

IAEA-TECDOC-CD-1692

# ***Water Chemistry and Clad Corrosion/Deposition Including Fuel Failures***

*Proceedings of a Technical Meeting  
held in Kiev, Ukraine, 2010*



**IAEA**

International Atomic Energy Agency

**WATER CHEMISTRY AND CLAD  
CORROSION/DEPOSITION INCLUDING  
FUEL FAILURES**

The following States are Members of the International Atomic Energy Agency:

AFGHANISTAN	GUATEMALA	PANAMA
ALBANIA	HAITI	PAPUA NEW GUINEA
ALGERIA	HOLY SEE	PARAGUAY
ANGOLA	HONDURAS	PERU
ARGENTINA	HUNGARY	PHILIPPINES
ARMENIA	ICELAND	POLAND
AUSTRALIA	INDIA	PORTUGAL
AUSTRIA	INDONESIA	QATAR
AZERBAIJAN	IRAN, ISLAMIC REPUBLIC OF	REPUBLIC OF MOLDOVA
BAHRAIN	IRAQ	ROMANIA
BANGLADESH	IRELAND	RUSSIAN FEDERATION
BELARUS	ISRAEL	RWANDA
BELGIUM	ITALY	SAUDI ARABIA
BELIZE	JAMAICA	SENEGAL
BENIN	JAPAN	SERBIA
BOLIVIA	JORDAN	SEYCHELLES
BOSNIA AND HERZEGOVINA	KAZAKHSTAN	SIERRA LEONE
BOTSWANA	KENYA	SINGAPORE
BRAZIL	KOREA, REPUBLIC OF	SLOVAKIA
BULGARIA	KUWAIT	SLOVENIA
BURKINA FASO	KYRGYZSTAN	SOUTH AFRICA
BURUNDI	LAO PEOPLE'S DEMOCRATIC REPUBLIC	SPAIN
CAMBODIA	LATVIA	SRI LANKA
CAMEROON	LEBANON	SUDAN
CANADA	LESOTHO	SWAZILAND
CENTRAL AFRICAN REPUBLIC	LIBERIA	SWEDEN
CHAD	LIBYA	SWITZERLAND
CHILE	LIECHTENSTEIN	SYRIAN ARAB REPUBLIC
CHINA	LITHUANIA	TAJIKISTAN
COLOMBIA	LUXEMBOURG	THAILAND
CONGO	MADAGASCAR	THE FORMER YUGOSLAV REPUBLIC OF MACEDONIA
COSTA RICA	MALAWI	TOGO
CÔTE D'IVOIRE	MALAYSIA	TRINIDAD AND TOBAGO
CROATIA	MALI	TUNISIA
CUBA	MALTA	TURKEY
CYPRUS	MARSHALL ISLANDS	UGANDA
CZECH REPUBLIC	MAURITANIA	UKRAINE
DEMOCRATIC REPUBLIC OF THE CONGO	MAURITIUS	UNITED ARAB EMIRATES
DENMARK	MEXICO	UNITED KINGDOM OF GREAT BRITAIN AND NORTHERN IRELAND
DOMINICA	MONACO	UNITED REPUBLIC OF TANZANIA
DOMINICAN REPUBLIC	MONGOLIA	UNITED STATES OF AMERICA
ECUADOR	MONTENEGRO	URUGUAY
EGYPT	MOROCCO	UZBEKISTAN
EL SALVADOR	MOZAMBIQUE	VENEZUELA
ERITREA	MYANMAR	VIETNAM
ESTONIA	NAMIBIA	YEMEN
ETHIOPIA	NEPAL	ZAMBIA
FIJI	NETHERLANDS	ZIMBABWE
FINLAND	NEW ZEALAND	
FRANCE	NICARAGUA	
GABON	NIGER	
GEORGIA	NIGERIA	
GERMANY	NORWAY	
GHANA	OMAN	
GREECE	PAKISTAN	
	PALAU	

The Agency's Statute was approved on 23 October 1956 by the Conference on the Statute of the IAEA held at United Nations Headquarters, New York; it entered into force on 29 July 1957. The Headquarters of the Agency are situated in Vienna. Its principal objective is "to accelerate and enlarge the contribution of atomic energy to peace, health and prosperity throughout the world".

IAEA-TECDOC-CD-1692

# WATER CHEMISTRY AND CLAD CORROSION/DEPOSITION INCLUDING FUEL FAILURES

PROCEEDINGS OF A TECHNICAL MEETING HELD IN  
KIEV, UKRAINE, 2010

INTERNATIONAL ATOMIC ENERGY AGENCY  
VIENNA, 2013

## COPYRIGHT NOTICE

All IAEA scientific and technical publications are protected by the terms of the Universal Copyright Convention as adopted in 1952 (Berne) and as revised in 1972 (Paris). The copyright has since been extended by the World Intellectual Property Organization (Geneva) to include electronic and virtual intellectual property. Permission to use whole or parts of texts contained in IAEA publications in printed or electronic form must be obtained and is usually subject to royalty agreements. Proposals for non-commercial reproductions and translations are welcomed and considered on a case-by-case basis. Enquiries should be addressed to the IAEA Publishing Section at:

Marketing and Sales Unit, Publishing Section  
International Atomic Energy Agency  
Vienna International Centre  
PO Box 100  
1400 Vienna, Austria  
fax: +43 1 2600 29302  
tel.: +43 1 2600 22417  
email: [sales.publications@iaea.org](mailto:sales.publications@iaea.org)  
<http://www.iaea.org/books>

For further information on this publication, please contact:

Nuclear Fuel Cycle and Materials Section  
International Atomic Energy Agency  
Vienna International Centre  
PO Box 100  
1400 Vienna, Austria  
Email: [Official.Mail@iaea.org](mailto:Official.Mail@iaea.org)

© IAEA, 2013

Printed by the IAEA in Austria  
March 2013

### IAEA Library Cataloguing in Publication Data

Water chemistry and clad corrosion/deposition including fuel failures : proceedings of a technical meeting held in Kiev, Ukraine, 2010. — Vienna : International Atomic Energy Agency, 2013.  
CD-ROM. — (IAEA-TECDOC-CD series, ISSN 1684-2073; no. 1692)  
ISBN 978-92-0-187510-5  
Includes bibliographical references.

1. Nuclear reactors – Corrosion – Congresses. 2. Nuclear fuel claddings – Effect of radiation on – Congresses. 3. Water cooled reactors – Safety measures. I. International Atomic Energy Agency. II. Series.

## FOREWORD

Corrosion is a principal life limiting degradation mechanism in nuclear steam supply systems, particularly taking into account the trends in increasing fuel burnup, thermal ratings and cycle length. Further, many plants have been operating with varying water chemistry regimes for many years, and issues of crud (deposition of corrosion products on other surfaces in the primary coolant circuit) are of significant concern for operators.

At the meeting of the Technical Working Group on Fuel Performance and Technology (TWGFPT) in 2007, it was recommended that a technical meeting be held on the subject of water chemistry and clad corrosion and deposition, including the potential consequences for fuel failures. This proposal was supported by both the Technical Working Group on Advanced Technologies for Light Water Reactors (TWG-LWR) and the Technical Working Group on Advanced Technologies for Heavy Water Reactors (TWG-HWR), with a recommendation to hold the meeting at the National Nuclear Energy Generating Company ENERGOATOM, Ukraine.

This technical meeting was part of the IAEA activities on water chemistry, which have included a series of coordinated research projects, the most recent of which, Optimisation of Water Chemistry to Ensure Reliable Water Reactor Fuel Performance at High Burnup and in Ageing Plant (FUWAC) (IAEATECDOC-1666), concluded in 2010. Previous technical meetings were held in Cadarache, France (1985), Portland, Oregon, USA (1989), Řež, Czech Republic (1993), and Hluboká nad Vltavou, Czech Republic (1998). This meeting focused on issues associated with the corrosion of fuel cladding and the deposition of corrosion products from the primary circuit onto the fuel assembly, which can cause overheating and cladding failure or lead to unplanned power shifts due to boron deposition in the clad deposits. Crud deposition on other surfaces increases radiation fields and operator dose and the meeting considered ways to minimize the generation of crud to avoid such problems.

The meeting was attended by 22 participants from 15 countries. Nineteen papers were presented in three technical sessions, covering operating experience, corrosion and oxidation, and clad deposition and its consequences.

The IAEA officer responsible for this publication was J. Killeen of the Division of Nuclear Fuel Cycle and Waste Technology.

### *EDITORIAL NOTE*

*This CD-ROM has been prepared from the original material as submitted by contributors. Neither the IAEA nor its Member States assume any responsibility for the information contained on this CD-ROM.*

*The use of particular designations of countries or territories does not imply any judgement by the publisher, the IAEA, as to the legal status of such countries or territories, of their authorities and institutions or of the delimitation of their boundaries.*

*The mention of names of specific companies or products (whether or not indicated as registered) does not imply any intention to infringe proprietary rights, nor should it be construed as an endorsement or recommendation on the part of the IAEA.*

## CONTENTS

SUMMARY .....	1
OPERATIONAL EXPERIENCE (Session 1)	
Bulgarian experience with the implementation of <sup>235</sup> U higher enriched fuel in WWER-1000 (water chemistry aspects) .....	11
<i>N. Zaharieva</i>	
NRI position in the water chemistry research and fuel inspection for Czech WWER-1000 reactors .....	19
<i>M. Mikloš, K. Mezhlumyan, J. Kysela, D. Ernst</i>	
Zinc addition and its challenge in Chinese NPP .....	25
<i>Shi Xiuqiang, Zhu Jun, Xu Xuelian</i>	
Primary water chemistry control at units of Paks Nuclear Power Plant .....	29
<i>J. Schunk, G. Patek, T. Pintér, P. Tilky, Á. Doma</i>	
Fuel assembly inspections performed during the refuelling outage of Paks Nuclear Power Plant Unit 4.....	35
<i>T. Pintér, P. Németh, Á. Menyhárt, I. Buránszky, J. Schunk, G. Patek</i>	
Comprehensive study of uranium and transuranium (Pu, Cm) accumulation on stainless steel and Zr+Nb cladding material surfaces .....	41
<i>K. Varga, P. Kádár, B. Baja, Z. Németh, T. Kristóf, N. Vajda, Zs. Stefánka, Z. Schay, T. Pintér, J. Schunk</i>	
Comparative study of the corrosion and surface analytical effects of the decontamination technologies .....	51
<i>K. Varga, B. Baja, E.H. Deák, K. Radó, Z. Németh, G. Patek, J. Schunk, A.N. Szabó</i>	
Primary system water chemistry follow-up and update in pressurized heavy water reactors .....	59
<i>M. Chocron, R. Bordoni, A.M. Olmedo, M. Strack, I. Rodríguez, R. Manera, J. Duca</i>	
CORROSION/OXIDATION (Session 2)	
The formation of oxide films under pressurized water reactor primary coolant conditions .....	71
<i>A. Luttikul, P. Srisukvatananan, D.H. Lister</i>	
Primary circuit water chemistry and impact on fuel cladding corrosion .....	87
<i>V. Marakhyan</i>	
The tests of water chemistry effect on corrosion behaviour of cladding .....	91
<i>B. Gong, X. Su, C. Li, Z. Zhou</i>	
Research into effects of coolant chemistry on corrosion processes of Ukrainian WWER-1000 core materials.....	107
<i>V.S. Krasnorutskyy, I.A. Petelguzov, V.M. Grytsyna, V.A. Zuyok, M.V. Tretyakov, R.A. Rud</i>	
CLAD DEPOSITION AND CONSEQUENCES (Session 3)	
Crud deposition on pressurized water reactor fuel in the Halden Reactor.....	113
<i>P.J. Bennett</i>	

Deposition of steel corrosion products on cladding surfaces and corrosion of zirconium ....	123
<i>V.G. Kritsky, I.G. Berezina, Y.A. Rodionov</i>	
Formation of corrosive deposits and their impact on operational safety of fuel elements in CANDU reactor.....	135
<i>I. Pirvan, M. Mihalache</i>	
The mechanisms for heat transfer in crud coated light water reactor fuel and their consequences .....	149
<i>S.P. Walker, I. Haq, N. Cinosi, M. Bluck, G.F. Hewitt</i>	
Experience in development and use of an ultrasonic plant for fuel assemblies cleaning of a WWER-440 reactor core .....	167
<i>A.V. Grishakov, O.P. Arkhipov, A.N. Prytkov</i>	
In situ experimental data on passivation of alloy 690 in hot conditioning water chemistry .....	173
<i>T. Saario</i>	
Optimization of water chemistry to control crud deposition on fuel clad in Indian pressurized heavy water reactors .....	187
<i>S. Velmurugan, S.V. Narasimhan</i>	
APPENDIX: PROPOSED FORM FOR REPORTING CRUD SAMPLING MEASUREMENTS .....	191
ABBREVIATIONS.....	193
List of participants.....	195

## SUMMARY

More than 95% of the nuclear power in the world is derived from water cooled reactors. In such reactor systems, water is used in primary circuits, secondary circuits (pressurized water reactors (PWR) and pressurized heavy water reactors (PHWR) and in a number of auxiliary systems. Water can be an aggressive medium especially at high temperature when in contact with structural materials. This means that the reliability of many nuclear power plant systems (fuel, steam generators, etc.) is dependent on the water chemistry during normal operations, startup, shutdown and abnormal operation conditions. Advanced water chemistry specifications have been developed for the existing water cooled reactors, but there is still room for improvement, particularly as fuel duty and burnups have increased, with new materials and enhanced requirements for reactivity control.

The sustainable development of nuclear energy depends on the safe and economic operation of nuclear fuel in current and future nuclear power plants. Innovative fuel cycles and improved fuel utilization are important elements in helping to achieve this goal and the fuel interaction with the coolant water plays a key role.

Limiting factors for fuel operation include the corrosion of fuel cladding and the deposition of corrosion products from the primary circuit onto the fuel assembly which can cause overheating and cladding failure or lead to unplanned power shifts due to boron deposition in the clad deposits. Further, issues of radiation dose to operation personnel are affected and proper control of crud can significantly reduce radiation fields in a power station.

The economic drive to increase the power and burnup of nuclear fuel can lead to higher corrosion of the cladding and changes in the coolant chemistry and improved cladding materials are countermeasures. It remains necessary to understand more fully the behaviour of fuel at burnups in excess of 50 GWd/tU.

Fuel clad failures can be caused by inappropriate water chemistry and clad sensitivity due to the combination of high temperature with high power flux and pH variation through changes in the concentrations of boric acid during a fuel cycle. As the burnup level increases and the fuel remains longer in the reactor, there is a need to better understand the corrosion processes. In particular it is necessary to consider the formation and development of corrosion throughout the primary circuit, the condition of any deposits arising and fuel rod behaviour during operation in the core.

This technical meeting was part of the IAEA activities on water chemistry, which have included a series of coordinated research projects [1–7], the most recent of which, “Optimization of water chemistry to ensure reliable water reactor fuel performance at high burnup and in ageing plant (FUWAC),” concluded in 2010. Previous technical meetings have been held in Cadarache, France (1985), Portland, Oregon, USA (1989), Řež, Czech Republic (1993) [8] and Hluboka nad Vltavou, Czech Republic (1998) [9].

## Opening session

The meeting was opened with a welcome from O. Godun, Head of Innovation Fuel Cycles Department, Scientific and Technical Centre of NNEG "Energoatom" based in Kiev. He provided an overview of the Ukrainian nuclear power programme, noting that all the Ukrainian operating nuclear power plants (NPP) are of the Russian designed pressurized water reactor (WWER) type and that the WWER-1000s are all using TVSA fuel supplied by TVEL from the Russian Federation. He provided fuel failure statistics, showing an improvement in the situation since 2005. Research is being undertaken to allow the Ukrainian WWER-1000 NPPs to operate in load follow mode. The Ukraine is considering the use of Westinghouse fuel (Vantage fuel type, known as TVS-W) and there are at the present time (2010) 42 assemblies of this type in the South Ukraine NPP. The Ukraine has experienced a number of fuel failures, but there is no capability to examine the failure to identify any cause.

J. Killeen (IAEA) also welcomed the participants and described the purpose of the meeting. He then presented an overview of IAEA work in the area of water chemistry.

### Session 1: Operating experience

Chairperson: F. Nordmann

N. Zaharieva (Bulgaria) described the operational experience of the Kosloduy NPP. The Steam Generators are of 8/18/10 SS. The new fuel being implemented is TVSA at 4.3% enrichment and with up to 5% Gd rods as a burnable poison. Coolant pH is maintained between 7.0 and 7.2 with a maximum KOH of 0.45mmol/kg. The amount of activated corrosion products in the circuit has not increased with the new advanced fuel cycle. There is concern with PWR problem experience and a programme is in place to check if such problems can occur in WWER [e.g. incomplete rod insertion (IRI) due to assembly distortion or crud induced power shifts (CIPS)].

M. Miklos (Czech Republic) reported on the experience at Temelin which has been using Westinghouse VVANTAGE-6 fuel. The coolant pH is maintained at a value of 7.1 with KOH limited to 20mg/kg. With this water chemistry there are no problems with deposition on the fuel clad (originally Zry-4 and now ZIRLOTM since 2008). Problems were experienced with excessive assembly growth leading to assembly distortion and IRI. There was also grid-rod fretting, which remains a problem. The assembly growth issue has now been solved, but Temelin is transitioning to Russian TVSA-T fuel, and is carrying out a whole core replacement rather than operate with a mixed core. They had had experience with fuel repair, and had decided not to repair assemblies where there was visible evidence of secondary hydriding, most failures having occurred on the outer fuel rods of the assemblies. The new TVSA-T fuel is designed with 9 fuel spacer grids to match the original Westinghouse fuel design.

Xiuqiang Shi (China) described the intention to use zinc addition in new Chinese PWRs to mitigate stress corrosion cracking (SCC) and to suppress general corrosion of primary circuit materials. He described the Chinese new build programme and expressed his concern about the lack of SCC testing where the Steam Generators (SGs) which are of Alloy 690, the effect of zinc on cladding corrosion and for the risk of CIPS following enhanced corrosion product in the coolant immediately after zinc addition. No current plant in China uses zinc addition, so there is no monitoring for Ni in the coolant and they are looking for a means to do this. To date testing has shown slower clad corrosion in the presence of zinc and tests will be done to examine the compatibility of zinc with Alloy 690 material. A full risk assessment for zinc addition will be carried out before any plant implementation which would be done during hot functional testing (HFT) before initial startup. In discussion it was noted that there was no need to add zinc to prevent SCC in Alloy 690, as this was not a susceptible material.

J. Schunk (Hungary) tabled four papers to the meeting, which are included in the proceedings. His presentation described empirical methods for determining leakage rates from failed fuel in

WWER-440 plants using fission product activity in the coolant. He described the history of fuel failure, with mostly very small leaks in units 1–4 at Paks NPP in the years 1990–96. In 2008 there was a large leaker in Unit 4. Iodine spiking was seen and one failed fuel assembly was identified through fuel sipping.

M. Chocron (Argentina) was unable to attend the meeting, but had provided a copy of the paper he had prepared for the meeting. It was presented on his behalf by J. Killeen, who described the operational experience from the Argentinean PHWR reactors. Details are provided of the Water Chemistry specifications for Embalse and Atucha NPPs.

## **Session 2: Corrosion and oxidation**

Chairperson: F. Nordmann

D.H. Lister (Canada) described laboratory studies comparing different steels, surface treatments and water chemistry effects on corrosion, both of steels and cladding materials. His detailed studies showed that the major effect on oxide formation was from steam generator (SG) alloy composition. The oxides formed on Ni-based alloys and SS304 were duplex, consisting of an Fe-rich crystallite layer and a Cr-rich underlying layer. The higher-Cr alloys produced a more compact oxide than the lower-Cr alloys. The oxides formed with the coolant containing boron and lithium were more compact than those in a coolant with just lithium. Boron incorporated in an inner oxide layer on Alloy 600 MA, Alloy 690 MA and Alloy 800 MA. He also noted that zinc addition enhances the formation of protective oxide on Ni-based alloys and on SS304 but had no apparent effect on the oxidation of zircaloy-4.

V. Marakhyan (Armenia) described the coolant chemistry used in Armenia, noting that there had been a crud corrosion fuel failure observed and that there was nitric acid generated from the hydrazine additions. This paper was presented later in the meeting and was, therefore, not considered during the general discussion for this session.

B. Gong (China) described a Chinese project to develop an advanced assembly and in particular he described the laboratory work being done to investigate the corrosion of advanced cladding materials in sub-cooled nucleate boiling (SNB) conditions with varying concentrations of boron and lithium in the coolant. His results show lower corrosion for modified Zr-4 compared with M5 cladding types, and that lithium increased corrosion rates. Test conditions were sufficiently challenging for spallation of the oxide to occur in some tests. There was some discussion about the test protocol, and it was noted that the water in the tests was saturated with oxygen, which made the tests non-representative of reactor conditions, but the results did show systematic changes in behaviour as the test parameters were modified. The oxygen level may explain why M5 oxidized more rapidly than modified Zr-4.

M. Tretyakov (Ukraine) described out of pile testing of E110 alloy to 35 000 hours, comparing surface condition, oxygen content and material fabrication. Additional work is being carried out on stainless steels. The concern is for the quantity of radioactive waste in WWER plant, as the water chemistry is working well. He reported early results of the effect of zinc addition on the corrosion of steels. During discussion of this paper, it was noted that WWER NPPs do not need zinc addition for either dose rate control nor to prevent stress corrosion cracking SCC. In WWERs, the precursors of the radioactive isotopes of cobalt are generally not present in the reactor materials and the cobalt contamination is much lower. However, zinc addition is under consideration for new NPPs to support passivation of the steam generators (SGs). One participant noted that for older WWER units there was a risk that zinc addition could interact with high temperature filters of titanium sponge, and should not be used in such plants.

## First discussion session

Following the presentations there was a general discussion, focusing initially on the use of zinc injection. It was recognized that there was a lot that can be done for new plant and replacement SGs with passivation treatments during HFT before startup. This would include zinc addition followed by a mild chemical clean. The methods used at Sizewell B were recognized to be good practice. It was recognized that the situation for WWER plants was different, there is no need to add zinc for dose rate control, due to the absence of stellite and high nickel steels in these plants, and hence very limited cobalt contamination. Further, there was no experience of zinc addition with Russian materials. Also for Canadian PHWR (CANDU) systems, zinc addition would be of little use for carbon steels. In general, zinc addition was of significant benefit for austenitic steels, but not for martensitics.

Questions were raised if there was any potential for the use of lithium by WWER NPPs or potassium by PWRs as the alkalizing agent, perhaps potassium might be suitable to help suppress CIPS in PWR., but there seemed to be no desire for a change from either reactor system users.

It was generally agreed that improvement in clad corrosion resistance is more driven by improvements to cladding composition than adjusting water chemistry, for example E110M is a new alloy, related to E110 but with the addition of 0.1%Fe shows superior corrosion resistance. Many new alloys are at various stages of testing, including E635M, HANA, MDA, and at least two Chinese alloys.

It was remarked that where there is localized sub-cooled nucleate boiling (SNB), all hydrogen will be stripped out from the coolant and radiolysis could produce similarly localized oxidizing conditions. Under CANDU conditions, with 40% voidage, reducing conditions remain, even though the hydrogen concentration is low compared with PWR.

### Session 3: Clad deposition and its consequences

Chairperson: D. Lister

P.J. Bennett (Norway) was unable to attend the meeting due to flight delays. His paper on Crud Deposition on PWR Fuel in the Halden Reactor, was not presented at the meeting, but is included in these proceedings. The paper describes the capabilities of the Halden Reactor Project which is capable of irradiation testing under representative PWR and boiling water reactor (BWR) conditions. The experimental observations are that zircaloy surfaces are often covered with crud, depending on the prevailing conditions, but that these are often easily removable by brushing. Tenacious crud can form where there are high concentrations of corrosion products in the water or there is high heat flux with a degree of surface boiling. Crud deposition can be rapid under conditions of high fuel duty where there has been a chemical intrusion. Various compositions of crud have been observed and it is noted that post irradiation examination on the crud does not necessarily give the composition or morphology that was present at power.

I. Berezina (Russian Federation) noted that deposition on fuel was causing a pressure differential rise during operation, and was a problem for most WWER-440 NPPs. There is anomalous mass transport following decontamination, and it is possible to use  $^{58}\text{Co}$  to indicate deposit growth. The target of her programme is to model and control  $\Delta P$ , which typically rises from 3.15MPa to 3.4MPa, by controlling water chemistry.

The second part of her talk covered zirconium alloy corrosion. A model of fuel cladding corrosion was developed to describe the effect of physical and chemical parameters of Zr alloys under light water reactor (LWR) conditions. The calculation formulae were verified on the base of experimental data on fuel cladding corrosion in the autoclave and NPPs LWR reactors. She noted that general corrosion on E110 alloy was low, but that crevice corrosion on the spacer grids can be much more severe with oxide thickness up to 200 $\mu\text{m}$ . She was asked what the nature of the crud was and if there was nickel included. It was noted that there had been some analysis of deposit from the top of

assemblies, and it was pure magnetite with no nickel, and had therefore derived from iron oxalate arising from decontamination procedures.

I. Pirvan (Romania) was concerned with corrosive deposits in CANDU plant and had investigated the causes of increased oxidation under crud. She used laboratory techniques as well as experiments in a loop of the TRIGA reactor, where unusual water conditions were examined. In the TRIGA test, varied cruds were observed which led to deep nodular corrosion underneath the crud. Corrosive deposits were formed in steam conditions at 400°C. The composition, thickness and evolution of crud of fuel assembly surfaces depend on operational condition, water chemistry conditions or different oxidation conditions of surface. During steady state operation of CANDU reactors with standard chemistry conditions, black and adherent magnetite crystallites, originating from corrosion of the carbon steel feeders, precipitated from the coolant onto Zr-4 surfaces. The presence of these corrosion deposits did not influence the oxidation or hydriding of zircaloy-4. In abnormal water chemistry conditions (pH>10.5 or oxygen concentration >100ppb) and in the presence of irradiation, CANDU fuel rods developed thick, non-adherent and porous deposits which provided an additional thermal barrier that led to nodular corrosion, and finally to perforation and failure of the sheath.

S.P. Walker (UK) presented a detailed model for the thermal-hydraulic behaviour of fuel coated with crud and how the physical structure of the crud can determine the local elemental composition of deposits. His model describes how coolant percolates through the crud and boils at the surface of “chimneys” in the crud, leaving boron deposits localized within the chimney.

H. Glasbrenner (Switzerland) was asked to provide a regulatory view of water chemistry issues for the meeting and she prepared a presentation for this purpose. She described the current practice in the Swiss NPPs, noting that regulatory limits were different between the plants e.g. maximum lithium concentrations. The BWR plants use on-line noble metal (OLNC) additions to prevent crack growth, but noted that this seems to move tramp uranium to the core, leading to an increase in fission products in the core. Measured crack growth rate in identified shroud cracks had been significantly reduced by OLNC. Laboratory tests are starting, which are designed to investigate how platinum behaves under BWR conditions. She asked what limits on coolant iodine activity were applied at other plants.

A. Grishakov (Russian Federation) described the ultrasonic cleaning equipment that has been developed for WWER-440 plants. He discussed the work done at Novovoronezh units 3 and 4 which had a particular problem with deposition on the fuel due to the specific material of the steam generators and the history of decontamination at the plant. The new industrial scale cleaning equipment can clean an assembly in around 40 minutes and is still under development to improve efficiency. All of the 3rd and 4th dwell fuel has been cleaned. Failed fuel is not cleaned. 23 “untight” fuel assemblies were found on an unplanned shutdown following fuel cleaning, but it is not thought that the cleaning had any causal influence on this event, approximately half of the failed assemblies had not been cleaned.

T. Saario (Finland) described in detail the procedure carried out by Sizewell-B NPP during the HFT. For the first ten days at operating temperature 1.5ppm Li + 30ccH<sub>2</sub>/kgH<sub>2</sub>O was used, followed by the same time with added boric acid. He discussed improvements since then, where the Japanese plant Tomori-3 has used zinc with lower lithium during HFT to reduce dose rates still further. His studies into the separate effects of the differing components of the passivation technique showed unusual behaviour of lithium and he considered that there was lithium hideout probably occurring. The conclusions of the study were that there is no international consensus on the optimal water chemistry to be used during HFT, though dissolved H<sub>2</sub> (25–35cc/kgH<sub>2</sub>O), zinc injection and boric acid are beneficial. Lithium should be around 0.5ppm based on an optimum pH determined from laboratory studies and it seemed likely that stabilization occurred in less than 50 hours.

Mr. Velmurugan described the control of deposition on cladding in PHWRs. He noted that the crud is magnetite, due to the use of carbon steel in the primary circuit. Conditioning of the circuit is done before fuel loading at a temperature of 260°C using lithium and hydrazine. Ideally it would be

preferable to have  $\text{pH}_a > 10.5$  to ensure solubility of the magnetite, but at the higher  $\text{pH}_a$  values, flow assisted corrosion (FAC) becomes a problem. Antimony deposition, activation and release in the core zircaloy surfaces have been observed in some reactors. Full system chemical decontamination is carried out in Indian PHWRs to reduce the radiation field. This procedure has been applied to 11 units with no problems identified.

M. Miklos (Czech Republic) gave a presentation on how best to record the results of crud examinations and studies in a consistent manner so that all could benefit from clear and comparable data. He provided a spreadsheet covering items he felt were important to record and asked participants for feedback. This form is given in Appendix 1.

## **Second discussion session**

Chairman: D. Lister

Following the final presentations an open discussion was held, D. Lister asked if the coolant in PWR and PHWR was in equilibrium with the load of corrosion products, and he felt that proper consideration should be given to kinetic effects as the solubility of the corrosion products varied through the circuit. There were differences of opinion on the presence of particulate in the circuit, one view was that oxygen in a sampling line would turn soluble material into particulate, providing misleading information, whilst others noted that material was trapped on filters, so some must be particulate, though some isotopes will be completely soluble. It was noted that there were issues associated with sampling both coolant concentrations of corrosion products and with the collection of crud scrape samples due to their solubility in shutdown conditions.

The potential effect of zinc addition on crud was discussed and recommended for further investigation. At the level of 5–10ppb used for dose rate control it does not seem to have an adverse effect, but there is not much experimental evidence. It was noted that failures seen at Farley following zinc injection were not thought to be associated with zinc, as similar failures occurred in another unit at Farley which had not had zinc injection.

There was interest in why WWER users were considering adding zinc to their systems as there was no need for dose rate control. There was a view that as fuel duty was increased in WWER it was appropriate to consider all relevant technologies that might help to prevent emergent problems. There is no experimental evidence of the effect of zinc on WWER circuit material and this has also led to reluctance to use this technology. One of the key issues associated with zinc addition in the older operating WWER units is the presence of high temperature filter containing titanium which may interact with zinc.

Open questions included the effect of enriched boron in the coolant; there were competing effects between lowering the lithium and the potential to affect CIPS. Further work was recommended to see if there was any effect of zinc on fuel crud.

### **Technical visit**

The Ukrainian hosts arranged a visit to the Chernobyl reactor and the participants were provided with details of the work being undertaken there. It provided a good reminder of the care needed in nuclear work and the need for a conservative approach to any change that might cause problems.

## RECOMMENDATIONS

The recommendations drawn from the panel discussions included the following:

- All new surfaces in the primary circuit of a nuclear power plant should be passivated if possible. New plants should be given a passivation treatment during hot functional testing;
- Zinc addition has a beneficial effect on the circuits of PWR plants, but was not necessary for WWER plants due to their stainless steel steam generators. In some cases adding zinc to WWER plant could be detrimental;
- There is no strong incentive to consider changing the alkalizing agents currently in use in PWR (lithium) or WWER (potassium);
- Decontamination of fuel assemblies is controversial, with a lot of bad experiences seen and strong recommendations were made that it should not be done, though some had not had any problems.

## REFERENCES

- [1] INTERNATIONAL ATOMIC ENERGY AGENCY, Fuel Cladding Interaction with Water Coolant in Power Reactors (A Survey Report of Co-ordinated Research Programme), IAEA-TECDOC-356, IAEA, Vienna (1985).
- [2] INTERNATIONAL ATOMIC ENERGY AGENCY, Coolant Technology of Water Cooled Reactors, Volume 1, Chemistry of Primary Coolant in Water Cooled Reactors, IAEATECDOC-667, IAEA, Vienna (1992).
- [3] INTERNATIONAL ATOMIC ENERGY AGENCY, Coolant Technology of Water Cooled Reactors, Volume 2, Corrosion in the Primary Coolant Systems of Water Cooled Reactors, IAEA-TECDOC-667, IAEA, Vienna (1992).
- [4] INTERNATIONAL ATOMIC ENERGY AGENCY, Coolant Technology of Water Cooled Reactors, Volume 3, Activity Transport Mechanisms in Water Cooled Reactors, IAEA-TECDOC-667, IAEA, Vienna (1992).
- [5] INTERNATIONAL ATOMIC ENERGY AGENCY, High Temperature On-line Monitoring of Water Chemistry and Corrosion Control in Water Cooled Power Reactors, IAEA-TECDOC-1303, IAEA, Vienna (2002).
- [6] INTERNATIONAL ATOMIC ENERGY AGENCY, Data Processing Technologies and Diagnostics for Water Chemistry and Corrosion Control in Nuclear Power plants High-Temperature On-line Monitoring of Water Chemistry and Corrosion in Nuclear Power Plants (DAWAC), IAEA-TECDOC-1505, IAEA, Vienna (2006).
- [7] INTERNATIONAL ATOMIC ENERGY AGENCY, Optimization of Water Chemistry to Ensure Reliable Water Reactor Fuel Performance at High Burnup and in Ageing Plant (FUWAC), IAEA-TECDOC-1666, IAEA, Vienna (2006)
- [8] INTERNATIONAL ATOMIC ENERGY AGENCY, Influence of Water Chemistry on Fuel Cladding Behaviour, IAEA-TECDOC-927, IAEA, Vienna (1997).
- [9] INTERNATIONAL ATOMIC ENERGY AGENCY, Water Chemistry and Corrosion Control of Cladding and Primary Circuit Components. IAEA-TECDOC-1128, IAEA, Vienna (1999).

**OPERATIONAL EXPERIENCE**

(Session 1)

**Chairperson**

**F. NORDMANN**  
France



# BULGARIAN EXPERIENCE WITH THE IMPLEMENTATION OF $^{235}\text{U}$ HIGHER ENRICHED FUEL IN WWER-1000 (WATER CHEMISTRY ASPECTS)

N. ZAHARIEVA  
Institute for Nuclear Research and Nuclear Energy,  
Bulgarian Academy of Sciences,  
Sofia, Bulgaria

## Abstract

Water chemistry and radiochemistry plant data from the WWER-1000 Units in NPP Kozloduy confirm that a realistic way for satisfactory implementation of  $^{235}\text{U}$  high enriched (up to 4.3%) fuel has been found. The main requirements are: implementation of solid neutron burnable absorbers; application of corrosion resistant fuel cladding; and the maintenance of suitable coolant water chemistry. The implementation at NPP Kozloduy is described.

## 1. INTRODUCTION

At Kozloduy NPP, Bulgaria, WWER-1000 reactors (V 320, produced in former Soviet Union) are operated as plant Unit 5 (in operation since 1988) and Unit 6 (in operation since 1993). A comparison of the main plant parameters of WWER-1000 reactors and Westinghouse supplied PWRs can be found in Table 1 [1].

TABLE 1. PLANT PARAMETER COMPARISON

Plant parameter	Westinghouse supplied PWRs		WWER-1000
Thermal power ( $\text{MW}_{\text{th}}$ )	2775	3441	3000
Number of coolant loops	3	4	4
Number of fuel assemblies	157	193	163
Core equivalent diameter (m)	3.04	3.37	3.17
Core volume ( $\text{m}^3$ )	26.6	32.6	28.7
Core uranium loading (MtU)	67–72	82–88	80.9
Core power density (kW/l)	105	105	105
Core specific power (kW/kg)	38–41	38–41	37
Core temperature rise ( $^{\circ}\text{C}$ )	36	36	32.6

The specific features of WWER-1000 units in the Bulgarian nuclear power plants are:

- The steam generators with austenitic stainless steel 08Cr18N10T tubing;
- The steam generators are with horizontal straight tubing;
- The fuel elements cladding material is Zr-1%Nb (Zr1Nb) alloy — recent trade name E 110;
- As a main neutron absorber is applied dissolved in coolant boric acid (with natural  $^{10}\text{B}$  content);
- Nowadays as a second (solid) burnable absorber, gadolinium (Gd) is integrated into the fuel — uranium-gadolinium ( $\text{U-Gd}_2\text{O}_3$ ) fuel — 5%  $\text{Gd}_2\text{O}_3$  is applied;

- As a pH control agent in the reactor coolant, potassium hydroxide is introduced (the high temperature coolant values —  $\text{pH}_T = \text{pH}_{300}$  are the main criteria determining the applied alkalizing reagent quantity necessary for the neutralization of boric acid in the coolant); The values of  $\text{pH}_{300}$  are required to be in the range of  $\text{pH}_{300} = 7,0\text{--}7,2$  for the entire operation period;
- Practically, as it is shown in Fig. 1, the buildup of lithium ( ${}^7\text{Li}$ ), based on the neutron reaction:  ${}^{10}\text{B} (n, \alpha) \rightarrow {}^7\text{Li} (n, \alpha)$ , takes place during the entire period of the cycle and even makes up a significant part of the total alkalizing ion concentration in the coolant;
- The necessary quantity of hydrogen in the primary circuit is generated by radiolysis of injected  $\text{NH}_3$ .

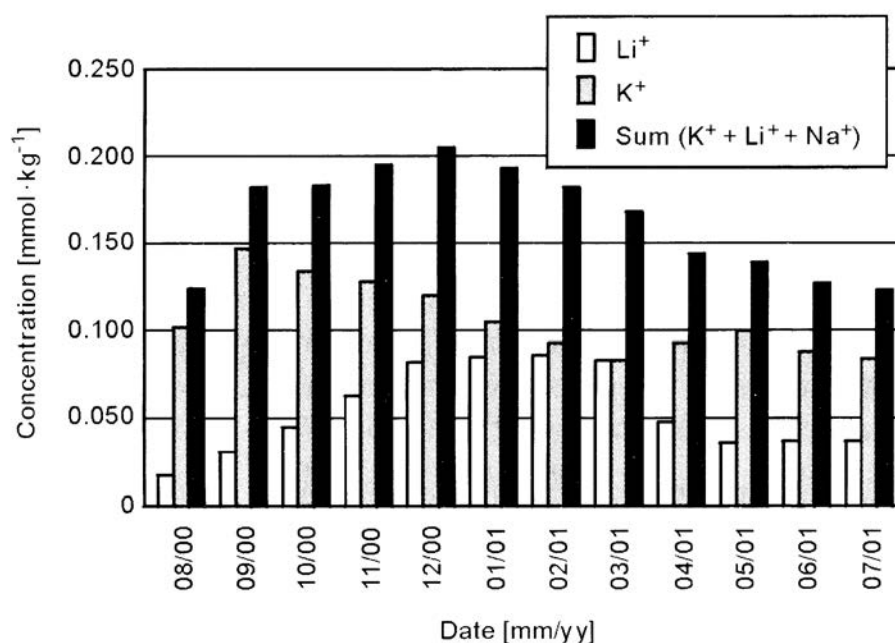


FIG. 1. Change in the coolant  $\text{Li}^+$ ,  $\text{K}^+$ , and total alkalizing ion concentrations (monthly average values) [2].

WWER-1000 reactors are in operation in the Russian Federation, Ukraine, Bulgaria, China and in the Czech Republic (NPP Temelin which WWER Units are Czech production).

## 2. USE OF ${}^{235}\text{U}$ HIGHER ENRICHED FUEL IN THE NUCEAR POWER PLANT KOZLODUY

In accordance with worldwide trends for the improvement of the nuclear power industry electricity production through the implementation of more highly enriched  ${}^{235}\text{U}$  uranium fuel, the management of NPP Kozloduy decided to introduce more highly enriched (up to 4,3%)  ${}^{235}\text{U}$  fuel in plant Units 5 & 6 (WWER-1000). This process was carried out over the course of four 12-month fuel cycles, by the implementation of advanced fuel assemblies of the type TVSA (imported from the Russian Federation — JSC TVEL Co), which have uranium fuel with up to 4,3%  ${}^{235}\text{U}$  enrichment. A burnable absorber (Gd) is integrated into the TVSA fuel-uranium-gadolinium (U-Gd $2\text{O}_3$ ) fuel — with 5% Gd $2\text{O}_3$ . A general view and cross section of the TVSA fuel assembly are presented in Fig. 2 [3]. The full implementation of the TVSA fuel was realized step by step, in accordance with a coordinated program between Kozloduy NPP and JSC TVEL.

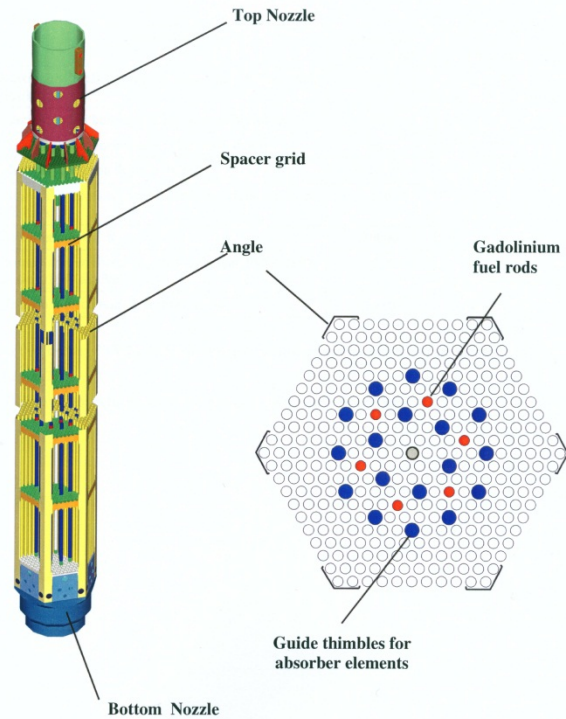


FIG. 2. TVSA general view and cartogram [3].

The 15th fuel cycle of Unit 5, NPP Kozloduy, was the first fuel cycle after the finalization of the step-by-step introduction of  $^{235}\text{U}$  higher enriched fuel, realized through the implementation of TVSA advanced fuel assemblies with gadolinium doped uranium fuel.

### 3. COOLANT WATER CHEMISTRY & RADIOCHEMISTRY PLANT DATA DURING THE POWER OPERATION PERIOD OF UNIT 5, 15<sup>TH</sup> FUEL CYCLE

The operation of Unit 5, NPP Kozloduy over all four fuel cycles during which  $^{235}\text{U}$  higher enriched fuel was introduced step-by-step, was realized in keeping with NPP Kozloduy primary circuit water chemistry requirements. These requirements, expressed in compact form in Fig. 3 require the high temperature coolant pH values:  $\text{pH}(300)=7.0$ ;  $\text{pH}(300)=7.1$ ;  $\text{pH}(300)=7.2$  (Area A in Fig. 3) to be kept, using the necessary coolant alkalizing agent concentrations, corresponding to the actual coolant boric acid concentrations.

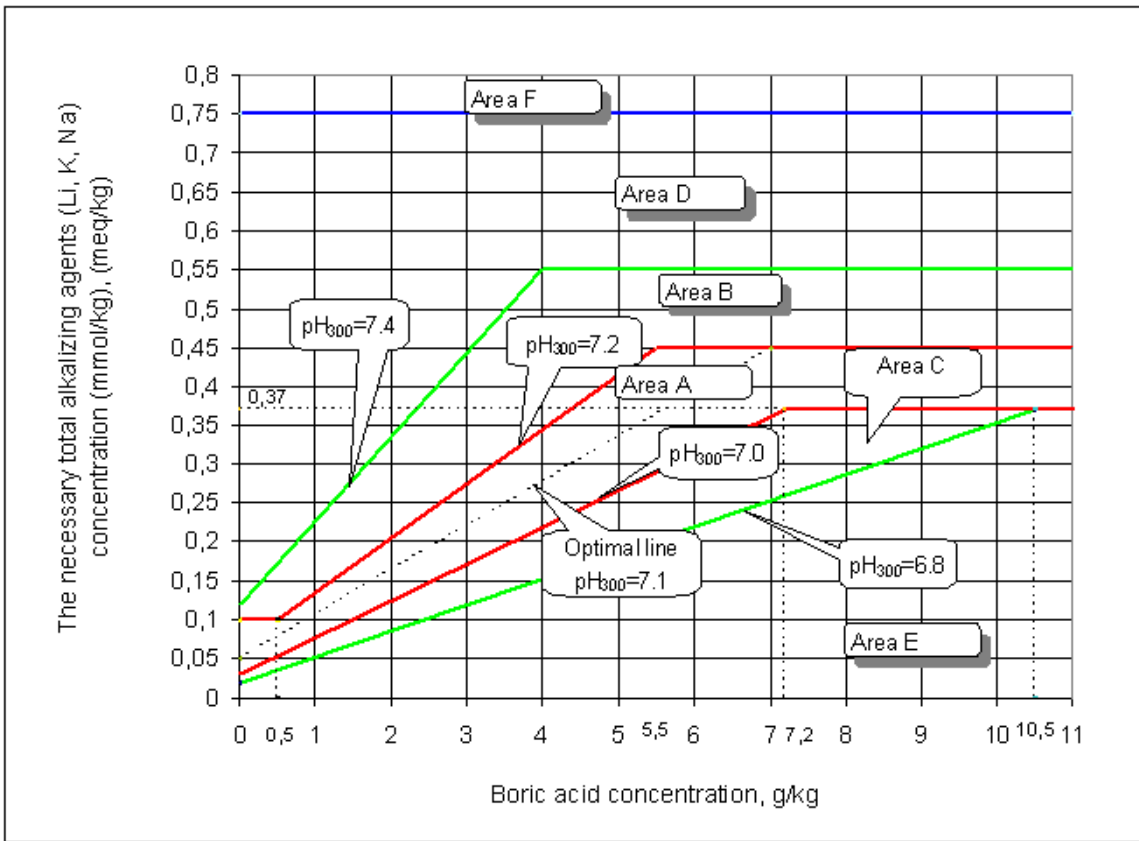


FIG. 3. Kozloduy NPP Coolant Water Chemistry Requirements.

The maintaining of these coolant water chemistry requirements ensured the necessary minimization corrosion processes in the construction materials of the primary circuit. As a consequence, the limitation of out-of-core corrosion product release ensured low activated corrosion product concentrations in the coolant.

The entire 15th fuel cycle water chemistry plant data are presented in Fig. 4.

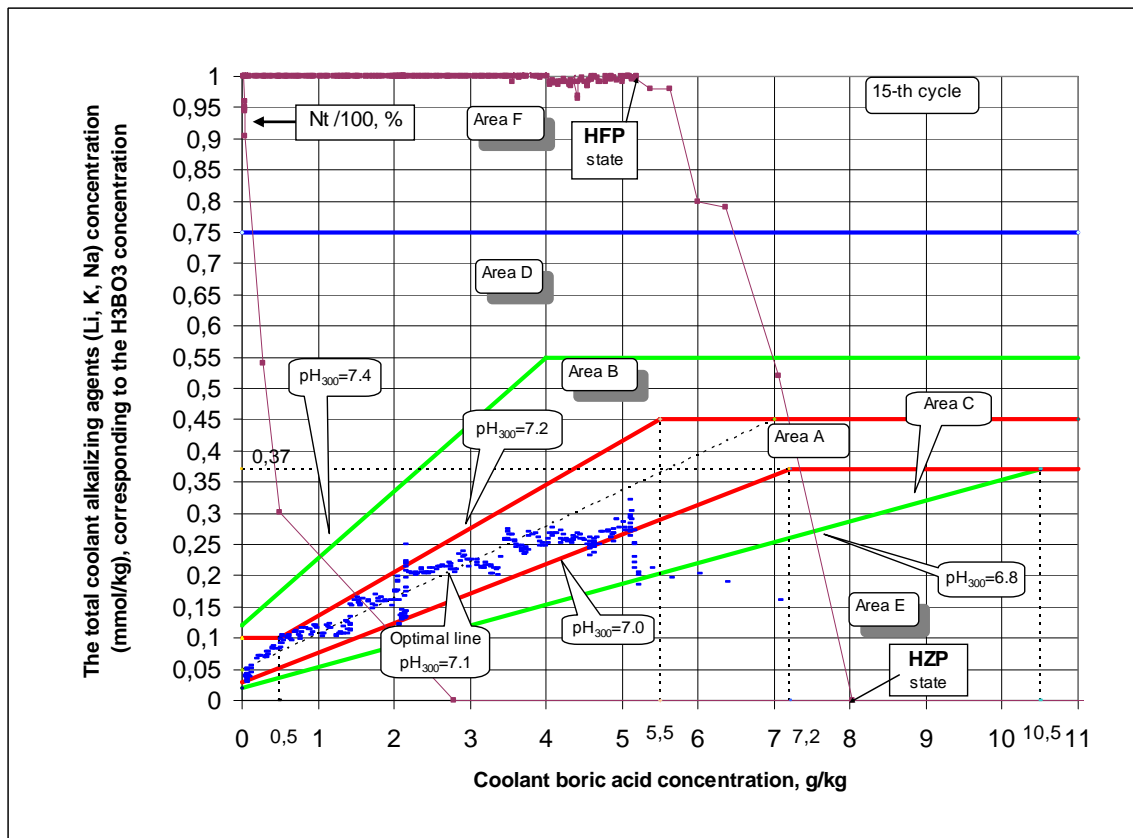


FIG. 4. Coolant Water Chemistry Plant Data for the entire 15th Fuel Cycle of Unit 5.

HWP — Hot Zero Power State

BOC — Beginning of Cycle

HFP — Hot Full Power State

EOC — End of Cycle

The fuel cycle's power operation period is the time period between the end of the Beginning of Cycle (BOC) and the start of shutdown period. For this reason the Hot Full Power (HFP) state point should be taken as the start of the operation period.

The data in Fig. 4 data allow a general evaluation to be made about the role, as a second absorber, of the gadolinia ( $Gd_2O_3$ ) uranium fuel (TVSA fuel assemblies).  $Gd_2O_3$  ensures great enough decrease in the initial coolant  $H_3BO_3$  concentration in fuel cycles operated with enriched  $^{235}U$  fuel, so that it can be neutralized with total alkalinizing agent concentrations below 0,45 mmol.kg-1 (The permitted maximal total coolant alkalinizing agent concentration).

The data in Fig. 4 show that during the fuel cycle operation period of the 15th fuel cycle of Unit 5, the unit's power is practically constant (100%) and under these conditions the coolant water chemistry plant data values are always in the range of Area A. This very important fact should be evaluated as a confirmation that the required coolant water chemistry plant values (within the range of Area A) are fully realizable through the implementation of 100% TVSA fuel assemblies in the reactor core. The obtained data indicate that staff efforts to keep the coolant water chemistry within the range of Area A were successful.

The data presented in Fig. 5 allow the conclusion to be made that the coolant activated corrosion product characteristics during the entire operation period of the 15th fuel cycle, Unit 5, are practically the same as the observed coolant activated corrosion product characteristics during the corresponding period of the previous fuel cycles of the Unit 5. This comparison shows that by 100% TVSA fuel assemblies in the reactor core of Unit 5 (15th fuel cycle), the corrosion processes in primary circuit remained on the same low level, i.e. under these conditions, an increase in coolant corrosion aggressiveness cannot be indicated.

NPP Kozloduy, Unit 5, 15th cycle

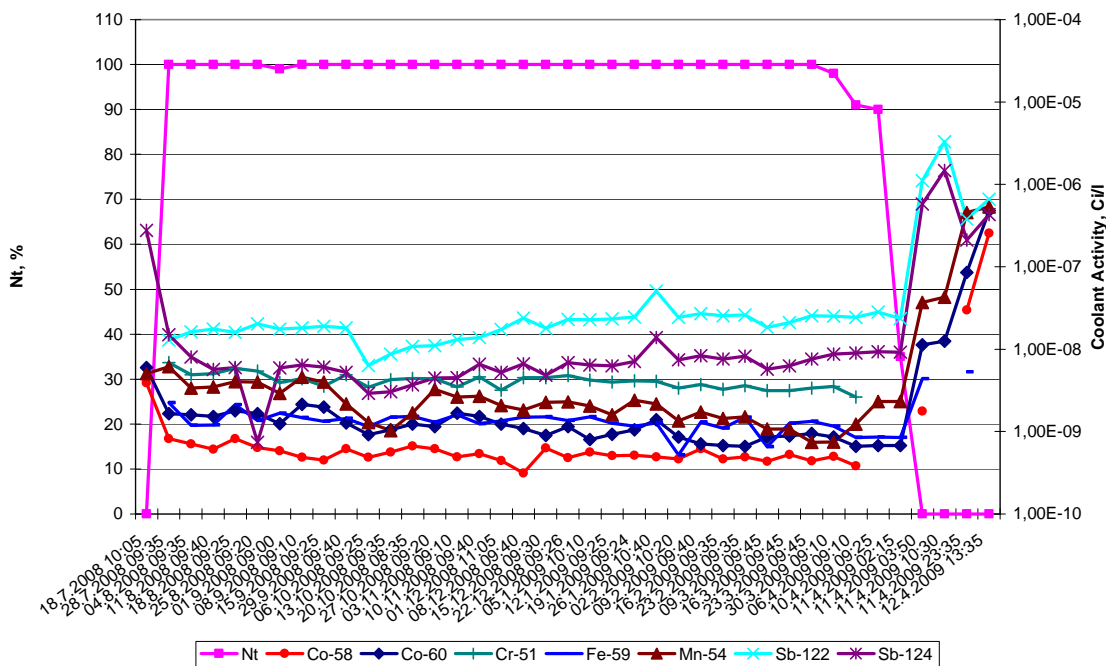


FIG. 5. Coolant activated corrosion products for the entire operation period of the 15th fuel cycle, Unit 5, Kozloduy NPP.

The excellent radiochemistry coolant plant data (low level of coolant activity), obtained during the entire operation period of the 15th fuel cycle of the Unit 5 are a good confirmation of the effectiveness of the coolant water chemistry, developed and applied in WWER-1000 Units in NPP Kozloduy, the main characteristic of which is the maintaining of coolant pH(300) values in the range of 7.0–7.2 (Area A).

The relatively unusual data for antimony isotopes, mainly  $^{122}\text{Sb}$ , in the coolant during the entire operation period and shutdown were subject to a special investigation, the results of which have been presented separately [4, 10].

According to M. Chatterton from the US Nuclear Regulatory Commission [5]: “Too high burnup or high (aggressive) fuel duty or both are related to incomplete control rod insertion (IRI) events, large axial offsets or axial offset anomalies (AOA), fuel failures due to high fuel duty, adverse effects of water chemistry, high crud buildup, and accelerated growth of rods and assemblies.” The US PWR practice shows that the higher duty cores (usually by implementation of more highly enriched  $^{235}\text{U}$  fuel) are always accompanied by increased boiling mainly on the feed fuel assemblies, and that the fuel cladding deposits tend to accumulate to the greatest extent in the higher sub-cooled nucleate boiling (SNB) regions of the core [6].

The boiling in the core causes a change in the type, thickness, and composition of deposits [7]: (a change in composition from a standard nickel ferrite based crud, to one that is dominated by nickel oxide formation) [7, 8].

The change in the deposit’s composition – the nickel oxide formation was the reason for our [9] opinion that the sub-cooled nucleate boiling (SNB) has a significant impact on the chemical environment of the Pressurized Water Reactor’s fuel cladding. This effect is not a direct consequence of the boiling but is a result of local (at cladding surfaces) stripping out of dissolved in coolant

hydrogen and the favouring of local water radiolysis. As a result of this water radiolysis process, the local oxidants: hydrogen peroxide ( $H_2O_2$ ) together with some radiolytical water radicals are produced.

It is clear that this change in cladding environment is in fact a result (consequence) of the synergic impact of the boiling and water radiolysis processes on the pressurized water reactor fuel cladding surfaces [9, 10].

This change in the fuel cladding environment characteristics creates a need for new criteria for corrosion resistance properties of fuel cladding materials in the presence of sub-cooled nucleate boiling. These materials should have high corrosion resistance due to this general change in the fuel cladding chemical environment.

A summary of the points discussed above shows that the main factors which have an impact on the potential onset of axial offset anomaly (AOA) are:

- (a) Sub-cooled nucleate boiling (SNB);
- (b) Primary circuit corrosion processes, respectively the coolant corrosion products.

These two phenomena are caused by two different independent reasons (plant conditions):

- Corrosion processes in the primary circuit and corrosion product transport depend directly on coolant water chemistry and out-of-core constructional materials.
- Sub-cooled nucleate boiling depends on the core duty; and its effects (change in the cladding chemical environment) are determined by the degree of local water radiolysis at cladding surfaces. The corrosion damages under these conditions depend mainly on the cladding material properties and cannot be influenced by the coolant water chemistry characteristics.

#### 4. CONCLUSIONS

The obtained water chemistry and radiochemistry plant data of WWER-1000 Units at NPP Kozloduy confirm that one realistic approach to problem free implementation of highly enriched  $^{235}U$  (up to 4,3%) fuel has been found.

The main features of this approach are:

- Implementation of solid neutron burnable absorbers together with the neutron absorber dissolved in the coolant – natural boric acid;
- Application of fuel cladding materials with enough corrosion resistance to the specific fuel cladding environment created by the presence of SNB;
- Maintaining of suitable coolant water chemistry which ensures low corrosion rates of primary circuit materials and limits cladding depositions and out-of-core radioactivity buildup.

The realization of this approach in the WWER-1000 Units at NPP Kozloduy was practically carried out through:

- The implementation of Russian fuel assemblies TVSA which:
  - Have as fuel cladding material E-110 alloy (Zr1Nb) with sufficient high corrosion resistance in the presence of SNB;
  - Use burnable absorber (Gd) integrated in the uranium-gadolinium ( $U-Gd_2O_3$ ) fuel (fuel rod with 5.0%  $Gd_2O_3$ );
- The development and implementation of water chemistry primary circuit guidelines, which require a relation between boric acid concentration and total alkalizing agent concentrations which ensures coolant  $pH_{300} = 7.0-7.2$  throughout the entire operation period.

The conditions discussed above created by the conversion of the WWER-1000 units at NPP Kozloduy to uranium fuel with 4.3% <sup>235</sup>U (TVSA fuel assemblies) practically ensured the avoidance of the creation of the conditions necessary for AOA and IRA onset.

## REFERENCES

- [1] SECKER, J., JOHANSEN, B., CASADEI, A., Long cycle and high burnup fuel experience at Westinghouse, Proceedings of the Third International Seminar WWER Fuel Performance, Modelling and Experimental Support, Pamporovo, Bulgaria, (1999).
- [2] DOBREVSKI, I., ZAHARIEVA, N., MINKOVA, K., IVANOVA, R., The concentration of the coolant <sup>7</sup>Li in Kozloduy nuclear power plant operating with potassium hydroxide as an alkalizing reagent (possible impact on the occurrence of axial offset anomaly), Power Plant Chemistry Journal, **Vol. 5** (2003) 197.
- [3] MOLCHANOV, V.L., DOLGOV, A.B., SAMOILOV, O.B., KAIDALOV, V.B., ROMANOV, A.I., LEVANOV, L.V., PETROV, I.V., AKSENOV, P.M., Results of development and operation experience of WWER1000 alternative FA, Proceedings of the 6<sup>th</sup> International Conference on WWER Fuel Performance, Modelling and Experimental Support, Albena, Bulgaria (2005).
- [4] DOBREVSKI, I., ZAHARIEVA, N., MINKOVA, K., GERCHEV, N., Behavior of antimony isotopes in the primary coolant of WWER1000type nuclear reactors in NPP Kozloduy during operation and shutdown, J, Power Plant Chem., **11** (2009) 312–319.
- [5] CHATTERTON, M.S., U.S. Nuclear Regulatory Commission, Regulatory perspectives on high burnup fuel issues and burnup extension, Proceedings of ICONE 8 — 8th International Conference on Nuclear Engineering (8232), Baltimore, MD USA, (2000).
- [6] EPRI Report TR-108320, (1997).
- [7] GARBETT, K., HENSHAW, J., SIMS, H.E., Radiolysis and nickel behaviour in PWR primary coolant, Proceedings of the Axial Offset Anomaly (AOA) Science Workshop, FRATTINI P. (Ed.), EPRI, (2000).
- [8] GARBETT, K., HENSHAW, J., Optimum primary coolant pH for high duty PWRs, EPRI Primary Water Chemistry Guidelines Meeting, Charlotte (USA), (2006).
- [9] DOBREVSKI, I., ZAHARIEVA, N., The impact of boiling on the chemical environment of heating surfaces in nuclear power plants, Power Plant Chemistry Journal (Germany), **9** (2007) 24–30.
- [10] DOBREVSKI, I., ZAHARIEVA, N., The synergic impact of the boiling of water radiolysis on the pressurized water reactor fuel cladding's environment, Proc. NPC 2010 (International Conference on Water Chemistry of Nuclear Reactor Systems), Quebec City, Canada, (2010).

## ACKNOWLEDGEMENTS

The presented text is based on the results of our (Iv. Dobrevski, N. Zaharieva) investigations carried out according to the Contract BG 13810/R, between the International Agency of Atomic Energy (IAEA) — Vienna, Austria and Institute for Nuclear Research and Nuclear Energy — Bulgarian Academy of Sciences — Sofia, Bulgaria, in the frame of the IAEA CRP “FUWAC” (Optimization of Water Chemistry Technologies and Management to Ensure Reliable Fuel Performance at High Burnup and in Ageing Plants) (2006–2009).

Here gratitude is expressed to:

- J. Killeen — Scientific Secretary of FUWAC CRP,
- The Executive Directors of NPP Kozloduy, Iv. Genov and D. Angelov, Director of Institute for Nuclear Research and Nuclear Energy, Corresponding Member of BAS, J. Stamenov for their support and encouragement in these investigations.
- Water Chemistry and Radiochemistry staff members of Unit 5, NPP Kozloduy and especially K. Minkova, P. Penev, G. Michailov, R. Ivanova, N. Gerchev for their participation and contribution to these investigations.

# **NRI POSITION IN THE WATER CHEMISTRY RESEARCH AND FUEL INSPECTION FOR CZECH WWER-1000 REACTORS**

M. MIKLOŠ, K. MEZHLUMYAN, J. KYSELA,  
Nuclear Research Institute Řež plc,  
Reactor Services Department,  
Husinec-Řež 130, 250 68 Řež

D. ERNST  
NPP Temelín, Fuel Management Department,  
373 05 Temelín

Czech Republic

## **Abstract**

Fuel failures and other fuel related issues can have significant operational impacts on nuclear power plants. Some nuclear power plants lost several millions per event to cover replacement power costs and the costs of a fuel reload due to fuel failures. Efforts to increase fuel utilization (longer cycles) and burnup are faced with real technical problems with facilities and components such as facility aging, fuel cladding corrosion, crud deposition and fuel fretting, the transport of activated crud from the active zone to other parts of the primary circuit and the subsequent need for frequent decontamination. While the industry has made substantial progress in reducing the frequency of fuel failures, continued attention to technical gaps impacting fuel reliability is needed. Since first reload, NPP Temelín, together with the fuel vendor, is performing post irradiation inspection on the fuel assemblies. However, the fuel vendor is changing and new plans for the fuel inspection are ready. The report describes past experiences with fuel inspections and repairs at the NPP Temelín and the role of Nuclear Research Institute (NRI) in the future cooperation with the new fuel vendor. In addition, NRI plays an important role in the Czech nuclear research market. The reactor services division carries out material irradiation and radioisotopes research and is involved in water chemistry research for PWR, BWR and WWER reactors and its impact on the crud deposition and fuel reliability. The main experimental loops and their utilization for water chemistry recommendations for Czech NPPs are also presented in paper.

## **1. INTRODUCTION**

In spite of the low fuel failure rates in current operation of water cooled nuclear power reactors, there is continued high interest in fuel failures for two reasons. First, problems and inconvenience caused by fuel failures in plant operation can still be significant. Second, the generally accepted goal to move towards zero failure rates as closely as possible, requires detailed knowledge of existing failure mechanisms, their root causes and remedies. Nuclear fuel continues to perform well around the world; however fuel failures still occur in all countries operating nuclear power reactors. According to the IAEA [1] the current fuel rod failure rates vary in different countries around an average between 10<sup>-5</sup> and 10<sup>-4</sup>, except in Japan where the reactors operate practically free from defects for more than ten years.

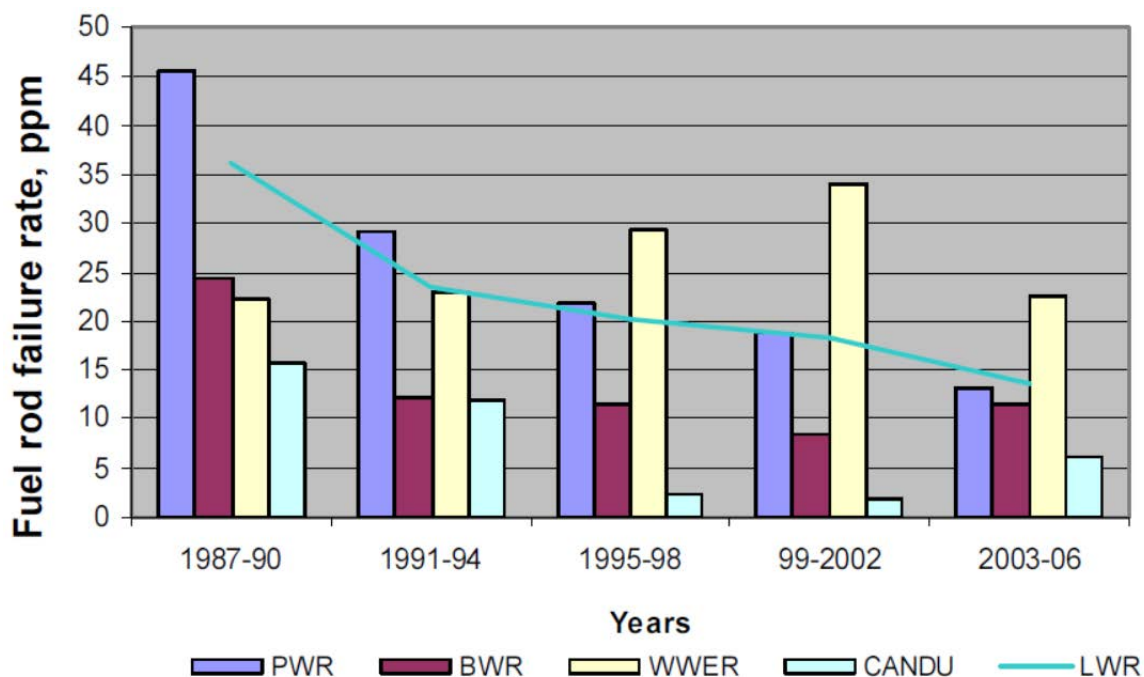


FIG. 1. Fuel failure rate according to IAEA [1].

Fuel failures and other fuel related issues can have significant operational impacts on nuclear power plants. Fuel failures, have cost some nuclear power plants several millions per event to cover replacement power costs and the costs of a fuel reload. While the industry has made substantial progress in reducing the frequency of fuel failures, continued attention to technical gaps impacting fuel reliability is needed.

## 2. FUEL FAILURES, INSPECTIONS AND REPAIRS IN CZECH REPUBLIC

The situation in Czech Republic is not digressing from the worldwide trends. Since first reload, provider of the WWER-1000 NPP Temelín (CEZ) together with the fuel vendor (Westinghouse Electric Company LCC) has performed post irradiation inspection on the fuel assemblies with the use of fuel repair inspection equipment (FRIE). There are several reasons to use of this equipment: additional proof of material compatibility, analytical method support and verification, overall thermomechanical performance demonstration, finding of a cause of an eventual fuel rod or assembly core component failure and independent check of the fuel system in-core behaviour.

Since the first cycle, the only fuel failure cause at NPP Temelín has been grid-to-rod fretting. Besides this problem, the inspection program (PIIP) was enlarged to specific and detailed inspection. In addition to fuel repair (FR), the PIIP was also aimed to study of FR failures and its causes. Tables 1 and 2 show that since first startup of Temelín NPP (cycles 1–7 for Unit 1 and cycles 1–6 for Unit 2), 62 leaking fuel assemblies at both units were found, and 26 of them were repaired and successfully reused in next cycles. Regarding incomplete rod insertion (IRI) due to strong bow and twist of the fuel assemblies, PIIP was specified, and different inspections were done to get large amount of data from the bow, twist and growth measurement. In several years many data were measured, root causes were found and many recommendations for new fuel design were applied (Fig. 2).

TABLE 1. LEAKING AND REPAIRED FUEL RODS AT UNIT 1

end of cycle	# of Leakers	# of Repaired Leakers	# of Leaked F/Rs
2	1	0	0
3	5	1	1
4	6	1	1
5	6	6	8
5A	4	2	3
6	7	7	10
7	3	1	1

TABLE 2. LEAKING AND REPAIRED FUEL RODS AT UNIT 2

End of Cycle	# of Leakers	# of Repaired Leakers	# of Leaked F/Rs
2	3	2	5
3	10	2	4
4	5	2	2
5	7	2	3
6	5	0	0

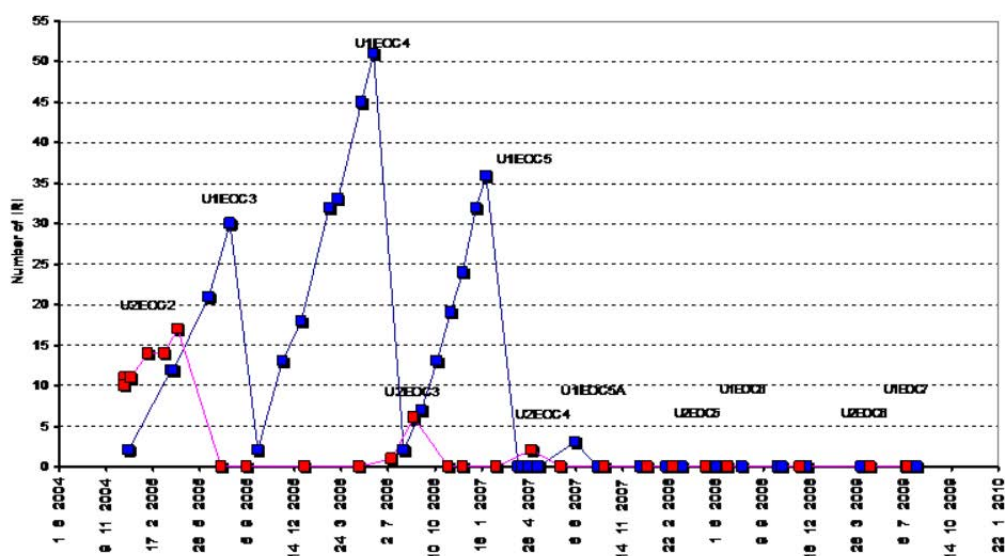


FIG. 2. Improvement in incomplete rod insertion [2].

Nuclear Research Institute plc together with NPP Temelín and Westinghouse Electric Company LLC is cooperating on the fuel inspection and repair since 2009. However, the fuel vendor is changing, and since August 2010 a new type of fuel TVSA-T from the Russian company TVEL is being used at Unit 1 NPP Temelín [3]. Since first cycle PIIP program will be implemented and NRI will participate on the fuel repair and inspection together with TVEL.

### 3. THE ROLE OF NRI IN WATER CHEMISTRY RESEARCH IN CZECH REPUBLIC

Nuclear Research Institute plc plays an important role in the Czech nuclear research market. Reactor services division besides the material irradiation and radioisotopes research is involved in the water chemistry research for PWR, BWR and WWER reactors and its impact on the crud deposition and fuel reliability. For this purpose light water research reactor LVR-15 and several experimental loops are used.

The research reactor LVR-15 is a tank type and currently uses two types of fuel manufactured by the NZCHK Company in Novosibirsk with 36% (IRT-2M) and <20% enrichment (IRT-4M). The

reactor's systems permit an output up to 10MW. The reactor's design and active zones permit the usage of various diameters of irradiation channels and thus flexibility from the standpoint of optimal neutron usage in the zone (Fig. 3).

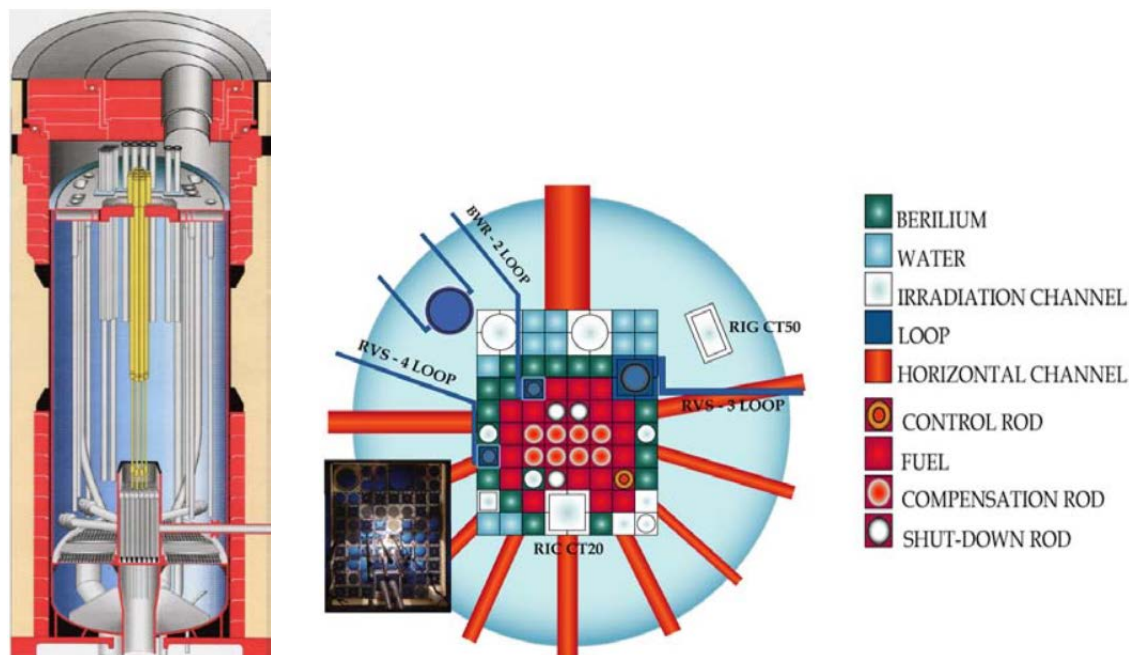


FIG. 3. Research reactor LVR-15, loops and rings.

Experimental loops are used to study the effect of environment on materials in the active zone of power reactors. Phenomena under study include corrosion, the influence of physical and radiation stresses on the rate of crack propagation, the interaction of fuel and coolant coverage, including cladding corrosion and the deposition of corrosion products on the surface of the fuel elements, further for the research of water chemistry of PWR, BWR and WWER reactors, including the development and testing of special measurement technology such as ECP measurement. All loops are equipped with high efficiency cleaning apparatus in order to achieve the high water purity which is necessary for tests. The loops thus permit flexible change of water chemistry, where direct injection of gaseous oxygen or hydrogen according to requirements.

A part of the research is oriented to the fuel clad reliability. In 2004 a two year project started between TVEL and NRI where four different types of Zr alloys (E110, E110M, E635, E635M) were tested in the experimental loop RVS-3 under conditions of the PWR water chemistry (Li=2,7-3,5 ppm, steam content up to 5 % mass) [4], see Fig. 4.

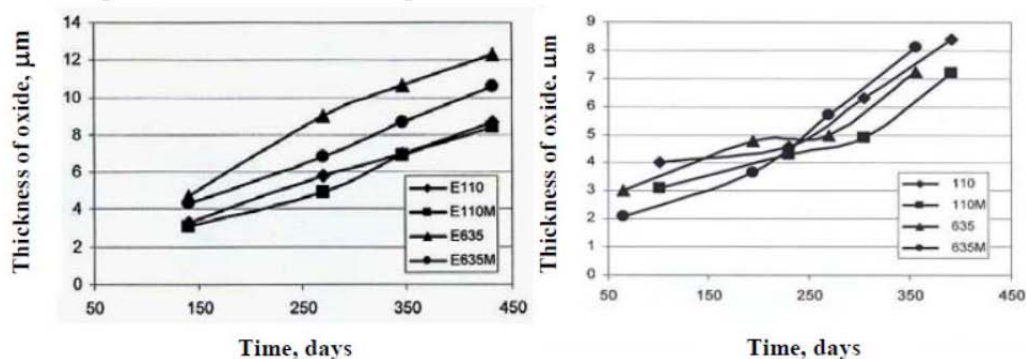


FIG. 4. Oxide thickness on the samples from (a) active and (b) inactive channel.

In present, similar experiment is preparing together with the Research Institute of Atomic Reactors (JSC SCC RIAR) in the field of the effect of different water chemistry (PWR, WWER) on

the fuel surface. The experiment is oriented to the study of the coolant chemistry influence and zinc dosing in the primary circuit on the corrosion behaviour of fuel rod's perspective zirconium alloys cladding and constructional materials of the in-vessel component in steady state and transient state modes in PWR and WWER reactors, subject to the present increasing of the plant's power, fuel burnup and longer cycles.

The LVR-15 reactor is an important facility, which serves for research into nuclear generating station materials and water chemistry. The main goal of the reactor's facilities is to model conditions that are as close as possible to real conditions, and thus secure the reproducibility and utilization of measured values. Experience that has been gained during the operation of research loops at NRI (RVS-3, RVS-4, zinc loop) is now used as the foundation of the water chemistry guidelines for Czech NPPs [5].

#### 4. CONCLUSIONS

Problems with fuel failures at NPP Temelín were introduced. All above mentioned problems are today under the control and all problems were solved together with the fuel vendor, mostly due to FA design changes. Nevertheless, with the change of fuel vendor new experiences in fuel operation and fuel post irradiation inspection in Czech Republic arrives.

Division of Reactor Services in Nuclear Research Institute plc and its focus in water chemistry and cladding reliability is introduced in the paper. Experience that has been gained during the past years at NRI is now used as water chemistry guidelines base ground for Czech NPPs. Together with the experiences from fuel inspection equipment at Temelín NPP; NRI has perfect tools for studying and improving of WWER water chemistry regimes.

#### REFERENCES

- [1] INTERNATIONAL ATOMIC ENERGY AGENCY Review of Fuel Failures in Water Cooled Reactors, IAEA Nuclear Energy Series Report NF-T-2.1 (2010).
- [2] HLAVINKA, V., International cooperation in development and supply of nuclear fuel for Czech NPPs. International Forum «ATOMEXPO 2009» Expocentre, Moscow, Russian Federation, (2009).
- [3] MOLCHANOV, V. Nuclear fuel for WWER reactors, actual state and trends. 8<sup>th</sup> WWER Fuel Performance, Modelling and Experimental Support, Helena Resort, Bulgaria. Bulgarian Academy of Science, (2009), 43–55.
- [4] MIKLOŠ, M.; et al. Research loops for the water chemistry, corrosion and crud depositing after deco. 8<sup>th</sup> WWER Fuel Performance, Modelling and Experimental Support, Helena Resort, Bulgaria, Bulgarian Academy of Science, (2009), 433–438.
- [5] MARKELOV, V.A., et al.: Corrosion behaviour of E110 and E635 type zirconium alloys under pwr irradiation simulating conditions. Water Reactor Fuel Performance Meeting, Seoul, Korean Republic, (2008), Paper No. 8023.



# ZINC ADDITION AND ITS CHALLENGE IN CHINESE NPP

Shi XIUQIANG, Zhu JUN,  
Shanghai Nuclear Engineering Research and Design Institute,  
SNPTC, Shanghai

Xu XUELIAN  
Shanghai Key Laboratory of Nuclear Engineering,  
200233, Shanghai

China

## Abstract

For primary water stress corrosion cracking mitigation and plant dose rates reduction, soluble zinc acetate will be added to reactor coolant in some new Chinese nuclear power plants in the next several years. In the nuclear power plant with zinc addition to reactor coolant, the effects of zinc on fuel cladding corrosion, fuel with sub-cooled nucleate boiling and corrosion product transport must be taken into account, and zinc implementation risk must be assessed. In order to deal with the challenge caused by zinc addition, some research, such as effect of zinc concentration on primary water stress corrosion cracking in reactor coolant system materials and analysis of corrosion product ion in reactor coolant, are being performed in China. Additionally, a zinc implementation risk assessment procedure will be developed for nuclear power plants. In the paper, the background and benefit/challenge of zinc addition are briefly described, and the work in hand for zinc addition is also summarized.

## 1. BACKGROUND

In order to mitigate primary water stress corrosion cracking (PWSCC) and reduce the general corrosion of primary system material thereby reducing plant dose rates, zinc addition to reactor coolant has been used since 1994 in United States Nuclear Power Plants (NPP). Now the technology is adopted in about 40 NPPs [1].

With the increasing need for energy, some NPPs are being constructed and some NPPs will be constructed in China. For the purposes of plant dose rates control and PWSCC mitigation, zinc addition will be used in some new NPPs in the next several years. In these NPPs, except for the benefits, the effect of zinc on materials and fuel must be taken into account.

## 2. MECHANISM

Due to exposure to reactor coolant at high temperature, duplex oxide film develops on the nickel base alloy and austenitic stainless steel material. The outer layer is active nickel/iron enriched layer, and the inner layer is passive chromium enriched layer. When zinc ions are in reactor coolant, zinc ions enter preferred lattice locations in the chromium enriched layer and other divalent cations are displaced and released into reactor coolant. The zinc-conditioned oxide film is more protective [2].

### 3. CHALLENGES

Although some benefits can be gained from zinc addition, the effects caused by zinc addition must be understood before its implementation. Until now, no NPP in mainland of China has zinc addition experience. In view of structural material and fuel, the challenges facing us occur at least in the following aspects:

- Reactor coolant system materials compatibility;
- Fuel material and performance;
- Reactor coolant system water chemistry monitoring.

It has been proven that zinc addition has beneficial effects on reactor coolant system materials, such as austenitic stainless steels and nickel base alloys. Zinc ions enter into the existing reactor coolant system materials oxide films and form more protective oxide film, which not only reduce general corrosion but also mitigate PWSCC [1]. About the research on PWSCC, tests were mainly focused on Alloy 600 material. Alloy 690 is widely used as steam generator tube material in Chinese NPPs. In the aspect of PWSCC mitigation with zinc addition, although Alloy 690 is believed having the same behaviour as Alloy 600, the data on Alloy 690 material PWSCC crack initiation and crack propagation are still lacking. The knowledge gap will affect the evaluation of steam generator tube.

The challenge on fuel is from fuel cladding integrity and fuel performance. As the primary barrier against the release of fission products, fuel cladding must maintain its integrity. In the zinc addition condition, it is important to understand the effect of zinc on zirconium alloy corrosion. For example, can zinc affect oxide on fuel cladding and can zinc enhance hydrogen pickup by fuel cladding? Besides corrosion, crud and crud induced power shift (CIPS) are issues. More corrosion product release into reactor coolant in the beginning period of zinc addition, and zinc enriched corrosion product deposits are more tenacious. This kind of zinc enriched corrosion product deposit creates a concern that it could lead to CIPS in PWR NPPs, because boron ( $^{10}\text{B}$ ) from reactor coolant concentrate within the deposit and cause neutron flux depression [1].

With zinc being added into reactor coolant system, zinc is preferentially incorporated into existing oxide film by displacing nickel, cobalt from the film, then nickel and cobalt dissolve into reactor coolant, so reactor coolant chemistry become more complex. According to experience in the NPPs with zinc addition, the nickel concentration in reactor coolant plays an important role in the assessment of CIPS risk. It is the third challenge. Due to no zinc addition in NPP in China, nickel in reactor coolant is not monitored now. Analysing such a low nickel concentration (ppb) in water is an issue, and a method must be found to carry out this analysis.

### 4. MEASURES

In order to understand zinc addition technology better, research has been and will be done in China. The finished autoclave test results show that carbon steel, austenitic stainless steel and nickel base alloy general corrosion rates in high temperature water with zinc ion are smaller. SSRT tests will be used for research on the effect of zinc on PWSCC. Crack initiation statistics and crack propagation measurement of Alloy 690 material will be performed in simulated reactor coolant with different zinc concentration.

For fuel impact assessment, after zinc addition application, a zinc implementation risk assessment procedure will be developed for NPP. Fuel cladding oxide measurement and corrosion product deposit scraping and analysis will be included. About the CIPS evaluation, some parameters will be collected and software will be used to calculate crud deposition and boron concentrated in crud.

## 5. SUMMARY

For some new Chinese NPPs, zinc addition will be used for plant dose rates reduction and primary water stress corrosion cracking mitigation in the beginning of operation. Due to no experience, research on corrosion has been and will be performed to understand the reactor coolant system materials compatibility with zinc environment. In the future, zinc implementation risk assessment procedure, including fuel cladding integrity and fuel performance, will be developed for these NPPs.

## REFERENCES

- [1] Pressurized water reactor primary water zinc application guidelines, 1013420, EPRI, December (2006).
- [2] BYERS, Zinc and CRUD, how they interact, EPRI Fuel Reliability Program WG1Meeting, (2005).



# **PRIMARY WATER CHEMISTRY CONTROL AT UNITS OF PAKS NUCLEAR POWER PLANT**

J. SCHUNK, G. PATEK T. PINTÉR, P. TILKY, Á. DOMA  
Paks Nuclear Power Plant Co. Ltd.  
Paks

J. ÖSZ  
Budapest University of Technology and Economics,  
Budapest

Hungary

## **Abstract**

The primary water chemistry of the four identical units of Paks Nuclear Power Plant has been developed based on Western type PWR units, taking into consideration some Russian modifications. The political changes in the 1990s have also influenced the water chemistry specifications and directions. At PWR units the transition operational modes have been developed while in case of WWER units – in lack of central uniform regulation – this question has become the competence and responsibility of each individual plant. This problem has resulted in separate water chemistry developments with a considerable time delay. The need for lifetime extensions worldwide has made the development of startup and shutdown chemistry procedures extremely important, since they considerably influence the long term and safe operation of plants. The uniformly structured limit value system, the principles applied for the system development, and the logic schemes for actions to be taken are discussed in the paper, both for normal operation and transition modes.

## **1. INTRODUCTION**

Numbers of steam generator decontamination were carried out prior to feed-water collector replacement for three out of the four WWER-440 type units of Paks Nuclear Power Plant. The internal surface of the steam generator heat exchanger tubes had not been sufficiently passivated after the decontamination, which caused the release of excess corrosion products into the main coolant loop.

The deposited corrosion products had reduced the flow cross section within the fuel rod bundles and, as a consequence, increased the hydraulic resistance of the fuel assemblies. Decision was made to remove the deposit from the fuel assemblies with the use of a chemical cleaning method. During these cleaning operations carried out in a separate tank, 30 fuel assemblies have been seriously damaged as a consequence of insufficient cooling due to a design error of the cleaning tank.

To minimize the rate of deposit on different primary surfaces, a new water regime was developed for the startup/shutdown operation conditions, for which we have a two-year operational experience now. This was especially important from units lifetime extension point of view. The water regime parameters used for normal operation conditions have also been revised and international experts were requested for expert opinion on the established modifications. The introduction of the modifications is in progress now.

The corrosion status of the primary surfaces greatly depends on the primary water regime applied for power operation mode, but a thorough knowledge of the water regime used in shutdown/startup conditions and during maintenance, and the effects of the maintenance work, is of similar importance.

## **2. REPLACEMENT OF THE STEAM GENERATOR FEEDWATER COLLECTOR AND THE EFFECTS OF THIS ACTION**

The WWER-440 type units at Paks Nuclear Power Plant have been constructed with six horizontal steam generators. The feedwater collectors of the steam generators are made of carbon

steel. Initially, the nozzles of the feed-water collectors were damaged by erosion, and, as the time has passed, the material of the collector itself has even heavily damaged.

The wearing was of such an extent that the old collectors had to be replaced with new ones of austenite steel material and a new design. The replacement included some work to be performed within the secondary side of the steam generators. To reduce the dose rate in the work place, the steam generators had been decontaminated at Units 1 to 3. This was followed by the feedwater collection replacement and the restart of the units.

After the restart, increased differential pressure, associated with reduced primary coolant mass flow was detected in the active core. The increase of the  $\Delta P$  and the development of the primary coolant flow rate during campaign 20 of Unit 1 are presented in Fig. 1.

The capacity of the unit was reduced to 96% as a response to the decrease in the primary flow rate. For one of the units, the coolant flow rate and the Unit power had reduced suddenly after a shutdown under accident conditions. All in all, it was stated that power reduction occurred in a different degree for all the units 1 to 3, which had been decontaminated. No decontamination work was performed for Unit 4 prior to the replacement of the feed-water collectors and the dose rate reduction was provided with the use of radiation protection procedures. Accordingly, no flow rate reduction was detected in the primary circuit of Unit 4.

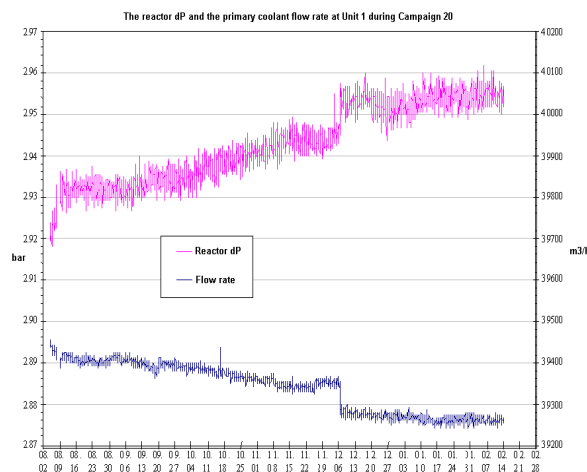


FIG. 1. Primary coolant flow rate ( $m^3/h$ ) and differential pressure (bar).

A working group was set up to address the problem. It was stated that the reason for the differential pressure increase was the presence of corrosion products at the inlet nozzle of the fuel assemblies. It was also concluded that the origin of this excess corrosion product was the structural components of the steam generator that had been insufficiently passivated after decontamination.

A cleaning procedure, to be carried out in an external tank, was developed for the removal of this deposit from the fuel assemblies. A tank designed for the accommodation of seven fuel assemblies was constructed for this work. One hundred and seventy fuel assemblies removed before from the reactor and decayed in the decay pool were successfully cleaned in this cleaning tank.

Due to their large number, the cleaning of the other fuel assemblies was scheduled for a date directly after shutting down of each unit for maintenance outage. The possibility of cleaning the fuel assemblies within the reactor was also studied but, finally, the cleaning outside the reactor was selected. A cleaning tank designed for the accommodation of 30 fuel assemblies was designed and constructed for this work. The cleaning operations commenced during the maintenance outage of Unit 2. Corrosion products equivalent to 1 to 2 kg iron was removed during the cleaning cycles, which included 30 fuel assemblies, which equals to 20–60 g iron from each fuel assembly. Initially, the cleaning process went smoothly, but after the completion of cycle six, initially it was not possible to

open the lid of the tank. Due to an error in the design of the cleaning tank, a steam cushion had developed in the tank, and, when the tank was finally opened, the fuel assemblies were damaged due to the cold boric acid streaming into the tank. Following the completion of long lasting preparatory work after the occurrence of the incident, the damaged fuel assemblies, and finally the cleaning tank too, were removed from pit 1 of Unit 2.

### 3. MINIMIZING THE DEPOSITION IN THE PRIMARY LOOP

The water regime used during the past 20–25 years operation of the Units was evaluated and the required corrective actions were identified as part of the work carried out for the service life extension, with due consideration of the power upgrading to 108% [1, 2].

#### 3.1. The purpose and the function of the primary water regime

The primary water regime has several purposes and functions that can be summarized in the following list:

- To provide compensation for the reactivity margin by continuous reduction of boric acid concentration and for the control/controllability of the reactor power (with follower assemblies);
- To ensure that the overall corrosion of the structural materials of the equipment is minimum;
- To minimize the risk of local corrosion of the structural materials;
- To minimize the deposit of corrosion products on the structural components and the fuel cladding;
- To keep the transport rate of corrosion products in the coolant and their deposition on the surfaces at a low level;
- To confine the rate of radiolytic decomposition in the primary coolant.

#### 3.2. Analysis of the water regime currently applied for the Paks units

##### 3.2.1. The work to be done

Three fundamental issues were answered by the complex and topical analysis:

- Is there anything to prevent the life time extension of WWER-440 Units of Paks Nuclear Power Plant from water regime point of view?
- To what extent the primary water regime of Paks Nuclear Power Plant complied with the design requirements and the knowledge level deriving from the recent technological developments?
- How was the corrosion degradation of the main primary equipment and to what extent were the main primary equipment degraded by the applied water regime?

##### 3.2.2. Statements

It was possible to keep the impurity concentration of the primary coolant as low as achievable from process system point of view.

The periodic increase in the quantity of the disperse corrosion products can be attributed to the extensive steam generator chemical decontamination work performed at Units 1–3.

Altogether two cases of fuel leakage were detected for the 79 campaigns involved. The total iodine concentration was higher than  $3.7 \text{ MBq/dm}^3$ , but never exceeded the Unit shutdown criteria of  $37 \text{ MBq/dm}^3$ .

The average corrosion loss for the equipment made from 08H10N10T type stainless steel was  $0.3\text{--}0.35 \text{ }\mu\text{m/year}$ , i.e.  $15\text{--}17.5 \text{ }\mu\text{m}$  during 50 years, which does not prevent the lifetime extension.

### 3.3. Recommendation for the implementation of the lifetime extension

The sampling line (TV20) upstream the water cleanup system No.1 does not provide a representative sample of the corrosion products during transition operational conditions, like startup and shutdown. Therefore, the installation of a new sampling line is necessary. On the basis of the inspection, acceptable samples can be taken from the operational boric acid measurement line, which obtains sample directly from the reactor vessel.

For the on-line measurement of the most important chemical parameters it is necessary to improve the reliability and to ensure the full scope use of the primary circuit continuous analytical monitoring system (FAM). The validation of FAM commenced and the results will be used to identify the measuring systems that can be used further on, and those that will need to be replaced.

The development of a water regime for transitional (startup and shutdown) conditions is a task with highlighted importance for the life time extension [3]. The startup and shutdown processes significantly affect and decisively identify the water regime parameters of the Unit for the whole campaign/cycle therefore, it is necessary to apply the filtration of the primary coolant in general at low (40–50 °C) temperature during these operation modes, in addition to the more frequent checking of some important chemical parameters. The improvement of the practice of feeding the chemicals (hydrazine, ammonium-hydroxide, potassium-hydroxide) to the coolant will also be initiated.

Physical and/or chemical procedures may need to be developed for the removal of the corrosion products accumulated during the long term operation in the primary circuit, which will be applied as required.

The reduction of the primary coolant hydrogen concentration from the originally specified range of 30–60 Nml/dm<sup>3</sup> to 25–50 Nml/dm<sup>3</sup> is also required to reduce the pH fluctuation range indirectly, through the ammonia dosage.

It is recommended that the simultaneous addition of ammonia and hydrazine, rather than the sole use of hydrazine be considered for the water chemistry regime of one or two units.

The reduction of the equivalent boric acid-potassium control range has a positive effect on the migration/transport/removal of corrosion products, being unavoidably present in the primary loops.

The difference between the presently used so called coordinated water regime and the proposed overall boric acid alkalization control is presented in the Figs 2, 3 and 4, 5 respectively. The reduction of the control range of the potassium equivalent (overall alkalization = potassium + lithium + sodium) and its breakdown between the boron acid concentrations of 3 and 3.5 g/kg and again below 1 g/kg is well marked in Fig. 4. The result of these changes can be studied by a comparison of the Figs 3 and 5. It is visible in Fig. 3, that the difference between the corrosion product concentrations calculated for the reactor vessel ( $C_R$ ) and those for the steam generators ( $C_{SG}$ ) has a negative value for a significant portion of the campaign. Consequently, the precipitation of the corrosion products will take place mostly in the active core, and will turn to the steam generators at the end of the campaign only.

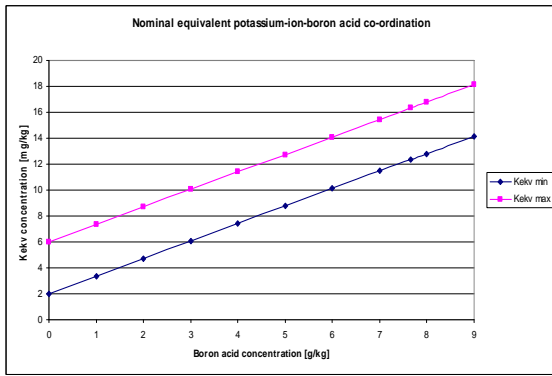


FIG. 2. The presently used alkalization control.

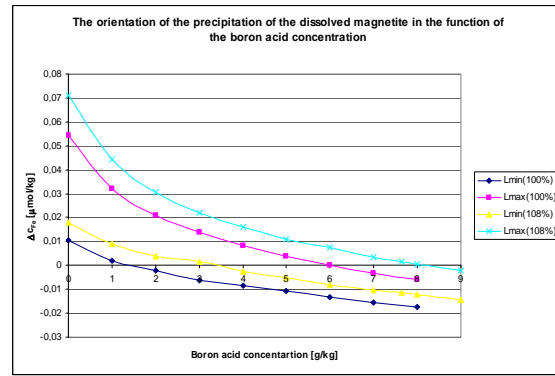


FIG. 3. The presently used  $C_R-C_{SG}$ .

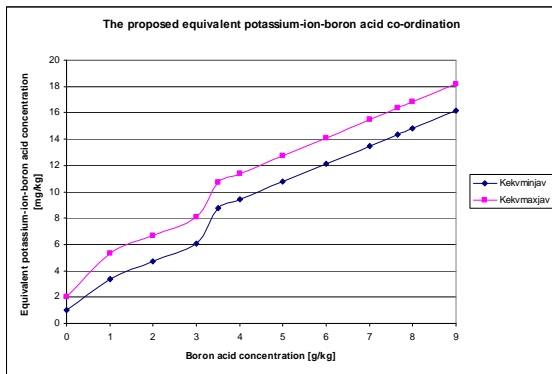


FIG. 4. The proposed alkalization control.

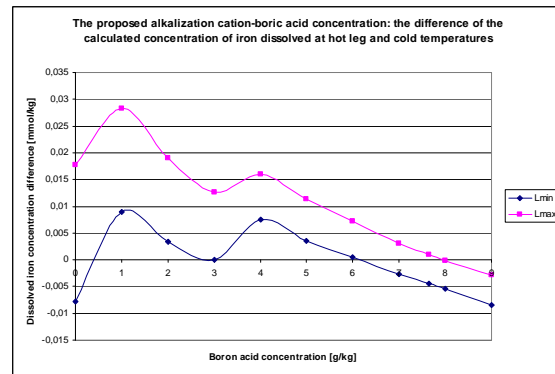


FIG. 5. The proposed  $C_R-C_{SG}$ .

This imposes unnecessary load to the active core and has an increasing effect on the radiation doses during maintenance outage.

It can be achieved by the implementation of the proposed modification as presented in Fig. 5 that the precipitation of the corrosion products takes place in the steam generators from the beginning of the campaign and it turns to the active core at the end of the campaign only. With this solution it is expected that the active core can be maintained in rather clean condition during steady operation and the portion of the corrosion products that precipitated in the active core can be removed every year by fuel unloading during refuelling outage. The re-orientation of the transport before maintenance outage will have a favourable effect on the radiation doses received during maintenance outage.

To achieve the aim outlined above, the overall alkali concentration should be kept (from the start of the cycle up to the time of achieving a concentration of 3.5 g/kg) in the upper part of the control range presented in Fig. 4. After this point, it should be changed to the lower part of the range and below 0.5 g/kg boron acid concentration further reduction of alkalization is required. The changeover of precipitation from the steam generators to the active core takes place during this period of some 500 hours.

#### 4. CONCLUSIONS

The newly introduced water regime successfully fulfills the requirements and complies with the preliminary expectations.

There is nothing to prevent the lifetime extension of the units of Paks Nuclear Power Plant from a water chemistry regime point of view.

The amount of deposits accumulating on the primary surfaces (and the subsequent dose rate during maintenance work) can be reduced to the minimum with the adaptation of the suggested,

appropriate water chemistry. This statement is based on detailed calculation, modeling and evaluation of corrosion product transport processes in the primary coolant system [3].

#### **REFERENCES**

- [1] LG Energia Kft, Comprehensive and thematic analysis of the water regime used at Paks Nuclear Power Plant during the period between 1983 and 2004 (2005).
- [2] LG Energia Kft, Review of the primary and secondary water regime used at A Paks Nuclear Power Plant for power upgrading (2005).
- [3] LG Energia Kft, Development of water regime for the primary and secondary system with consideration of the service life extension. Development of water regime for startup and shutdown conditions (2006).

# FUEL ASSEMBLY INSPECTIONS PERFORMED DURING THE REFUELLING OUTAGE OF PAKS NUCLEAR POWER PLANT UNIT 4

T. PINTÉR, P. NÉMETH, Á. MENYHÁRT, I. BURÁNSZKY, J. SCHUNK, G. PATEK  
Paks Nuclear Power Plant Co. Ltd.  
P.O.Box: 71, Paks,  
Hungary

## Abstract

Based on the trend of the measured radioactivity concentration in the primary coolant during the 22nd cycle of Unit 4 it was found probable that there were 1–2 failed fuels in the reactor core. Because of the value of caesium activity concentration and presence of strontium and barium isotopes in the coolant it could be predicted that it was a fresh failure and there was a direct contact between the fuel pellet and the coolant. This theory was supported by the spiking effects of iodine and caesium isotopes. The telescopic sipping method for the successful identification of failed fuel are presented in the paper. Values for the sure identification are discussed. The comparison between the estimation from the measured data during the 22nd cycle and that of the real failed fuel are also discussed. The proper identification of the failed fuel is verified by the activity level trend after startup of Unit 4. A slight contamination with fissile nuclides has been determined by activity concentration of iodine isotopes in the coolant. The exemption from failed fuel in the reactor core has been proven by a slightly increased but stable activity level in the coolant.

## 1. INTRODUCTION

Shortly after the restart of Unit 4 in 2008 a strong iodine activity increase was experienced. The value of  $^{131}\text{I}$  activity exceeded the value belonging to the first action level of the Technical Operational Rules (MÜSZ), and the total iodine activity approximated the first action level relating to it, Fig. 1. This level remained high for several days without rising any further. During the course of the campaign after a slow decrease it stabilized, but at a higher value than during earlier campaigns or than the values of other units. The increase and the nature of the activity assumed the presence of a leaking fuel assembly. The size of the activity did not justify the immediate shutdown of the unit, but a decision has been made to find the leaking fuel assembly during the main repair of the unit in 2009.

Fig. 1 shows that the total iodine activity concentration meaning the sum of the five iodine isotopes ( $^{131}\text{I}$ – $^{135}\text{I}$ ) only approximated to that of the total iodine action level 1, while, for a short time,  $^{131}\text{I}$  activity concentration exceeded, by a little, the  $^{131}\text{I}$  action level 1.

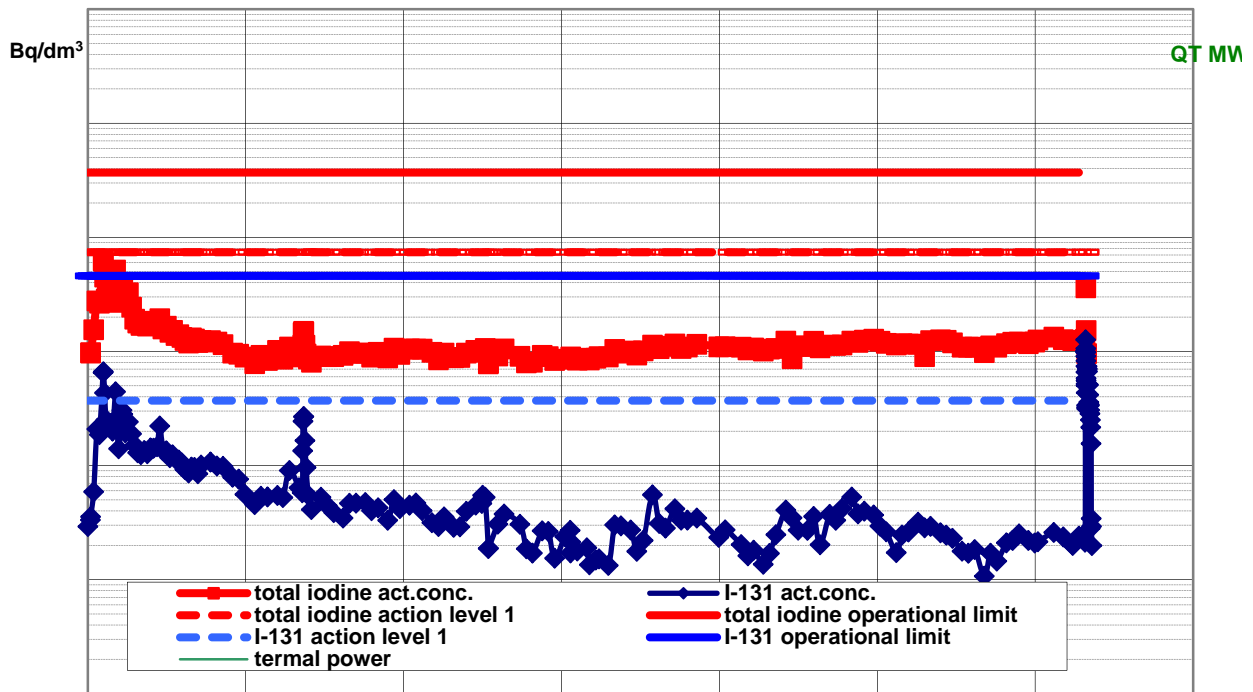


FIG. 1. The activity change of the iodine isotopes indicating the leakage of the fuel assembly during the 22<sup>nd</sup> campaign of Unit 4.

In spite of the fact that during the campaign the activity values did not reach the technical operational rules (MÜSZ) limit levels, the decision remained to select the leaking fuel assembly. Based on the preliminary calculations, it was likely that one of the one year old fuel rods was leaking, possibly being in a control rod. The nature of the defect indicated a macro fault, i.e. there was direct contact between the water and the fuel pastille.

349 fuel assemblies can be found within the active zone of the reactor; of which 312 are working fuel assemblies and 37 are fuel assemblies with control rods. One fuel assembly contains 126 fuel rods, which means approximately 44000 fuel rods. One rod became leaking and the task was to find that one. Because of one leaking rod an entire fuel assembly had to be removed from the core.

Spiking which occurred during the outage of the unit confirmed the presence of the leaking fuel assembly. Fig. 2 shows well the spiking peak occurring due to the download and depressurization effects.

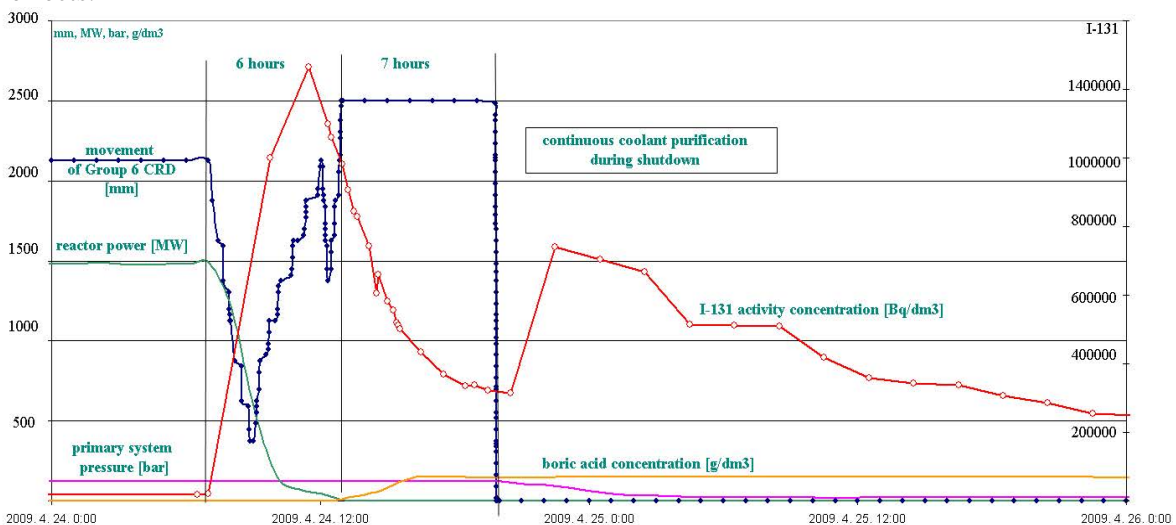


FIG. 2. <sup>131</sup>I spiking data measured at the outage of 22nd campaign of Unit 4.

## 2. SIPPING INVESTIGATION PREPARATIONS

A newly procured H&B telescope sipping equipment had been tested successfully in the resting pool of Unit 2, and we wanted to use this to achieve the selection of the leaking fuel assembly during the refuelling of Unit 4. The advantage of the telescope sipping equipment compared to our other available inspection equipment is that during normal refuelling operations, the fuel inspection can be performed only extending it up to a bearable extent. In order to use the sipping machine it was necessary to make several modifications to the refuelling machine and some of its equipment. All of these were done with the permission of the relevant authority.

The most important modification was that to the refuelling machine's fuel gripper during which we had to ensure that the water which had soaked through the fuel assembly was able to get into the inspection apparatus. Further, not insignificant alterations were those modifications to the software of the refuelling machine, the creation of a hose tensioning device which allows safe movement, and the power supply of the same safety as the refuelling machine.

The necessary alterations and permissions had been prepared prior to the outage for the maintenance of Unit 4, and based on the appropriate cartogram the inspection and refuelling of the zone could start.

## 3. SIPPING INSPECTION RESULT

After the outage of Unit 4, sipping inspections were performed on each fuel assembly. In the course of the inspection, the fuel assemblies were lifted one by one by the refuelling machine. The inert gas activity retrieved in the gas separator from the water which had soaked through the assembly was continuously registered with a scintillation detector. After sampling the composition of the water which had soaked through the assembly, was analysed in the laboratory. We took sample once a day from the ATM for laboratory analysis to track the inspection background.

The sipping program started on 2 May 2009. Apart from minor issues which have no influence on the reliability of the sipping results, the refuelling and the sipping inspection passed off undisturbed.

During the course of the implementation tests the sipping background was recorded. Where the detector was located, the gamma background was approximately 3 cps, which equalled the value found during the measurements made on Unit 2 in November 2008. The value of the first measured sipping background — using the sipping water from the reactor — was in the range of 4000 cps.

Through the sipping inspection we started to detect signal (at this point the sipping protocol had been started), when the fuel gripper was connected to the fuel. Afterwards, the refuelling machine lifted the fuel assembly to a height of 500 mm below the transportation height. Following the measurement, the fuel assembly was lifted to transportation height and was moved to the next position according to the cartogram. There, it was put down, and after coming to rest in its place, the fuel gripper was released. The refuelling machine was moved to the next position, where the procedure was started from the beginning again.

The sipping inspection protocol was stopped directly before grabbing the next fuel assembly for the purpose of sipping inspection.

For the sipping signal the warning and alarm threshold values were set as multiples of the background calculation speed (1.5 fold background = warning, 3 fold background = alarm). The background calculation speed was continuously monitored by the managing personnel of the sipping and in case of a background change it was reset.

Until the start of the inspection of the control rods no sipping signal indicating a leaking fuel assembly was detected. Continuing the inspections on 9 May 2009 the operator of the sipping

observed a strong sipping signal increase. At a several thousand fold signal increase the sipping measurements were stopped, after taking the water sample, in order to avoid the contamination of the detector and the equipment. Based on the signal, the 6th control rod in the 3<sup>rd</sup> group was leaking (in the 351st step). At the sipping apparatus the maximum signal size was 132600 cps, while at the same time being below 100 cps background signal number. The leakage of the fuel assembly was verified by the laboratory result of the water sample.

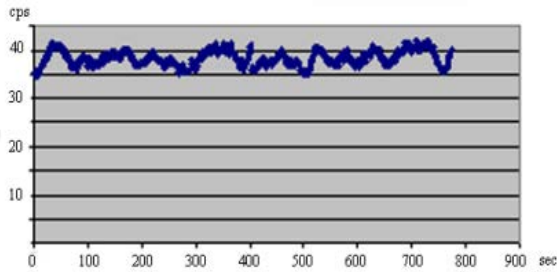


FIG. 3. The sipping signal of the measurement before the leaking fuel assembly.

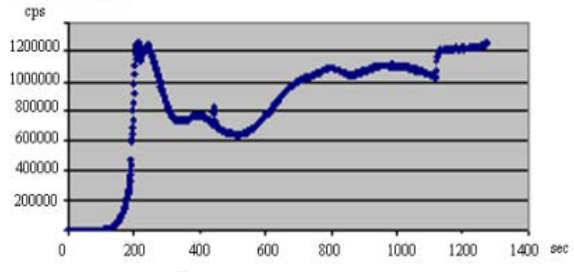


FIG. 4. The sipping signal of the leaking fuel assembly.

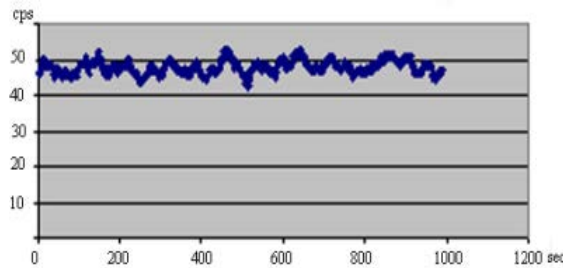


FIG. 5. The sipping signal of the measurement after the leaking fuel assembly.

Figures 3, 4 and 5 show the trace of the sipping signal of the leaking fuel assembly and the fuel assemblies measured before and after the leaking fuel assemblies. The fuel assembly verified as leaking was removed from the zone.

During the further steps of the refuelling and the sipping inspection a suspicious fuel assembly was found, the signal size of which did not exceed the three times background mark, therefore it was not considered to be leaking and it was left in the reactor for further operation.

#### 4. CONCLUSIONS

In the 22<sup>nd</sup> campaign of Unit 4 the selection of the leaking fuel assembly — probably production faulty — which caused significant activity increase, was carried out successfully with the telescope sipping equipment. The assessment made from the data measured during the campaign shows a good match with the data related to the leaking fuel assembly found.

The correctness of the selection of the leaking fuel assembly causing an activity increase in the 22<sup>nd</sup> campaign is verified by the activity trend of the restart campaign. Based on the activity data of the iodine isotopes it can be seen that the zone is slightly contaminated with fissionable nuclides. This causes the higher activity values.

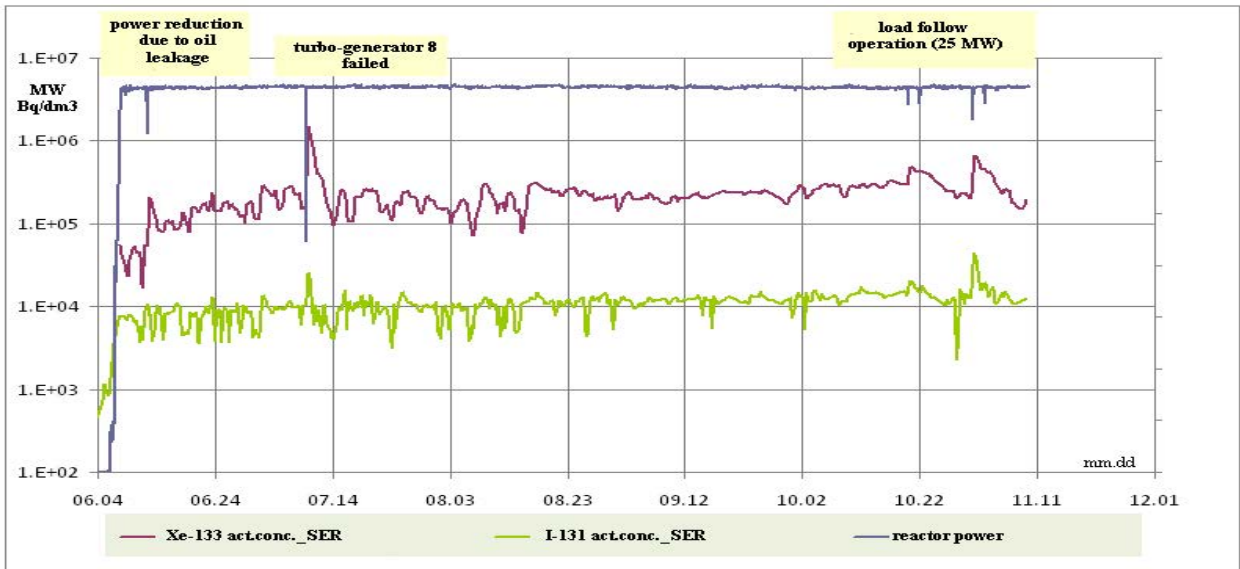


FIG. 6. <sup>131</sup>I and <sup>133</sup>Xe activity concentrations measured at the restart of Unit 4.

Figure 6 shows that when changing the power, a minor activity transient occurs. This is probably caused by the “presumably leaking” fuel assembly which stayed in. With regard to this fuel assembly, it became apparent that due to this highly accurate and sensitive measuring equipment, such leakage can be detected, which was not possible earlier. This requires further thinking of the fuel management, as there is a need to have some basis upon which a decision can be made about the tight status and what should we do with the fuel assemblies deemed to be leaking. For this reason further inspections and analyses are needed.



# **COMPREHENSIVE STUDY OF URANIUM AND TRANSURANIUM (PU, CM) ACCUMULATION ON STAINLESS STEEL AND ZR+NB CLADDING MATERIAL SURFACES**

K. VARGA, P. KÁDÁR, B. BAJA, Z. NÉMETH  
Institute of Radiochemistry and Radioecology, University of Pannonia  
Veszprém

T. KRISTÓF  
Institute of Chemistry, Department of Physical Chemistry, University of Pannonia  
Veszprém

N. VAJDA  
RadAnal Ltd.,  
Budapest

Zs. STEFÁNKA, Z. SCHAY  
Institute of Isotopes, Hungarian Academy of Science,  
Budapest

T. PINTÉR, J. SCHUNK  
Paks NPP Ltd. Paks

Hungary

## **Abstract**

Within the frame of a joint project, accumulation of the uranium and transuranium (TRU) species on construction materials (such as stainless steel and Zr+Nb cladding material) has been studied. The sorption studies were carried out in a static model system, in boric acid coolants provided by the Paks NPP. Solution and samples obtained in the course of below experiments were analysed by independent ( $\alpha$ -spectrometry, ICP-MS, SEM-EDX, voltammetry) methods. The experimental results reveal that the solution concentration of uranium and TRU nuclides in each experiment decreases significantly within a relatively short period of time, giving a direct evidence of the fast sorption kinetics. It should however be noted that the mechanistic features of the contamination processes are decisively dependent upon the very nature of radionuclides studied and the chemical structure and composition of the surface oxide layer formed on stainless steel.

## **1. INTRODUCTION**

As a result of the breakdown on 10 April 2003 there was a significant contamination by uranium and transuranium (Pu, Am, Cm) nuclides in some technological units (such as reactor pit No.1, fuel transfer pond) of the reactor block 2 of the Paks Nuclear Power Plant (PNPP). It was of special importance to know the contamination processes (adsorption-desorption) of uranium and transuranium (TRU) nuclides during the release of the damaged fuel assemblies. In the reactor pit No.1 uranium and TRU nuclides can be present in different chemical forms (molecular, colloidal and/or disperse) in the boric acid coolant. A reliable evaluation of the extent and kinetic of the above contamination phenomena on the constructional materials used in the fuel transfer pond seemed to be fundamental to perform the safe removal of the damaged fuel started at October 2006. However, there were only limited pieces of information about the extent, chemical forms and kinetic behaviours of the uranium and transuranium species accumulated on the surface of the main structural materials [1].

## 2. EXPERIMENTAL

The static experiments of the accumulation processes on the surfaces of the stainless steel canister material and Zr+Nb cladding material were carried out in boric acid coolants provided by the Paks NPP in the model systems detailed below (see Fig 1.).

The accumulation of uranium and TRU species was studied by the so-called “electrode” radioactive tracer method [2]. The “electrode” method is a direct and sensible radioactive tracer technique. Main characteristics of the studied samples as well as of the sorption experiments are summarized in Table 1. During the sorption experiments in different time periods sample surfaces were taken for analysis, the surface activity of uranium and TRU (Pu, Am, Cm) nuclides in the solution samples were detected by alpha spectrometry and or ICP-MS method. In addition at the sorption experiments of the Zr+Nb alloys, speciation studies of solution samples were carried out to analyse the chemical form of uranium and TRU (Pu, Am, Cm) nuclides. In addition surface analysis was performed of the original and treated samples with voltammetric and SEM-EDX methods.

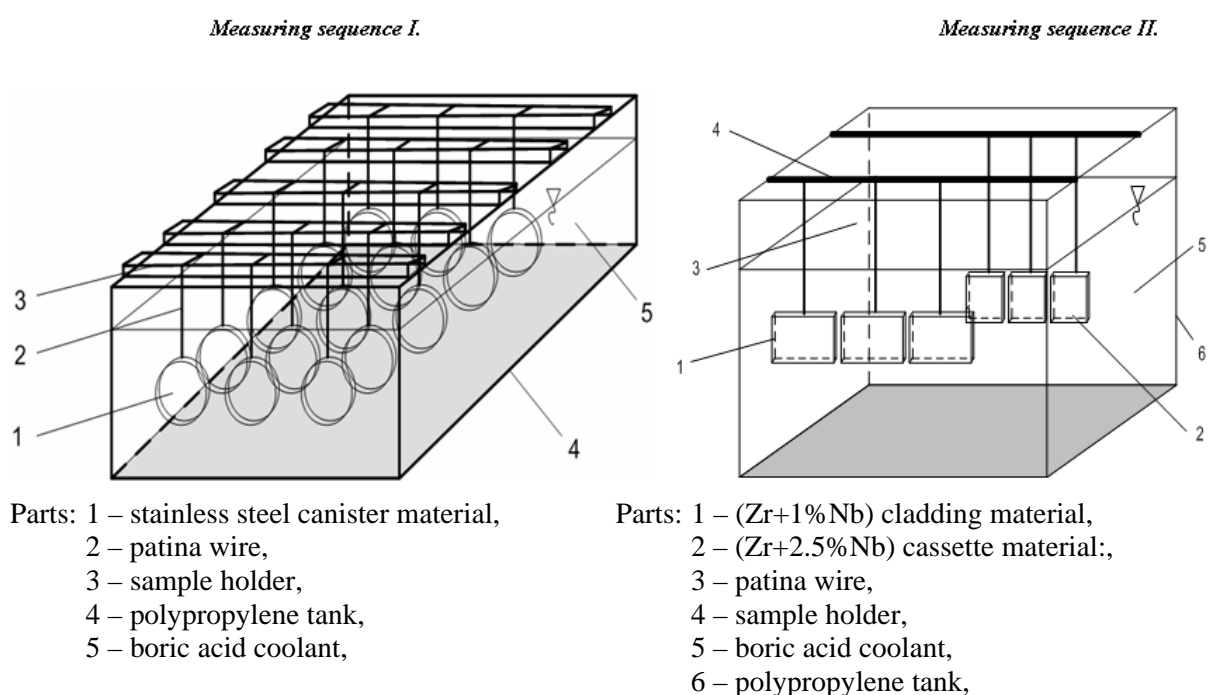


FIG. 1. Illustrative images of the static model systems used in measuring sequence I–II.

TABLE 1. MAIN CHARACTERISTICS OF SORPTION EXPERIMENTS.

Measuring sequence	Experimental parameters				
	Composition of solution	Solution pH	Studied surface	Temperature	Sampling time / h
I.	boric acid coolant ( $c = 27.7 \text{ g} \cdot \text{dm}^3$ )	3.5	stainless steel can material (12x18H10T GOSZT): 2 cm diameter	RT	1, 5, 15, 30, 60
II.	boric acid coolant ( $c = 17.0 \text{ g} \cdot \text{dm}^3$ )	4.2	Zr+1%Nb cladding material: 3.5x3 cm Zr+2.5%Nb cassette material: 1x1 cm	RT	5, 10, 24, 120, 1440

### 3. RESULTS AND DISCUSSION

Prior to the detailed description of the sorption characteristics of stainless steel and Zr+Nb alloy surfaces, it is worth mentioning that the general corrosion state, morphology and chemical composition of the samples have been comprehensively studied. In this section, only some SEM-EDX and voltammetric results characterizing the surface of stainless steel and Zr+Nb alloy samples are presented (see Figs. 2–3, respectively). The experimental data shown in Fig. 1 reveal that the oxide-layer grown on the surfaces of stainless steel canister material used in the present work is thin (the thickness is less than 0.1  $\mu\text{m}$ ) and no significant enrichment of Cr can be detected next to the surface. In the case of the Zr+Nb alloy samples experimental data shown that the (Zr+1%Nb) cladding material has a smooth surface in contrast to the (Zr+2.5%Nb) cassette material which surfaces is more rough, the metallographic cross section of the Zr+Nb alloy samples shows, that both surfaces are covered with a thin  $\text{ZrO}_2$  layer, the thickness of which is less than 1  $\mu\text{m}$ . Furthermore, no significant change in the morphology and chemical composition of surface oxide-layers can be observed after the sorption experiment (see treated surfaces in Fig. 2). The surfaces of each sample have a passive character in a wide potential interval next to the corrosion potential (see Fig. 3). As demonstrated in Fig. 3, the average corrosion rates for these surfaces in boric acid solution are very low ( $v_c \leq 0.8 \mu\text{m}/\text{year}$ ). Moreover, the polarization measurements performed on three different specimens before and after the sorption experiments reveal that the treatment of the surfaces in boric acid coolant does not exert significant influences on the  $E_c$  and  $v_c$  values.

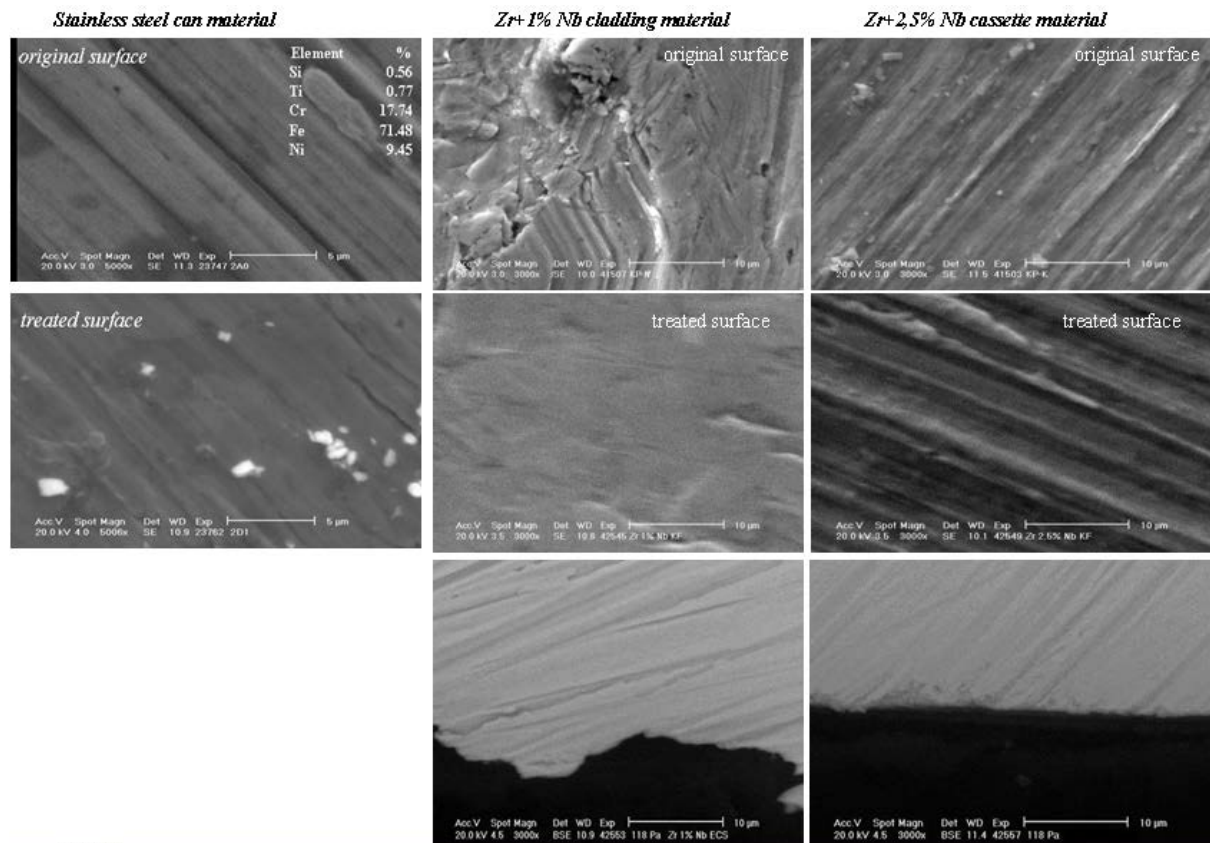


FIG. 2. Some illustrative SEM micrographs and images of the metallographic cross section (at the bottom) of the stainless steel can material and Zr+Nb alloys, representing morphology of surface oxide-layer right before and after the adsorption experiments.

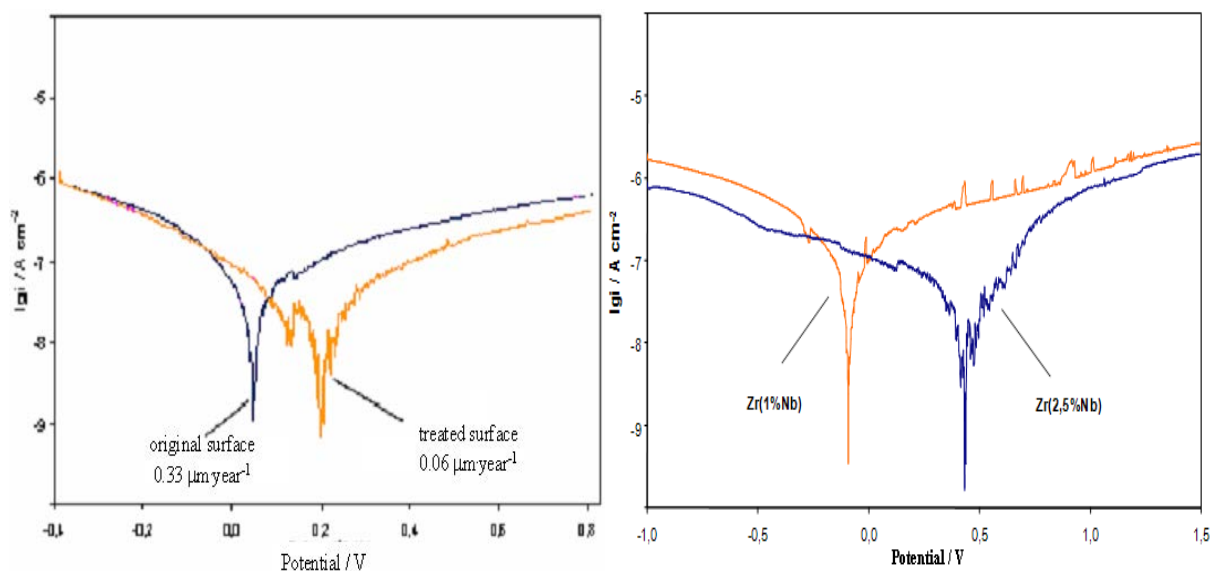


FIG. 3. Potentiostatic polarization curves measured at the stainless steel can material (left) and Zr+Nb alloy (right) studied in boric acid solution ( $c = 12 \text{ g}\cdot\text{dm}^{-3}$ ). Scan rate:  $10 \text{ mV}\cdot\text{min}^{-1}$ . Curves were recorded under identical experimental conditions.

In light of the above considerations, the results of the sorption studies in sequence I. are as follows, the time dependence curves of the accumulation of alpha emitter radionuclides evaluated from the alpha spectrometric measurements of the surface as well as of uranium accumulation evaluated from the ICP-MS studies are presented in Figs. 4–5, respectively:

- The surface concentration of uranium and TRU nuclides in the experiment increases significantly within a relatively short period of time (~15 hour), giving a direct evidence of the fast sorption kinetics.
- The time dependence curves of the sorption of alpha emitter radionuclides exhibit maximum character. In the case of Pu, Am and Cm isotopes the previously mentioned phenomena above can be interpreted with the significant exhaustion of the solution. At the same time the anomaly of the uranium accumulation can be correlated to corrosion and solution chemistry (dissolution of corrosion products, co precipitation).

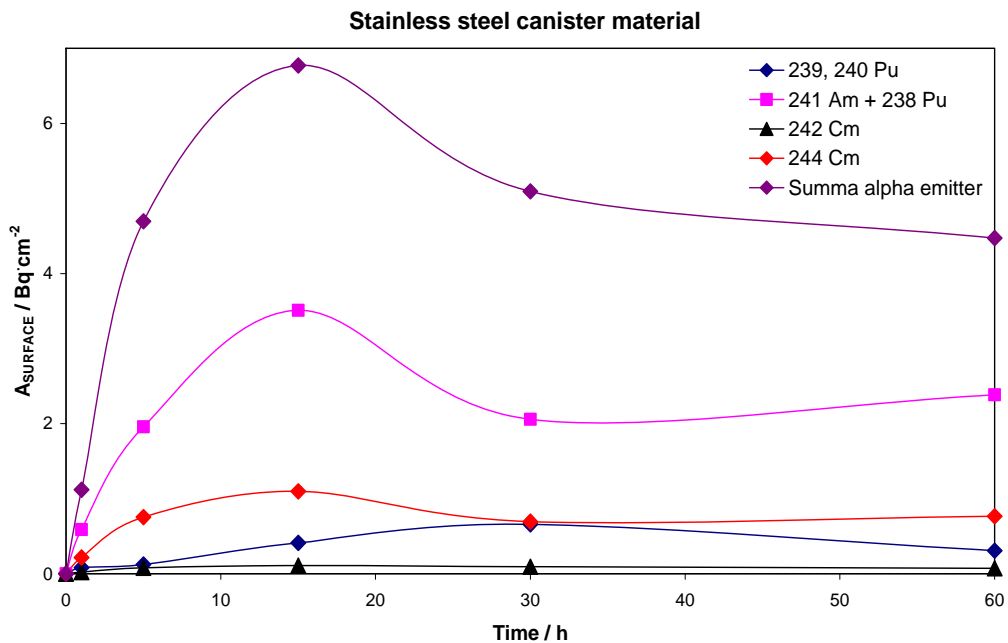


FIG. 4. The time dependence of surface activity of alpha emitter radionuclides on a stainless steel canister material surface.

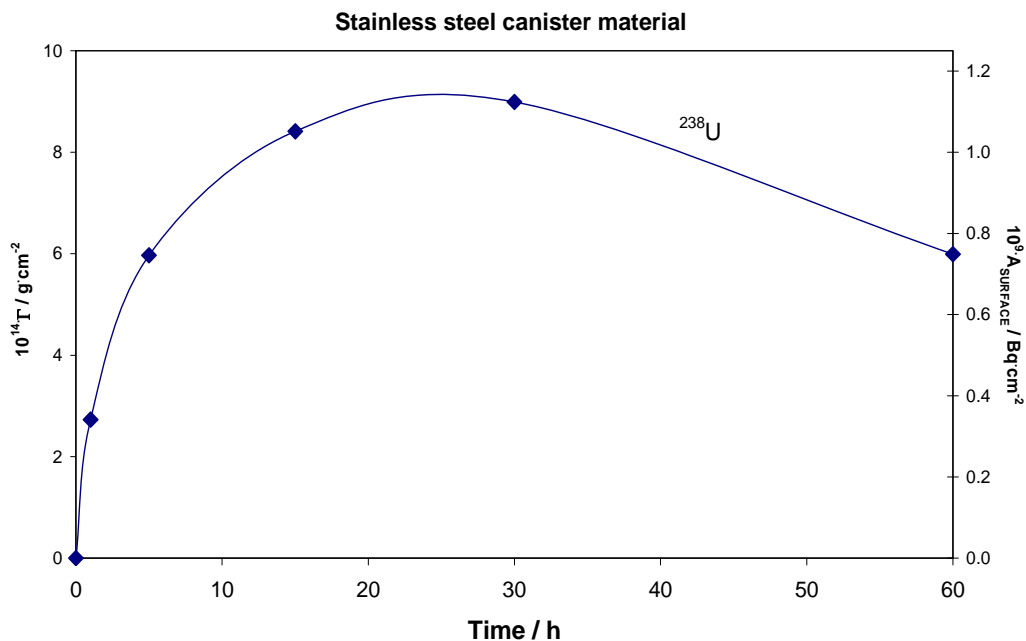


FIG. 5. The time dependence of surface activity ( $A_{SURFACE}$ ), as well as surface excess ( $\Gamma$ ) of  $^{238}\text{U}$  on a stainless steel canister material surface.

The results of the sorption studies in sequence II are as follows, the time dependence curves of the accumulation of plutonium and curium evaluated from the alpha spectrometric measurements of the surface and solution as well as of uranium accumulation evaluated from the ICP-MS studies are presented in Figs. 6–8, respectively. In addition, relative fractions obtained by the speciation studies of

solution samples after various adsorption periods are compiled in Figs. 6. (a)–8. (a). The experimental results shown in Figs. 6–8 reveal that:

- The surface concentration of plutonium and curium isotopes are extremely low ( $\Gamma \leq 2 \cdot 10^{-11} \text{ g} \cdot \text{cm}^{-2}$ ;  $A_F \leq 76 \text{ mBq} \cdot \text{cm}^{-2}$ ) on a Zr+Nb alloy surface, and the sorption kinetics is slow. The calculated surface excess of the mentioned radionuclides is under the 0.01% of the monolayer coverage. The speciation results show that the chemical form of the radionuclides fluctuates continuously during the experiment, and the sorbed species are mostly accumulated on the Zr+2.5%Nb cassette material surface.
- The extent of uranium accumulation is much higher than the above mentioned radionuclides ( $\Gamma = 0.5 \text{ } \mu\text{g} \cdot \text{cm}^{-2} \text{ U} \approx 1.8 \cdot 10^{-9} \text{ mol} \cdot \text{cm}^{-2} \text{ UO}_2$ ), after 1440 hours exceeds to monolayer coverage. When comparing the charge of uranium species with the surface charge of the Zr+Nb alloy adsorbent, the extent and character of the uranium accumulation can be estimated (see Fig. 6.). Namely,  $\text{pH}=4.2$  is smaller than  $pzc$  (i.e. pH value of the zero surface charge). Consequently, the Zr+Nb alloy surface is positively charged, and the accumulation of cations (as dominant fraction of uranium) cannot primarily be considered. In the notice of the previous findings the accumulation of uranium can be considered as deposition of colloidal particles on both Zr+Nb alloy surfaces.
- The corrosion of Zr+Nb alloy surfaces and the dissolution of surface contaminants (Fe) may have significant effects on the extent and nature of contamination. In the current case, the surface analyses (SEM-EDX) and voltammetry shows the passive character of the Zr+Nb alloy surface.

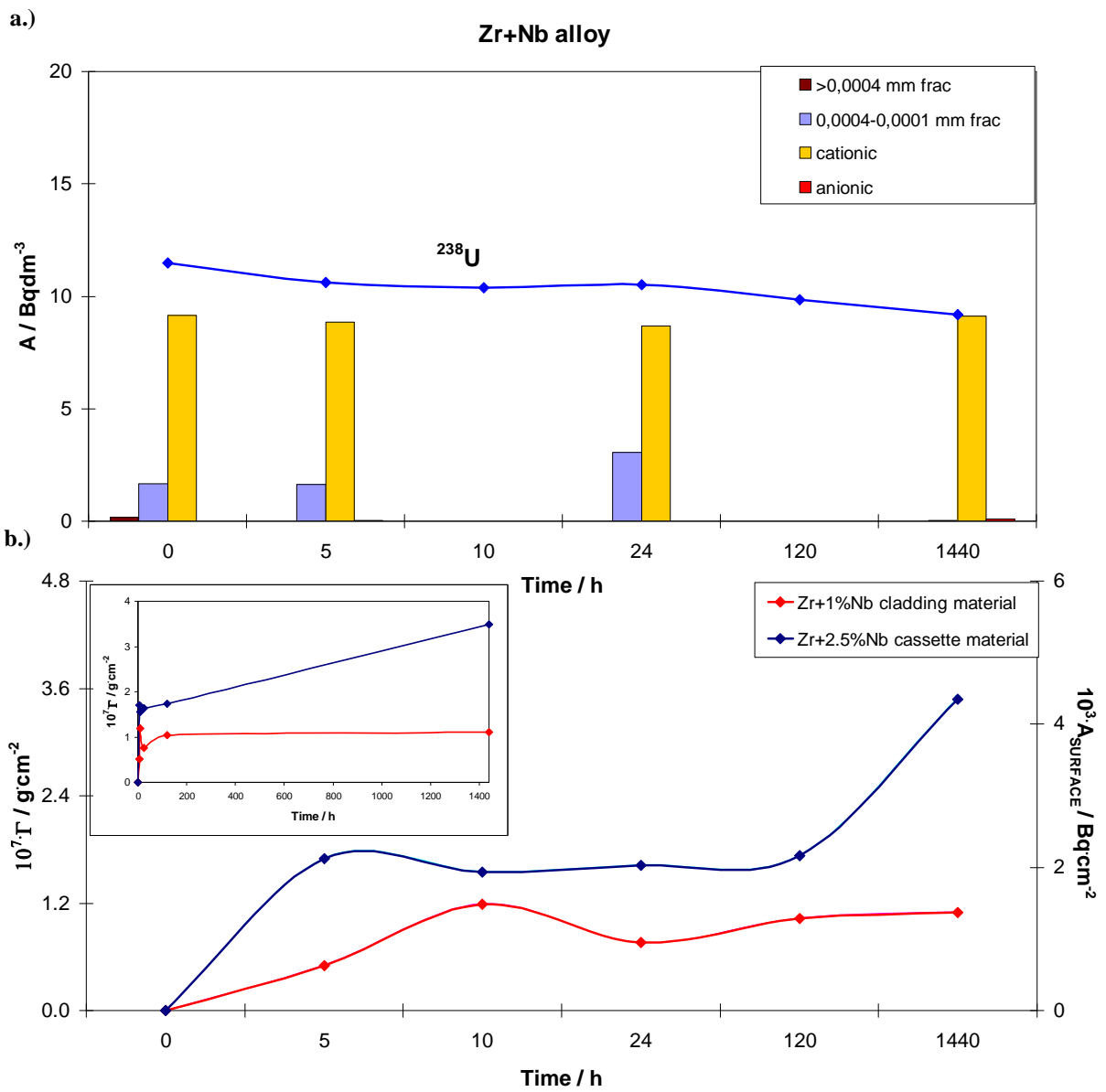


FIG. 6. The solution activity concentration of (a)  $^{238}\text{U}$  and (b) surface excess ( $\Gamma$ ) and surface activity ( $A_{\text{SURFACE}}$ ) vs. time on stainless steel canister material surfaces. The histogram in (.) also shows results of speciation studies after various adsorption periods.

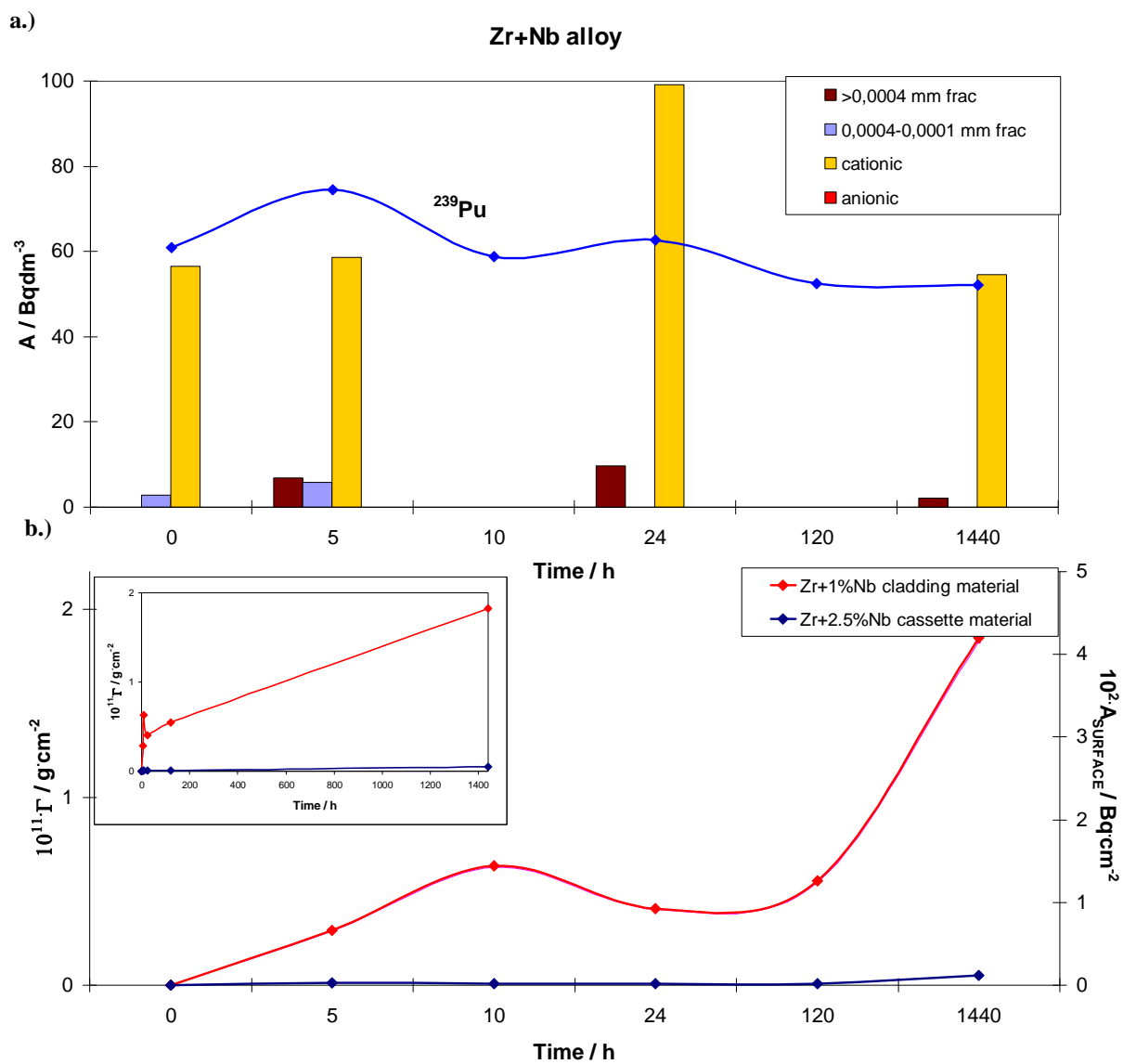
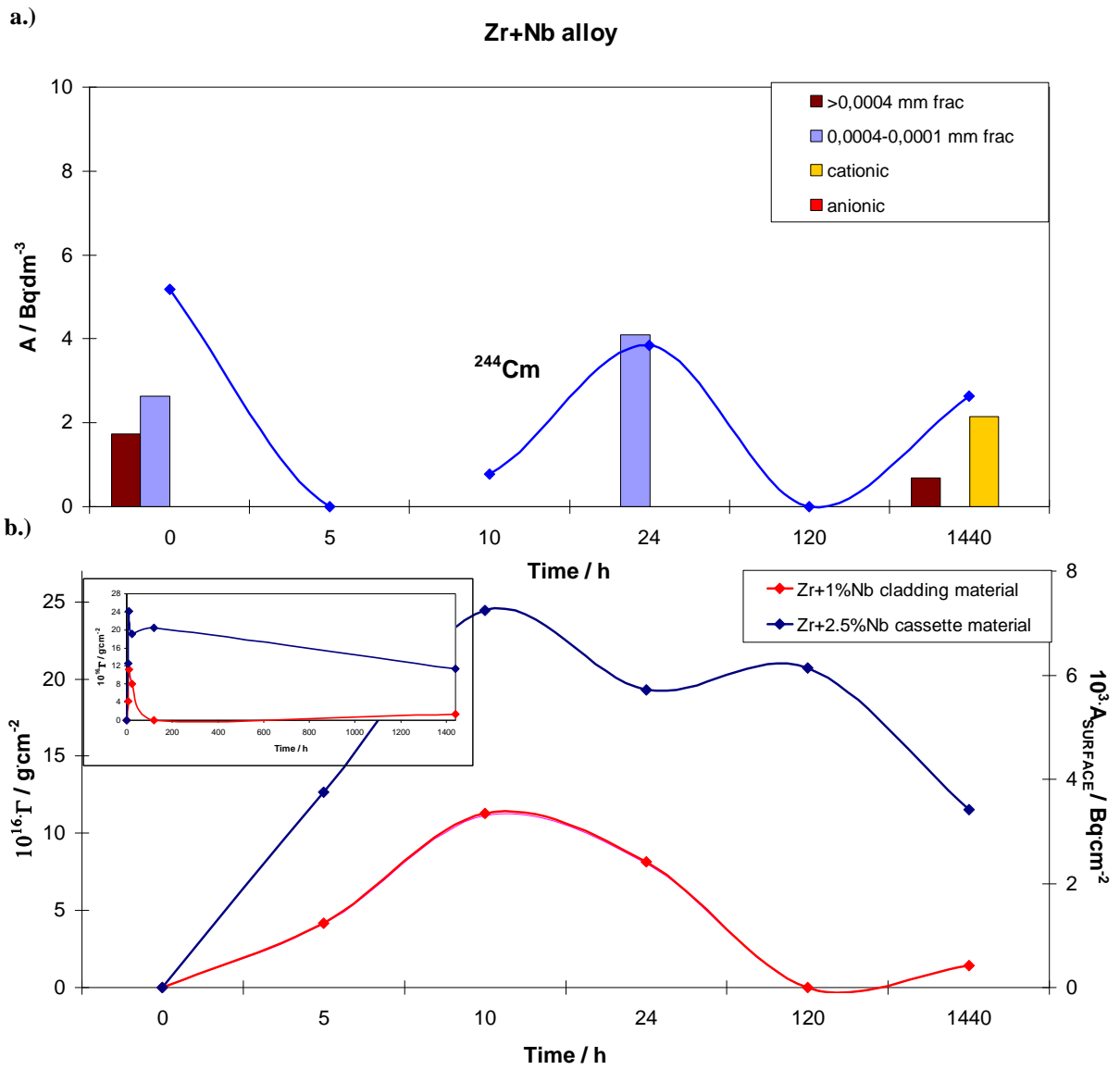


FIG. 7. Time dependence of solution activity concentration of (a)  $^{239}\text{Pu}$  and (b) surface excess ( $\Gamma$ ) and surface activity ( $A_{\text{SURFACE}}$ ) on stainless steel canister material surfaces. The histogram on (a) shows the results of speciation studies after various adsorption periods.



#### 4. CONCLUSIONS

In this paper, we have presented and discussed some experimental findings on the time dependences of uranium and TRU accumulations obtained in a static laboratory model system using stainless steel canister material and Zr+Nb alloy samples provided by the Paks NPP.

The alpha spectrometric, voltammetric, SEM-EDX and ICP-MS studies clearly demonstrate that the extent and the kinetics of uranium and TRU accumulations are primarily influenced by the:

- pH of the boric acid solution, and the chemical concentration of the radionuclides;
- Corrosion state of the surfaces and dissolution of surface contaminants.

#### ACKNOWLEDGEMENTS

This work was supported by the Paks NPP Co. Ltd.

#### REFERENCES

- [1] KÁDÁR, P., VARGA, K., NÉMETH, Z., VAJDA, N., PINTÉR, T., SCHUNK, J.J., Radioanal. Nucl. Chem. **284** (2010) 303–318.
- [2] VARGA, K., The role of interfacial phenomena in the contamination and decontamination of nuclear reactor”, In: Radiotracer Studies of Interfaces HORÁNYI G. (Ed.) Interface Science and Technology, Elsevier B.V., Amsterdam, Vol. 3 (2004).

# COMPARATIVE STUDY OF THE CORROSION AND SURFACE ANALYTICAL EFFECTS OF THE DECONTAMINATION TECHNOLOGIES

K. VARGA, B. BAJA, E. H. DEÁK, K. RADÓ, Z. NÉMETH  
Institute of Radiochemistry and Radioecology, University of Pannonia  
Veszprém

G. PATEK, J. SCHUNK  
Paks NPP Ltd.,  
Paks

A.N. SZABÓ  
Department of Physics and Chemistry, University of István Széchenyi  
Győr

Hungary

## Abstract

Decontamination technologies are generally developed to reduce the collective dose of the maintenance and operation personnel at nuclear power plants (NPP). The highest efficiency (i.e. the highest decontamination factors) available without detrimental modification of the treated surface of structural material is the most important goal in the course of the application of a decontamination technology. At the Paks NPP the AP-CITROX procedure has been utilized for the decontamination of the primary coolant circuit's components (e.g. main circulating pump (MCP) and steam generators (SGs)). Our previous studies have revealed that a "hybrid" structure of the amorphous and crystalline phases was formed in the outermost surface region of the austenitic stainless steel tubes of SGs as an undesired consequence of the industrial application of the AP-CITROX decontamination technology during the period of 1993–2001. In the paper, we report some comparative findings on the corrosion and surface chemical effects of the AP-CITROX procedure and the novel decontamination technology elaborated at our institution. On optimizing the operational parameters the latter technology may become suitable for the effective decontamination of both dismountable (e.g. MCP swivel) and separable (e.g. SGs) equipment. For this purpose experiments were performed. In this laboratory scale experiments, the passivity, morphology and chemical compositions of the treated surfaces of tube specimens were investigated by voltammetry, and SEM-EDX methods, respectively. The SEM-EDX results have revealed that the oxide removal is surprisingly uniform even after two or three consecutive cycles. The electrochemical studies have provided evidence that no unfavourable tendencies in the general corrosion state of the tube samples can be detected in the course of the chemical treatments.

## 1. INTRODUCTION

In some Soviet made WWER-type pressurized water reactors different versions of the so-called AP-CITROX method (AP: alkaline permanganate; CITROX: citric and oxalic acid) have been widely used for the chemical decontamination of the austenitic stainless steel piping of steam generators (SGs) [1–3]. This technology has mainly been utilized for the decontamination of the primary coolant circuit's components (e.g. main circulating pump (MCP) and steam generators (SGs) at the Paks NPP (Hungary). During the time period of 1993–2001 chemical decontamination of 24 SGs in the reactor blocks 1–3 of the Paks NPP were carried out by a non-regenerative version of APCITROX technology, sometimes in two or three consecutive cycles.

Our previous studies have revealed that a hybrid structure of the amorphous and crystalline phases is formed in the outermost surface region of the austenitic stainless steel tubes as an undesired consequence of the industrial application of the AP-CITROX technology [3–6]. The formation of this mobile oxide-layer significantly increased the amount of the corrosion products in the primary circuit, resulting in magnetite deposition on fuel assemblies. As deposits blocked the cooling channels, the flow rate of water coolant through the reactor core decreased. Consequently, the power capacity of three nuclear reactor units had to be reduced, and full core fuel replacement became necessary.

In the light of the above events, the analysis of this data and the comprehensive study of the corrosion effects of the technology reveal that fundamental issues of analytical chemistry, corrosion science and chemical engineering were not taken into consideration during the elaboration of the AP-CITROX procedure, suggested in steam generator manual, and utilized at Paks NPP. Therefore, the non-regenerative version of the AP-CITROX technology is not an adequate method for the chemical decontamination of any reactor equipment having large steel surfaces (e.g. SGs). As a consequence of the lack of the appropriate decontamination method, an R&D project focused on the elaboration of the required technology was initiated in 2005.

In this work, we present a brief overview on the fundamental issues of the R&D project focused on the elaboration of the required technologies. Based on the results of some recent laboratory studies we summarize the main corrosion and surface analytical effects of the AP-CITROX procedure and the novel decontamination technology including an oxidizing pre-treatment of the surface with acid permanganate followed by washing with oxalic acid developed at our institution.

## 2. EXPERIMENTAL

### 2.1. Preparation of the steel samples

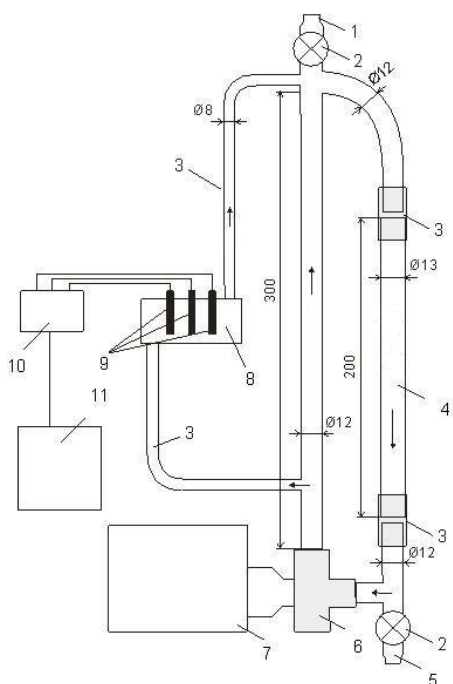
The experiments have been performed on austenitic stainless steel specimens (type: 08X18H10T (GOST 563261) which correspond to AISI 321 and DIN 1.4541; outer diameter: 16 mm, average wall thickness: 1.6 mm) originating from different SGs of the Paks NPP. With no steel sample cut from MCP materials, all experiments were carried out using SGs tube specimens. The austenitic stainless steel heat exchanger tubes were investigated before and after chemical treatments. The tube specimens studied can be classified into two groups: (1) samples that have never been decontaminated at Paks NPP; and (2) samples decontaminated by AP-CITROX procedure at Paks NPP.

On modelling the decontamination method for separable equipment (SGs decontamination), tube samples of 200 mm were cut, while in case of dismantlable devices (MCP decontamination) specimens of 26 mm were used. After chemical treatment specimens of 20 mm were cut from the tube samples for voltammetric and SEM-EDX studies. The tube pieces were cut into two halves along their axes and then — for the voltammetry — flattened gently. In order to protect the oxide layer on the specimens from possible chemical effect of organic solvents, the surfaces were not degreased. The corrosion properties of the stainless steel samples prepared by the above technique were studied mainly on their original inner surfaces which had been in contact with the primary coolant. In addition, the metallographic cross sections of tube specimens were prepared and analysed by SEM-EDX method.

### 2.2. Laboratory model systems

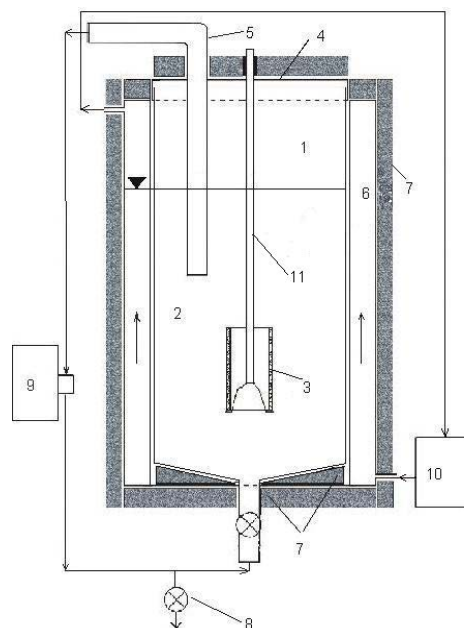
Two different model systems were developed for the laboratory study of the decontamination techniques (Fig. 1). While the applied temperature at SGs decontamination was 30°C, temperature applied for MCP decontamination was 90°C. The SGs model system consists of two parts. The main circulation part is made of PVC elements. The tube sample is mounted into the system with two silicone tubes. PH electrode, temperature sensor, conductivity electrode were placed in a secondary circle. Volume of decontamination solution to treated surface area ratio was  $2.4 \text{ cm}^3 \cdot \text{cm}^{-2}$ . The applied flow rate was  $1.5 \text{ m} \cdot \text{s}^{-1}$ , maintained by a centrifugal pump.

The decontamination of dismantlable devices was carried out in big tanks at Paks NPP. Therefore, a laboratory decontamination tank with a volume of  $500 \text{ cm}^3$  was used for laboratory modeling (see Fig 1.). The temperature during the experiments was controlled by a thermostat. The tubes sample was located in the middle of the tank. The material sample holder was prepared from austenitic stainless steel (type: 08X18H10T (GOST 5632-61). Volume of decontamination solution to treated surface area ratio was  $15 \text{ cm}^3 \cdot \text{cm}^{-2}$ . Decontamination solution was exchanged twice every hour by making use of a peristaltic pump.



Laboratory system for SGs decontamination

1. deaerator stud
2. bullet valve
3. silicon tubes
4. examined tube sample
5. filling up/draining stud
6. centrifugal pump (Cole-Parmer type U75225-15)
7. pump drive (electric motor)
8. measuring cell
9. electrodes (pH, conductivity, temperature sensor)
10. measuring instrument (Consort C861)
11. PC



Laboratory system for MCP decontamination

1. decontamination tank
2. decontamination solution
3. examined tube sample
4. cover
5. siphon
6. thermostat casing
7. insulating layer
8. filling up/draining stud
9. peristaltic pump
10. thermostat
11. sample holder

FIG. 1. Laboratory systems developed for chemical decontaminations.

### 2.3. Investigation of the corrosion state of tube specimens by voltammetry

The passivity of the tube samples was studied by potentiostatic polarization method. The experiments were carried out by the means of a VoltaLab 40 (RADIOMETER) type electrochemical measuring system controlled by PC. In the course of potentiostatic polarization experiments the potential ( $E$ ) of the specimen (working electrode) was continuously shifted towards anodic direction at a constant rate of  $10 \text{ mV} \cdot \text{min}^{-1}$  and the current density ( $i$ ) related to the inner surface area of the specimen was recorded. The measurements were carried out in boric acid model solution of the primary coolant ( $c=12 \text{ g} \cdot \text{dm}^{-3}$ ) in argon gas atmosphere (99.999 v/v % Ar). The schematic of the measuring system, the detailed experimental procedure and the determination of the corrosion parameters (such as corrosion potential ( $E_c$ ), corrosion current density ( $i_c$ ), and corrosion rate ( $v_c$ ) derived by so-called Stern method have been described in our earlier papers [1, 2, 6] The electrode potential values quoted in this paper are given on the saturated calomel electrode (SCE) scale.

## 2.4. Study of the surfaces by SEM-EDX method

The morphology and chemical composition of the oxide layer developed on the inner surfaces of the stainless steel specimens were studied by scanning electron microscopy (SEM), equipped with an energy dispersive X ray microanalyzer (EDX) (Type: PHILIPS XL 30 ESEM). In case of each specimen at least two different surface areas were studied by making use of the combined SEM-EDX equipment. The comparative evaluation of surface morphology was performed by analyzing the SEM micrographs obtained at two different magnifications,  $M=3000$  and  $M=1000$  respectively. The chemical composition of the sample surfaces was determined on two different areas of  $1 \text{ mm}^2$  by EDX method. Metallographic cross sections of some tube specimens were also prepared and analysed [4, 6].

## 3. RESULTS AND DISCUSSION

### 3.1. Corrosion effect of the AP-CITROX decontamination technology

In the period from 2000–2007, within the frame of a joint project, the corrosion state of the steam generators of the Paks NPP have been studied. These studies provide evidence that some adverse features (formation of a “hybrid” layer with accelerated corrosion rate and great mobility) can be detected after 1–3 years of applying the AP-CITROX procedure [4, 6]. The inner surfaces of all tube samples have passive character in a wide potential interval next to the corrosion potential. The average corrosion rates calculated for all samples are not higher than the literature data which were measured for the stainless steels type 08X18H10T and AISI 321 in aqueous solutions having similar composition ( $0.3\text{--}4 \mu\text{m}\cdot\text{year}^{-1}$ ) ([7–11] and references therein). The average corrosion rates of steel specimens never decontaminated are very low ( $v_c \leq 0.8 \mu\text{m}\cdot\text{year}^{-1}$ ), a bit higher corrosion rates can be detected at the decontaminated tube samples. However, it is to be noted that two samples which were cut out four years after the chemical decontamination exhibit ca. five times higher corrosion rate ( $v_c = 3.5$  and  $3.9 \mu\text{m}\cdot\text{year}^{-1}$ ).

### 3.2. General corrosion state of the tube samples after using the novel decontamination technology

The potentiostatic polarization curves measured in boric acid solution at the inner surface of the stainless steel specimens are shown in Fig. 2. The calculated corrosion rates are summarized in Table 1. In addition, Table 1 provides a compilation of the main corrosion and metallographic characteristics of the steel specimens studied.

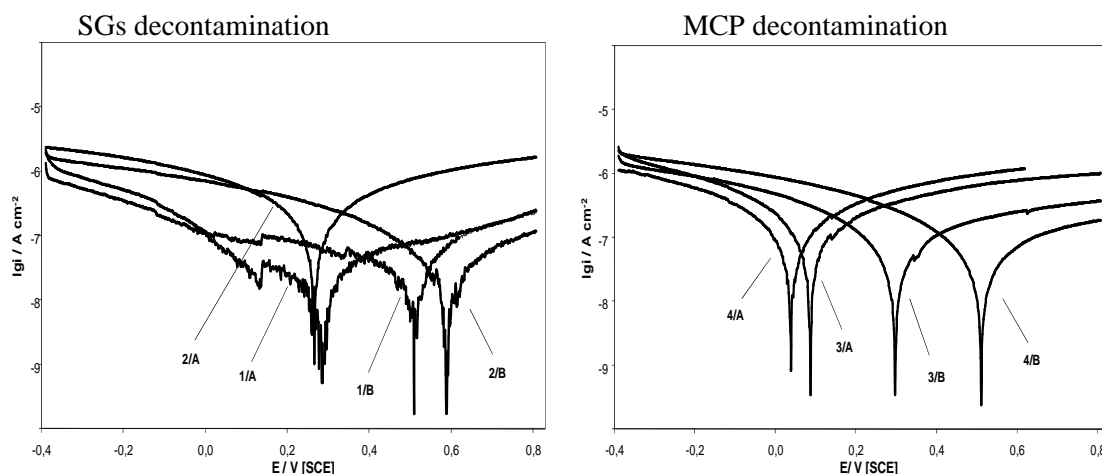


FIG. 2. Potentiostatic polarization curves measured at the inner surface of the samples in boric acid solution ( $c = 12 \text{ g}\cdot\text{dm}^{-3}$ ). Scan rate:  $10 \text{ mV}\cdot\text{min}^{-1}$ .

It is apparent that after applying the novel decontamination treatment, the average corrosion rates decreased, while corrosion potentials increased, giving a strong indication of the more passive character of treated surfaces (see Table 1).





As can be seen in Fig. 4, the effects of MCP decontamination on surface morphology can be detected by SEM-EDX method. On the surface of the samples never decontaminated at Paks NPP (No. 3) a thin oxide-film covered by crystalline deposits can be seen before the decontamination and some crystals remain also after the treatment. Samples decontaminated earlier by AP-CITROX procedure at Paks NPP (No. 4) have a medium thick oxide layer (~ 5 µm) before treatment and the total oxide layer can be removed by the novel decontamination procedure. Fig. 4 No. 4/B shows that the part of the bulk steel can also be dissolved as a consequence of the application of this technology.

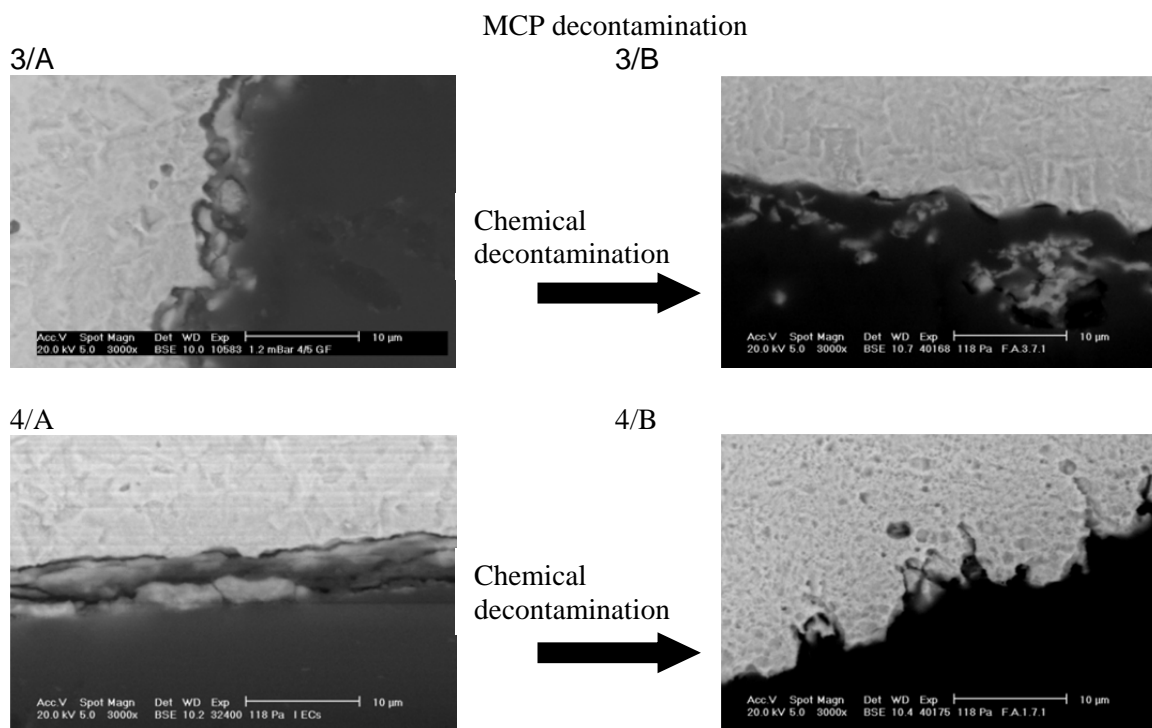


FIG. 4. Effects of MCP decontamination on the structure and morphology of surfaces.

#### 4. CONCLUSIONS

In this work the corrosion, surface chemical and morphological effects of the AP-CITROX procedure as well as of the novel decontamination technology elaborated at our institution were studied and compared.

The average corrosion rates of samples originating from SG never decontaminated by AP-CITROX procedure are very low. A bit higher corrosion rates can be detected at the decontaminated tube samples. However, our studies reveal that a "hybrid" structure of the amorphous and crystalline phases is formed in the outermost surface region of the austenitic stainless steel tubes as an undesired consequence of the industrial application of the AP-CITROX technology.

The laboratory scale experiments attest that the novel technology elaborated for the austenitic stainless steel surfaces may become suitable for the effective decontamination of both dismantlable (e.g. MCP) and separable (e.g. SGs) equipment. By applying this method the oxide removal is surprisingly uniform, even after two or three consecutive cycles. Moreover, no unfavourable tendencies in the general corrosion state, surface structure and morphology of the tube samples can be detected in the course of the chemical treatments.

## ACKNOWLEDGEMENT

This work was supported by the Paks NPP Co. Ltd (Paks, Hungary).

## REFERENCES

- [1] VARGA, K., NÉMETH, Z., SOMLAI, J., VARGA, I., SZÁNTHÓ, R., BORSZÉKI, J., HALMOS, P., SCHUNK, J., AND TILKY, P., *J. Radioanal. Nucl. Chem.*, **254** (2002) 589.
- [2] VARGA, K., BARADLAI, P., HIRSCHBERG, G., NÉMETH, Z., ORAVETZ, D., SCHUNK, J. AND TILKY, P., *Electrochim. Acta*, **46** (2001) 3783
- [3] VARGA, K., NÉMETH, Z., SZABÓ, A., RADÓ, K., ORAVETZ, D., MAKÓ, K. É., HOMONNAY, Z., KUZMANN, E., STICHLAUTNER, S., TILKY, P., SCHUNK, J., OSZVALD, F., PATEK, G., Comprehensive investigation of the corrosion state of the heat exchanger tubes of steam generators, WANO-MC Workshop Experiences and techniques of SG Decontamination in WWER Plants Paks NPP Paks Hungary (on CD-ROM), (2004).
- [4] SZABÓ, A., VARGA, K., NÉMETH, Z., RADÓ, K., ORAVETZ, D., MAKÓ, K. É., HOMONNAY, Z., KUZMANN, E., TILKY, P., SCHUNK, J., PATEK, G., *Corrosion Sci.*, **48** (2006) 2727.
- [5] RADÓ, K., NÉMETH, Z., VARGA, K., SCHUNK, J., KŐRÖSI, F., *J. Radioanal. Nucl. Chem.*, **268** (2006) 313.
- [6] (a) VARGA, K., NÉMETH, Z., HOMONNAY, Z., SZABÓ, A., RADÓ, K., ORAVETZ, D., SCHUNK, J., TILKY, P., OSZVALD, F., *J. Nucl. Mater.* **348** (2006) 181.  
(b) HOMONNAY, Z., KUZMANN, E., STICHLAUTNER, S., VARGA, K., NÉMETH, Z., SZABÓ, A., RADÓ, K., MAKÓ, K. É., KÖVÉR, L., CSERNY, I., VARGA, D., TÓTH, J., SCHUNK, J., TILKY, P., PATEK, G. AND OSZVALD, F., *J. Nucl. Mater.* **348** (2006) 191.
- [7] SHOESMITH, D. W., MANCEY, D.S., DOERN, D.C., BAILEY, M.G., *Corrosion*, **45** (1989) 149.
- [8] BAUMGARTNER, E., BLESÁ, M.A., MARINOVICH, H.A., MAROTO A.J.G., *Inorg. Chem.*, **22** (1983) 2226.
- [9] BORGHI, E. B., ALÍ, S. P., MORANDO, P. J. BLESÁ, M. A., *J. Nucl. Mater.*, **229** (1996) 115.
- [10] GERASZIMOV, V. V. MONAHOV, Sz., *Materiali Jadernoj Techniki Atomizdat Moskva*, (1981), (Hungarian translation).
- [11] LISTER, D. H., Some aspects of corrosion in cooling water systems and their effects on corrosion product transport, EUROCORR 2003, Budapest, Proceedings (on CD-ROM), (2003).

# PRIMARY SYSTEM WATER CHEMISTRY FOLLOW-UP AND UPDATE IN PRESSURIZED HEAVY WATER REACTORS

M. CHOCRON, R. BORDONI, A.M. OLMEDO, M. STRACK, I. RODRÍGUEZ,  
Comisión Nacional de Energía Atómica,  
Av. Del Libertador 8250, 1429, Buenos Aires

R. MANERA,  
Central Nuclear Embalse

J. DUCA  
Proyecto Atucha II, Nucleoeléctrica Argentina

Argentina

## Abstract

Argentina has two nuclear power plants in operation: Atucha I, a pressurized vessel heavy water reactor designed and built by the former SIEMENS-KWU and Embalse a CANDU 600, a Pressurized Heavy Water Reactor designed and built by Atomic Energy of Canada, AECL. A third plant, Atucha II, very similar to Atucha I in design is in advanced state of construction. The three are currently operated by Nucleoeléctrica Argentina S.A. (N.A.S.A.) while the Comisión Nacional de Energía Atómica (C.N.E.A.) is the Institution that, among many other things, provides research and technological support to the plants. Although the three stations are cooled and moderated by heavy water, Atucha I and Atucha II have a very different primary system design and structural materials compared to Embalse. It has also to be taken into account that Atucha I and Embalse have been in operation several years which allowed to introduce updated concepts in water chemistry to them. For Embalse the Water Chemistry Manual Rev. 7 has been issued in 2009. Finally, for Atucha II and considering that the project has passed through several years of delay and the proximity of the commissioning tests, an entire new version of the water chemistry manual is going to be released soon. In the present paper a review of the primary system control parameters is presented, including impurities that could exert some specific corrosion and/or deposition effects (diagnostic parameters) and radiochemistry data where available. Also a synopsis of the updated chemistry manuals together with the supporting reasons that lead to the modifications will be included.

## 1. INTRODUCTION

Argentina has two operating Pressurized Heavy Water Reactor (PHWRs): Atucha I, designed and built by the former SIEMENS-KWU; and Embalse, designed and built by Atomic Energy of Canada (AECL). A third one, Atucha II, which is similar to Atucha I, is in an advanced state of construction. The three plants are currently operated by Nucleoeléctrica Argentina S.A. In what follows a summary of their characteristics is presented. Later on, the primary system water chemistry specifications are given plus a depiction of the failed fuel detection system for each plant. Finally main Water Chemistry (WC) operating experience and/or modifications are discussed.

## 2. DESCRIPTION OF EMBALSE NUCLEAR POWER PLANT

It is a CANDU 600 PHWR designed and built by Atomic Energy of Canada and is in operation since 1984.

- Total fission power: 2155 MW;
- Power transferred at the Steam generators: 2097 MW;
- Moderator: 93.7 MW;
- End shield: 5.9 MW;
- Auxiliary systems: 9.3 MW;
- Nominal channel power: 6.5 MW — fuel bundle: 800 kW.

The reactor assembly comprises [1]:

- Moderator calandria: cylindrical shell made of CS with the calandria tubes. It is filled with the moderator (D<sub>2</sub>O) : 70°C. It also contains the reactivity control mechanisms;
- Calandria tubes: material Zr-4;
- Pressure tubes: they house the fuel bundles;
- Number of fuel channels: 380.Total length: 10.82 m;
- Coolant data (D<sub>2</sub>O): 266 °C/312 °C, 11.04–10.03 MPa, max. flow rate 24 kg/sec;
- Annulus gas: fills the gap between calandria and pressure tubes. The purpose is an early detection of a pressure tube leakage;
- End shield: front and back end of the reactor assembly.

Main materials of the primary heat transport system (PHTS):

- Feeders piping: carbon steel;
- Steam generators tubing: A800;
- Pressure Tubes: Zr-Nb;
- Fuel sheet: Zr-4;
- End fittings: SS 403.

Fuel — on-load refuelling:

- Type: natural uranium, compacted and sintered;
- Number of fuel bundles per channel: 12 — total 4560;
- Fuel bundle length: 495 mm, OD: 102.9 mm, 37 elements, weight 23.5 kg;
- Element OD: 13.08 mm, ID: 12.16 mm, 30 pellets, cylindrical;
- Total weight of U: 95 Mg;
- Fuel burnup: 7000 MW·d/tU — heat flux : 260 W/cm;
- Service cycle: 110 bundles/week = 15.7 bundles/day.

## 2.1. Embalse primary circuit water chemistry

PHTS water chemistry has been fully reviewed for the Phase I studies of the Extended Operation Project [2, 3]. Main results are connected to their impact on feeders piping whose main degradation mechanism is flow accelerated corrosion and pressure tubes deuterium uptake. Conclusions are that pHa management, also reduced in 1996, has had a beneficial impact on both effects on compared to other reactors [4]. Considering the above mentioned modifications plus others carried out at the secondary circuit and the local and worldwide experience which has been gathered along the operation years, an entirely new version of the water chemistry manual has been issued in June 2009 [5, 6]. The summary of the current PHTS specifications is presented in Table 1 and PS diagnostic parameters for power operation in Table 2.

TABLE 1. PRIMARY SYSTEM CONTROL PARAMETER, FOR POWER OPERATION.

Control Parameters		Expected Values	Action Level 1	Action Level 2	Action Level 3
Lithium	[mg/kg]	>0.35/ < 0.56	< 0.35/>0.56	---	---
Deuterium	[mg/kg]	> 0.35 / < 1.8	< 0.35	< 0.2 / >1.8	< 0.1 / >3.3
	[mID <sub>2</sub> /kg]	> 2 / <10	< 2	< 1.2 / >10	< 0.6 / >18.3
Oxygen	[mg/kg]	< 0.005 <sup>1)</sup>	<sup>1)</sup>	<sup>1)</sup>	<sup>1)</sup>
Chlorides	[mg/kg]	< 0.01	> 0.1	> 0.2	> 1
Sulfates	[mg/kg]	< 0.01	> 0.1	> 0.2	> 1

<sup>1)</sup> The value is established by achieving reducing conditions (hydrogen injection).

TABLE 2. PRIMARY SYSTEM DIAGNOSTIC PARAMETERS FOR POWER OPERATION.

Diagnostic Parameters		Expected Values
pH <sub>a</sub> at 25°C <sup>1)</sup>		10.2–10.4
Total conductivity	[μS/cm]	9–35
Isotopic concentration	[wt %]	>97,5
Crud	[mg/kg]	< 0.1
Ammonia	[mg/kg]	< 0.3
Fluorides	[mg/kg]	< 0.1
SiO <sub>2</sub>	[mg/kg]	< 0.7
TOC <sup>2)</sup>	[mg/kg]	< 0.2

<sup>1)</sup> The value is correlated with lithium concentration.

<sup>2)</sup> Total Organic Carbon

Figures 1 and 2 show the control parameters for the last two years, pH-Li-Conductivity and D<sub>2</sub>. It can be seen that they are maintained inside a narrow band during the operation period. Figures 3 and 4 show some of the diagnostic parameters for the same period of time. Among them, iron is higher than in PWR reactors due to the presence of carbon steel piping (feeders). Silica is most of the period under specifications. It has to be considered that the D<sub>2</sub>O coolant is continuously upgraded and recycled to the system.

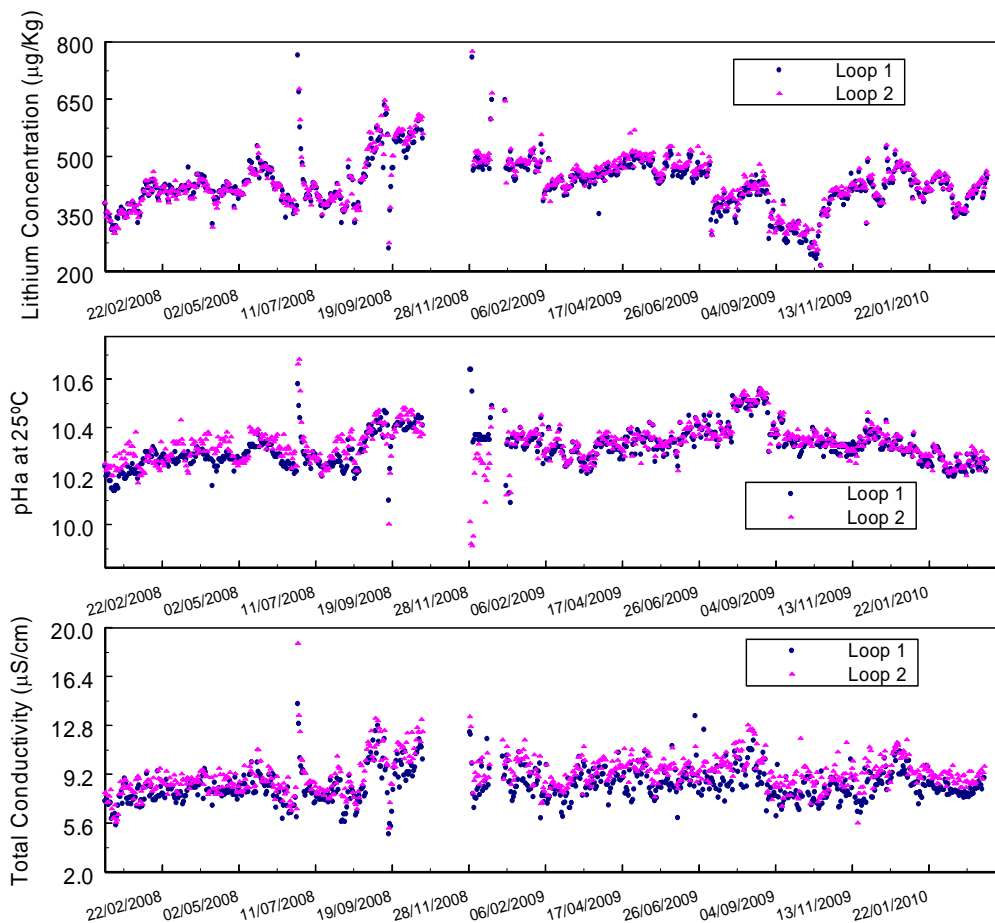


FIG. 1. Li - pH<sub>a</sub> - Conductivity in Embalse PHTS.

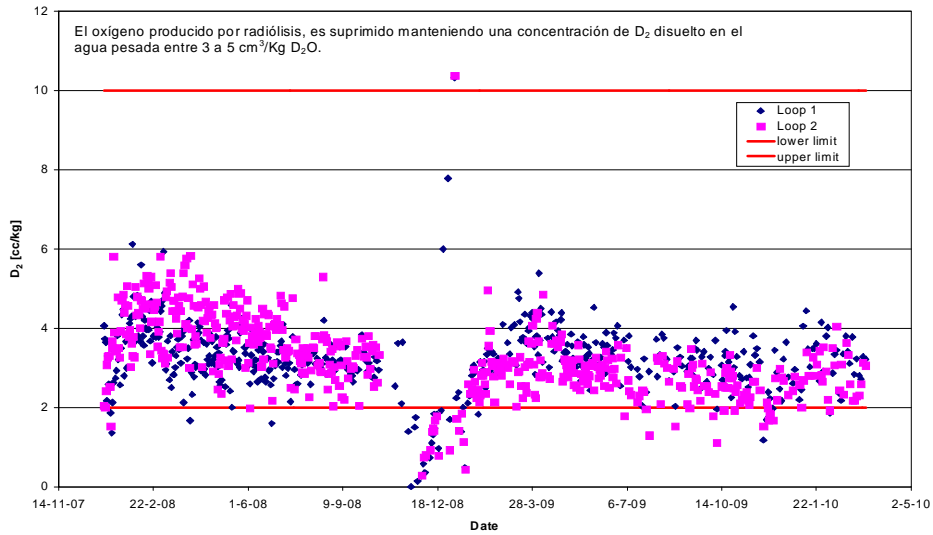


FIG. 2. Deuterium concentration in Embalse PHTS.

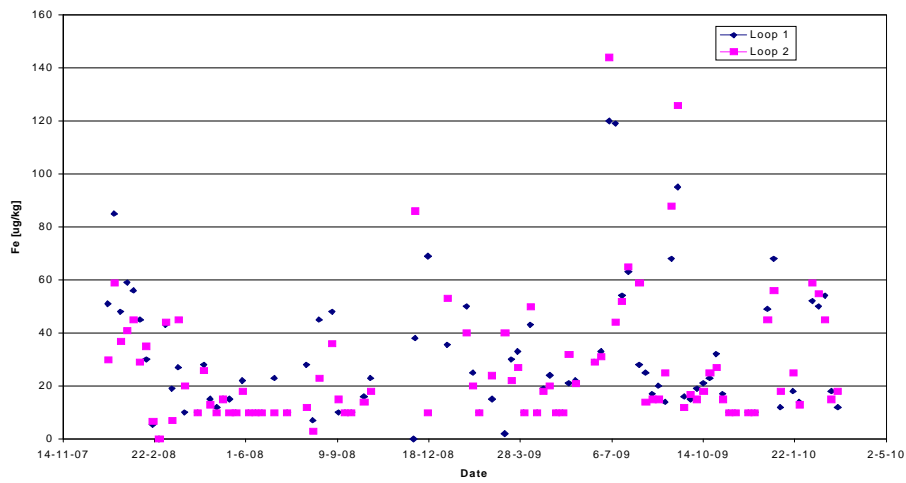


FIG. 3. Iron concentration in Embalse PHTS.

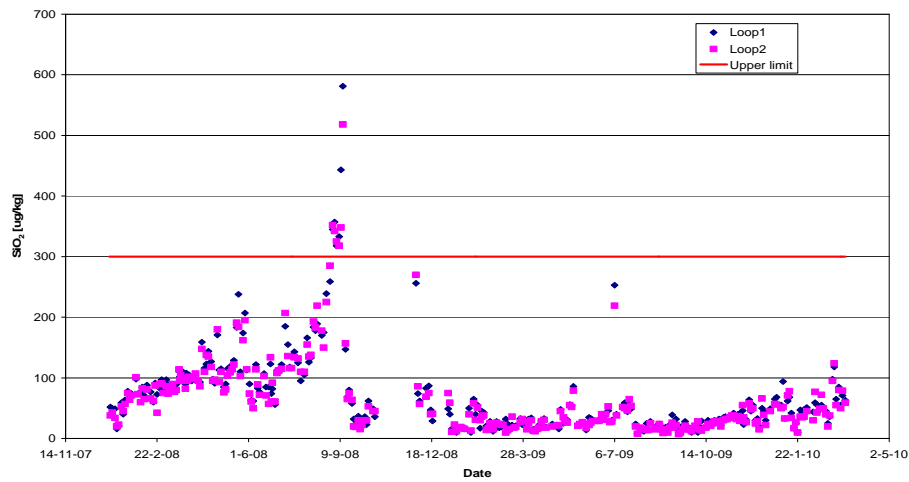


FIG. 4. Silica in Embalse PHTS.

A detailed survey of PHTS materials and corrosion trends has been presented elsewhere [7, 8].

## 2.2. Failed fuel monitoring and detection systems (FFMDSs) at Embalse

Embalse has two FFMDSs as follows:

- Total activity monitoring system: It follows global activity in both reactor loops, i.e.  $^{88}\text{Kr}$ ,  $^{131}\text{I}$ ,  $^{133}\text{I}$ ,  $^{135}\text{Xe}$  and  $^{133}\text{Xe}$ ;
- Failed fuel localization system: it identifies the channel where the failed fuel is located and this in turn allows to track it, through the refuelling machine up to the fuel pool. The system takes a coolant sample from each fuel channel taking advantage of the PHTS reactor assembly and performs a cycle sweeping the 380 fuel channels looking for  $^{87}\text{Br}$  and  $^{137}\text{I}$  delayed neutrons. It is divided in four subsystems each one with 95 sampling lines [9, 10].

Figures 5 and 6 present the evolution of activity of some important fission products along the same operation period. Operating experience has proved that trend of noble gases activity ratios are much more sensitive than iodine isotopes for the surveillance of fuel elements integrity.

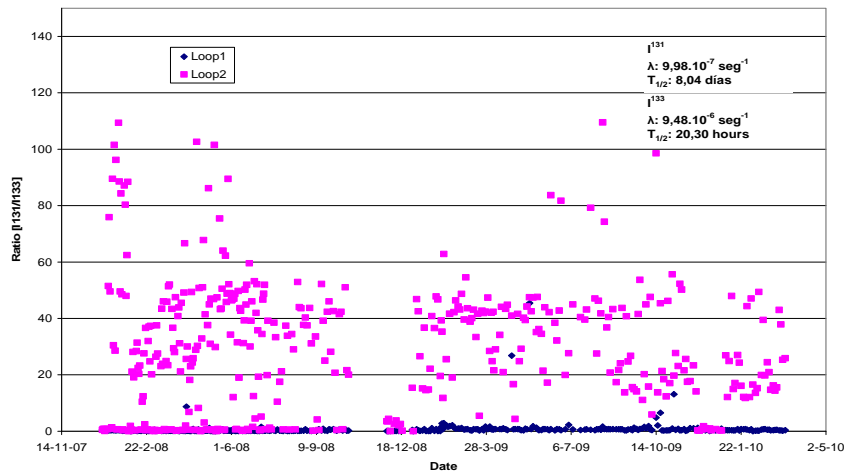


FIG. 5.  $^{131}\text{I}/^{133}\text{I}$  ratio in Embalse PHTS.

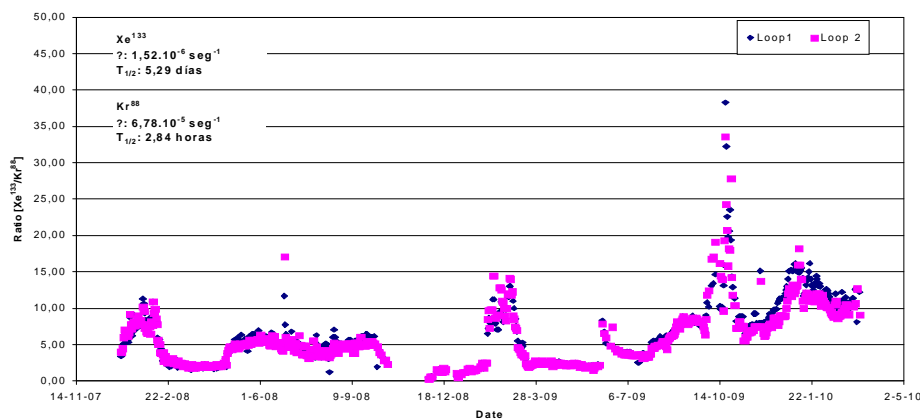


FIG. 6.  $^{133}\text{Xe}/^{88}\text{Kr}$  in Embalse PHTS

### 3. DESCRIPTION OF ATUCHA I/II NUCLEAR POWER PLANTS

Atucha I and Atucha II are PHWRs designed and built by the former SIEMENS-KWU. Atucha I is in operation since 1974 (360 MWe) while Atucha II is in an advanced state of construction.

#### 3.1. Atucha II main features:

- Total Fission power: 2160 MW — electric power 745 MW;
- Power transferred at the steam generators: 1953.5 MW;
- Moderator: 220 MW;
- Average channel power: 4.79 MW/fuel.

The reactor assembly comprises [11]:

- Reactor Pressure Vessel: vertical. Two circuits;
- Coolant data (D2O): 278 °C–312 °C;
- Active core length: 5300 mm;
- Moderator tank inside the RPV. Moderator (D2O) Temperature 170 °C–220 °C. Some mixing with the coolant and heat transmission by conduction exist;
- Fuel channels: they house the fuel bundles. Number of fuel channels: 451.

Main Materials of the Primary Heat Transport System (PHTS):

- RPV cladding and PHTS piping cladding: SS 4550
- Steam generators tubing: A800
- Fuel channels and external insulation foil: Zr-4
- Fuel Sheet: Zr-4

Fuel — on-load refuelling:

- Type: Natural uranium, compacted and sintered;
- Number of fuel bundles per fuel channel: 1;
- Fuel bundle length: 5300 mm, OD: 102.9 mm, 37 rod elements, weight 23.5 kg;
- Lattice: 272 mm;
- Rod OD: 11.9 mm, thickness: 0.55 mm, 30 pellets, cylindrical;
- Total weight of U: 85 Mg;
- Fuel burnup: 7500 MW·d/tU — heat flux: 244 W/cm;
- Service cycle: 1.8 bundles/day.

#### 3.2. Atucha II primary circuit water chemistry

At CNAII project, water chemistry design has been chosen based on the same theoretical principles as for Embalse and on international experience. Parameters have been defined according to best international practices. The water chemistry manual has been preliminary issued and its final version is currently under review by AREVA specialists [12]. It is also under consideration the use of Zinc addition as a measure to reduce radiation fields in Atucha I and Atucha II as well [13]. For Atucha II chemistry specification and alarms are presented in Table 3, and diagnostic parameters and complimentary specifications, respectively, in Tables 4 and 5.

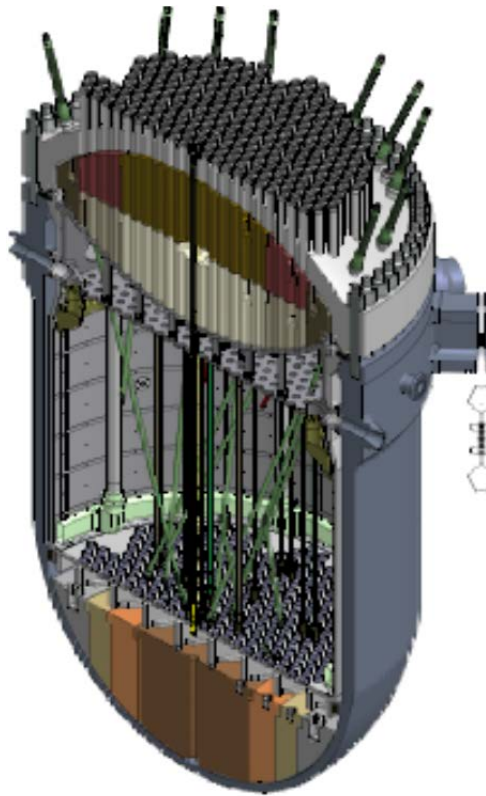


FIG. 7. Atucha II reactor assembly. A fuel channel and control rods can be appreciated in the figure.

TABLE 3. CHEMISTRY SPECIFICATIONS AND ALARMS FOR CNA II

Control Parameters	Specifications	Limit Value	AL 1	AL 2	AL 3
Lithium-7(mg/kg)	0.2–0.7	0.5–0.7	>0.7	>1.0	<0.2 / >2.5
D <sub>2</sub> (mg/kg)	0.6–2	1.6–2	<1.6	<1.0	<0.6 / >3
(cc/kg)	3–12	8–12	<8	<5.6	<3 / >17
O <sub>2</sub> (mg/kg)	<0.005	<0.005	>0.005	>0.01	>0.02
Cl <sup>-</sup> (mg/kg)	<0.1	<0.005	>0.05	>0.1	>0.5

AL 1: Action level 1, four weeks of operation.

AL 2: Action level 2, one week of operation.

AL 3: Action level 3, plant shutdown in 12 hours.

TABLE 4. DIAGNOSTIC PARAMETERS FOR CNA II (cont.)

Diagnostic Parameters	Expected Values	Operating Range
pH <sub>A</sub> <sup>a</sup>	10–10.5	10.3–10.5
$\Lambda$ (25°C– $\mu$ S/cm) <sup>a</sup>	<20	13–8
Boron (mg/kg) <sup>b</sup>	---	---

<sup>a</sup> The expected value has to correlate to the control parameter Lithium.

<sup>b</sup> Following the reactivity control requirement.

TABLE 5. COMPLEMENTARY SPECIFICATIONS FOR CNA II

Parameter	Expected Value	Limit Value
Iron, Nickel and Chromium as suspended solids or "crud" (mg/kg) <sup>1)</sup>	<0.1	<0.01
Soluble Iron (mg/kg) <sup>1)</sup>	<0.05	<0.005
Silica (mg/kg) <sup>1)</sup>	<0.5	<0.1

<sup>1)</sup> If the control parameters are between the expected values and correlate with the Diagnostic Parameters, the Complementary Control Parameters have to be maintained within the expected values.

### 3.3. Failed fuel monitoring and detection systems (FFMDSs) at Atucha

Atucha has two FFMDSs as follows:

- Total activity monitoring system (NE). It follows global activity in both reactor loops.
- Failed fuel localization system (NX): it identifies the channel where the failed fuel is located and this in turn allows to track it, through the refuelling machine up to the fuel pool. The system is provided with two multiport valves that sample coolant water from each fuel channel. It performs a cycle sweeping the 451 fuel channels looking for fission products.
- At Atucha I, taking advantage of the installed system (NX), an on purpose derivation was added for the detection of <sup>87</sup>Br delayed neutrons.

## 4. CONCLUSIONS

The purpose of the present paper has been, in the frame of the reference meeting, to present a detail of the Argentina PHWRs, reactor assembly, materials of construction and PHTS water chemistry. For the case of these plants rather than fuel, other internals like fuel channels or pressure tubes are perhaps a subject of major concern taking into account continuous refuelling of the former and life time operation of the later. Water chemistry specifications, updates and later operating experience, where available, have been presented, showing that design values are satisfied and also that, according to international reviews they might have had beneficial effect on long time operation. Failed fuel detection system has also the function of detecting a coolant flow reduction or partial blockage. These systems have also been improved, taking into account advantages of PHWRs along the years for the early detection and localization of a failed fuel bundle.

## REFERENCES

- [1] INTERNATIONAL ATOMIC ENERGY AGENCY, Assessment and Management of Major NPP Components Important to Safety: CANDU Reactor Assemblies, IAEA-TECDOC-1197, IAEA, Vienna (2001).
- [2] CHOCHRÓN, M., Circuito primario y moderador. controles de la química, CNE-GVI-EV-MODERADOR-IX (2006).
- [3] QIU, L., Chemistry assessment of Embalse PHTS, AECL. (2007).
- [4] ELLIOT, J., International Atomic Energy Agency, Water Chemistry Specialists Meeting. Embalse, Argentina (1999).
- [5] CHOCRON, M., DIAZ, V., HORNOS, L., STRACK, M., RODRIGUEZ, I., FERNANDEZ, N., MANERA, R., QUINTEROS, D., OVANDO, L., SAINZ, R. Modifications in the water chemistry for long term operation. plant experience and design manual updated issue. Workshop on Plant Life Management and Long Term Operation of NPPs under the Technical Cooperation Programme Enhancing Operational Safety in Nuclear Installations (RLA 9060), Buenos Aires, Argentina (2009).
- [6] FERNÁNDEZ, N., MANERA, R., QUINTEROS, D., OVANDO, L., SAÍN Z, R., CHOCRON, M., HORNOS, L., STRACK, M., RODRÍGUEZ I., Embalse modifications in the water chemistry for plim. plant experience and design manual updated issue. Nuclear Plant Chemistry Conference 2010-NPC2010, Quebec City, Canada (2010).
- [7] MAROTO, A.J.G., Water chemistry and corrosion control of cladding and primary circuit components, IAEA-TECDOC-1128, IAEA, Vienna (1999).
- [8] BORDONI, R., OLMEDO, A.M., MIYAGUSUKU, M., CHOCRON, M., FERNÁNDEZ, N., QUINTEROS, D., OVANDO, L., SAÍN Z, R., Corrosion monitoring of structural materials in the primary coolant circuit of Embalse N.P.P., International Conference on Water Chemistry of Nuclear Reactor Systems NPC'08, Berlin, Germany (2008).
- [9] Embalse DM 63103.
- [10] Embalse DM 63105.
- [11] Siemens-KWU, Nuclear power plant with PHWR (1979).
- [12] CHOCHRÓN M., Ingenieria de la química del agua de la central nuclear Atucha II. Nucleo Eléctrica Argentina S.A., CP-CNAII-UAQ-3/06 (2006).
- [13] CHOCHRÓN, M., RODRIGUEZ, I., BORDONI, R., OLMEDO, A., MIYAGUSUKU, M., Evaluacion de la ingenieria de la inyeccion de zinc a los sistemas primario-moderador de la central nuclear Atucha I. CP-I-1/10 (2010).



**CORROSION/OXIDATION**

(Session 2)

**Chairperson**

**F. NORDMANN**

France



# THE FORMATION OF OXIDE FILMS UNDER PRESSURIZED WATER REACTOR PRIMARY COOLANT CONDITIONS

A. LUTTIKUL, P. SRISUKVATANANAN and D.H. LISTER  
UNB Nuclear, Department of Chemical Engineering,  
University of New Brunswick,  
PO Box 4400, Fredericton, NB, E3B 5A3  
Canada

## Abstract

The study investigated the effects of steam generator (SG) alloy composition and post-processing (e.g. heat treatment), and coolant boron concentration and zinc addition, on oxide film formation under PWR primary coolant conditions. Specimens of Alloy 600, Alloy 690, Alloy 800, type 304 stainless steel (SS304) and zircaloy-4 — the major materials of construction of primary circuits — were exposed to high-temperature coolant of different chemistries in autoclaves. In experiments with heat flux, surface-area ratios of specimens involved just the heated or cooled portions of zircaloy or SG alloy while the SS was isothermal; ratios were typical of actual reactor systems. In isothermal experiments, the ratios involved all wetted surfaces. After exposures of several days, specimens were removed and the oxides characterized with surface analysis techniques. As expected, the results revealed that Ni-based alloys and SS304 were both covered with iron rich crystallites overlaying an amorphous chromium rich layer, while zircaloy-4 was covered with a single oxide layer. For the SG tubing of the same post-processing, the higher chromium alloys apparently produced a more compact oxide than the lower chromium alloys. This effect of post-processing was observed on all alloys, but was not as obvious as the effect of alloy composition. The most compact oxides were formed in coolant containing boron, which tended to concentrate in the inner oxide layers. Thicker and looser outer layer oxides were found on Alloy 600 exposed for 30 days to coolant with pH300°C of 7.4 than on the same alloy for five or ten days to coolant with pH300°C of 7.1. Zinc in the coolant was incorporated in the inner oxide layer on SG material but had different effects on the outer layers on different materials. Observed differences in oxide morphologies may account for differences in crud behaviour in operating plants.

## 1. INTRODUCTION

Crud induced power shift (CIPS — also known as Axial Offset Anomaly, AOA) was first observed at Callaway in cycles 4–6 (1989–93) [1]. It has been a recurring problem in some Pressurized Water Reactors (PWRs) with a core exit temperature in excess of 325°C. However, not all high duty cores have experienced CIPS. European plants have been operated at high thermal duty without experiencing CIPS — apparently because crud levels there are very low [2]. It is now known that CIPS is caused by a combination of high crud level in the coolant, high boiling intensity in the core and the presence of boron, which is sequestered in fuel deposits and skews the neutron flux distribution. Cladding deposits also give rise to out-core radiation fields. Corrosion products found in the cores are rich in Ni, which originates mainly in the Ni-based alloy steam generator (SG) tubing. Therefore, the SG tubing is the primary concern for corrosion product inventory that has led to the development of CIPS.

In a typical PWR, the three major materials contacting the primary coolant are zircaloy-4 (as fuel sheath), nickel alloy (as SG tubing) and stainless steel (SS — as piping and cladding of the reactor vessel and SG channel heads). For the SG tubing, the Ni-based alloys used worldwide are alloy 600, Alloy 690 and Alloy 800, which are post processed in different ways, such as mill annealing (MA), thermal treating (TT), cold drawing (CD) and shot peening (SP). In the USA, SG tubes are either Alloy 600 MA, Alloy 600 TT or Alloy 690 TT [3], while Alloy 800 is commonly used in European plants [2]. In some PWRs, it is believed that the SG tubing is fully passivated and shutdown releases of corrosion products (and, subsequently, CIPS) cannot occur [4]. The most important factors affecting tube passivation are its composition and alloy post-processing, and coolant chemistry is expected to interact with the resulting different surface conditions in different ways.

A preceding study of the metallurgical properties of SG tubing specimens by the authors [5] indicated that CD specimens were the hardest, as expected, while MA and TT specimens had similar hardness. All SG specimens met grain size standard specification [6, 7]. Thus, Alloy 600 exhibited the smallest grain size of about 10 µm, whereas the grain sizes of Alloy 690 and 800 were between 15 and

35  $\mu\text{m}$ . The grain boundaries of etched TT samples were sharp and clear, in contrast with those of MA and CD samples. It is believed that TT allows more precipitation of compounds or elements, resulting in a uniform precipitate distribution. There was no consistent effect of heat treatment on grain size seen in the study.

In terms of primary coolant chemistry, it is found that operating at elevated pH (pH300°C = 7.4) is beneficial in reducing the amount of deposit on cladding surfaces [8] and, in turn, reducing the likelihood of CIPS. Activity transport and radiation field growth are also minimized. Zinc addition has been implemented in several PWRs and shown to be one of the ways to reduce CIPS by promoting more protective oxide on the surfaces of SG alloys and decreasing the quantity of corrosion products and transported crud. This treatment also minimizes activity transport; Byers and Jacko [9] reported that zinc limited the corrosion product release rate by as much as a factor of five as compared to the same coolant without added zinc.

The objectives of this current study were to characterize the oxide film formed on Alloy 600, Alloy 690, Alloy 800, 304 stainless steel (SS304) and zircaloy-4 (zirc-4) and to evaluate the effects of boron addition, zinc addition, SG alloy composition and post-processing on oxide film formation under PWR primary coolant conditions. The characterization might then indicate properties that could affect corrosion product release during plant operation.

## 2. EXPERIMENTAL

### 2.1. Test materials

The materials used in this work were those investigated in the preceding study, viz. SG alloys, SS304 and zirc-4. The SG alloys were Alloy 600 (MA and CD, both from Westinghouse), Alloy 690 (MA, TT and CD, all from Valinox) and Alloy 800 (MA, from an unknown manufacturer and SP, from Sandvik). The compositions of these alloys are given in Table 1. Specimens were cut from the supplied materials (as received tubing) in different shapes of shell section, depending on the surface areas required for keeping the surface ratio of the SS, SG alloy and Zirc-4 the same in all tests.

TABLE 1. COMPOSITIONS OF THE SG ALLOYS (WT %)

Alloy	Ni	Cr	Fe	Mn	Al	Ti	Si	S	Cl	Mo
600	71.2	15.24	9.52	0.25	0.31	0.34	0.20	0.01	0.10	0.57
690	57.46	27.49	9.56	0.26	0.26	0.36	0.44	-	0.22	0.46
800	31.76	20.12	42.50	0.64	0.46	0.45	0.49	0.01	0.08	0.52

## 2.2. Oxide formation tests

The corrosion tests were carried out in two autoclaves simulating PWR primary conditions at 295–300°C and saturation pressure. The first set of experiments was conducted in a static 1 L titanium autoclave (Ti-2), where there was heat flux through the Zirc-4 and SG alloy specimens to simulate the heat source and sink, respectively, in a reactor primary circuit. The specimens were mounted on tubes passing through the autoclave lid. The heat flux through the Zirc-4 was 325 kW/m<sup>2</sup>, provided by an internal electrical heater, and that through the SG alloy samples was 20 kW/m<sup>2</sup>, provided by a stream of coolant from a high temperature loop. With the given heat flux, sub-cooled boiling was expected to occur on the Zirc-4 surface and the boiling rate was calculated to be 1,045 kg/ m<sup>2</sup>h<sup>-1</sup>. There was no heat through SS304 specimen. The surface area ratio of the three materials is typical of PWR primary circuit, which is 25% Zr-4, 65% SG alloy tubing and 10% SS304 piping. Note that in the experiments with heat flux, the “active” proportion of the Zr-4 surface is considered to be only the heated area. The high temperature, high pressure loop was used to circulate water and remove heat from the autoclave. The test durations were 120 and 240 hours. A schematic diagram of the loop and the configuration of the autoclave are shown in Fig. 1 and Fig. 2 (a), respectively.

The second set of experiments was isothermal (no heat flux through the specimens), conducted in 1 L titanium and 2 L stainless steel autoclaves maintained at saturation pressure. The total surface areas of materials were the same as in the first set, but this time ratios were based on the whole wetted surface, rather than heated or cooled areas. This made the surface area proportions 40% Zr-4, 23% SG alloy and 37% SS304. The configuration of specimens in the isothermal experiments is shown in Fig. 2(b). The test durations were between 120 and 720 h.

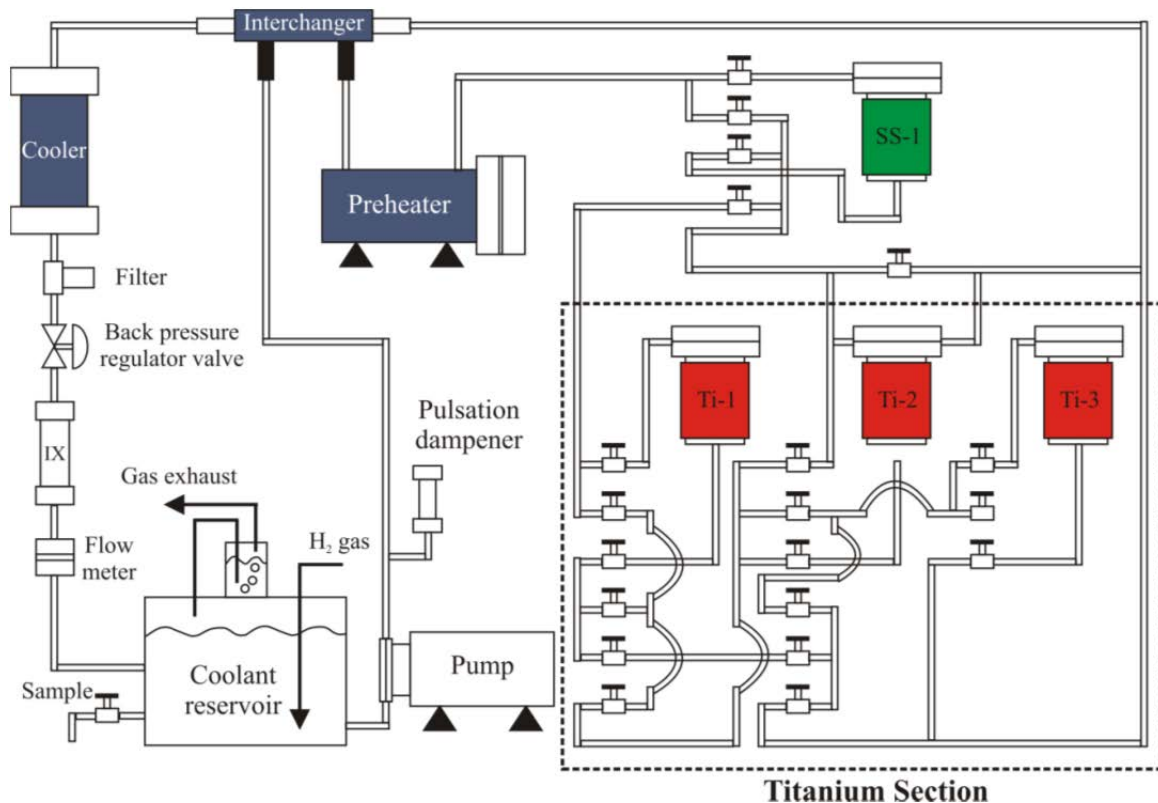


FIG. 1. Diagram of the high temperature, high pressure loop.

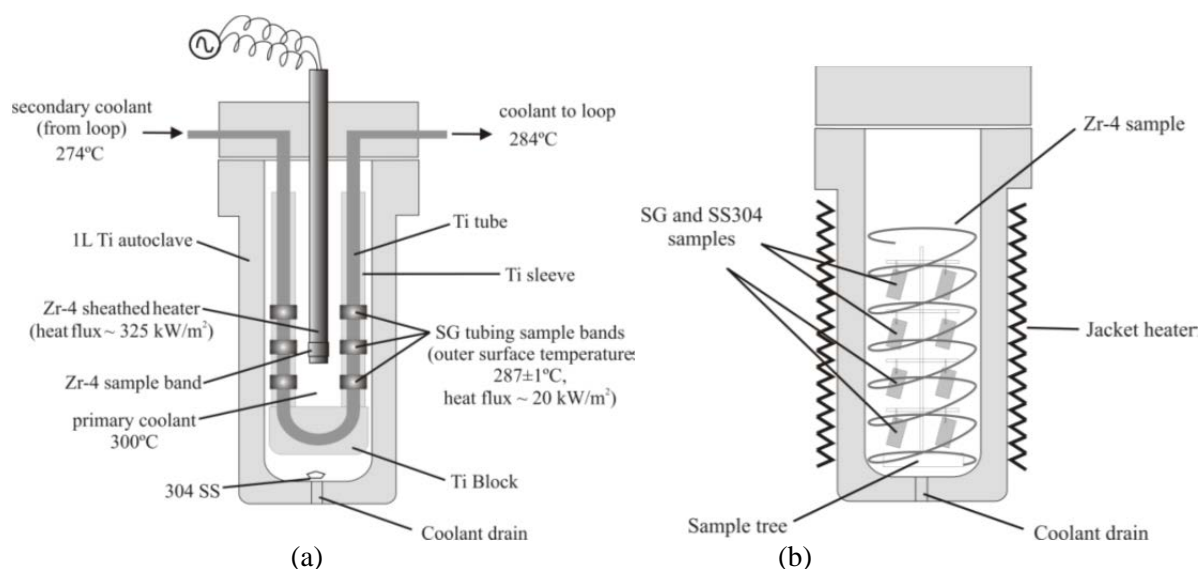


FIG. 2. Test section: (a) with heat flux through zirc-4 and SG samples and (b) without heat flux.

### 2.3. Coolant chemistry

PWR primary coolant chemistry conditions were simulated with a solution of boric acid (0–2 000 ppm as B), lithium hydroxide (0.28–12.92 ppm as Li for adjusting  $\text{pH}_{300^\circ\text{C}}$  to be 6.9–7.4) and 18 cc/kg dissolved hydrogen. In the experiments with zinc addition, zinc stock solution was prepared by equilibrating ZnO with water at room temperature; the appropriate amount of zinc stock solution was added to coolant containing boron and lithium to obtain a zinc concentration of 20 ppb.

### 2.4. Oxide characterization

After specimen exposure, typical surface morphology and elemental composition of oxides were investigated with SEM and EDX (Model JSM6400). On some samples, elemental depth profiles of oxide films were determined with SIMS and oxide phases were identified with XPS. Surface characterization was performed on the convex surfaces of specimens. Laser-Raman Spectra analyses were performed on some samples to identify the type of oxides. The SIMS analyses employed a Cameca IMS-3f ion microprobe using a  $\text{Cs}^+$  beam to monitor oxygen and various negative secondary ions of interest, e.g. Fe, Ni, Cr, Ti, Zr. The analysed area was 60  $\mu\text{m}$  in diameter.

The XPS analyses were performed using a Kratos Axis Ultra X ray photoelectron spectrometer. The XPS survey spectra were obtained from an area of approximately  $300 \times 700 \mu\text{m}$  using a pass energy of 160 eV. XPS high resolution spectra were obtained from an area of approximately  $300 \times 700 \mu\text{m}$  using a pass energy of 20 eV. The SIMS and XPS analyses were done at Surface Science Western, University of Western Ontario, Canada.

### 2.5. Test matrices

Several experimental runs were conducted in this study. Two test matrices are shown here, based on the effects of parameters on oxides to be discussed. The effect of boron was investigated by comparing results from Run 1, Run 2, Run 6 and Run 7 as shown in Table 2.

TABLE 2. TEST MATRIX FOR EFFECT OF BORON

1 L titanium autoclave				
Run	1	2	6	7
	With heat flux	With heat flux	No heat flux	No heat flux
SG alloy sample				
-Alloy 600	MA	MA	MA	MA
Coolant chemistry				
-pH <sub>300°C</sub>	7.01	7.01	7.01	7.01
-[B] (ppm)	2 000	0	2 000	0
-[Li] (ppm)	4.89	0.28	4.89	0.28
-[H <sub>2</sub> ] (cc/kg) nominal	18	18	18	18
Exposure time (days)	10	5	5	5
Pressure (psig)	1 140	1 140	1 230	1 230
Bulk temperature (°C)	295	295	300	300

Effects of SG composition, post-processing and zinc addition were examined in Run 4, Run 5, Run 8 and Run 9. The conditions of these runs are detailed in Table 3.

TABLE 3. TEST MATRIX FOR EFFECTS OF SG COMPOSITION, POST-PROCESSING AND ZINC ADDITION

Run	1 L titanium autoclave		2 L stainless steel autoclave	
	4	5	8	9
	No heat flux	No heat flux	No heat flux	No heat flux
SG alloy sample				
-Alloy 600	MA, TT	MA, TT	MA, TT	MA, TT
-Alloy 690	MA, TT, CD	MA, TT, CD	MA, TT, CD	MA, TT, CD
-Alloy 800	MA, SP	MA, SP	MA, SP	MA, SP
Coolant chemistry				
-pH <sub>300°C</sub>	7.4	7.4	7.4	7.4
-[B] (ppm)	2000	2000	2000	2000
-[Li] (ppm)	12.92	12.92	12.92	12.92
-[Zn] (ppb)	0	20	0	20
-[H <sub>2</sub> ] (cc/kg) nominal	18	18	18	18
Exposure time (days)	30	30	30	30
Pressure (psig)	1230	1230	1230	1230
Bulk temperature (°C)	300	300	300	300

### 3. RESULTS AND DISCUSSION

#### 3.1. General observations on oxide morphology

During exposure in all tests, all samples were darkened. The oxides formed on SG alloys and SS304 consisted of two layers; a Fe rich crystallite layer and a Cr rich underlying layer. The crystallite layer presented a bimodal size distribution of large, sparse crystallites and a more uniform distribution of small crystallites. zircaloy-4 was covered with a single oxide layer, presumably ZrO<sub>2</sub>. Platelet and needle like oxides were commonly found on Alloy 600 samples, whereas on Alloy 690 and Alloy 800 the oxides were mostly octahedral.

### 3.2. Effect of boron

The effect of boron was studied in two cases: with and without heat flux through the SG alloy and Zirc-4 surfaces. Oxides formed on Alloy 600 MA, SS304 and Zirc-4 in the coolant containing both boron and lithium (~2000 ppm B, 4.89 ppm Li) and just lithium (0 ppm B, 0.28 ppm Li) are shown in Fig. 3 (with heat flux) and Fig. 4 (without heat flux). For both cases — with and without heat flux — and in the presence of boron, the oxides formed on Alloy 600 MA and SS304 were more compact than those in the coolant without boron. It should be noted that the exposure time of Run 1 was twice that of Run 2. Nonetheless, similar observations were made for Run 6 and Run 7, except that isothermal Alloy 600 MA tended to develop more very small crystallites.

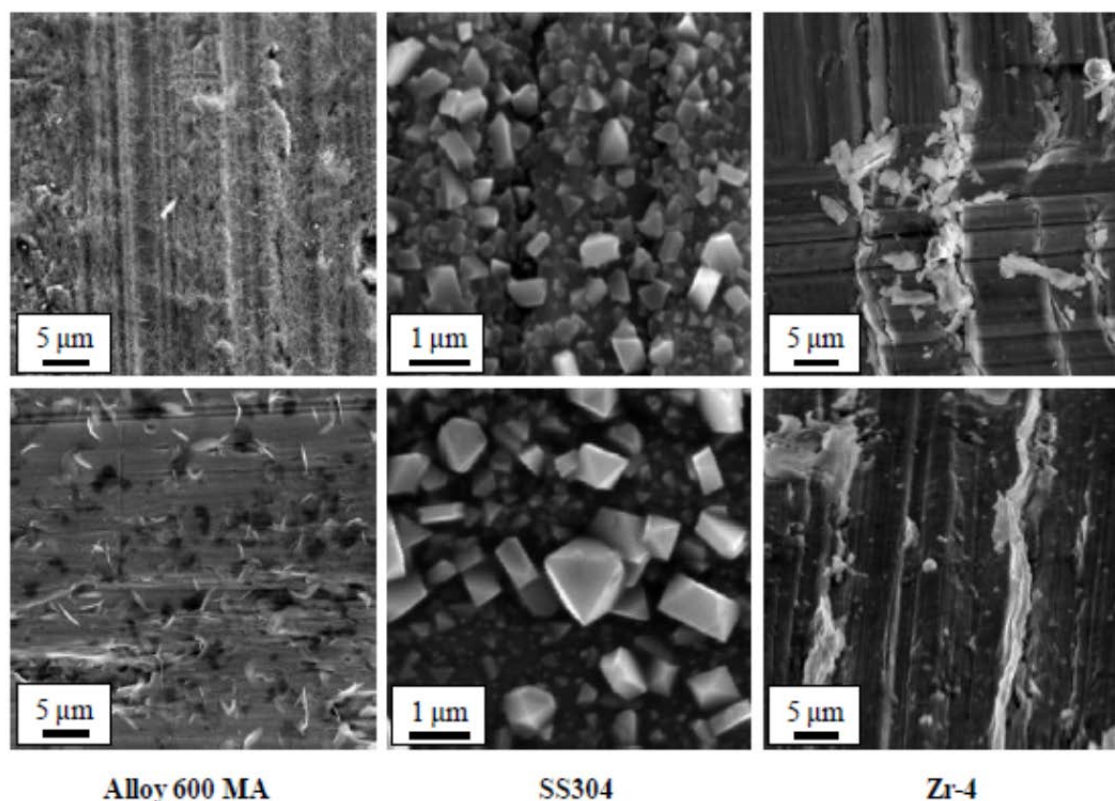


FIG. 3. SEM images of oxides formed on specimens in the coolant with boron (top row) and without boron (bottom row) in the presence of heat flux.

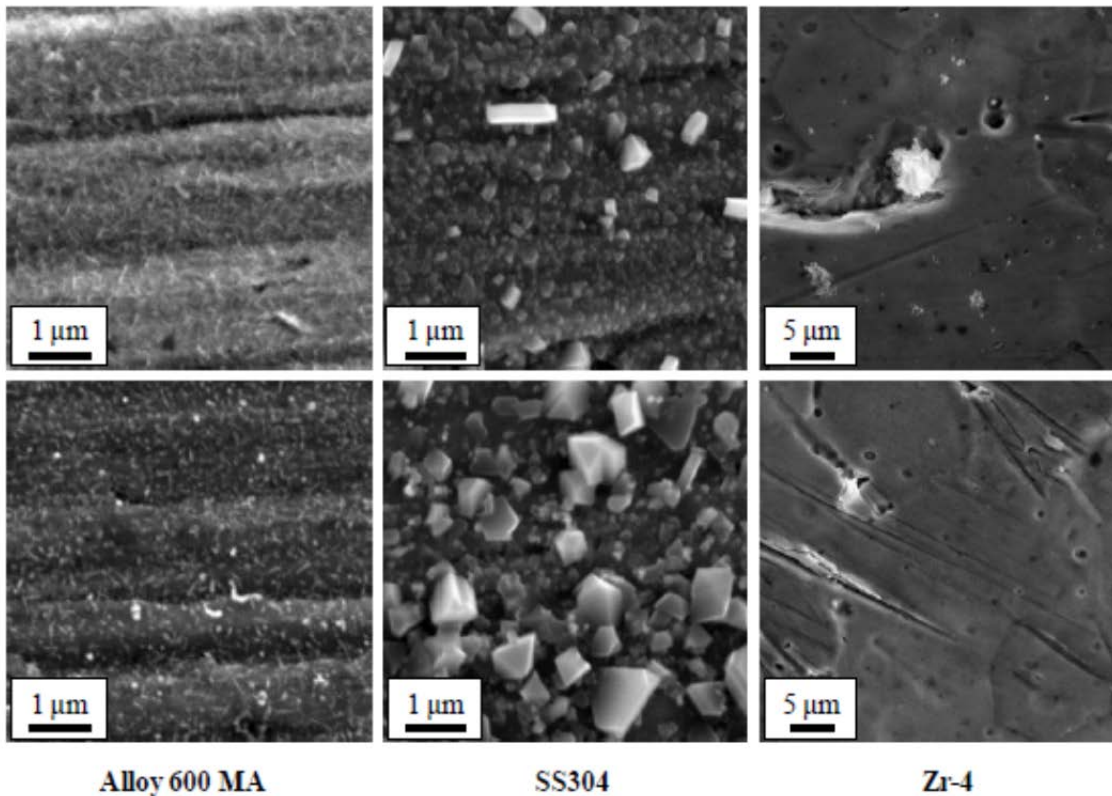


FIG. 4. SEM images of oxides formed on specimens in the coolant with boron (top row) and without boron (bottom row) in the absence of heat flux 10.

On the zirc-4 surface, oxide crystallites were not readily apparent via the SEM but the effects of boron and heat flux were clear when corrosion rates were determined using weight gain, as shown in Table 4. A corrosion rate as high as  $3.36 \text{ mg}\cdot\text{dm}^{-2}\cdot\text{day}$  (mdd) was obtained in the condition where there was heat flux and no boron. The presence of boron under the heat flux condition lowered the average corrosion rate by ~9%, when determined by interpolation of the ten-day exposure results from Run 1 to five days using cubic kinetics. This may be due to the fact that in the presence of heat flux there was sub-cooled boiling on the zirc-4 surface, resulting in the concentration of solutes in the oxide pores [10]. Concentrated lithium may then have accelerated the corrosion of the zirconium alloy in the coolant without boron. There was no significant effect of boron on zirc-4 corrosion under non-heat flux conditions.

TABLE 4. CORROSION RATE OF ZIRC-4

	Heat flux through surface	Boron (ppm)	Lithium (ppm)	Temp. (°C)	Exposure time (days)	Corrosion rate by wt. gain (mdd)
Run1	Yes	2 000	4.89	295	10	1.92 (3.05 <sup>a</sup> )
Run2	Yes	0	0.28	295	5	3.36
Run6	No	2 000	4.89	300	5	1.66
Run7	No	0	0.28	300	5	1.59

<sup>a</sup> interpolated to 5 days using cubic kinetics

### 3.3. Effect of SG alloy composition

Figure 5 shows the SEM micrographs of Alloy 600, Alloy 690 and Alloy 800, which were processed by MA (top row) and TT (bottom row), from Run 4. It is evident that SG alloy composition had a significant effect on the oxide morphology. Platelet oxides were observed on Alloy 600 specimens, whereas on Alloy 690 and Alloy 800 oxides were octahedral. The compactness of the oxide formed on Alloy 690 MA suggests that it may have been more protective than that on Alloy 800 MA and on Alloy 600 MA. It is most likely a result of Cr content in the alloys, since the weight percentage of Cr in Alloy 690 is higher than that in Alloy 800, which in turn is higher than that in Alloy 600. A similar result was observed on TT specimens, where Alloy 690 had more compact oxide than Alloy 600 TT. The abundance of large crystallites formed on Alloy 600 over 30 days at  $\text{pH}_{300^\circ\text{C}}$  of 7.4 is in contrast to the results of Runs 1, 2, 6 and 7, which operated for five or ten days at  $\text{pH}_{300^\circ\text{C}}$  of 7.1. The apparently looser outer layer may be more prone to release in the higher flow regime in an operating steam generator.

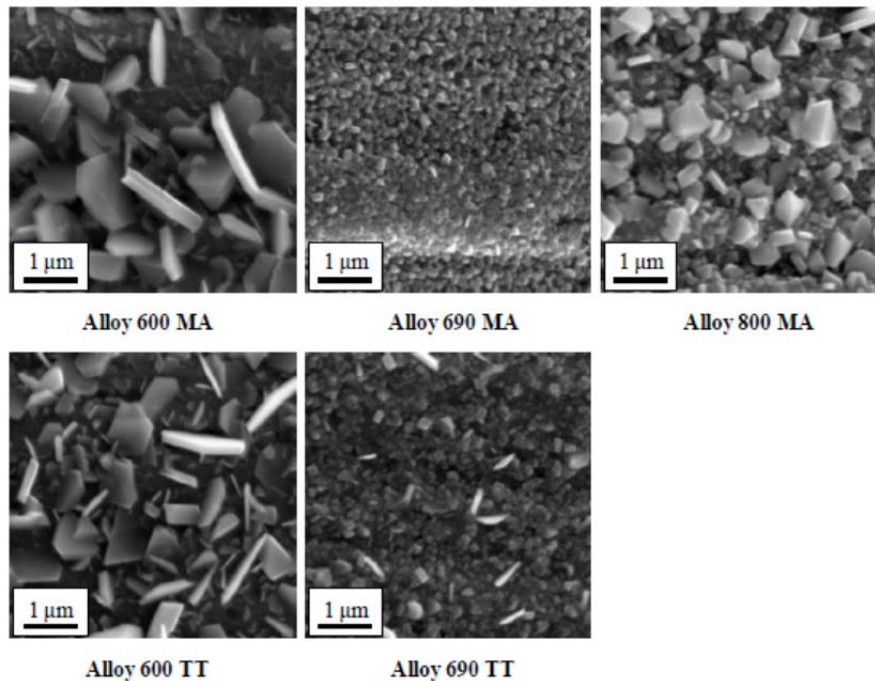


FIG. 5. SEM images of oxides formed on MA specimens (top row) and TT specimens (bottom row) in Run 4.

TABLE 5. EDX ANALYSES ON OXIDES AND UNDERLYING LAYERS OF SPECIMENS FROM RUN 4

Sample	Wt%						
	Ni	Fe	Cr	Ti	Cu	Zr	O
Alloy 600 MA							
-Platelet	34.66	24.04	7.00	4.86	0.61	0.10	28.73
-Underlying layer	64.19	12.40	15.69	1.20	1.04	0.07	5.41
-Before exposure	70.83	9.63	15.40	0.39	-	-	2.00
Alloy 690 MA							
-Crystallite	12.57	49.44	7.41	1.64	0.34	0.17	28.43
-Underlying layer	53.49	12.01	28.99	1.26	0.85	0.1	3.3
-Before exposure	56.37	9.47	27.41	0.33	-	-	6.42
Alloy 800 MA							
-Crystallite	21.54	39.4	8.78	1.95	0.59	0.16	27.58
-Underlying layer	31.55	41.70	21.87	1.12	1.14	0.14	2.48
-Before exposure	31.94	43.04	19.29	0.35	-	-	5.38

Table 5 shows EDX qualitative analyses of specimens from Run 4 on the crystallites and on the underlying layers. The crystallites and underlying layers were Fe-rich and Cr-rich, respectively. Laser-Raman analyses confirm that the crystallites are nickel ferrite; however, there are different spectral shifts from different alloys. These shifts and the differences in Ni/Fe ratio of the crystallites suggest that the stoichiometric ratios of Ni and Fe in the nickel ferrite are different for the oxides on different alloys.

SIMS analyses were performed on Alloy 600 MA and Alloy 690 MA specimens obtained from Run 8; their elemental profiles shown in Fig. 6. The profiles were divided into three domains. The first domain was attributed to the outer oxide layer, which was enriched in Fe. The second domain was attributed to the inner oxide layer, which was enriched in Cr. The first two domains were defined by the point where the Cr intensity reached its maximum value. The third domain was a transition to the base metal, where the intensity of the O reached 50% of its original value. Alloy 600 MA showed no clear zone, since the concentration of most elements decreases with increasing sputtering time. Nonetheless, the boundary between the inner and outer oxide layers was assumed to be where the Cr intensity leveled off before decreasing. Alloy 690 MA and Alloy 800 MA, on the other hand, showed distinct domains. The overall and the outer oxide thicknesses of the three samples were estimated based on the sputtering rate of 1 nm/s, as shown in Table 6. Alloy 800 MA clearly had thicker oxide layers, presumably due to higher Fe content in the base alloy. It is also evident that B from the coolant was incorporated into the inner oxide.

Figure 7 shows Cr 2p<sub>3/2</sub> core level spectra of oxide films formed on Alloy 600 MA, Alloy 690 MA and Alloy 800 MA in Run 8. A main feature of these spectra was observed at a binding energy of about 577 eV, which is a characteristic of Cr<sup>3+</sup>. By using standardized fitting procedures [11], it is evident that the majority of Cr was present as FeCr<sub>2</sub>O<sub>4</sub> – nearly 100% for Alloy 690 MA. Small amounts of Cr<sub>2</sub>O<sub>3</sub> and Cr(OH)<sub>3</sub> were seen. The Cr 2p<sub>3/2</sub> peak intensity on Alloy 690 MA was the highest, followed by Alloy 600 MA and Alloy 800 MA. Since SIMS results indicated that Alloy 600 MA and Alloy 690 had similar thicknesses of oxide film, the amount of Cr in the oxide solely depended on that in the base metal. Alloy 800 MA, on the other hand, had a much thicker oxide film, and XPS analysis could not detect significant amounts of Cr, which was mostly formed as an inner oxide. XPS analysis of the Fe 2p peaks suggested that there was a mixture of Fe<sup>2+</sup> and Fe<sup>3+</sup> as well as a significant amount of FeCr<sub>2</sub>O<sub>4</sub>. It should be noted that since there was a large Ni content, there was an overlap of the Fe 2p signal with a Ni Auger signal, making it more difficult to identify the compound accurately. XPS analysis of the Ni 2p spectra suggested the existence of Ni<sup>2+</sup> species, which includes NiO, NiCr<sub>2</sub>O<sub>4</sub>, NiFe<sub>2</sub>O<sub>4</sub> and Ni(OH)<sub>2</sub>. However, standard peak-fitting procedures failed to generate a good fit [12].

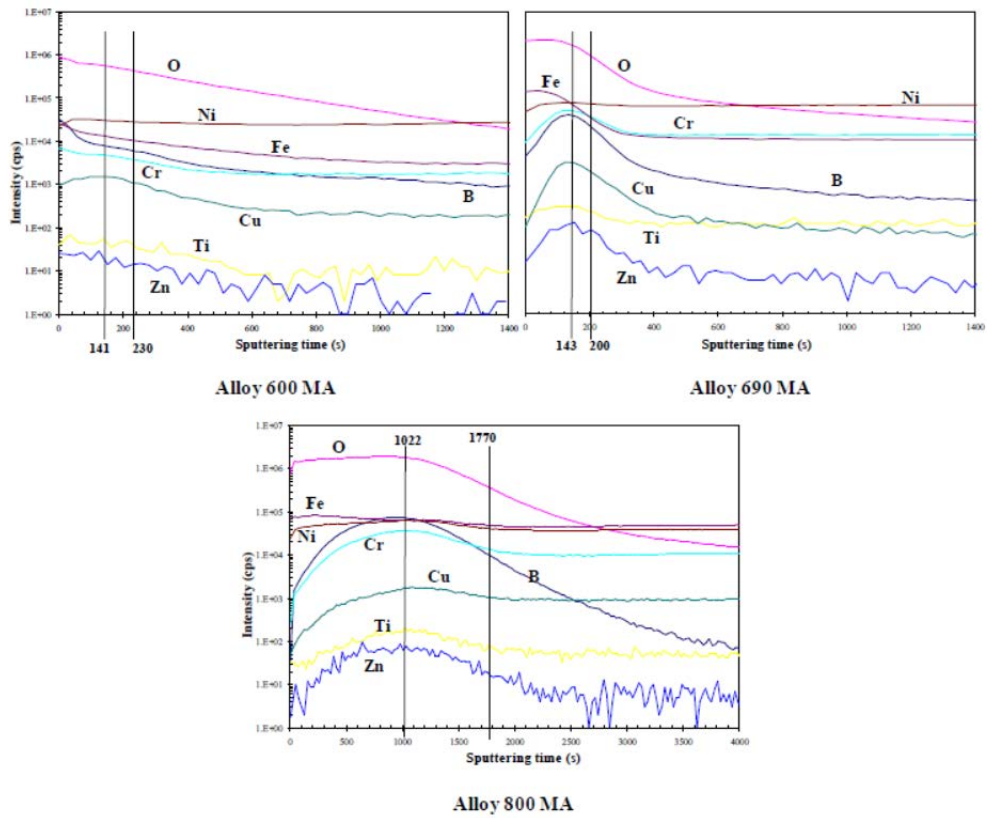


FIG. 6. SIMS elemental profiles of Alloy 600 MA, Alloy 690 MA and Alloy 800 MA in Run 8.

TABLE 6. OXIDE THICKNESSES OF RUN 8 SPECIMENS DETERMINED FROM SIMS

Run 8 specimen	Overall oxide thickness ( $\mu\text{m}$ )	Outer oxide thickness ( $\mu\text{m}$ )
Alloy 600 MA	0.23	0.14
Alloy 690 MA	0.20	0.14
Alloy 800 MA	1.77	1.02

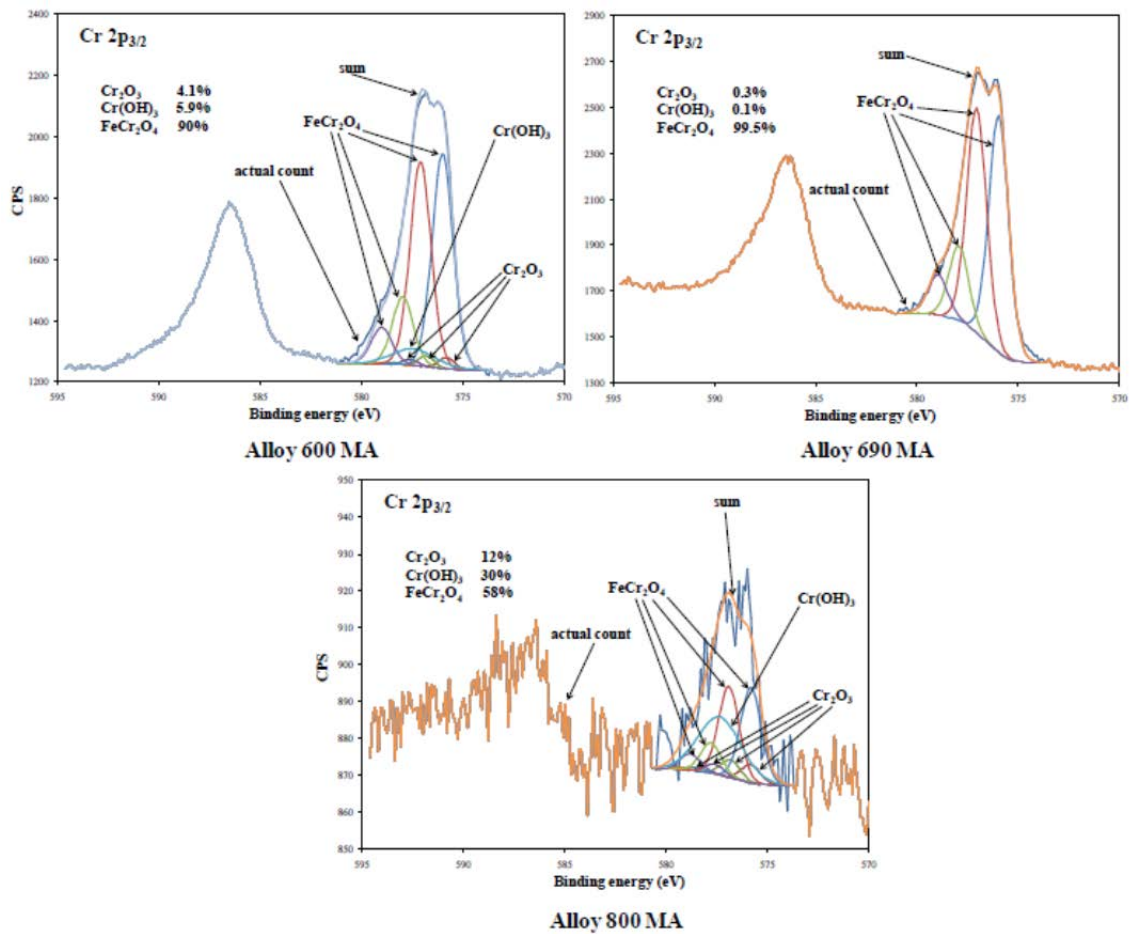


FIG. 7. Cr 2p<sub>3/2</sub> core level spectra of oxide film grown on Alloy 600 MA, Alloy 690 MA and Alloy 800 MA in Run 8.

### 3.4. Effect of SG alloy post-processing

SEM images of Alloy 600, Alloy 690 and Alloy 800 specimens with different post-processing from Run 4 are shown in Fig. 8. It appears that for Alloy 600 and Alloy 690, oxides on TT samples were slightly denser and more compact than those on MA and CD, the two latter having similar morphologies. The largest difference was on Alloy 800, for which SP specimens showed a significantly more compact oxide than MA specimens. This is possibly due to the fact that SP specimens would have had more surface defects, resulting in more oxide nucleation sites. It is clear from Fig. 8 that the effect of post-processing was not so obvious, compared to the effect of alloy composition. These differences may contribute to different material release rates in actual nuclear plants.

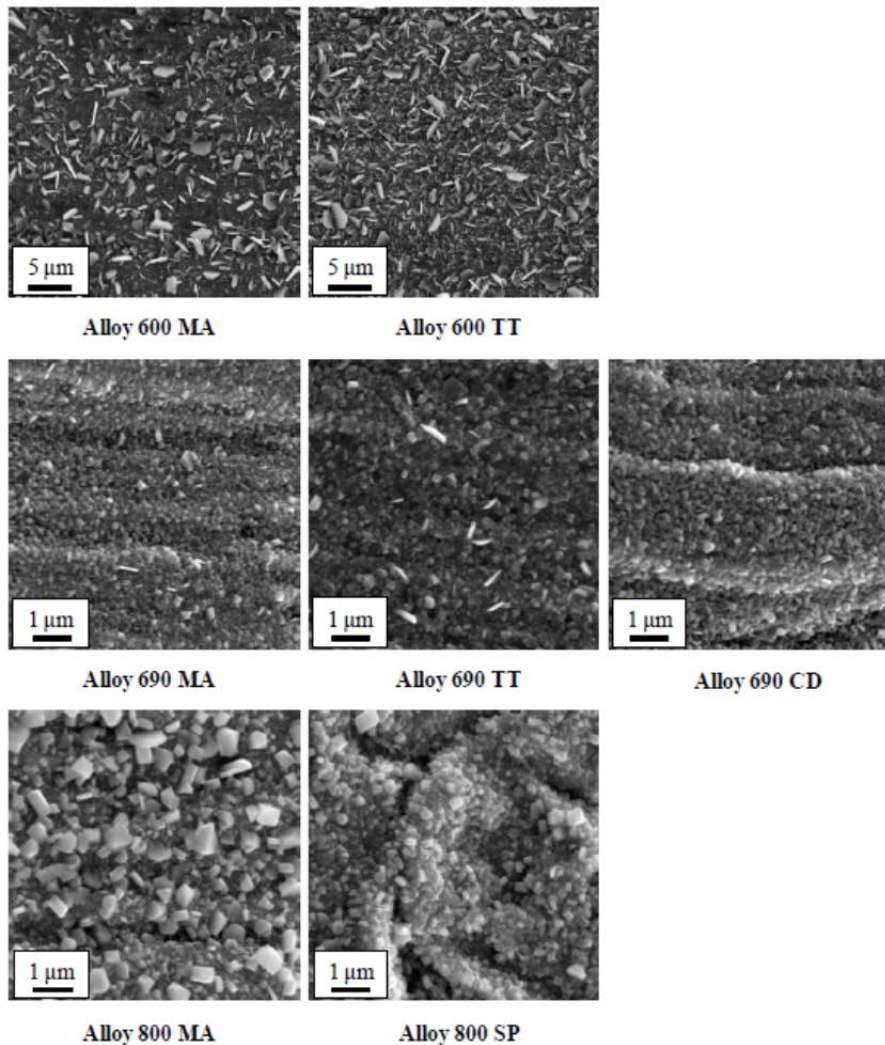


FIG. 8. SEM images of oxides formed on Alloy 600 (top row), Alloy 690 (middle row) and Alloy 800 (bottom row) specimens in Run 4.

### 3.5. Effect of zinc addition

A comparison of oxides formed on specimens exposed to the nominally Zn-free coolant and those exposed to the coolant with 20 ppb Zn is shown in Fig. 9. In both cases, all specimens were covered with large and small crystallites, which were non-uniformly and uniformly distributed, respectively. The small crystallites formed in the coolant containing added Zn were smaller and had higher coverage than those formed in the Zn-free coolant. SIMS results confirmed that Zn prefers to be incorporated in the inner oxide, as shown in Fig. 10. It is generally accepted that  $Zn^{2+}$  is incorporated in the oxide in preference to the other divalent ions  $Ni^{2+}$  and  $Fe^{2+}$ , resulting in a “release” of such displaced ions by diffusion through the oxide to the coolant [13]. The concentration of Zn in the inner layer presumably accounts for why Zn was not detected by XPS, which just scanned the outer surfaces. This observation is discussed later. The same authors [13] also suggest that the incorporation of Zn can result in the formation of more stable oxides, e.g.  $ZnCr_2O_4$  in the inner oxide and  $ZnFe_2O_4$  in the outer oxide. The stability of the former oxide, but not the latter, has been established for some time [14]. The change of the structure and the more stable oxide increase oxide nucleation rate, causing the formation of a large number of small crystallites at the base of the outer layer close to the inner layer. This is consistent with the observations in this study, as shown in Fig. 9.

Under the same criteria to identify the overall and the inner oxide thicknesses as previously discussed, the thicknesses of oxides formed on Alloy 690 MA in the Zn-free and the 20-ppb Zn

coolants are tabulated and compared in Table 7. Unexpectedly, because Zn is usually an effective inhibitor, the results show thicker oxides in the coolant with Zn. However, it is clear from Fig. 9 that Zn was present also in the experiment that was supposed to be Zn-free, since the inner layer on the Alloy 690 MA in that run incorporated a significant amount of Zn, no doubt from impurity contamination. In fact, measurements of the Zn content of the de-ionised water used in Run 8 and of the Zn content of the coolant after the run, and a review of the experimental procedures, led to the conclusion that the Zn contamination in that run originated in a lubricant that was applied to the autoclave bolts before assembly.

As mentioned earlier, XPS results in Table 8 show no Zn on the specimens. This was presumably because the outer oxide layer obscured the inner layer. Interestingly, however, specimens from both runs showed significant amounts of Cr, which would have been in the inner layers (the lesser proportion of Cr analysed by XPS on the specimen exposed to Zn-containing solution is consistent with its having a thicker outer layer). Unfortunately, the presence of Zn in both Runs 8 and 9 makes conclusions about its effect uncertain, although it is clear that it concentrates in the inner oxide layers.

There were no observations of Zn effects on the oxides formed on zirc-4.

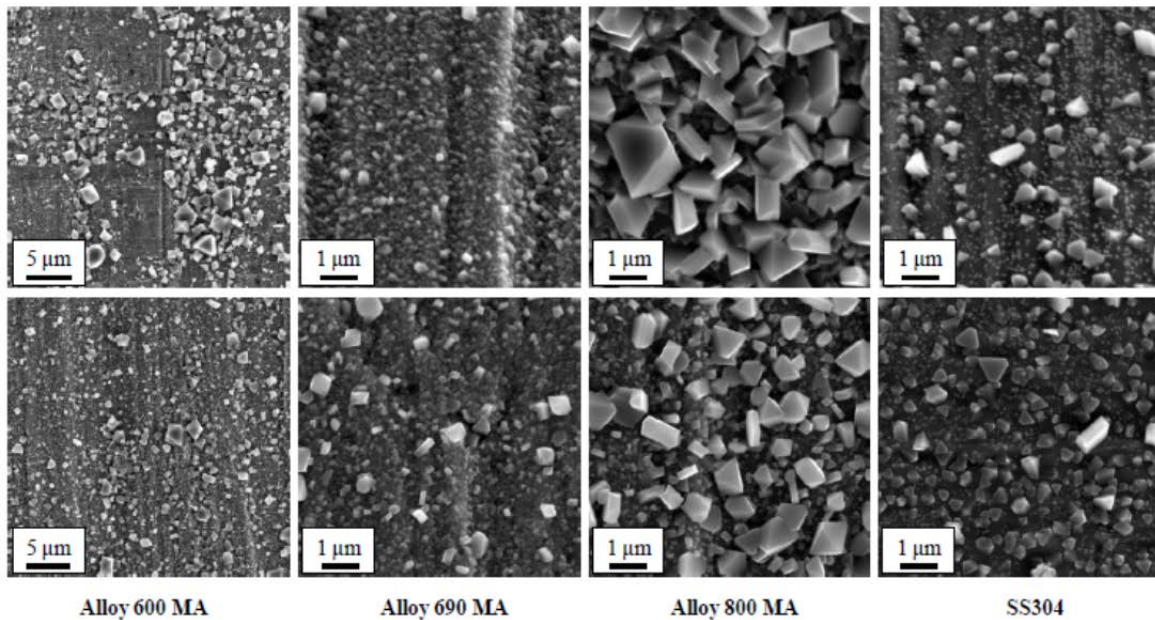


FIG. 9. SEM images of oxides on specimens exposed to coolant without Zn (top row) and with 20 ppb Zn (bottom row) from Runs 8 and 9.

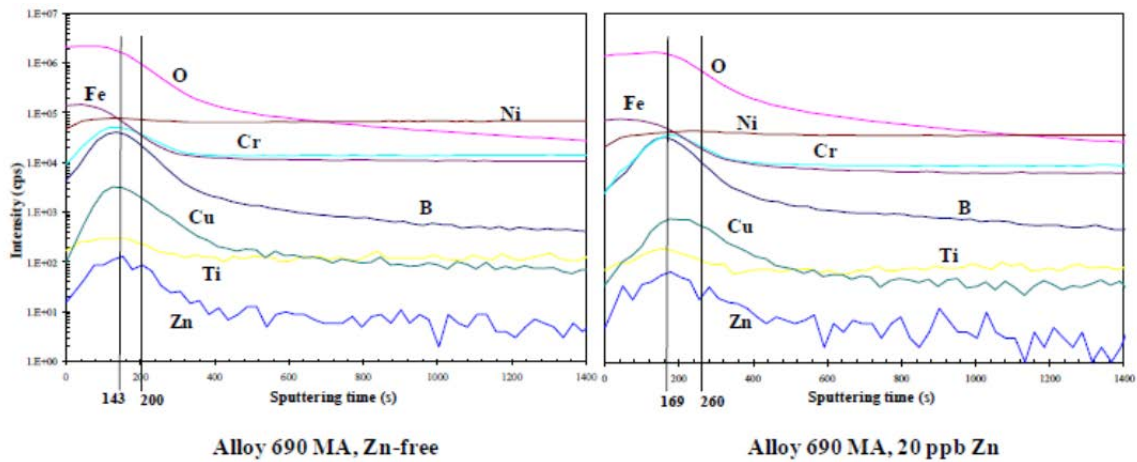


FIG. 10. SIMS elemental profiles of Alloy 690 MA specimens in zinc-free and 20-ppb-zinc coolant from Runs 8 and 9.

TABLE 7. OXIDE THICKNESSES OF ALLOY 690 MA SPECIMENS DETERMINED FROM SIMS

Sample	Overall oxide thickness ( $\mu\text{m}$ )	Inner oxide thickness ( $\mu\text{m}$ )
Run 8 (Zn-free) Alloy 690 MA	0.20	0.06
Run 9 (20 ppb Zn) Alloy 690 MA	0.26	0.09

TABLE 8: XPS ANALYSIS OF OXIDE FILM GROWN ON ALLOY 690 MA SPECIMENS

Sample	At%					
	Ni	Fe	Cr	O	B	Si
Run 8 (Zn-free) Alloy 690 MA	4.7	13.2	9.2	71.1	0.6	1.2
Run 9 (20 ppb Zn) Alloy 690 MA	9.3	16.7	4.1	69.5	very low	0.4

#### 4. CONCLUSIONS

This paper presents the characterization of oxide films grown on SG materials (Ni-based alloys), type 304 stainless steel and zircaloy-4 in simulated PWR primary coolant. The results indicate that the morphologies of these oxides depend on coolant chemistry, composition of the material and post-processing. The oxides formed on SG materials and SS304 were duplex – an Fe-rich layer (apparently based on  $\text{NiFe}_2\text{O}_4$ ) overlaying a Cr-rich layer (apparently based on  $\text{FeCr}_2\text{O}_4$ ) – while the oxide formed on zirc-4 was a single oxide layer (presumably  $\text{ZrO}_2$ ).

The major effect on oxide morphology was from SG alloy composition. For the outer oxide layer, platelet crystallites were found on Alloy 600, whereas on Alloy 690 and Alloy 800, the crystallites were octahedral.

The oxides formed on SG alloys and SS304 in the coolant containing both boron and lithium were more compact than those in the coolant without boron. The effect of boron on zirc-4 was observed only in the presence of heat flux through the zirc-4 surface, where the presence of boron

reduced corrosion rate somewhat. Boron was incorporated in the inner oxide layer on Alloy 600 MA, Alloy 690 MA and Alloy 800 MA.

For the same post-processing treatment of SG alloys, the higher the Cr content of the alloy, the more compact the oxide. Effects of SG alloy post-processing were also observed on all alloys, but were not so obvious as the effects of alloy composition. The largest effect was for Alloy 800, for which SP material formed significantly more compact oxide with smaller outer-layer crystallites than MA material.

Alloy 600 grew a heavier oxide layer during 30 days in coolant at  $pH_{300^{\circ}C}$  of 7.4 than during five or ten days in coolant at  $pH_{300^{\circ}C}$  of 7.1.

Zinc as a coolant additive was incorporated in the inner oxide layers on SG alloys and SS304. There was no effect of Zn on oxide formed on zirc-4.

Observed differences in oxide characteristics may contribute to different material release rates from steam generators in nuclear plants.

## ACKNOWLEDGEMENT

The authors would like to thank the Natural Sciences and Research Council of Canada and the CANDU Owners Group for financial support.

## REFERENCES

- [1] Root cause investigation of axial power offset anomaly. EPRI TR-108320, (1997).
- [2] Primary water chemistry, fuel rod corrosion, and crud deposition in PWRs: A comparison of the European and U.S. plant performance. EPRI TR-107255, (1996).
- [3] US NRC, Steam generator tube issues. (2004).
- [4] BATES, J.C., LANCASTER, G.A., SCRANCHER, M., GARBETT, K., Corrosion product monitoring during the seventh refuelling outage at Sizewell B. Proc. Int. Conf. on Water Chemistry of Nuclear Reactor Systems, Jeju Island, South Korea, (2006)
- [5] LISTER, D.H., SRISUKVATANANAN, P., FEICHT, A., INTASOPA, G., LUTTIKUL, A. Final report on laboratory studies of the effects of steam generator tube characteristics on oxide formation under PWR primary coolant conditions, IAEA Coordinated Research Project FUWAC (2006–2010) — Optimization of Water Chemistry to ensure Reliable Water Reactor Fuel Performance at High Burnup and in Aging Plant. IAEA-TECDOC-1666, IAEA, Vienna (2011).
- [6] Standard specification for seamless nickel and nickel alloy condenser and heat exchanger tubes. ASTM B163-04, (2005).
- [7] ASM Handbook: Heat Treating. Vol. 4. ASM International. (1991)
- [8] Review of in-reactor Zircaloy corrosion and crud deposition experience at AECL. EPRI NP-1254 (1979).
- [9] BYERS, W.A., JACKO, R.J. The influence of zinc additions and PWR primary water chemistry on surface films that form on nickel base alloys and stainless steels. Proc. Sixth International Symposium on Environmental Degradation of Materials in Nuclear Power Systems – Water Reactors, San Diego, California, (1993).
- [10] COX, B., UNGURELU, M., WONG, Y.M., WU, C. Mechanism of LiOH degradation and H<sub>3</sub>BO<sub>3</sub> repair of ZrO<sub>2</sub> film. Proc. Zirconium in the Nuclear Industry: Eleventh International Symposium, ASTM STP 1295, (1996).
- [11] BIESINGER, M.C., BROWN, C., MYCROFT, J.R., DAVIDSON, R.D., MCINTYRE, N.S. XPS studies of chromium compounds. Surface and Interface Analysis, **36** (2004) 1550–1563.

- [12] BIESINGER, M.C., PAYNE, B.P., LAU, L.W.M., GERSON, A., AND SMART, R.S.C. "X-ray photoelectron spectroscopic chemical state quantification of mixed nickel metal, oxide and hydroxide systems". *Surface and Interface Analysis*, **41** (2009) 324–332.
- [13] ZIEMNIAK, S.E. AND HANSON, M., Zinc treatment effects on corrosion behaviour of 304 stainless steel in high temperature, hydrogenated water. *Corrosion Science*, **48** (2006), 2525–2546.
- [14] LISTER, D.H. Activity transport and corrosion processes in PWRs. *Nuclear Energy*, **32** (1993) 103–114.

# PRIMARY CIRCUIT WATER CHEMISTRY AND IMPACT ON FUEL CLADDING CORROSION

V. MARAKHYAN  
Armenia NPP,  
Armenia

## Abstract

It is intended to extend the operation of the Armenia NPP. To help this project it is necessary to understand the processes used in foreign WWER-440 NPPs for controlling and maintaining water chemistry parameters. The paper describes the issues around cladding corrosion for Armenia NPP.

## 1. INTRODUCTION

Chemistry control is one of the most important factors affecting the safe, economical and safe operation of nuclear power plants.

## 2. OPERATIONAL REQUIREMENTS

There are a number of basic requirements for nuclear power plant water chemistry, including:

- Nuclear power plant water chemistry should be established to organize and sustain in such a way as to protect the integrity of protective barriers.
- Corrosion effect of coolant and other working environments on construction materials, equipment and piping systems and other plant should not lead to a breach of the limits and conditions for safe operation of nuclear power plants.
- Nuclear power plant water chemistry should provide a minimum amount of deposits on heat transfer surfaces of equipment and pipelines.
- Nuclear power plant water chemistry should be directed at reducing the radiation fields arising from ionizing radiation activated corrosion products, forming deposits on the surfaces of equipment and pipelines of nuclear power plants.
- To reduce the intensity of corrosion processes necessary to ensure sustainable maintenance of the coolant and to limit the concentration of aggressive, corrosive impurities: chloride, fluoride ions and oxygen.

The high concentration of chloride and fluoride ions in the coolant requires removing their source from make-up water or dosed reagents, as well as increasing the efficiency of cleaning fluid on the special water purification.

The high concentration of oxygen in the coolant requires removal of the oxygen concentration in the make-up water or also dosing with solutions of reagents to ensure efficient binding of oxygen by increasing the concentration of hydrogen in the normalized range of additional input or hydrazine hydrate.

## 3. FUEL BEHAVIOUR

Profitability of nuclear power reactors depends on fuel efficiency, which is determined by the level of burnup achieved. Among the key factors determining the efficiency of fuel at high burnup, is changing the elemental composition of the fuel due to the accumulation of fission products.

Alloys based on zirconium are the most important element of structural material in the cores of power reactors with coolant water under pressure.

### 3.1. Oxidation

In operating nuclear power plants, corrosion processes occur due to exposure to water. On the zirconium fuel cladding different types of corrosion phenomena take place:

- Uniform or front corrosion;
- Fretting corrosion;
- Debris corrosion;
- Corrosion under the sediment and deposition of suspended and dissolved particles in the coolant.

The last two types of corrosion observed for deviations from the standard indicators of water — chemical conditions (water chemistry) or in violation of the operating rules.

Corrosion of zirconium alloys is the oxidation of the samples and their hydrogenation. At the initial stage of oxidation, water molecules are adsorbed on to the corrosive surface of the sample and capturing electrons dissociate to oxygen ions and protons. Further, the oxygen dissolves in the metal and when its concentration reaches 30% of the surface oxide film occurs zirconium oxide. The newly formed oxygen ions diffuse through the film and reaching the metal increasing its thickness.

When the film thickness reaches 2–3  $\mu\text{m}$ , a transition to linear oxidation kinetics occurs. In general, the process of destruction of the hydrogenated alloy takes place in three stages:

- Cracks in the brittle phase;
- Destruction of hydride and out of cracks in the matrix;
- Distribute crack in the matrix.

Frequent cases of damage to the shells of zirconium hydride is the formation of large blisters, known as “solar explosions” (sunbursts).

### 3.2. Deposition

Deposits on heat transfer surfaces of reactors, in particular the fuel cladding, leads to a reduction of the heat transfer coefficient, and consequently to increase the temperature of the shells, which may yield a fuel element failure.

The formation of sediments is the physical and chemical processes occurring near the heat transfer surface, resulting in the formation of solid particles that can be deposited on the heat transfer surface.

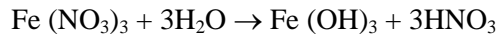
Corrosion products that have fallen into the water, are in dissolved and undissolved forms. Insoluble corrosion products having particle sizes exceeding 10 microns are deposited in stagnant zones and zones with reduced speed of water circulation, for example in the deaerator. Fine corrosion products and substances in the dissolved and colloidal states, carried by water and deposited on the surface of the main circulation circuit. Only a small fraction of corrosion products remain suspended in the circulating water.

The chemical composition of sediments are determined by the material as the main circulation circuit, and the condensate feed tract. The bulk of the sediment was iron oxides followed by oxides of nickel and chromium. Changing the pH and oxygen content in water has a significant influence on the corrosion of structural materials and the removal of corrosion products. It would be logical to assume a similar effect of these factors on the rate of deposition. In practice, there is a different picture: in the ammonia-hydrazine water regime with a high pH of circulating water in the fuel rods produce large deposits of low thermal conductivity, there have been cases burnout cladding. A satisfactory explanation for this phenomenon is not found.

Obviously only that, the neutral water regime corrosion products contained in the water in the form of oxides of different degrees of dispersion, with the water passing through the reactor core does not take a strong liking to the fuel cladding. Later the particles apparently connected to each other, larger and accumulate in stagnant zones.

With an ammonia-hydrazine water regime, a consequence of the radiolysis of ammonia in the presence of oxygen is a nitric acid concentration up to 1.5 mg/liter.

Radiolysis of water enhances the corrosion of austenitic stainless steel as a consequence of large quantities of oxygen. Corrosion is aggravated by chlorine ion. Nitric acid also increases the corrosion rate and accelerates the formation of deposits on the surfaces of fuel rods. Nitric acid is neutralized with ammonia, which at high temperature is little dissociated.



Iron hydroxide will deposit. Maximum deposition of corrosion products occurs in the zone of boiling.

On the one hand, the high rate of circulating water through high flow turbulence increases the frequency of particle collisions with the walls and each other, which may contribute to coagulation and deposition of particles.

On the other hand, a higher flow rate may have erosive effects on the sediment. In fact, noted that the deposits occur mainly in the field where the velocity of the fluid is around  $5\text{--}6 \text{ m}\cdot\text{s}^{-1}$ . Increase of the heat flow leads to an increase in deposits. This is most evident in a marked increase in the number of deposits on fuel cladding in the core center as compared with the amount of deposits in the peripheral areas, where the level of energy is lower.

Measures to prevent deposition of corrosion products in the first circuit unit with WWER-440 may include:

- Filling loop de-aerated water with hydrazine;
- Raising the pH of circulating water with the addition of ammonia;
- Maintaining optimal water regime, including the suppression of radiolysis;
- Conservation equipment available during a reactor outage.

When operating a fuel element in WWER-type reactor consider the following mechanical and thermal processes:

- Thermoelastic expansion of the fuel and cladding ;
- Creep of fuel and cladding;
- Plastic deformation of the shell, if implemented at the output of the fuel element to the nominal power, and manoeuvring power;
- Swelling of the fuel;
- Radiation growth shell;
- Separation of gaseous fission products under the cladding;
- Cracking and fragmentation of the fuel pellets;
- Reconstruction of the microstructure of fuel;
- Molecular, contact, radioactive conductivity of the gas gap;
- Mechanical interaction between fuel column to sheath;
- Damage and fracture of the shell material under stress corrosion.

One of the important requirements for core materials of reactors is the low absorption of hydrogen. The degree of hydrogenation of zirconium alloys for long term use is determined primarily by the intensity of corrosion and temperature.

#### 4. CONCLUSION

The need to justify the extension of station operation requires highly complex works in the collection, storage and processing of data from foreign nuclear power plants with WWER-440, as well as possible, and to develop additional approaches to the improvement of water chemistry.

# THE TESTS OF WATER CHEMISTRY EFFECT ON CORROSION BEHAVIOUR OF CLADDING

B. GONG,  
Reactor Engineering Research Sub Institute,  
Nuclear Power Institute of China

X. SU, C. LI, Z. ZHOU  
Materials Research Sub Institute,  
Nuclear Power Institute of China

China

## Abstract

To investigate the effect of improved primary water chemistry of PWR on corrosion behaviour of cladding, a project on compatibility of high content water chemistry and advanced cladding materials is in progress in NPIC during recent years. The modified Zr-4 and M5 alloys were tested in water with lithium at 3.50~6.48mg/L and boron at 983~3000mg/L for 3000 hours. For simulation of water-vapor environment around the surface of cladding, electrical heating elements were manufactured from modified Zr-4 and M5 cladding tubes. These elements were tested in water loops at 310°C and 15.5MPa with surface temperature of 346°C. The test results revealed that high concentration of lithium at same pH will accelerate the general corrosion rate and the hydrogen pick-up to a certain extent. Variation of pH300°C from 6.5 to 7.2 had no obvious influence on corrosion rate at 3.50 mg/l lithium. But the weight loss occurred when the boric acid content decreased to 6.48mg/l lithium. The weight gain difference between M5 and modified Zr-4 in single water phase was imperceptible. The thicker oxide layer with heavy deposits was formed on the boiling section of M5 elements; however the hydrogen absorption did not exceed that of modified Zr-4. It may imply that the M5 alloy is more sensitive to “oxidation introduced deposition” under sub-cooled nucleate boiling condition, especially when oxygen is saturated.

## 1. INTRODUCTION

In order to realize higher burnup of fuel elements in advanced reactors, the initial inventory of  $^{235}\text{U}$  is designed to be increased and the content of boric acid will be also increased for necessary neutron absorption. To maintain the pH of coolants in normal ranges and inhibit corrosion of structure materials, the content of lithium hydroxide will be improved proportionately. However, the higher concentration of lithium may accelerate corrosion and deposition on the cladding surface that will result in the low heat transfer efficiency, even in the failures of fuel elements.

To investigate improved water chemistry effect on the corrosion behaviours of cladding for PWR, a project on the compatibility of the high content water chemistry and advanced cladding materials is in progress in NPIC during recent years. The out-of-pile experiments have been performed to evaluate oxidation and deposition on modified zircaloy-4 and M5 [1] cladding tubes in the different water chemistry with increased lithium and boric content.

## 2. EXPERIMENTS

### 2.1. Test objects

Modified zircaloy-4 (low tin content) tubing (9.5 mm OD, 0.57 mm thick), AFA-2G and M5 alloy tubing (9.5 mm OD, 0.57 mm thick) for AFA-3G are used for the long term corrosion tests. The main chemical composition of materials is listed in Table 1 and Table 2.

TABLE 1. THE MAIN CHEMICAL COMPOSITION OF MODIFIED ZIRCALOY-4 (WT%)

Element	wt%
C	0.0133~0.0180
Cr	0.07~0.11
Fe	0.18~0.24
Fe+Cr	0.28~0.33
O	0.1000~0.1500
Si	0.0070~0.0120
Sn	1.20~1.50
Zr	balance

TABLE 2. THE MAIN CHEMICAL COMPOSITION OF M5 (WT%)

O	Nb	S	Zr
0.1390~0.1450	0.98~1.01	0.0022~0.0035	balance

For investigating the effect of sub-cooled nucleate boiling on the development of oxide layer and deposits, these tubes are manufactured into self-heating elements (9.5 mm OD, full length of 525mm, heat length of 100mm) to generate heat flux and water-steam environment around the tube wall. As the structure showed in Fig. 1, the internal tubes with electrical wires and insulators are extruded into heating elements and installed into the tested tubes with vacuum electron beam welding at both ends. This element-in-tube structure is designed to keep primary size and surface state before tests. Helium is injected between the gap of internal element and tested tube for the general heat transfer. A 4×4 unit (50.8mm×50.8mm×43.0mm) of spacer grid is fixed on the heating section of elements group (two modified zircaloy-4 elements and two M5 elements) for a simulation of concentrated crevice chemistry, as shown in Fig. 2.

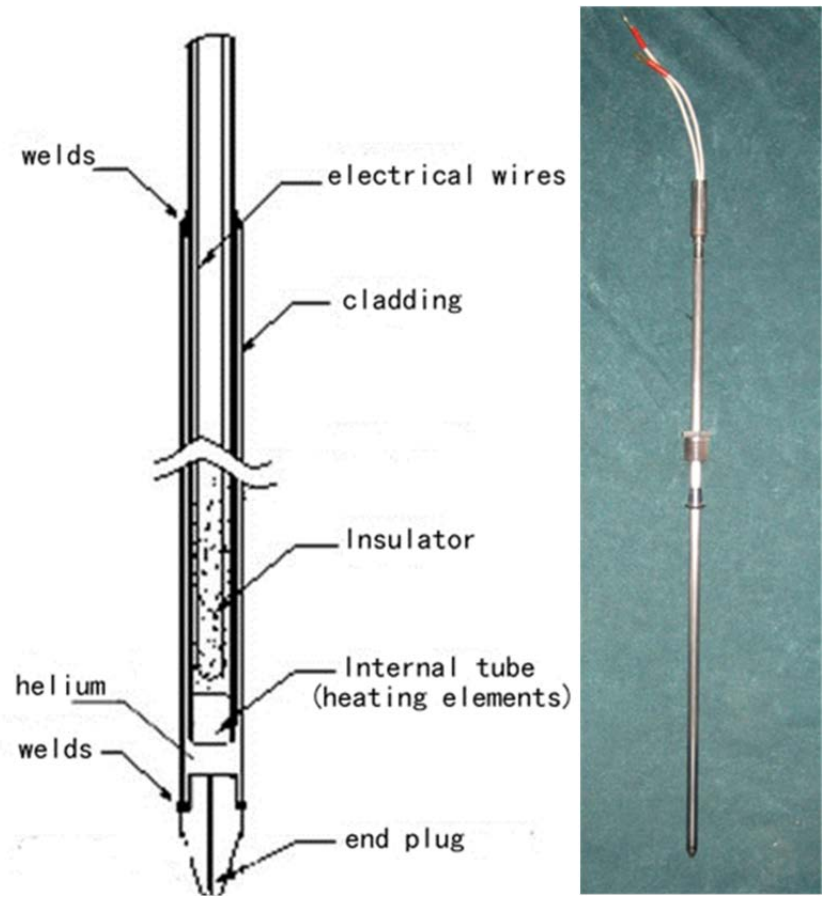


FIG. 1. Structure and appearance of self-heating elements.

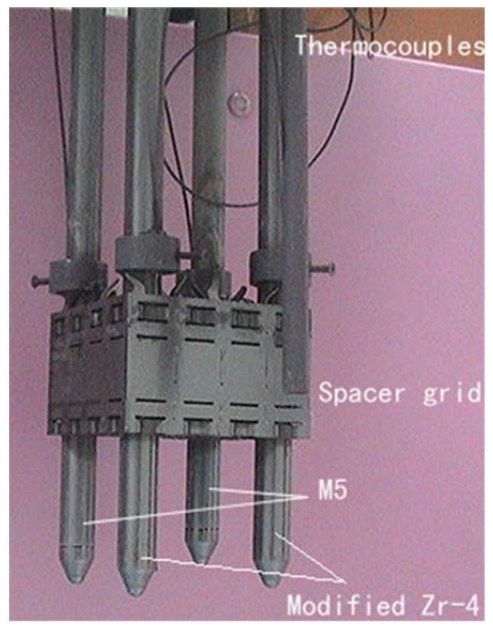


FIG. 2. Elements group before tests.

In addition, some samples of modified zircaloy-4 and M5 tubes are installed around the elements to follow the weight gain in single phase water, as shown in Fig. 3.



FIG. 3. Samples of tubes for weight gain measurement.

## 2.2. Test equipment

The element groups are immersed in the two Hastelloy C276 autoclaves for corrosion tests, as showed in Fig. 4. The temperature of elements and autoclaves are controlled separately. Thermocouples are fixed on the heating section of elements and in the different area of the autoclave for precise temperature monitoring. A mini type recirculation loop manufactured of Hastelloy C-276 and 316SS is connected with each autoclave for continuous water replenishment (5L/h flow rate) and maintenance of heat balance between elements surface and fluid. The loop is composed of high pressure pump, heat exchanger, preheater, coolers, pressure regulator and water sample and purification system, shown in Fig. 5.

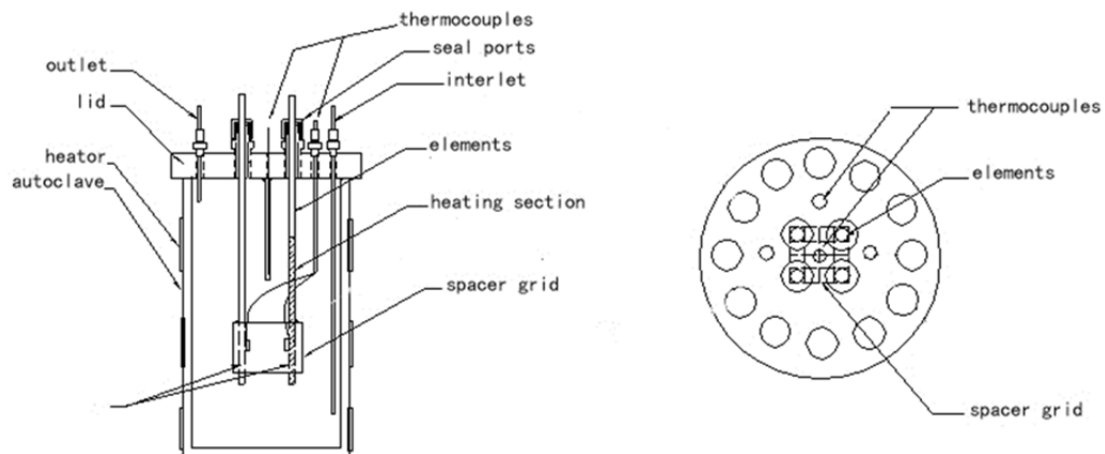
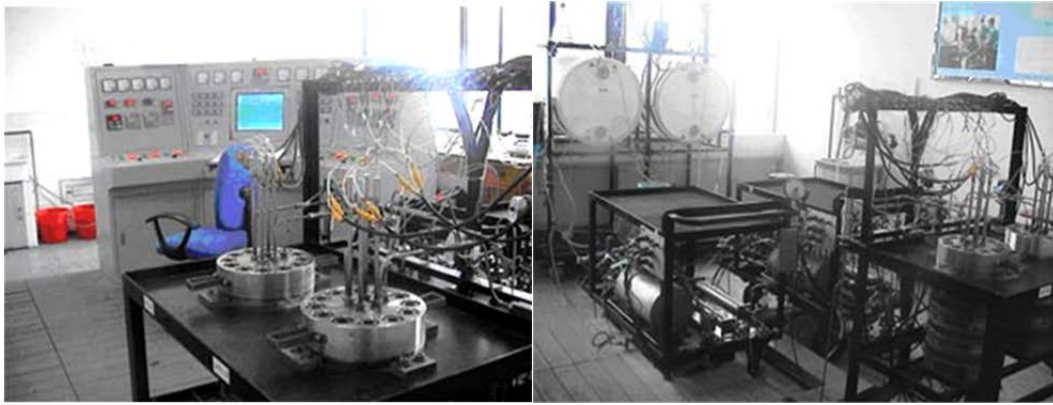
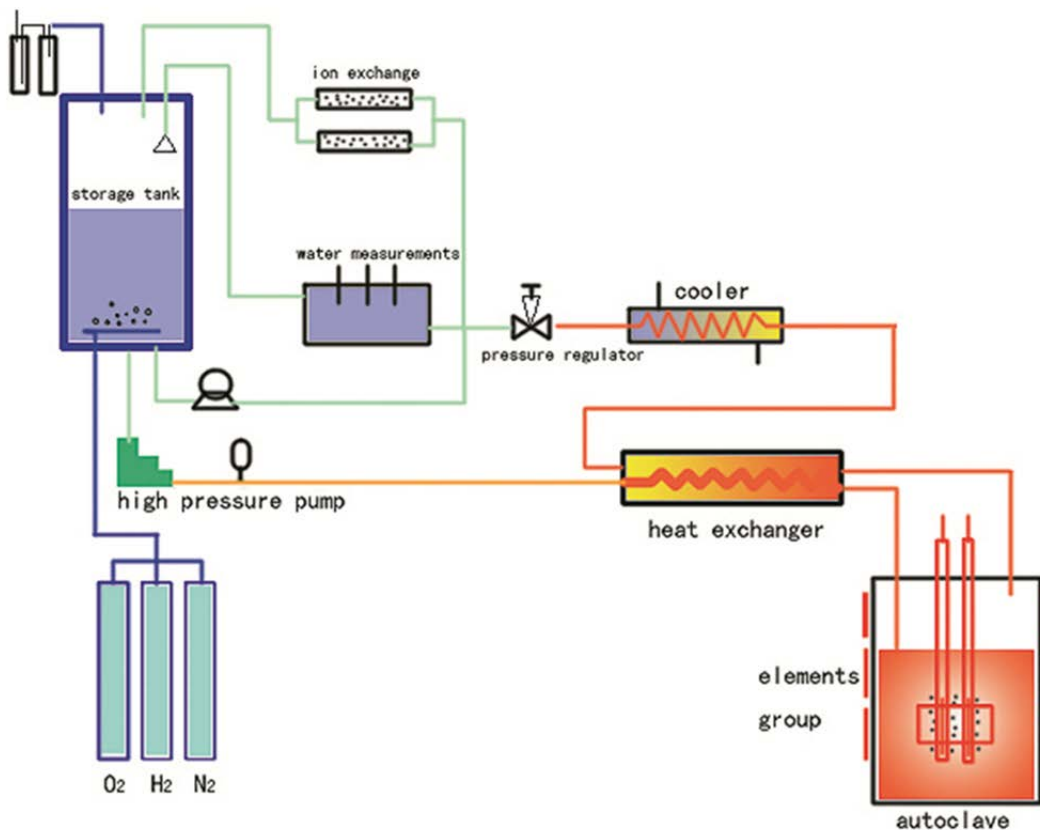


FIG. 4. Elements group in the autoclave.



(a) Autoclaves mounted with elements      (b) Mini type recirculation loops



(c) The flow diagram of recirculation loop

FIG. 5. The Mini type recirculation loops for corrosion tests.

### 2.3. Test variables

Four types of water chemistry conditions are chosen for the tests. The two solutions contain 3.50 mg/L lithium are used for evaluation on the corrosion risk in the maximum limit or an “out-of-specification” water chemistry in the plants. The other two solutions contain 6.48 mg/L lithium for evaluation on the corrosion extent at higher concentration of lithium. The pH values at 300°C are calculated to be 6.9 and 7.2 with different boric and lithium content listed in Table 3. All solutions are not deoxidized and dissolved oxygen content is 8ppm for acceleration of corrosion.

TABLE 3. WATER CHEMISTRY CONDITIONS

	1#	2#	3#	4#
pH <sub>300°C</sub>	6.9	7.2	6.9	7.2
B (mg/L)	1887	983	3000	1703
Li (mg/L)	3.5	3.5	6.48	6.48

Under each water chemistry, the elements of modified zircaloy-4 and M5 are tested at 310°C and 15.5 MPa for 3000 hours. The surface temperature of elements is controlled to be 346°C with heat flux density of 200000W/m<sup>2</sup>. According to the calculation, the temperature difference between elements wall and fluid will produce nucleate boiling on the surface of elements without bulk boiling in the autoclave.

### 3. RESULTS AND DISCUSSION

#### 3.1. General corrosion in single phase water

The corrosion kinetic curves in the single phase water are shown in Fig. 6. Both materials show slow weight gain when exposed to the 1#, 2# and 3# water conditions. The maximum weight gain is obtained in 3# condition, 23mg/dm<sup>2</sup> for M5 and 19mg/dm<sup>2</sup> for modified zircaloy-4. The minimum weight gain is obtained in 1# condition, 17mg/dm<sup>2</sup> for M5 and 14mg/dm<sup>2</sup> for modified zircaloy-4, respectively. When exposed to the 4# condition, both materials show weight loss after the weight gain reaches a peak value in 500 hours. Compared with modified zircaloy-4, the M5 samples show higher weight gain in the first three water conditions and greater weight loss in the 4# condition.

The colour of samples after the tests in four water conditions is black and quite similar. No evidence of local corrosion is found by visual inspections, as shown in Fig. 7.

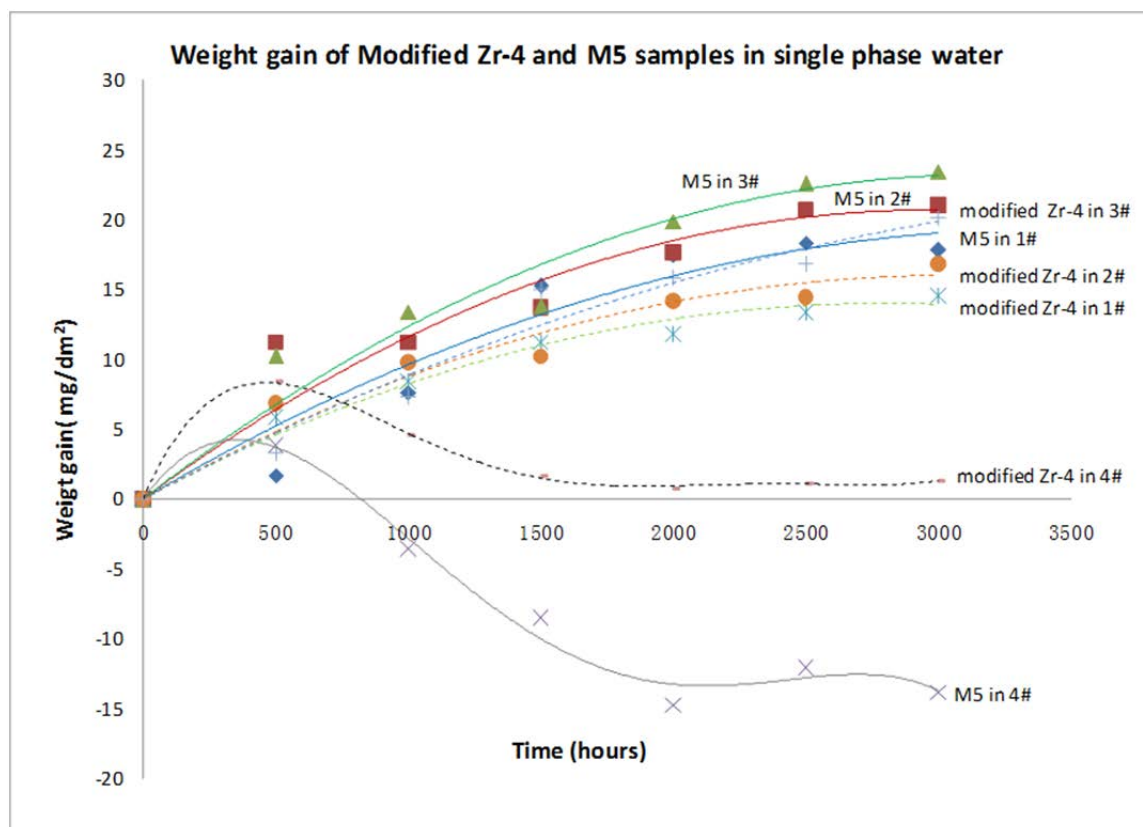
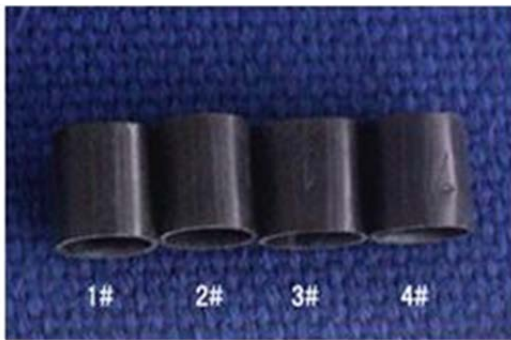
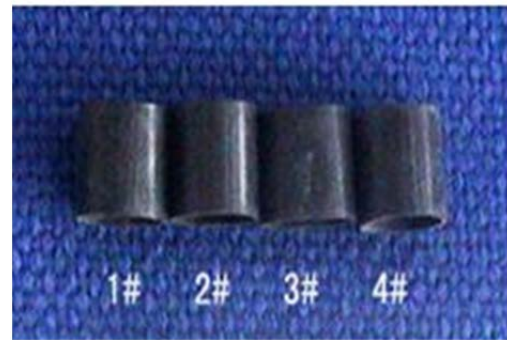


FIG. 6. The weight gain vs. time of modified Zr-4 and M5 exposed to 1#~4# water chemistry conditions at 310°C and 15.5 MPa.



(a) M5



(b) Modified Zr-4

FIG. 7. Tube samples after 3000h tests at 310°C and 15.5 MPa in the 1#~4# conditions.

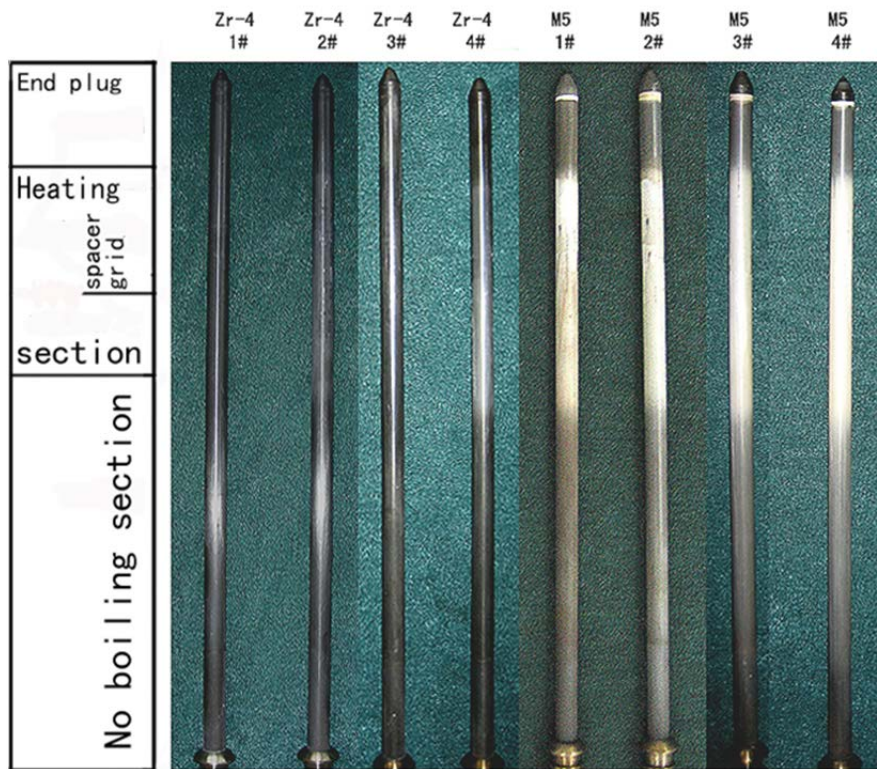
### 3.2. Corrosion and deposits under surface boiling conditions

The appearance of elements after tests in four conditions is shown in Fig. 8. No local corrosion attack is found in the area between element and spacer grid. However, for the M5 elements, the heating section where surface boiling happened is covered by white layer. A white ring is also found near the welding seam and the grey film is formed on other regions where the temperature is lower than heating section. The modified zircaloy-4 elements show black appearance as that of tube samples only except a slight transition to white on the heat section of elements in 4# condition.



(a) Elements group after 3000h test in 4# water condition.

FIG. 8. The appearance of elements after 3000h tests in 1#~4# water conditions.



(b) Elements after 300h test in 1#~ 4# water conditions.

FIG. 8. The appearance of elements after 3000h tests in 1#~4# water conditions.

The XRD analysis indicates that the white layer formed on the M5 elements consist of  $ZrO_2$  and Zeolite deposits. The black film formed on the modified zircaloy-4 elements has been revealed [2] to be protective  $ZrO_2$  with high proportion of tetragonal structure.

The cross section and thickness of layer is inspected by optical microscopy, as shown in Figs 9 and 10. The layer on the heating section of M5 elements is about five times thicker than that of Modified zircaloy-4 elements. With increase of lithium content or decrease of boric at same lithium content, the layer thickness of M5 elements increases from  $15\mu m$  to  $25\mu m$ . Different from M5 elements, the layer thickness of modified zircaloy-4 elements increases slightly from  $3.0\mu m$  to  $3.6\mu m$ .

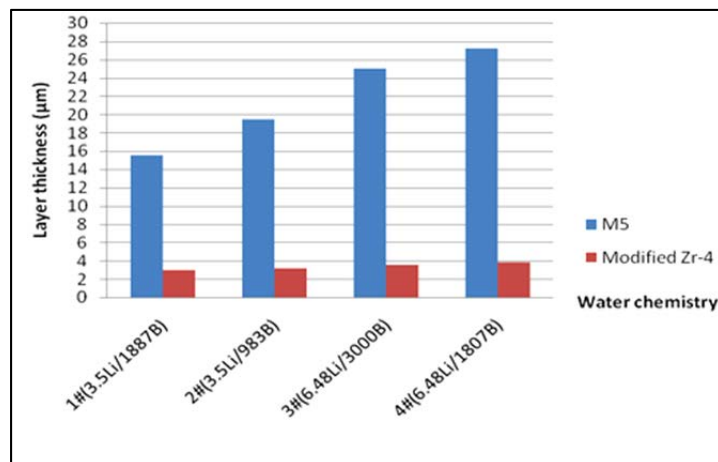


FIG. 9. Layer thickness of the heating section of modified Zr-4 and M5 elements after 3000h tests.

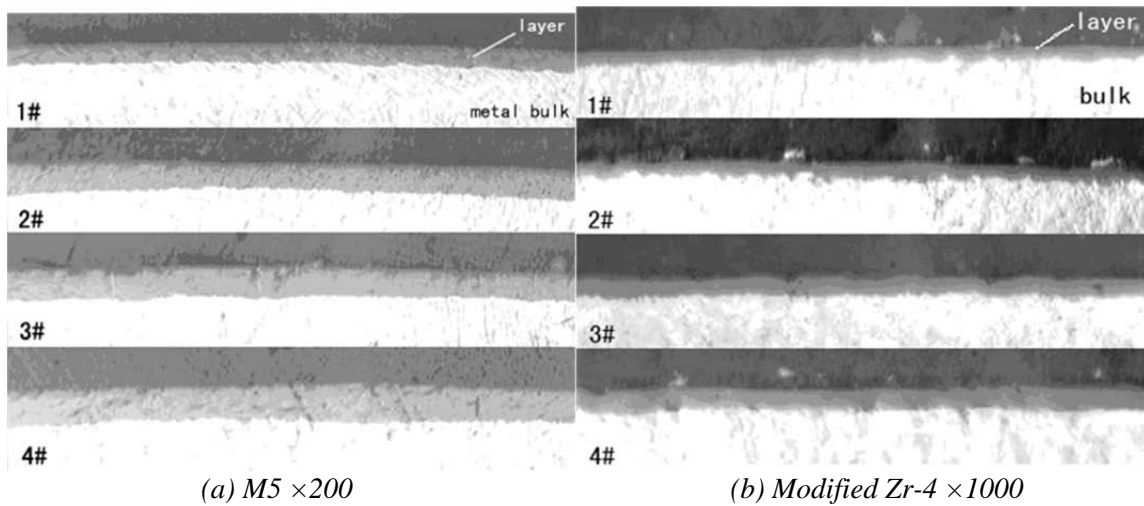


FIG. 10. The metallograph of crud layer on the heating section of M5 and modified Zr-4 after 3000h tests in 1#-4# water conditions.

As shown in the Fig. 11, a double structure is observed in the oxide layer formed on the M5 elements. The inner layer is identified to be zirconia that has a similar thickness as layer of modified zircaloy-4 elements. The outer layer is porous and easy to crack, which is identified by EPMA to be deposits with a high proportion of calcliothorite and magnesia. It can be noticed that the deposits contribute the majority of the layer thickness on the heated section of M5 elements. Figure 12 shows the layer morphology investigated by SEM. The continuous and spread deposits are formed on the M5 elements. Loose fragments and pores can also be observed in the deposits on the M5 elements. Relatively fewer deposits are formed on the modified zircaloy-4 elements, however, the suspected hydrides are also observed on the elements tested in 3# and 4# conditions whereas they were not found on the M5 elements.

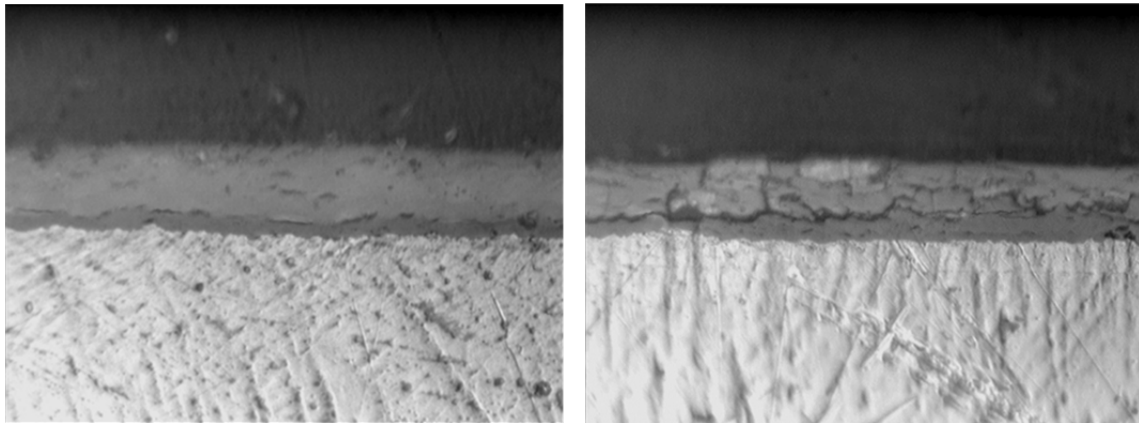
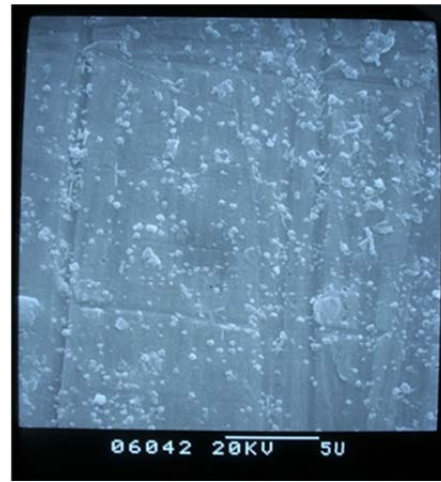


FIG. 11. The double structure and cracks in the crud layer of M5 elements after 3000h tests in 4# water condition.



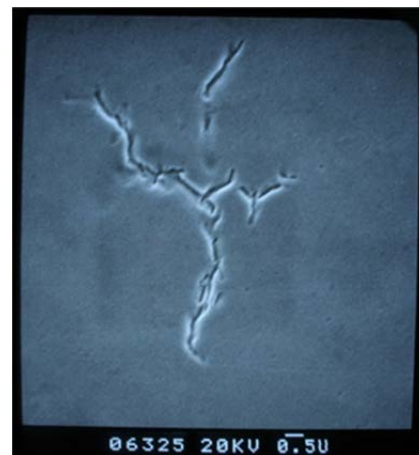
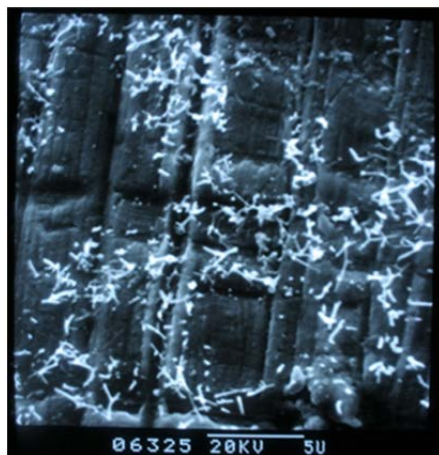
(a) Deposits on the M5 elements



(b) Deposits on the Modified Zr-4 elements



(c) Pores in the crud layer of M5 elements



(d) Susceptive Hydride in the crud layer of Modified Zr-4 elements

FIG. 12. SEM morphology of layer on the heating section of elements in 4# water condition.

The hydrogen pick-up of the heated section is analysed by an infrared detection method. The data indicate that the hydrogen content of both materials increases with lithium content and keeps almost constant with decrease of boric at constant lithium content. No obvious change of hydrogen pick-up is found when pH is improved from 6.8 to 7.2 at the same lithium content. In addition, the modified zircaloy-4 elements show higher hydrogen pick-up than M5 in each water condition, as shown in Fig. 13. The metallograph of hydride in the heated section of elements is shown in Fig. 14. Hydride can be observed in all elements. The orientation of hydride in M5 elements is irregular, whereas the tangential orientated hydride precipitates in modified zircaloy-4 elements. It can be noticed that the quantity or length of hydride increased slightly in 3# and 4 conditions.

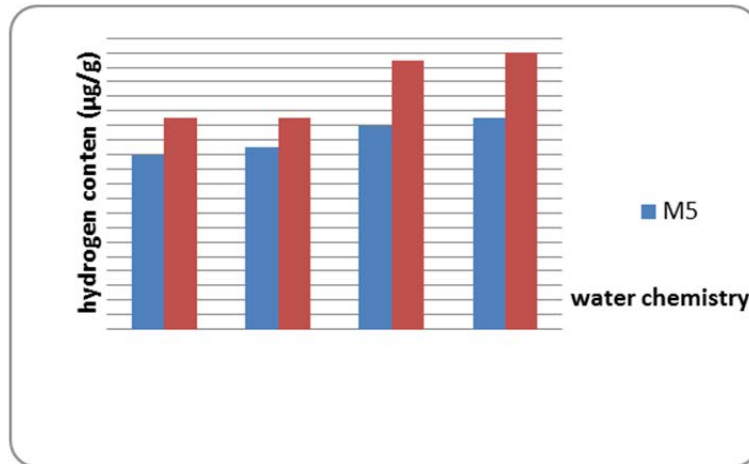


FIG. 13. The hydrogen pick-up of heating section after 3000h tests in 1#~4# water conditions.

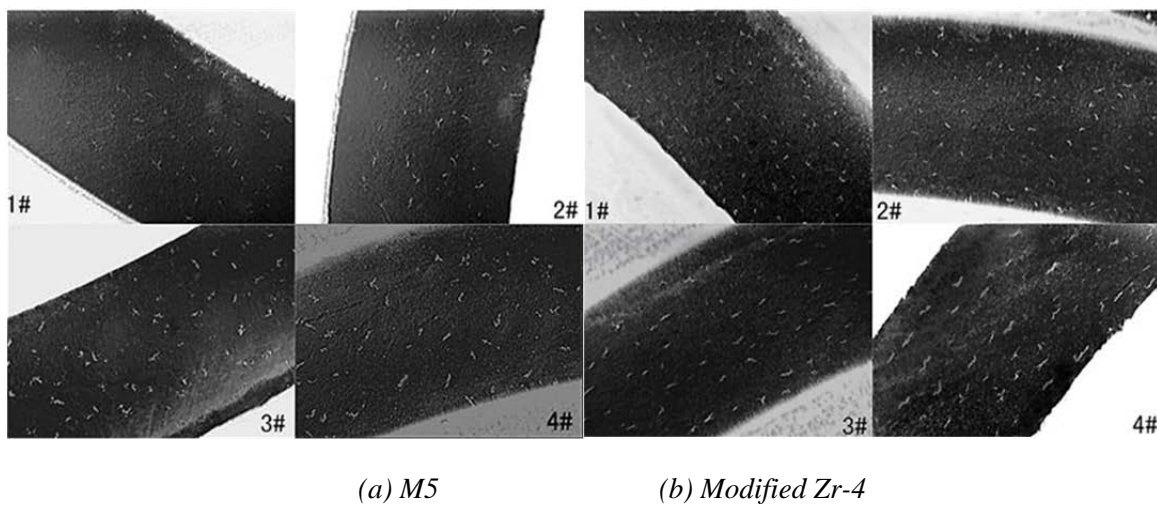


FIG. 14. Hydride in the heating section of elements in 1#~4# water conditions.

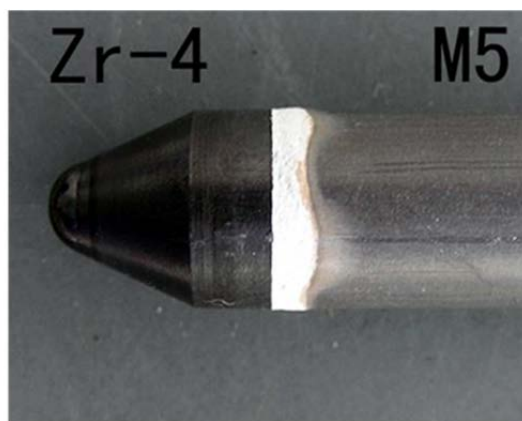


FIG. 15. The white ring appears on the end plug welds of M5 elements.

#### 4. DISCUSSION

The corrosion kinetics of zirconium alloy has been summarized [3] to be two stages of pre-and post-transition. In the pre-transition stage, the weight gain obeys the cubic kinetics and the oxide film is protective with black colors and dense microstructure. After the transition, the oxidation rate is usually accelerated and the weight gain may show a linear or cyclic increase. The oxide layer turns into gray or white with increase of thickness and becomes un-protective due to porosity and cracking.

The present weight gain of tube samples in 1# ~ 3# water conditions seems to be still in the stage of pre-transition with the characters of black and glossy surface as well as slow and exponential weight increase. The samples in 3# and 4# conditions show the most weight gain or unusually weight loss that indicates an effect of lithium hydroxide concentration. One of theories [4] is lithium generates pores in layer as the rapid transport of oxygen that accelerates reaction in the oxide/ metal interface. Recent researches in NPIC [5] propose an assume that the comprehensive action of  $\text{Li}^+$  and  $\text{OH}^-$  will decrease the surface free energy of film and accelerate the transition of microstructure from cubic (c) to monoclinic (m), and more pores are generated during the transition. According to these theories, it is not difficult to understand weight gain increases with improved lithium content.

For the reasons of losing weight in 4# water condition, even if the lithium content is the same, the influence of lithium on the stability of oxide layer could be magnified when the boron content is decreased. To some extent, it can be explained by the corrosion inhibition of boric acid with the following mechanisms [4]:

- Removal of surface OLi groups by reaction with non-ionized boric acid molecules;
- To change the caustic chemistry at the bottom of pores and produces a buffer effect on the dissolution of  $\text{ZrO}_2$ ;
- To plug pores and prevent the diffusion of anode pieces in the pores up to the reaction interface.

The obviously inhibiting effect of boron has been found by previous research [6]. In our tests, the weight gain curves or the measured layer thickness also reflect a slight decrease with increased boron content at the same lithium content. The water with 1703mg/kg boric acid shows insufficient ability to prevent the dissolution of samples at 6.4 mg/L lithium. For the detailed mechanism, further research will be carried out in NPIC to find the relationship of weight change and porosity of oxide layer under effect of boric acid with high concentrated lithium.

Unlike the tube samples in single phase water, the elements experience more serious oxidation and deposition under surface boiling condition especially for M5. The possible influencing factors include:

#### 4.1. Effect of surface boiling:

Because the temperature of elements exceeds the saturation temperature at pressure of 15.5 MPa, sub-cooled nucleate boiling is generated and two-phase fluid produced around the elements. Under this condition, lithium hydroxide is easier to concentrate on the surface because of its non-volatile feature, which will accelerate the oxidation rate of zirconium alloys.

#### 4.2. Effect of temperature:

Weight gain will increase with temperature due to higher oxygen diffusion coefficient and oxidation rate constant, which has been proved by early studies [7]. In our tests, the surface temperature of elements is about 36°C higher than that of tube samples and the higher extent of oxidation is as expected.

#### 4.3. Effect of contaminations:

In our tests, deionized water is used for the preparation of solutions, but to accelerate the process of the deposition, the re-purification system is not always used. Because solubility is influenced by negative temperature coefficient, the contaminants such as Ca and Mg, in the form of calciothorite and magnesia, prefer to deposit on the elements where the temperature is highest. This kind of deposit is hard, impervious and more easily leads to a drop of heat transfer efficiency. For an example, the elements that have thicker crud layers in 3# and 4# water conditions experienced the higher probability of over-heat alarm near the end of tests.

From Fig. 11, the boundary between deposits and ZrO<sub>2</sub> layer is not very clear. It seems the deposits participate in the formation of a crud layer mixed with ZrO<sub>2</sub> and the thickness changes with different water chemistry. Figure 11 also shows some cracks that appear to be “steam filled cracks” [4] within the crud layer. These cracks may become new traps for ionic concentration and accelerate the oxidation of inner layer or even failures. Therefore the deposits should be considered harmful to the corrosion resistance of elements.

Since the heat flux and temperature of elements are same, the sensitivity and level of deposition are assumed to be directly relevant to the properties (e.g. porous and lattice structure) of the ZrO<sub>2</sub> layer, which is affected by water chemistry. Therefore, the serious deposition on M5 elements may imply an unstable ZrO<sub>2</sub> layer formed in the tested water conditions.

Previous research [8] has revealed the excellent corrosion resistance of M5 alloy by in-pile or out-of-pile tests. Compared with zircaloy-4, these tests prove that M5 has much lower corrosion kinetics in various water chemistry conditions (Li: 10 to 70ppm as Li, B:0 to 650 ppm as boric acid). In our tests, the modified zircaloy-4 shows temporary lower corrosion kinetics than that of the M5 alloy. Besides the effect of different water chemistry, the suspected factors also include:

- Contamination during the manufacture of specimens: Some impurities, such as nitrogen, have been considered harmful to the corrosion resistance of zirconium alloys. When introduced during the manufacture (e.g. welding), the nitrogen would replace the oxygen ion in the lattice structure and increase the vacancies in the surroundings. However, the chemical examination on the tubes before tests has shown that there is no contamination of nitrogen or other harmful elements.
- Insufficient time for corrosion kinetics comparison: The previous data [8] indicate the difference of weight gains between M5 and zircaloy-4 is very subtle before 150 days and starts to be widened after about 200 days. It seems 3000 hours (125 days) is not sufficient for comparison because the transition of oxide film may not yet happen. In spite of this, the higher level of deposition on the M5 elements in a short time should be noticed. In our opinions, the most likely culprit is dissolved oxygen.

#### 4.4. Effect of dissolved oxygen:

Based on the data collected from various research [4], the Zr-Nb alloys would show increased corrosion rate whereas the zircalloys are quite immune when exposed to water containing dissolved oxygen. Especially in the mixture of water and steam, the weight gain or oxidation of ZrNb alloys may increase significantly with the DO level [9].

The principle for this phenomenon is considered to be preferential reaction on the Zr-Nb alloys with free oxygen in the participation of niobium rather than water to produce the oxide layer. This kind of oxide layer may experience a rapid growth and would be more porous under effect of lithium hydroxide, and therefore high affinity to the deposits.

Another important characteristic is that the hydrogen pick-up of Zr-Nb alloys still remains at lower levels irrespective of changes on weight gain when exposes to the water-steam with mixture of dissolved oxygen. Since the hydrogen entering the metal is originated from reaction of zirconium and water, the final hydrogen pick-up should depend on the degree of this reaction. The previous tests data [8] revealed that the hydrogen pick-up increased linearly or cyclically with the thickness of oxide layer when exposed in the deoxidized water. For the M5 alloy, the layer thickness of 3~4 $\mu\text{m}$  would accompany by the about 35ppm hydrogen pick-up. If the layer thickness reached to the 20 $\mu\text{m}$ , the hydrogen pick-up would exceed 100ppm and serious hydride precipitation will occur. Nevertheless, in spite of thickest layer over than 20 $\mu\text{m}$  formed on the M5 elements, the actual measured hydrogen pick-up is still within 30ppm and lower than that of modified zircaloy-4. It indicates the mechanism for the layer formation of M5 alloy is not same as zircaloy-4 and layer is produced not only by the reaction of metal with water.

Besides, the factors leading to the lower hydrogen pick-up of M5 alloy also include the fine grain structure with tiny and general dispersed phase of  $\beta_{\text{Nb}}$ , which can stop efficiently the adhesion and diffusion of hydrogen. As for the difference of hydride orientation, the tangential orientation is considered least harmful to mechanical properties of tubes. The influence of irregular hydride can be ignored if the hydrogen content does not exceed the critical value, 500ppm [10] for zircaloy-4 and is unclear for M5 alloy.

In addition, the fact of corrosion on the end plug welds of elements also indicates the quite different oxidation behaviour of both materials in water with dissolved oxygen. The white ring only appeared on the side of M5 tubes whereas the end plug made from zircaloy-4 maintained the black and gloss finish shown in Fig. 15. The weld was polished to get rid of the ring and retested in the same water condition, however, the ring appeared again only after 500h. Different from the layer on the heating section, the white ring is mainly composed of  $\text{ZrO}_2$  without zeolite deposits. The micro zone analysis will be done to find if Nb depletion exist below the layer of white ring due to preferential oxidation.

## 5. CONCLUSION

The recent studies and tests on the corrosion and deposition of cladding materials performed in the water chemistry and corrosion laboratory of NPIC, lead to the following conclusions:

- In single phase conditions, the general corrosion rate of modified zircaloy-4 and M5 alloy increases with concentration of lithium. The protection of the oxide layer decreases and weight loss will appear when the content of boric acid decreases to a certain degree at a high content of lithium.
- Under surface boiling conditions, the growth of a crud layer increases with concentration of lithium and decrease of boric acid. The M5 alloy seems to prefer reacting with free oxygen instead of water and to absorb deposits readily when exposed to water-steam containing dissolved oxygen and lithium, whereas the modified zircaloy-4 shows a lower tendency for deposition but has a higher hydrogen pick-up. Dissolved oxygen and contaminations should be

controlled more strictly to avoid the “oxidation introduced deposition”, especially for the Zr-Nb alloys cladding in the out-of-specification water chemistry.

Because of the unexpected effect of oxygen and insufficient test time, the studies on the real difference of the corrosion kinetics in these water conditions should be continued. For further identifying which factor, dissolved oxygen or lithium, plays a decisive role on the deposition, the next phase of research in NPIC will focus on the corrosion and deposition behaviour of M5 alloy in high lithium concentrations with different levels of dissolved oxygen. The research objects also include new type zirconium alloys developed in China, such as N18 and N36. For the better simulation of test conditions, a special corrosion experiments platform is under construction which includes two small testing systems (up to 650°C and 25MPa) for screening water chemistry and materials, and an integrative loop for engineering evaluation.

## REFERENCES

- [1] ZHAO, W., Summary on out-of-pile and in-pile properties of M5 alloy, *Nuclear Power Engineering*, **1** (2001) 22.
- [2] ZHENG, X., Isothermal transformation from tetragonal (t) to monoclinic (m) in ZrO<sub>2</sub> ceramics, *Mat. Sci. Eng.* **1** (1999).
- [3] BILLOT, P., ROBIN, J-C., GIORDANO, A., PEYBERNES, J., Experimental and theoretical studies of parameters that influence corrosion of zircaloy-4, *Zirconium in Nuclear Industry: Tenth International Symposium, ASTM STP 1245*, American Society for Testing and Materials, Philadelphia, (1994), 351–377.
- [4] INTERNATIONAL ATOMIC ENERGY AGENCY, *Water Corrosion of Zirconium Alloys in Nuclear Power Plants*, IAEA-TECDOC-996, IAEA, Vienna (1998).
- [5] ZHOU, B., LI, Q., YAO, M., LIU, W., ZHU Y., Microstructure of oxide film formed on zircaloy-4, *Corrosion & Protection*, **90** (2009) 9.
- [6] PÈCHEUR, D., GIORDANO, A., PICARD, E., BILLOT, Ph., THOMAZET, J., Effect of elevated lithium on the waterside corrosion of zircaloy-4. Experimental and predictive studies. Influence of Water Chemistry on Fuel Cladding Behavior: Proceedings of a Technical Committee Meeting. Feb. IAEA-TECDOC-499, IAEA, Vienna (1997) 111–130.
- [7] KLEIN, A.C., REYES, JR J.N., MAGUIRE, M.A., Thermal gradient effects on the oxidation of zircaloy fuel cladding, *Technical Committee Meeting on Fundamental Aspects of Corrosion of Zirconium-based Alloys in Water Reactor Environments*, Portland, OR USA, (1989).
- [8] THOMAZET, J., DALMAIS, A., BOSSIS, P., GODLEWSKI, J., BLAZT, M., MIQUET, A., The corrosion of the alloy M5<sup>TM</sup>: an overview, *iaea technical committee meeting on behaviour of high corrosion Zr-based alloys*, web publication, [www.iaea.org](http://www.iaea.org) (2012).
- [9] KUMAR, K., AGGARWAL, S., KAIN, V., SAARIO, T., BOJINOV, M., Effect of dissolved oxygen on oxidation and hydrogen pick up behaviour — Zircaloy vs. ZrNb alloys, *Nucl. Eng. and Des.* **240** (2010) 985–994.
- [10] CHEN, H., MA, C., BAI, X., *Corrosion and Protection of Nuclear Reactor Materials*, Atomic Energy Press (1984).



# RESEARCH INTO EFFECTS OF COOLANT CHEMISTRY ON CORROSION PROCESSES OF UKRAINIAN WWER-1000 CORE MATERIALS

V.S. KRASNORUTSKYY, I.A. PETELGUZOV, V.M. GRYSYNA, V.A. ZUYOK,  
M.V. TRETAKOV, R.A. RUD  
Nuclear Fuel Cycle Science and Technology Establishment (NFC STE),  
National Science Center Kharkov Institute of Physics and Technology (NSC KIPT),  
Kharkov, Ukraine

## Abstract

The paper presents the results of E110 out-of-pile tests of and research into oxidation kinetics during 35 000 hours (five fuel cycles) under conditions that simulate primary coolant composition and parameters of WWER-1000 at power operation and in steam at 400°C. The test data revealed that the weight gains of E110 did not exceed 200 mg/dm<sup>2</sup> for water environment at 350°C and 900 mg/dm<sup>2</sup> for steam at 400°C during long term oxidation. Oxide films on all specimens and in the areas of weld joints have high corrosion resistance. Also, we will provide autoclave tests results for austenitic stainless steels type Ch18N10T in the environment simulating primary coolant composition and parameters of WWER-1000 reactors. The corrosion process on stainless steels is non-monotonic and is accompanied by weight loss of specimens. Chemical composition of corrosion environment and concentration of oxidizing components exert an essential impact on corrosion rate and oxidation mechanism. It is well known that corrosion processes are less intensive at pH=7.2. Also, initial surface treatment drastically affects corrosion kinetics of stainless steel specimens. Moreover, it should be mentioned that the National Science Academy of Sciences of Ukraine started a programme "Problems of Lifetime and Safe Operation of Structures, Buildings and Machines". In the framework of this programme NFC STE is carrying out a number of research activities under the project "Improvement of Lifetime and Reliability of Aging WWER-1000 RCS Equipment by Water Chemistry Optimization", namely, to establish the influence of zinc injection on corrosion rate and properties of oxide films on stainless steels and zirconium alloys under conditions simulating composition and parameters of WWER-1000 primary coolant.

## 1. INTRODUCTION

This report provides results of E110 out-of-pile tests of and research into oxidation kinetics during dwells of 35 000 hours, and autoclave tests results for austenitic stainless steels type Ch18N10T in the environment simulating primary coolant composition and parameters of WWER-1000 reactors. The NFC STE is carrying out a number of research activities under the project "Improvement of Lifetime and Reliability of Aging WWER-1000 RCS Equipment by Water Chemistry Optimization".

## 2. RESULTS

Figure 1 provides the results of the autoclave testing of WWER materials for 35 000 hours.

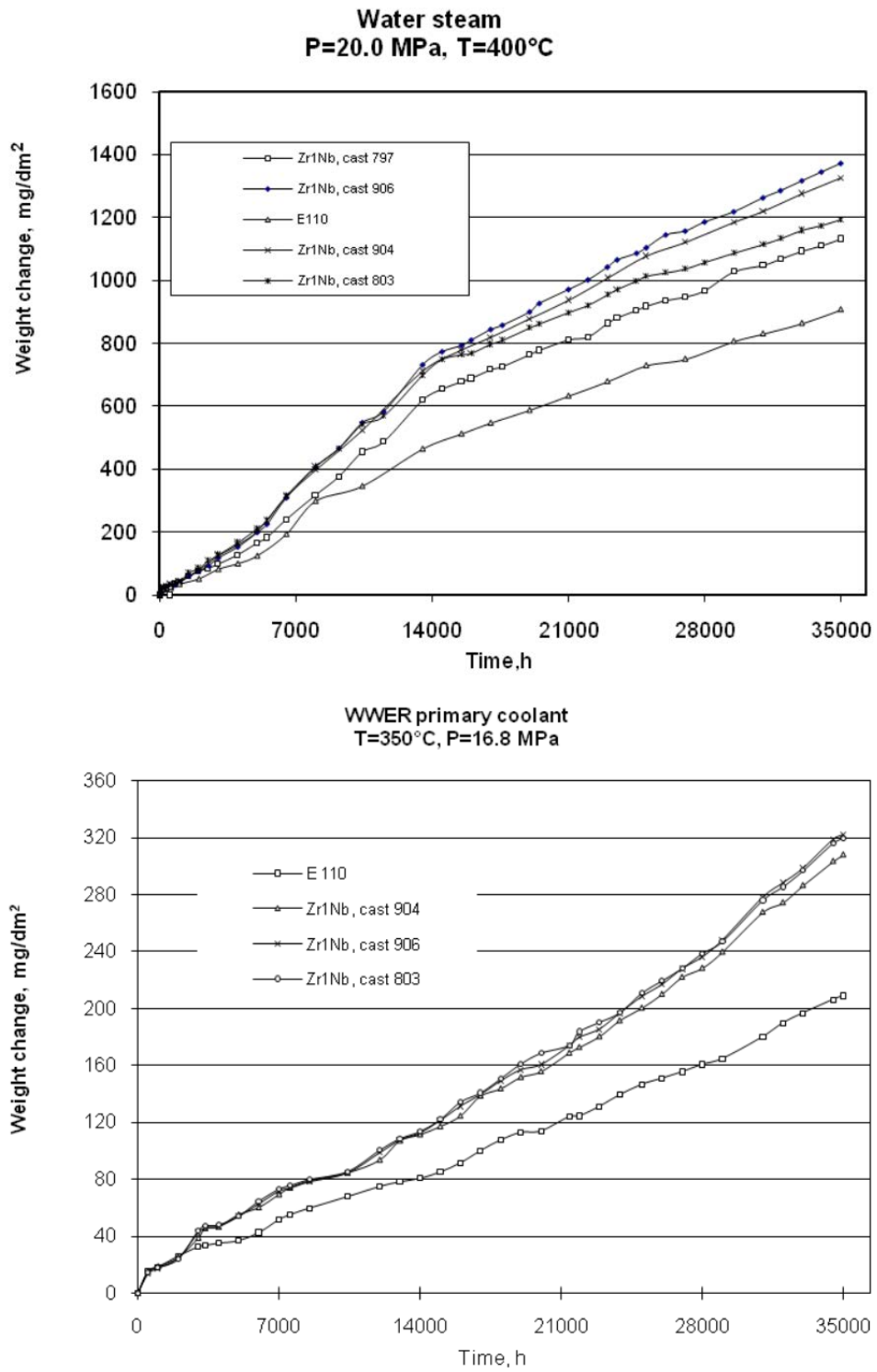


FIG. 1. Results of autoclave tests on WWER materials.

Figure 2 provides the results from the autoclave tests of austenitic stainless steels type Ch18N10T in the environment simulating primary coolant composition and parameters of WWER-1000 reactors.

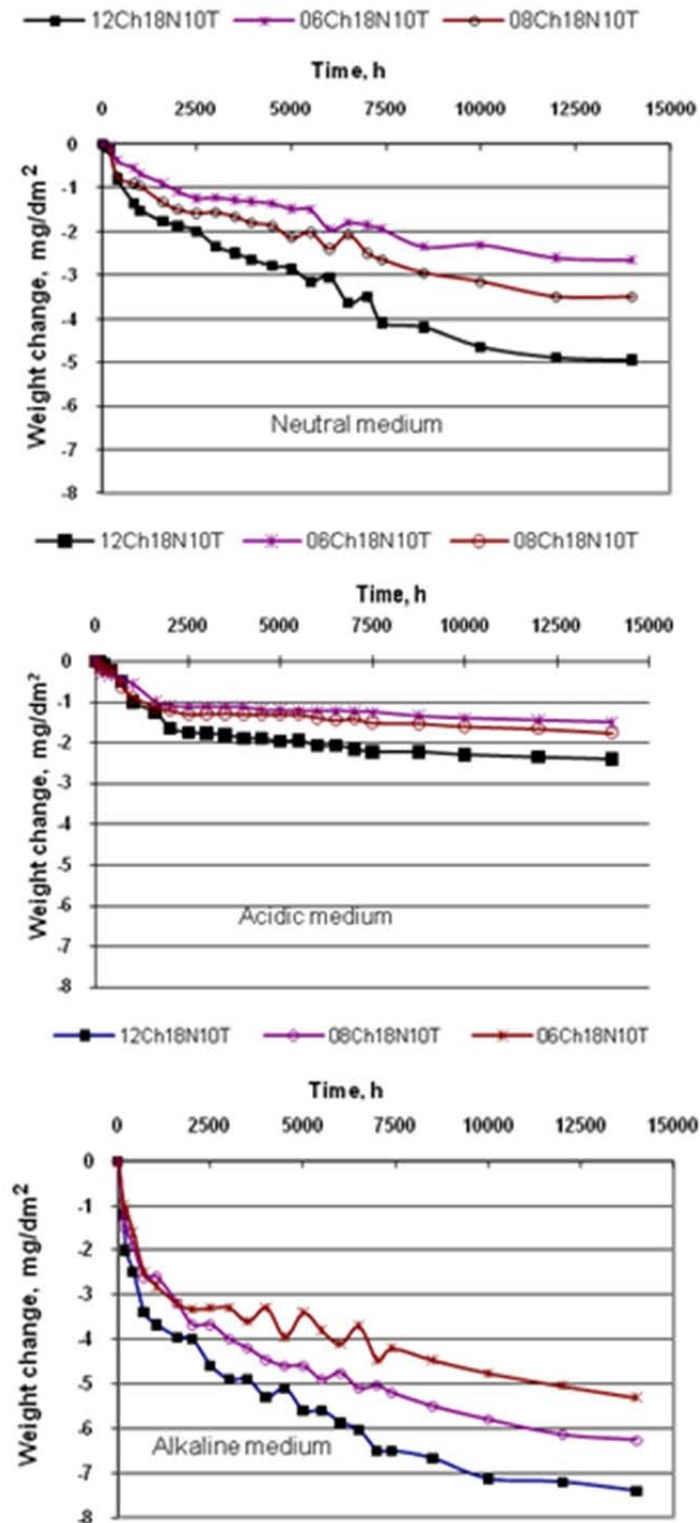


FIG. 2. Autoclave tests of WWER steel types in neutral, acidic and alkaline media.

### 3. SCIENTIFIC SUBSTANTIATION OF PRIMARY WATER CHEMISTRY OPTIMIZATION.

Primary water chemistry regime provides safe and reliable operation of fuel and the entire RCS equipment.

Despite great positive experience in primary water treatment of WWER reactors, there are still some disadvantages, in particular the need for the disposal of bulk quantities of radioactive waste.

According to the above said in the framework of a programme “Problems of Lifetime and Safe Operation of Structures, Buildings and Machines” started by the National Science Academy of Sciences of Ukraine, NFC STE NSC KIPT is carrying out a number of research activities under the project “Improvement of Lifetime and Reliability of Aging WWER-1000 RCS Equipment by Water Chemistry Optimization”, namely, to establish the influence of zinc injection on corrosion rate and properties of oxide films on stainless steels and zirconium alloys under conditions simulating composition and parameters of WWER-1000 primary coolant.

### 4. CONCLUSIONS

WWER-1000 RCS construction materials possess high performance capabilities at operation under primary circuit conditions (at heat power, which is lower than at PWRs). Hence activities of primary chemistry optimization at Ukrainian NPPs should be concentrated on reduction of radioactive wastes (the amount directly depends on primary water chemistry) and RCS equipment activity (which is lower than at PWRs).

# CLAD DEPOSITION AND CONSEQUENCES

(Session 3)

**Chairperson**

**D. LISTER**

Canada



# CRUD DEPOSITION ON PRESSURIZED WATER REACTOR FUEL IN THE HALDEN REACTOR

P.J. BENNETT  
Institutt for Energiteknikk,  
Halden,  
Norway

## Abstract

Many nuclear power plants are operating at higher power and coolant temperatures than were common previously. Increasing fuel duty can increase rates of crud deposition and hideout of harmful chemical species. Thus, water chemistry conditions that were previously acceptable may no longer provide adequate margin for maintaining fuel reliability. In PWRs, heavy crud deposits can lead to axial offset anomaly (AOA), where localized boron hideout in crud deposits cause a shift in reactor power output towards the bottom of the core. AOA can necessitate plant de-rates or adoption of less efficient cores to avoid the phenomenon. In extreme cases, crud deposits can lead to fuel failures, where steam blanketing within the crud impedes heat transfer from the fuel to the coolant and thus increases fuel clad temperature. The major factors determining crud deposition are the heat flux at the clad surface, coolant corrosion product concentrations and steam void fraction along the clad surface. In the Halden reactor, crud has often deposited on fuel rods irradiated under PWR conditions. This paper discusses the effects of coolant thermal-hydraulics and water chemistry on crud formation and composition.

## 1. INTRODUCTION

Many nuclear power plants are operating at higher power and coolant temperatures than were common previously. Increasing fuel duty can increase rates of crud deposition and hideout of harmful chemical species. Thus, water chemistry conditions that were previously acceptable may no longer provide adequate margin for maintaining fuel reliability.

Historically, boiling conditions (which promote crud deposition) have existed predominantly in BWRs. Without zinc injection, the majority of the crud is formed of hematite ( $\text{Fe}_2\text{O}_3$ ), which is loose and fluffy and has little heat impeding effect [1]. However, with zinc addition and other factors, such as high coolant copper levels, fuel failures have occurred that have been associated with tenacious crud layers. It is thought that the presence of steam blankets within pores in the crud causes a significant rise in clad temperature, resulting in increased clad oxidation and failure.

In PWRs, heavy crud deposits can lead to axial offset anomaly (AOA), where localized boron hideout in crud deposits cause a shift in reactor power output towards the bottom of the core [1]. AOA can necessitate plant de-rates or adoption of less efficient cores to avoid the phenomenon. In extreme cases, crud deposits can lead to fuel failures. Crud-induced cladding corrosion failures have occurred in the TMI-1 PWR [2]. Nine rods failed after 121 days at power. Hot cell analyses of the rods showed that there were crud deposits along the upper spans. Higher than expected clad temperatures in the crudded region were evinced by thicker than expected oxide layers and hydrogen pick-up, together with regions of recrystallized cladding. In conclusion, the failures were attributed to local penetration of the cladding caused by high cladding temperatures due to steam blanketing within the crud deposits.

The major factors determining crud deposition are the heat flux at the clad surface, coolant corrosion product concentrations and steam void fraction along the clad surface.

The Halden Boiling Water Reactor (HBWR) is a test reactor with a maximum power of 20 MW that is cooled and moderated by boiling heavy water (normal operating temperature 235°C and pressure 34 bar). For tests requiring representative light water reactor (LWR) conditions, test rigs are housed in pressure flasks that are positioned in fuel channels in the reactor and connected to dedicated water loops. The reactor operates for two ~100 day reactor cycles each year. Typical fast fluxes are  $3 \times 10^{13} \text{ n} \cdot \text{cm}^{-2} \text{ s}^{-1}$ , equivalent to an accumulated fluence of  $6 \times 10^{20} \text{ n} \cdot \text{cm}^{-2}$  in a calendar year.

A typical experiment contains from one to six test fuel rods, with an active fuel length of up to 60 cm. PWR water chemistry is simulated by additions of LiOH, B(OH)<sub>3</sub> and dissolved hydrogen, together with any required additives, for example zinc. Although the coolant flow rate through the test section (1–1.8 m/s) is a factor of three lower than that in a commercial PWR, a representative degree of sub-cooled nucleate boiling (SNB) can be achieved by adjustment of the coolant inlet temperature and fuel rod power.

In-reactor tests to study PWR cladding corrosion and hydriding have been conducted in the Halden reactor for more than 20 years. Although studies of crud formation and composition have not been an objective of these tests, crud deposits do form, and have affected the test results. In addition, some experiments have been performed in which crud formation was a specific objective. This paper will discuss the effects of fuel heat flux, coolant thermal-hydraulics and water chemistry on crud formation and composition.

## 2. SUMMARY OF EXPERIMENTAL OBSERVATIONS

### 2.1. Zircaloy surfaces with heat flux will be covered in crud deposits. However, depending on thermal-hydraulic and chemistry conditions, these are often loose and easily removed by brushing.

Figure 1 shows test rods from a cladding corrosion test, with three segmented fuel rods, comprising a range of modern PWR cladding materials. Test conditions were fuel rod heat flux: 500–1140 kW/m<sup>2</sup>, coolant temp: 305–320°C, void fraction: 0–0.05. Water chemistry conditions were 3 ppm Li, 1000 ppm B (pH<sub>300</sub> 7.1), with mean soluble corrosion product concentrations of 5 ppb Fe and 0.15 ppb Ni.

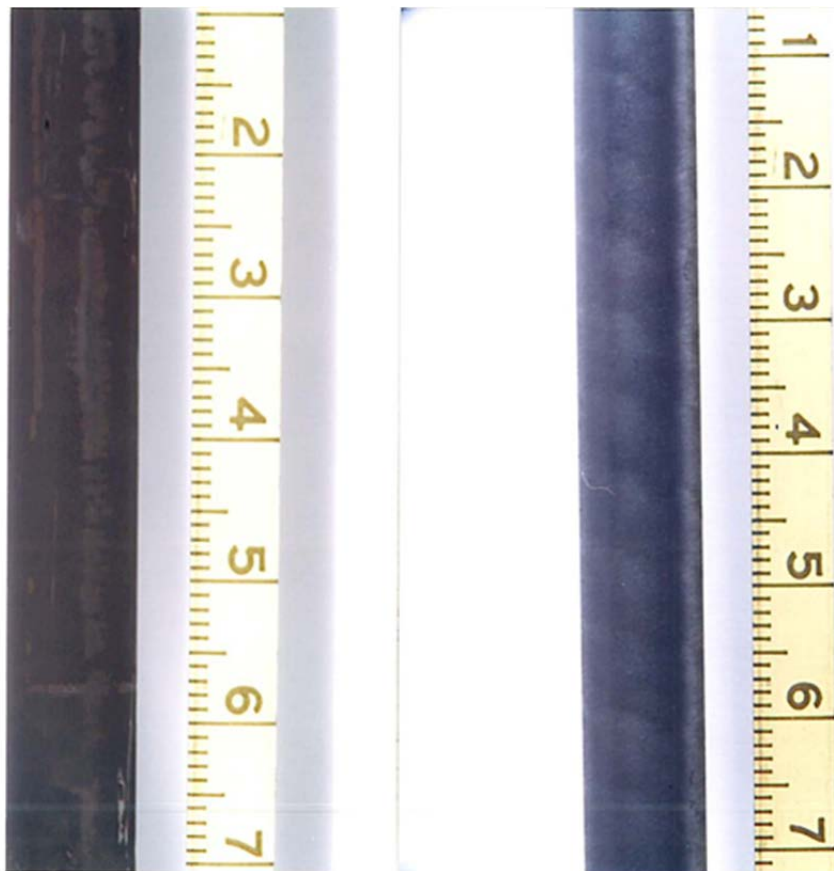
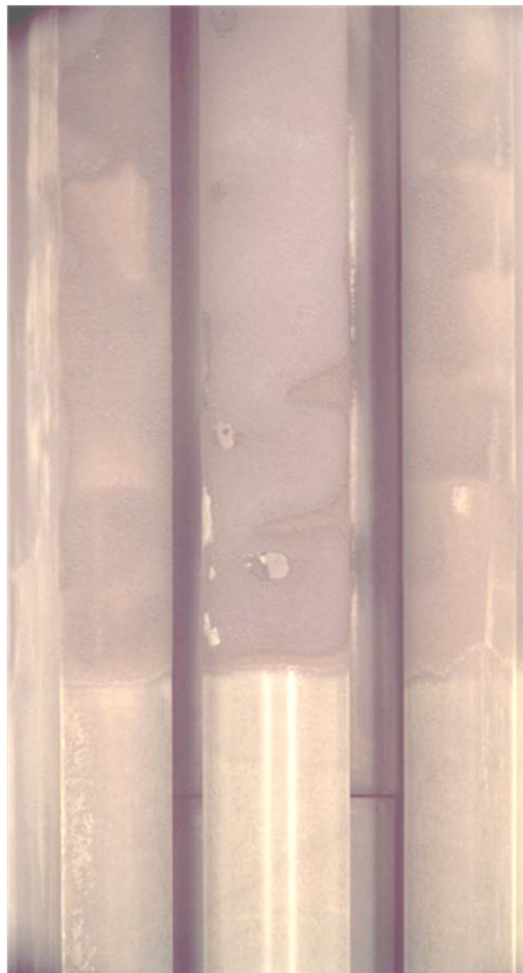


FIG. 1. Zry-4 fuel rod before and after brushing, showing removal of loose crud.

Oxide thickness measurements were performed after every ~180 days at power. According to standard practice at Halden, the rods were brushed before the oxide thickness measurements were made. Brushing is done in a specially designed rig, in which four stainless steel brushes are arranged at 90° to each other. The brushes are fitted to a diameter 0.5 mm smaller than the test rods, and the rods are moved (up and down) five times through the rig. The rod is moved axially through the brushes whilst being rotated. In each measurement, a layer of loose crud was normally observed, which was easily brushed away.

## 2.2. High corrosion product concentrations may lead to tenacious crud deposits under benign fuel duty.

Figure 2 shows a picture of a test rod from an experiment performed to demonstrate the axial offset anomaly in the Halden reactor [3]. The fuel rods were fuelled with low enrichment pellets in the bottom third section to ensure single phase coolant flow, and with higher enrichment pellets in the upper two thirds to achieve SNB. In the lower section, the heat flux was 450 kW/m<sup>2</sup>, while it was 980 kW/m<sup>2</sup> along the upper section. There was no void along the lower section, and a maximum value of 0.02 along the upper section.



*FIG. 2. Crud deposition commencing at boundary between single phase coolant flow and sub-cooled nucleate boiling.*

At the beginning of the test (Phase 1), the conditions were chosen to be representative of those of a high duty PWR. Under these conditions, no build-up of crud was observed. In phase 2 of the experiment, the test rod power and coolant inlet temperature were increased such that the mass evaporation rate was doubled. Coolant Fe and Ni levels were increased by injecting a soluble organic complex; measured levels of Fe and Ni were 15 and 2 ppb respectively. These changes in thermal-

hydraulics and water chemistry resulted in thick crud deposits along the section of the fuel undergoing SNB; however, the high Fe/Ni levels did not lead to crud on the section of the fuel undergoing single phase heat transfer.

Figure 3 shows crud deposits on test rods that had been operated under relatively benign thermal-hydraulic conditions (ALHR 15–25 kW/m, coolant temperature 300–310°C, maximum void fraction: 0.002 %. Water chemistry conditions were 3 ppm Li and 1000 ppm B (pH<sub>300</sub> 7.1). The crud deposition occurred after an operation period in which elevated levels of corrosion product iron and nickel were measured (Fig. 4): with maximum Fe and Ni levels of 35 and 4 ppb respectively.

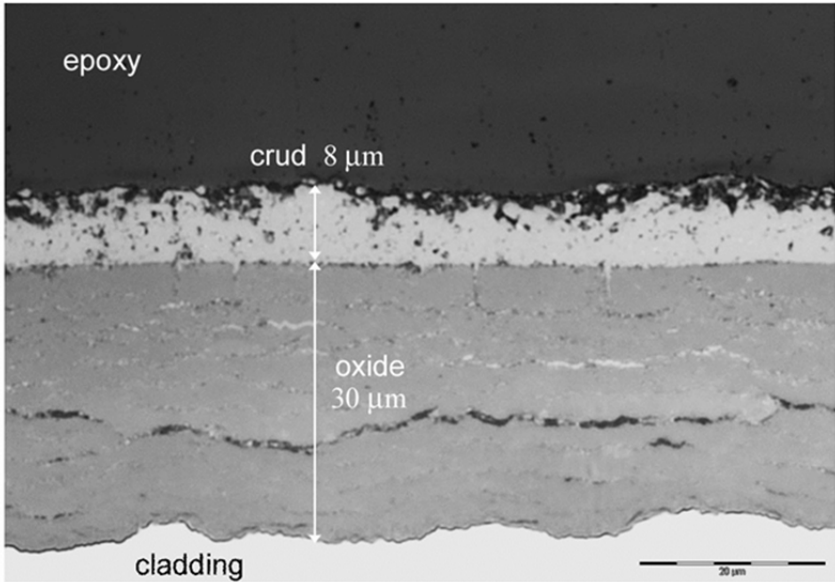


FIG. 3. Crud deposits on low duty fuel.

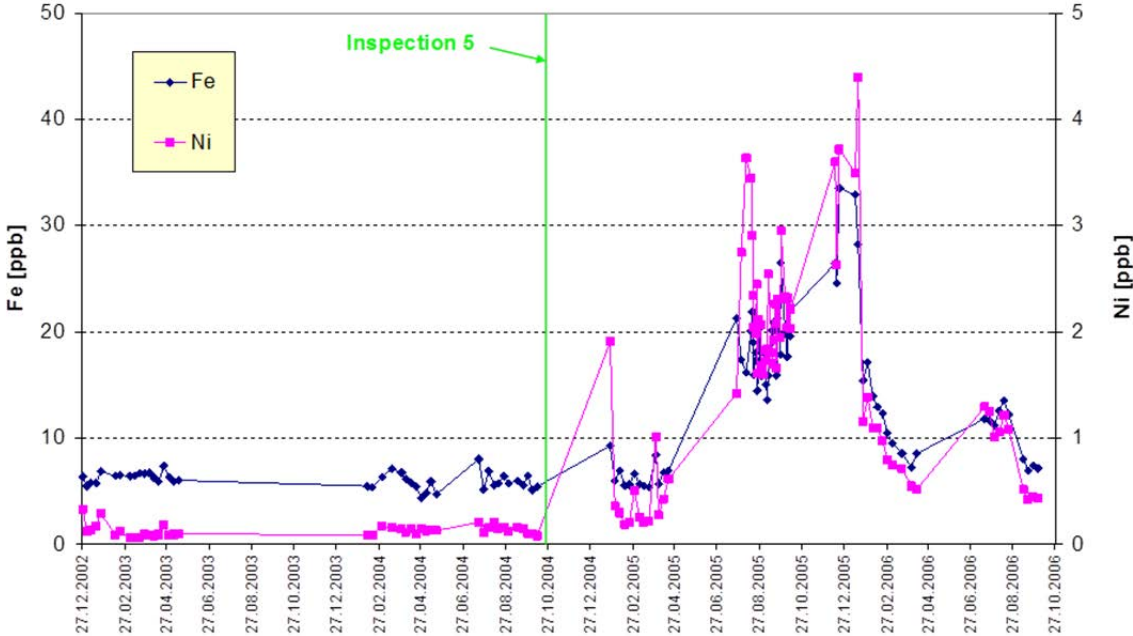


FIG. 4. Elevated Fe and Ni concentrations, correlating with crud formation.

### 2.3. Above a critical degree of fuel duty (void fraction, degree of SNB, mass evaporation rate), “normal” concentrations of Fe and Ni can lead to tenacious crud deposits.

Figure 5 shows oxide thickness measurements from a zircaloy-4 corrosion test, with six fuel rods, each divided into two segments of length 250 mm. The lower segments contained fuel of 10 w/o  $^{235}\text{U}$ , and the upper segments contained 6.5 w/o  $^{235}\text{U}$ . Test conditions were fuel rod heat flux: 900–1200 kW/m<sup>2</sup>, coolant temp: 320–330°C, maximum void fraction: 0.13. Water chemistry conditions were 3 ppm Li and 1000 ppm B (pH<sub>300</sub> 7.1).

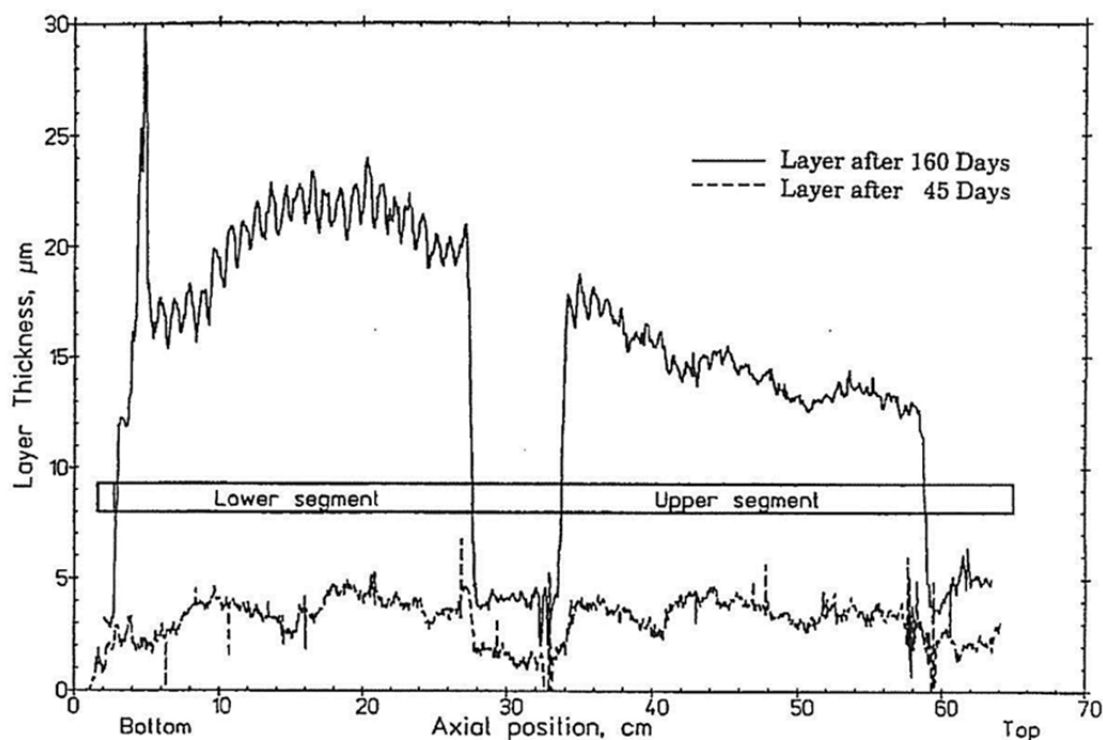


FIG. 5. Formation of crud deposits during 160 days of irradiation.

Anomalous crud build-up on the rodlets was detected by out-of-pile eddy current measurements of oxide thickness, taken after 45 and 160 days at power. After 45 days, a layer of (oxide + crud) of approximately 6 µm was observed. There were no significant differences between the thickness on the lower and upper segments. After 160 days, the lower segment had a layer of approx. 20 µm, while the layer on the upper segment was approximately 10 µm; i.e. the crud was thicker on the section with the higher heat flux. Heated and unheated axial zones were clearly distinguishable. In the non-heated region, the layer thickness was approximately 5 µm. In the heated regions, there were minima at pellet-pellet interfaces and maxima at the pellet centres. Thermal-hydraulic analyses showed that bulk boiling did not lead to a higher crud deposition than nucleate boiling.

### 2.4. Chemical intrusions together with high fuel duty can lead to rapid formation of crud deposits. These may be tenacious, depending on chemical composition.

Crud was formed in an experiment conducted to measure on-line creep behaviour of zircaloy fuel cladding materials, using an in-core diameter gauge. The test assembly contained both unfuelled and fuelled clad sections. This test is of interest because the diameter gauge gave in-core measurements of crud deposition. Test conditions were fuel rod heat flux: 1180 kW/m<sup>2</sup>, coolant temp: 310–320 °C, void fraction: 0.12–0.19. Water chemistry conditions were 2.3 ppm Li and 1170 ppm B (pH<sub>300</sub> 6.93). Soluble zinc, at a target concentration of 50 ppb, was added as zinc formate.

The fuelled clad segment exhibited two periods of anomalously large increases in diameter, which corresponded with measured peaks in coolant zinc of 150–200 ppb shortly after the start of zinc injection. These increases were attributed to the formation of a tenacious crud layer (detailed features of the diameter traces could be seen after repeated measurements. The diameter gauge pressed onto the clad surface with a force of 10 N, which was not sufficient to remove the crud). Figure 6 shows two diameter profiles, taken before and after one of the zinc concentration peaks. It can be seen that the crud deposition took place only on that part of the cladding with fuel pellets inside; no deposition occurred at the axial position with no heat flux (i.e. in the regions containing a mid-plug connecting the two fuelled areas), while there was less crud deposition in the regions containing fuel pellet — pellet interfaces (since the fuel pellets are chamfered at the edges, heat flux at the cladding outer surface is lower in the regions around pellet-pellet interfaces).

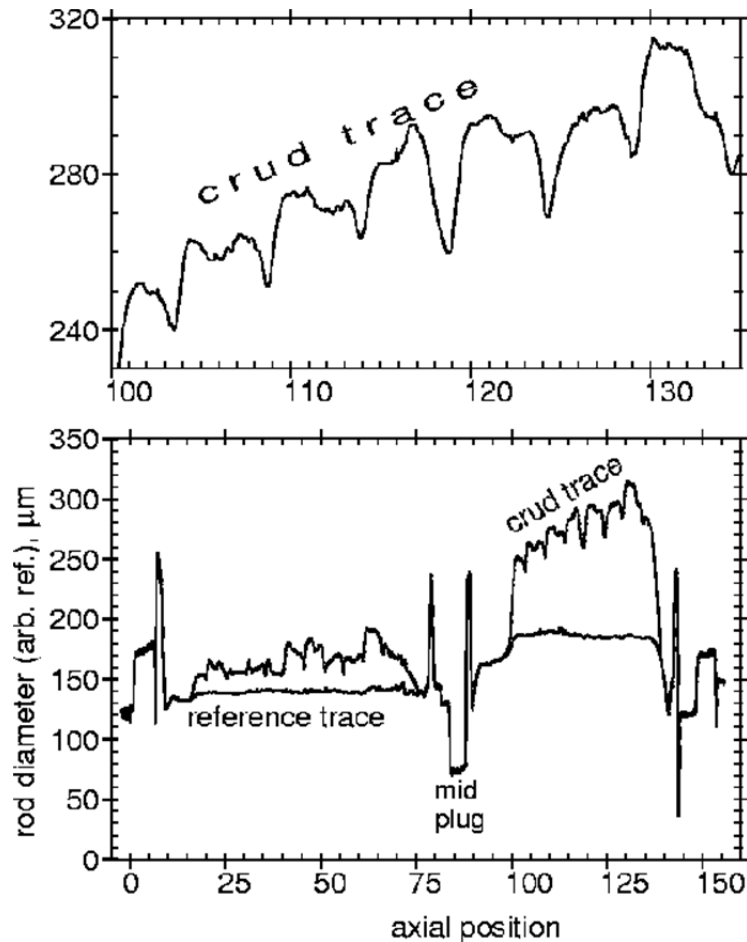


FIG. 6. In-core rod diameter profiles, before and after soluble zinc spike.

The dependence of crud deposition rate with heat flux above the flux value required for onset of nucleate boiling was very strong (Fig. 7), and could be expressed as a fifth power:

$$D \propto \left( \frac{LHR}{LHR_{\min}} \right)^5$$

where

- $D$  is the crud deposition rate,
- $LHR$  is the local linear heat rate and
- $LHR_{\min}$  is a constant heat rate, equivalent to the minimum needed to produce sub-cooled nucleate boiling at the coolant temperature and pressure.

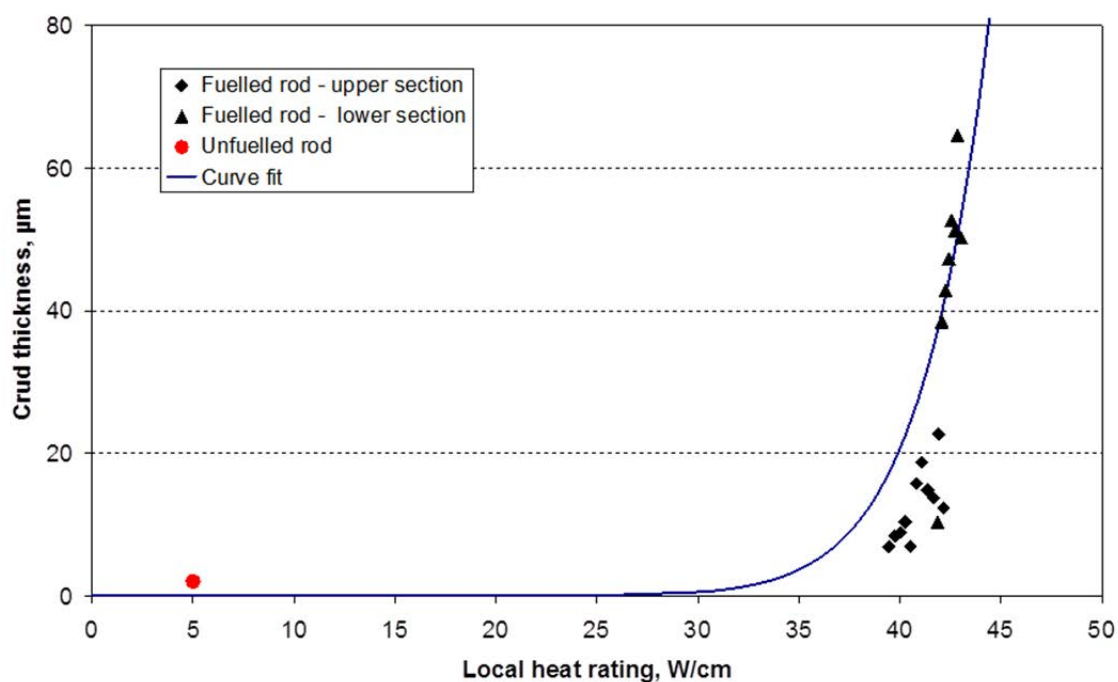


FIG. 7. Dependence of crud deposition on heat rating.

After the peaks in zinc concentration, no further episodes of large scale deposition were observed, while diameter increase rates returned to pre-zinc addition values once the zinc was stabilized at 50 ppb. A pronounced decrease in diameter was observed during a reactor shutdown approximately 83 days after the Zn peaks, indicating that the crud dissolved at lower temperatures (90°C), with Li and B levels maintained. Throughout the period, no increases in diameter were observed on the unfueled clad section.

## 2.5. Crud composition

Table 1 summarizes crud elemental compositions from several of the tests.

TABLE 1. CRUD COMPOSITION

Corrosion product levels, ppb	Composition, wt%			
	Fe	Ni	Cr	Zn
5 Fe, 0.2 Ni	56	12	22	BDL
1–20 Fe, 1.4 Ni	48	7	7	BDL
15 Fe, 2 Ni	27–40	60–68	BDL	BDL
3–15 Fe, 0.5 Ni, 50 Zn	25–37	1–4	BDL	10–15

BDL: below detection limit

While the first two lines in the table indicate that higher coolant nickel levels do not necessarily result in enhanced incorporation into crud, the results from the third line (with nickel injections) show clearly formation of nickel-enriched crud. Whether this behaviour can be explained by a critical Fe:Ni ratio or whether it shows experimental variability is not clear. The results from the final line show that even 50 ppb of coolant zinc did not result in a crud Zn fraction of more than 15 wt%. However, since the creep test discussed above showed crud releases both at power (when zinc levels were reduced) and during temperature changes, it is important to remember that post-irradiation examinations are not necessarily representative of crud compositions at power.

A comprehensive analysis was made of the crud deposits from the test with Fe and Ni additions [4]. The crud deposits were located along the upper 40 cm of the fuelled sections; i.e. those with high enrichment fuel resulting in sub-nucleate boiling. Crud samples were examined by light microscopy, SEM/EDS, X ray diffraction and gamma spectrometry.

The crud from the upper sub-cooled boiling sections of the rods showed a well developed chimney morphology (Fig. 8), and the EDS analysis indicated high Ni/Fe ratios, 1.2 to 1.4. These high Ni/Fe ratios can be compared to the 1:1 addition of soluble Ni:Fe during the experiment. In general, the deposits consisted of sub-micron, equiaxed particles, but at the uppermost elevations acicular particles were observed, with local regions varying from almost entirely acicular particles to regions containing few acicular particles in a matrix of fine particles (Figs 9 and 10). The acicular particles were very high in Ni, with only a little Fe. As XRD indicated the presence of NiO and NiFe<sub>2</sub>O<sub>4</sub>, the acicular particles are believed to be NiO, or bunsenite.

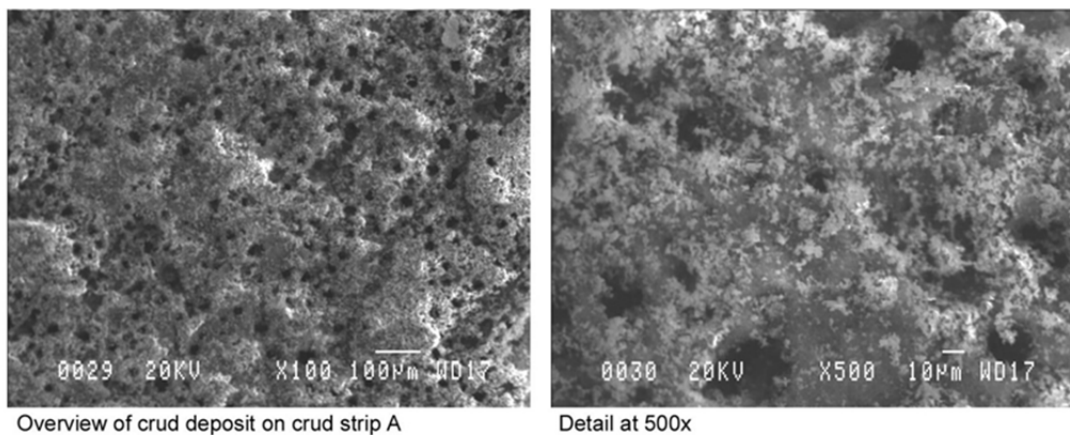


*FIG. 8. SEM micrographs showing chimney morphology of crud.*

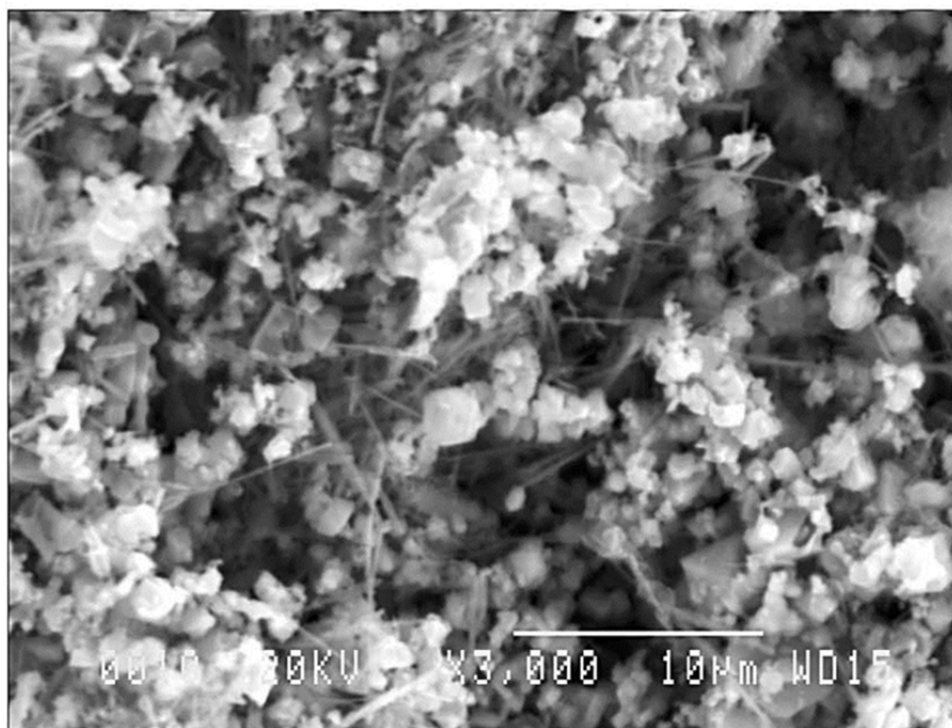


*FIG. 9. SEM micrograph of crud showing equiaxed and acicular particles.*

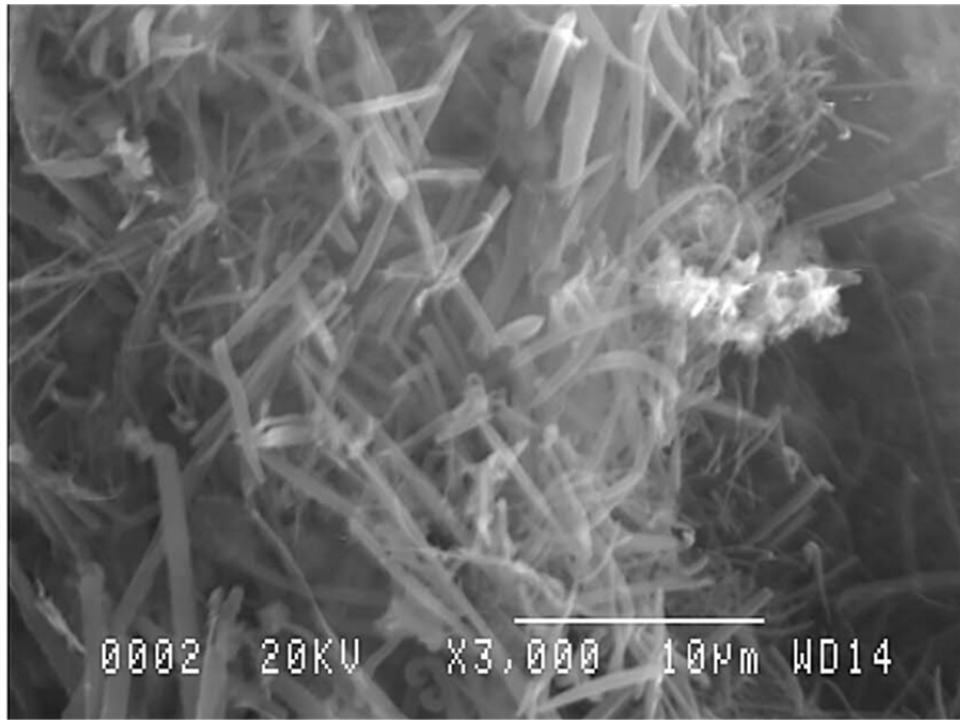


*FIG. 10. SEM micrograph showing equiaxed and acicular crud particles.*

### 3. CONCLUSIONS

- Avoiding crud deposits is difficult.
  - High duty can result in crud formation even with low corrosion product concentrations.
  - Elevated corrosion product concentrations can result in crud formation with low fuel duty.
- Chemical intrusions, leading to rapid formation of crud, show the importance of good chemistry control.
- PIE on crud does not necessarily give information on crud composition and morphology at power.

### REFERENCES

- [1] CHENG, B., SMITH, D., ARMSTRONG, E., TURNAGE, K., BOND, G., Water chemistry and fuel performance in LWRs, ANS TOPFUEL (2000).
- [2] TROPASSO, R., WILLSE, J., CHENG, B., Crud-induced cladding corrosion failures in TMI-1 Cycle 10, 2004 International Conference on LWR Fuel Performance, Orlando, USA (2004).
- [3] EPRI, Halden in-reactor test to exhibit PWR axial offset anomaly, EPRI, Palo Alto, CA: 1008106 (2004).
- [4] EPRI, Analysis of crud deposits from Halden in-reactor test to exhibit PWR axial offset anomaly, EPRI, Palo Alto, CA: 1013521 (2006).



# DEPOSITION OF STEEL CORROSION PRODUCTS ON CLADDING SURFACES AND CORROSION OF ZIRCONIUM

V.G. KRITSKY, I.G. BEREZINA, Y.A. RODIONOV  
Leading Institute "VNIPIET"  
Saint Petersburg, 197183, Russian Federation

## Abstract

If due to incorrect water chemistry, conditions for corrosion product deposition in the core are created, not only the activity of the coolant increases but the hydraulic resistance of the reactor also grows, which results in an increase of pressure drop in the reactor. The phenomenon of "pressure drop" which takes place in NPP with WWER reactors was considered. A model has been developed to explain the pressure drop rise in-core and deposit redistribution in the core and primary circuit of WWER-440 NPPs. The physico-chemical basis of the model is the transport corrosion product dependence on temperature, pH<sub>T</sub> value of coolant, and the correlation between rates of corrosion product (Fe) formation (after steam generators decontamination) and their removal from the circuit. Deposition along fuel rods causes sub-boiling and results in an acceleration of corrosion product and boron precipitation on the fuel cladding surface, an increase of the nuclide activation period and consequently coolant radioactivity. Activity of Co-58 is the indicator of deposit growth acceleration. The corrosion mechanism for Zr-Nb alloys shows complex character and depends on many parameters described in detail.

## 1. INVESTIGATION OF DEPOSIT GROWTH ON WWER-440 FUEL ASSEMBLIES AND OF PRESSURE DROP CHANGES

Growth of deposits on the reactor core surfaces results in a higher pressure difference across the reactor (reactor pressure difference—PDR), the value of which depends, apart from the section's hydraulic characteristic, on many parameters: the density of heat release in fuel assemblies, the nature of deposits on the surface, and others. The thickness of deposits is determined by the balance between the ingress and removal of corrosion products and impurities in the circuit, the power unit's age, decontamination operations, hydrodynamic parameters of coolant, and water chemistry. Operating experience has shown that migration of corrosion products in the circuit gives rise to certain problems. An empirical approach is often used in trying to solve such problems, and not always with success. This is because the deposit growth rate is a multiparametric function of the power unit operating conditions. Among the negative consequences stemming from growth of deposits in the core and increase in the pressure difference across the reactor are that the flow rate of coolant through the reactor tends to drop, that the maximum permissible rise of temperature is reached in some fuel assemblies, and that the reactor power has to be forcibly reduced up to complete shutdown when the PDR reaches its operational limit. Incidents connected with an increase in the pressure difference across the reactor are nowadays observed at almost all nuclear power plants (NPPs) equipped with WWER-440 reactors.

The coolant flow circulating in WWER reactors has a single-phase structure almost at all times during operation under steady conditions. A steam phase may appear in it only if an emergency drop of flow rate occurs. One factor due to which such a drop may occur is growth of deposits in the reactor core, which can precipitate, depending on the content of corrosion products (CPs) in the circuit and chemical composition of coolant:

- On the surface of the lower part of fuel rods due to gradient between the solubility of CPs on the surface and their concentration in the coolant [1]; it depends on water chemistry;
- On the surface of the upper part of fuel rods (the eighth spacer grid) due to the effect in which the density of heat release is anomalously distributed along the fuel rod axis, known as axial offset anomaly (AOA) [2];
- On spacer grids as a result of crude precipitating on them (the second spacer grid) [3];
- On the surface of casing tubes.

The dependence of increase rate of pressure drop upon pH<sub>T</sub> before decontamination (Fig. 1 (a)) and after decontamination (Fig. 1 (b)) is modified.

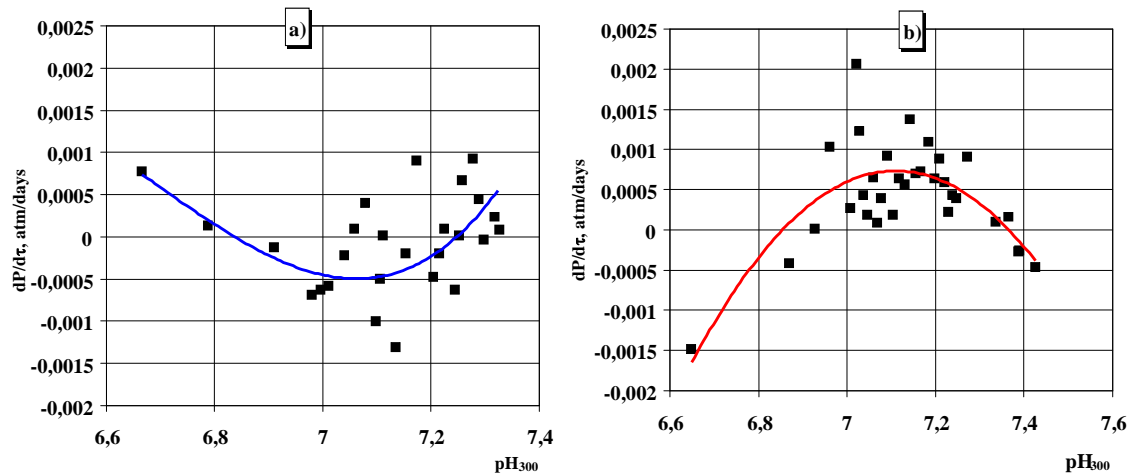


FIG. 1. The change of pressure drop increase rate depending on high temperature  $pH_{300}$  under different conditions of deposits formation (a) "classic" mass transfer, (b) anomalous mass transfer).

The reasons of this fact are the following:

- The great removal of corrosion products (CP) from steam generator surfaces after decontamination, change of CP behaviour and then consequent deposit of CP on the fuel element surfaces;
- Sub-cooled boiling takes place on some of the fuel element and results in the acceleration of corrosion products deposit, the increase of nuclide activation period and coolant radioactivity. This is a key problem.

The deposits along fuel rod can cause sub-boiling conditions and result in an acceleration of corrosion products and boron precipitation on the fuel cladding surface, an increase of nuclide activation period and coolant radioactivity (see Fig. 2).

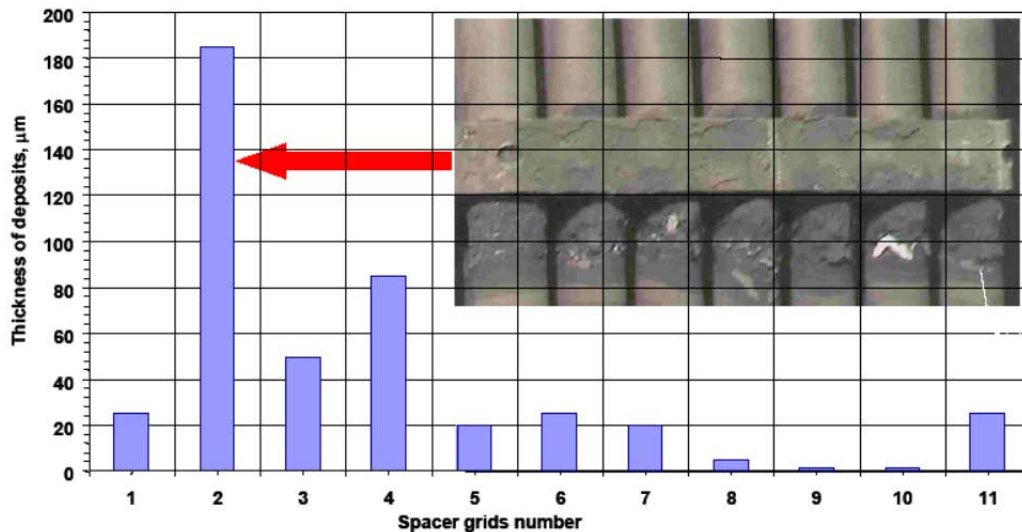


FIG. 2. The deposit value and acceleration of cladding corrosion along fuel rod N7 under spacer grids plates of fuel assembly after 4 years operation.

It is extremely difficult to take into account the effect a large number of physicochemical indicators and processes have on mass transfer of CPs. The activity, for example, of Co-58 is the indication of deposit growth acceleration (see Fig. 3).

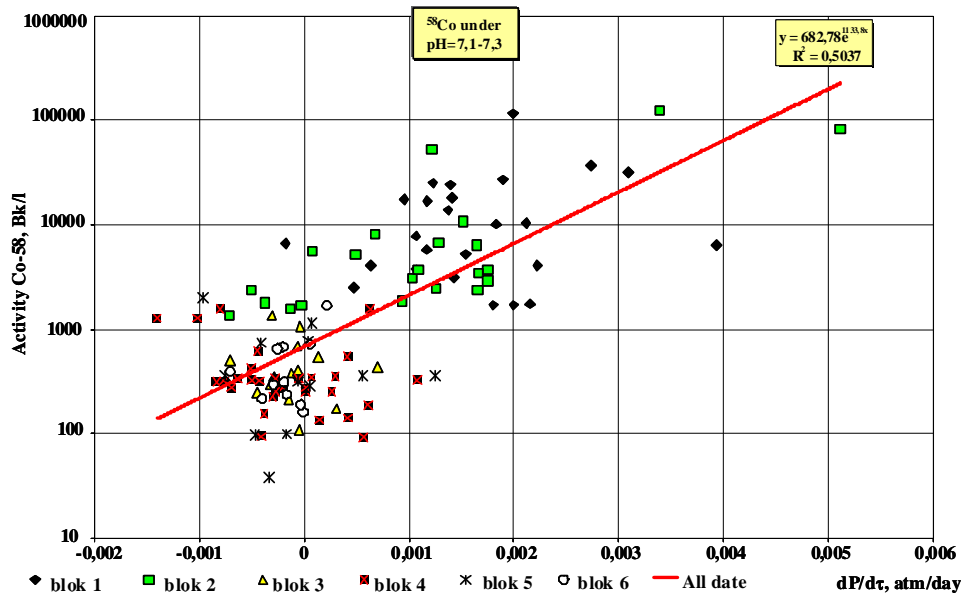


FIG. 3. Correlation between  $^{58}\text{Co}$  specific activity in NPP WWER coolant and rate of pressure drop change in pHT 7.1–7.3.

The aim of our modeling is to predict the growth of pressure difference on the basis of regular data available at an NPP and correct the water chemistry so that the pressure drop across the reactor is kept at a stable level by adjusting the concentrations of KOH,  $\text{H}_2$ , and  $\text{NH}_3$ .

The parameters that have been included in the model are:

- Operating parameters: reactor thermal power and concentration of boric acid. The concentration of boric acid is reduced and the reactor power output is decreased during the campaign to reduce the negative consequences stemming from a growth of pressure drop;
- Standardized and monitored parameters prescribed by the standards for the quality of water chemistry;
- Parameters determining the redox potential of the system: concentrations of hydrogen and ammonia;
- Parameters of the physicochemical model of mass transfer that characterize the direction of mass transfer;
- Parameters characterizing the composition of corrosion products in coolant.

The problem has been studied on the example of WWER-440 units, which have no anticorrosive surfacing on the vessel. The influence of water chemistry parameters and power unit characteristics (pressure drop at the beginning of the cycle, the number of decontaminations, the relationships of FA quantity of different age) were determined. The mathematical rate increase model of pressure drop has been developed (see equation (1)).

To construct a mathematical model all the data on units A and B for the 29–32 lifetimes have been summarized in one data file (2 147 points). The following equation has been used for preliminary calculations based on the physical and chemical models of mass transfer:

$$\Delta P_i = \Delta P_{in_k}^j + \Delta P_0^{(uni)} + a_0 + a_1 S_{Fe_i} T + a_2 \frac{\Delta S_{Fe_i}}{25} \Delta T + a_3 \lg(B/K)_i + a_4 W_i \quad (1)$$

where :

$a_0, a_1, a_2, a_3, a_4$  are coefficients;

$\Delta P_i$  is pressure drop in the  $i$ -th measurement,  $i$  — the number of point from 1 to 2147;

- $\Delta P_{ink}^j$  is the initial pressure drop in k-th lifetime after i-th shutdown. This indicator includes in-core CP mass;
- $\Delta P_0^{(unit)}$  is the value of pressure drop of the unit to be determined by unit characteristics;
- $S_{Fei}$  is calculated iron (out of magnetite) solubility at 300°C;
- $T$  is the temperature, it is introduced to take into account in-core coolant overheating due to PD rise;
- $\Delta S_{Fei}$  is iron solubility difference at 300 and 275°C;
- $\Delta T$  is actual temperature gradient between the wall and coolant temperatures;
- $lg(B/K)$  is decimal logarithm of boron-potassium proportion taken in molar concentrations. This magnitude specifies pH<sub>300</sub> value;
- $W$  is reactor thermal capacity.

The calculated and actual values of the pressure drop rates (PDR) are shown in Fig. 4. We see the good correlation between calculated and actual data.

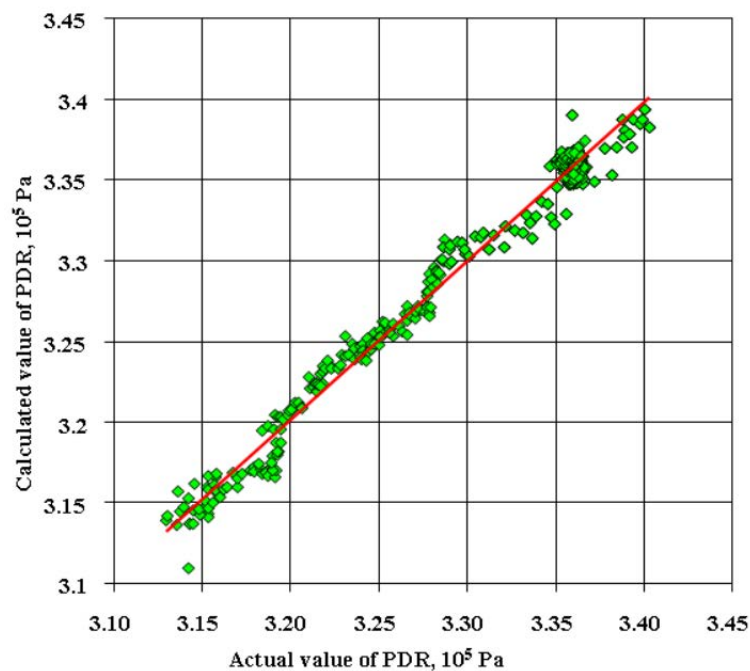


FIG. 4. Correlation between experimental and calculated values of PDR in Unit 4 at the Novovoronezh NPP (the 32nd campaign).

Thus, we can make the following summary:

- The phenomenon of "pressure drop" which takes place in NPP with WWER reactors was considered.
- A model was developed to explain pressure drop rise in-core and deposits redistribution in the core and in the primary circuit of NPP with WWER-440. The physical-chemical basis of the model is the transport corrosion products dependence on temperature, pHT value of coolant, and correlation between rates of corrosion products (Fe) formation (after steam generators decontamination) and their removing from the circuit.
- Deposits along the fuel rod cause sub-boiling and result in an acceleration of corrosion product and boron precipitation on the fuel cladding surface, an increase of nuclide activation period and coolant radioactivity. Activity of Co-58 is the indicator of deposit growth acceleration.

## 2. THE MODELLING OF ZIRCONIUM ALLOY CORROSION IN NPP COOLANTS. CORROSIVE STATE OF WWER FUEL ASSEMBLIES CONSTRUCTIVE ELEMENTS

Consolidated data on corrosive state of fuel assemblies constructive elements made from zirconium alloy E110 are shown in the Table 1.

TABLE 1. CORROSION DATA FOR ASSEMBLY COMPONENTS OF E110 ALLOY

Element	Thickness of oxide film ( $\mu\text{m}$ )	
	3–4 fuel cycle	5–6 fuel cycle
Fuel element cladding	2–7	15–16
Zirconium space grid	up to 90	upon to 200

The corrosive state of E-110 fuel elements claddings after six fuel cycles without sub-boiling is shown in Fig. 5. Frontal corrosion leads to the formation of uniform dense oxide film with  $10 \mu\text{m}$  of thickness in the upper part of fuel element. In the rare cases the hot-spot corrosion with oxide film thickness up to  $18 \mu\text{m}$  is observed. The increased corrosion of WWER-440 and WWER-1000 fuel elements claddings operated under design conditions up to high fuel burnup was not observed.

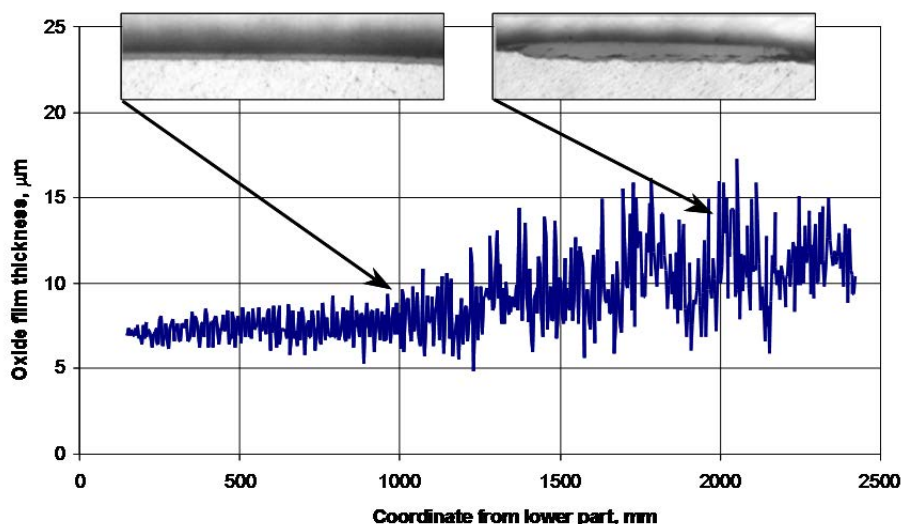


FIG. 5. Corrosive state of fuel elements claddings E 110 after operation within 6 fuel cycles without sub boiling.

In the WWER-440 zirconium spacer grids cells operated up to five fuel cycles the moderate amount of hydrides with advantageously tangential orientation is observed. The hydrides size achieves  $100 \mu\text{m}$ . In the most of welds of space grid cells the crevice corrosion is missing. The local crevice corrosion with thickness up to  $\sim 200 \mu\text{m}$  is observed for negligible number of cells (Fig. 6).

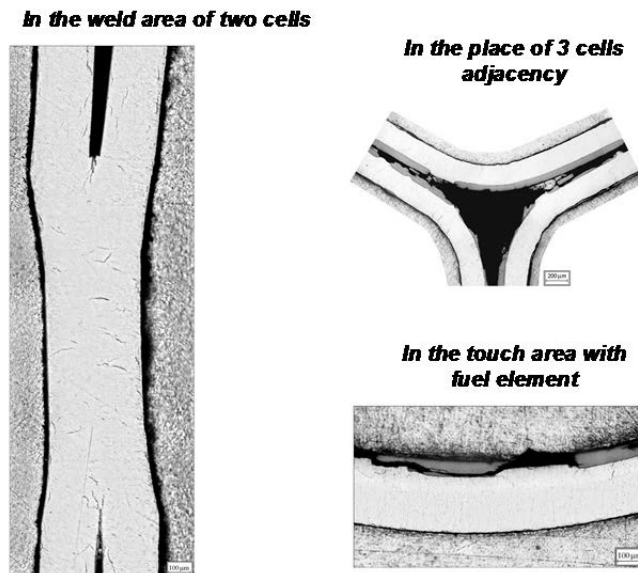


FIG. 6. The microstructure of various parts of WWER-440 zirconium spacer grids.

## 2.1. Influence of water chemistry and alloys composition on corrosion behaviour of Zr alloy in NPP

The corrosion mechanism for Zr-Nb alloys shows complex character and depends on many parameters described in detail. The oxidation rate can be expressed as  $V = dS/dt = k_T + k_\Phi$ , where  $k_T$  and  $k_\Phi$  are the heat and neutron radiation components respectively.

Empirical studies of numerous oxidation reactions have shown that under constant oxygen pressure in the environment the temperature dependence on the oxidation rate of Zr alloys can be described by the Arrhenius equation:

$$k_T = k_0 \exp\left[-\frac{Q}{R(T + \Delta T)}\right] \quad (2)$$

where

- Q** is the activation energy,
- R** is the gas constant,
- T** is the absolute temperature at the coolant/cladding interface,
- $\Delta T$**  is the growth of cladding temperature under corrosion deposits layer.

The experimental value of  $Q/R$  is  $(6.5-13) \cdot 10^3 K$  [1-3]. The following experimental facts have revealed the influence of water chemistry on Zr-alloys corrosion:

- Influence of water pH (Fig. 7b,c);
- Influence of  $H_2O_2$  concentration;
- Decrease of corrosion film thickness in the transient stage (i.e. practically its partial dissolution [4]);
- Morphology of > 3-5 mm thick films (formation of grains and pores of different size but the same geometric form) [4];
- Crystallization of the dissolved phase in the form of fine  $ZrO_2$  powder in the water volume of the steam separator of RBMK reactor.

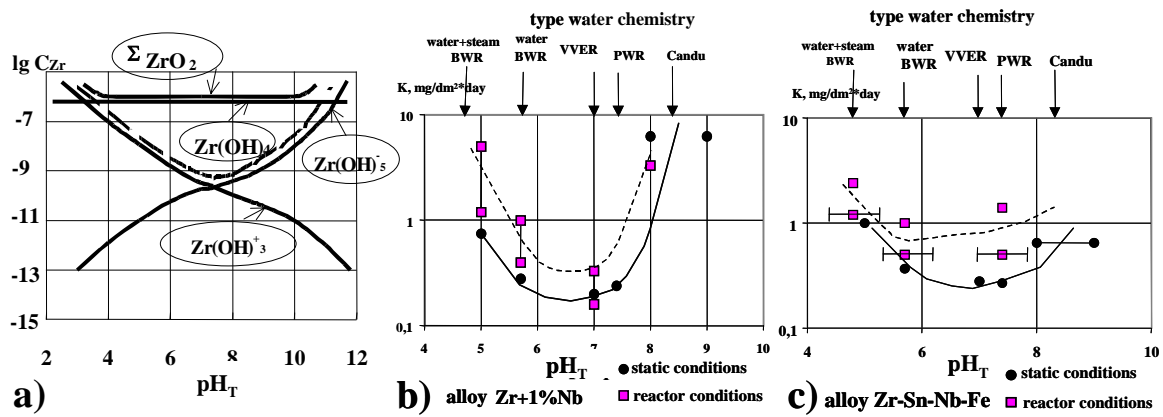


FIG. 7. (a) The values of calculated solubilities of zirconium corrosion products (mole/kg) In PWR conditions [5] versus  $pH_T$ , - - - - envelope  $[Zr(OH)_5 + Zr(OH)_3]$  (b),(c) The Zr alloys corrosion dependence on  $pH_T$  value under static conditions, 360°C (—) and under operation (- - - -); testing time: 300–600 days.

It is well known that the solubility of oxides is dependent on T, pH and the concentrations of salts and impurities in solution. The solubility was determined [5, 6] for the systems: zirconium corrosion products ( $ZrO_2$ ,  $Zr(OH)_4$ ) — water ( $H_2O$ ) — corrective additives (HCl, KOH) over the temperature range of 298–623 K and the correlation between the solubility and Zr alloys corrosion rate was analysed. Fig. 7(a) shows the calculated solubilities of zirconium corrosion products in LWR conditions. Comparing the data in Fig. 7(a) with Figs 7(b) and 7(c) shows that the change of the corrosion rate with  $pH_T$  is adequate to that of the sum of  $Zr(OH)_3$  and  $Zr(OH)_5$  — concentrations, which fact confirms the validity of the model adopted. According to [5], the equilibrium solubility of  $ZrO_2$  dependence on the temperature is described by an equation similar to Eq.2, with  $Q/R = (5 \div 15) \times 10^3$  K.

The rate of Zr alloy corrosion under reactor irradiation depends on heat flux through fuel cladding coolant chemistry (in addition to  $H_2O_2$ ,  $OH^-$ ,  $O^{2-}$  concentrations one should account for the concentrations of hydrogen, ammonia, strong alkalis — LiOH, KOH, pH, etc.) and some other parameters [7].

The activation energy of radiation corrosion is very small so  $Q\phi=0$ . The concentration of dissolved oxygen and products of water coolant radiolysis ( $H_2O_2$ ) is one of the important factors that influences on the radiation corrosion [1]. Probably, the  $H_2O_2$  influence is based on the formation of unstable compound  $ZrO_3 \cdot nH_2O$  and compound with high solubility  $Zr(OH)_4$ . It produces strong effect on the stationary concentrations of practically all products of water coolant radiolysis. In the case of two-phase flow (BWR conditions) we have expression:

$$k_{\Phi}^{BWR} = N \frac{K_G^{H_2}}{p} \Phi^{n\alpha} \quad (3)$$

where

- N is constant;
- $\Phi$  is fast neutron fluence;
- $n = 0.5-1$ ;
- $K_G^{H_2}$  is Henry constant;
- p is pressure;
- $\alpha$  is mass vapour content ( $\alpha = 0 \dots 1$ ).

Figure 8 shows the vapour content influence on linear Zr-alloy corrosion LWR environment.

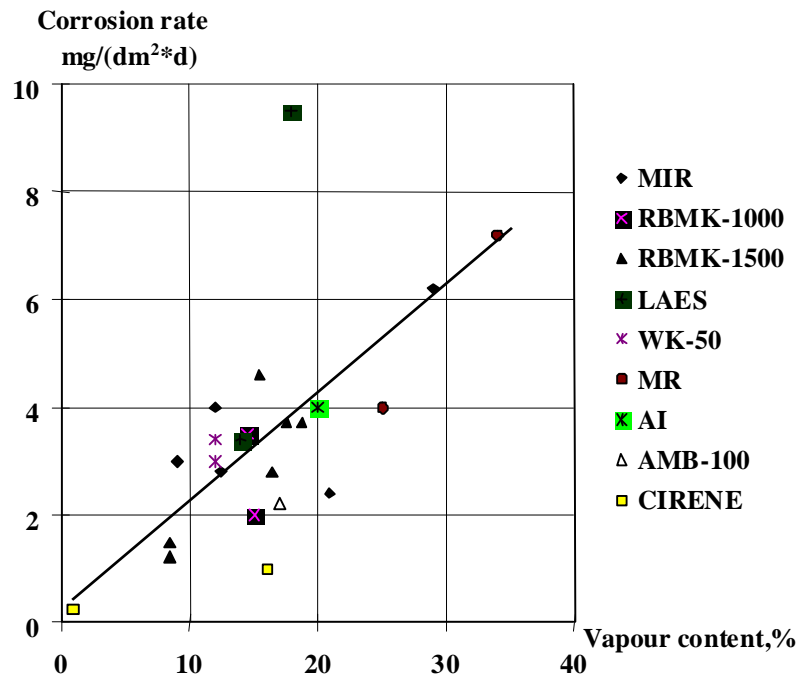


FIG. 8. The vapour content influence on linear Zr-alloy corrosion in various LWR environments.

In the case of single-phase flow (PWRs) the material balance equation has another solution. For the first approximation for PWRs, if  $\alpha=0$  one can assume that  $k_{\phi}^{\text{PWR}} \gg 0$ .

A system of equations, which take into account the above mentioned factors for producing a generalized model for calculating Zr alloys corrosion is presented in Table 2.

TABLE 2. SYSTEM OF EQUATIONS FOR GENERALISED MODEL OF ZR-ALLOYS CORROSION AND FUEL FAILURE INTENSITY

No	Parameter	Equation
1	Composition of alloy	$\ln K_i \sim \frac{\Sigma \Delta G_{Me} - \Sigma \Delta G_{Me_m O_n}}{RT}$ <p><math>K_i</math> — corrosion rate; <math>R</math> — universal gas constant; <math>T</math> — the environment temperature</p>
2	Temperature, heat flow	$K_i \sim K_{i0} \exp[-\Delta G / (R(T + \Delta T))]$ <p><math>\Delta G</math> — energy activation of corrosion process,  <math>\Delta T \sim \Delta \delta q / \lambda</math> — temperature drop on oxide thickness, <math>\Delta \delta</math> — the thickness of oxide film, <math>q</math> — heat flux through wall of fuel element, <math>\lambda</math> — effective heat conduction of oxide layer</p>
3	Radiation, vapour content	$K_j \sim K_{j0} \alpha \Phi^n$ <p><math>n</math> — constant</p>
4	Water chemistry, coolant impurities	$pH_T \rightarrow C_{Zr(OH)_n^{4-n}}$ $K_i \sim K_{i1}$ $K_{i1} \sim C_x (RT/h) \exp(\Sigma \Delta G_{ij} / RT)$ <p><math>C_x</math> — concentration of ion "x" in the coolant; <math>h</math> — Plank constant</p>
5	General corrosion equation	$K = k_1 \left[ \frac{1}{1 - \alpha} \exp\left(-\frac{\Sigma \Delta G}{R(T + \Delta T)}\right) \right] + k_2 \frac{1}{1 - \alpha + \beta} \Phi^n$ <p><math>\Delta T \sim \Delta \delta q / \lambda</math>  <math>\Sigma \Delta G = \Delta G_o + \Delta G_{TZrO_2} + \Delta G^\#</math>  <math>\Delta G^\# = \Sigma \Delta G_i</math>, were <math>\Delta G_i</math> is energy contributions of alloying components and water impurities to oxide formation, <math>k_1</math> — the constant depending on water chemistry; <math>k_2</math> — the constant depending on neutron radiation, <math>\beta</math> — the constant taking into account impurities concentration, which depresses the radiolysis process</p>

These equations describe the uniform and nodular corrosion of E-110 alloy under LWR's operation conditions. The correlation analysis has proved the applicability of the before developed model [3] which include the equations 2 and 3 from Table 2 and derived equations for describing the experimental data.

Equation 1 from Table 2 takes into account the effect of alloying components, which can be considered through the energies of mixed oxides formation by the model of ideal solutions. The energy of mixed oxide is calculating as the sum of alloy components energies with accounting of stoichiometric coefficients.

The correlation between corrosion rates of Zr+1% alloying component in steam at 400°C and the energy of alloying component oxide formation is shown in Fig. 9.

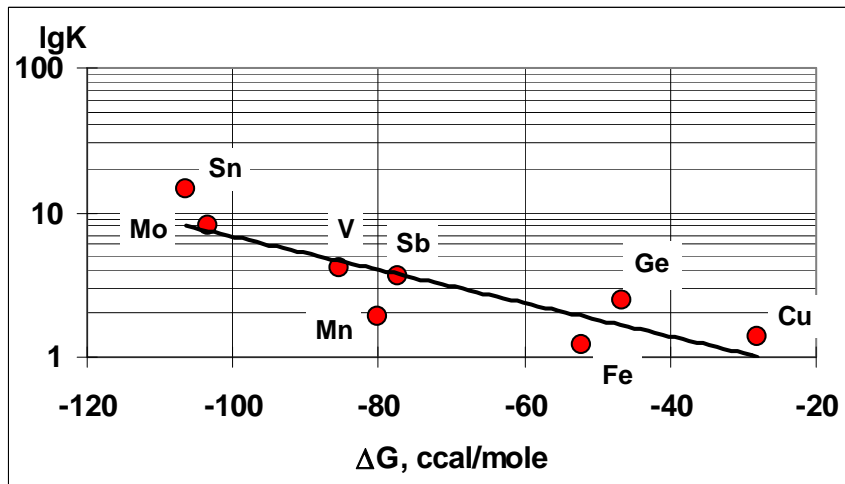


FIG. 9. Correlation between corrosion rates of Zr+1%alloys ( $\text{mg}/(\text{dm}^2 \cdot \text{day})$ ) in steam at  $400^\circ\text{C}$  and 17 MPa and the heat of formation of alloying component oxide.

Figure 10 represents the influence of alloying components on Zr-alloy corrosion (data from [8, 9] have been used). Figure 11 gives a correlation between the corrosion rates for various Zr-based alloys in PWR and the energy of mixed oxides formation (calculated with the data from [9–12]).

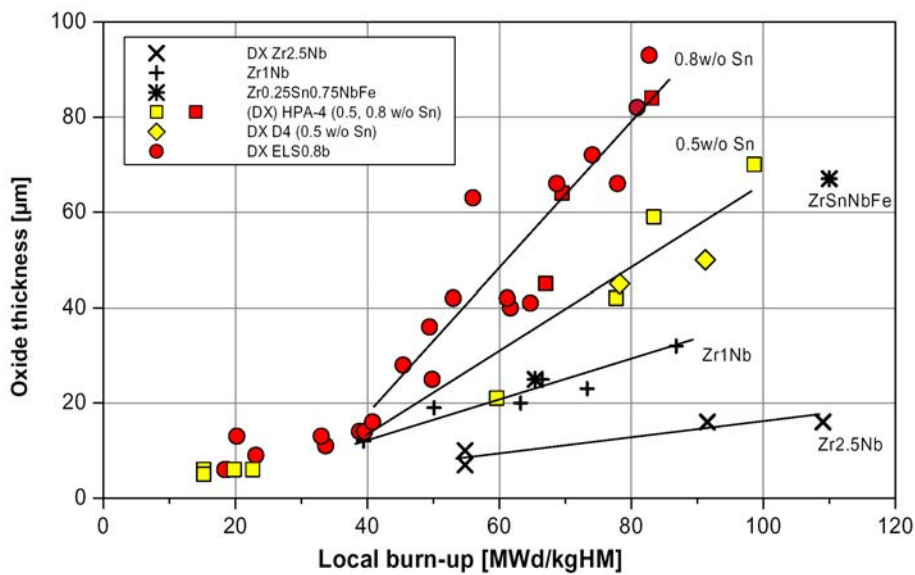


FIG. 10. Influence of alloying components on Zr-alloy corrosion (Goll V., Helvig Ch., Hoffman P. et al., The behaviour of  $\text{UO}_2$ -fuel with burnup  $105 \text{ MW} \cdot \text{d}/\text{kgU}$ .)

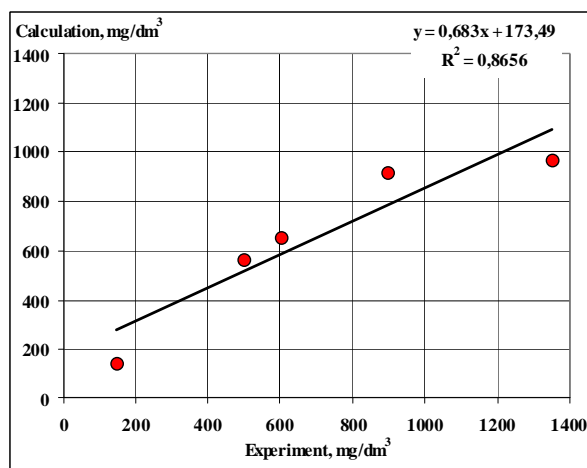


FIG. 11. Correlation between calculating and experimental data on over weight ( $\text{mg}/\text{dm}^3$ ) of zirconium alloys M5, Zr-2.5Nb, Zr-0.25Sn,0.75Nb; Zr0.5Sn, ELS08 under corrosion tests in PWR NPP up to burnup 80 MW-d/kgU (see Fig. 10).

The success of such approach makes possible to propose a generalized model for calculating the corrosion of Zr-alloys. Thus, we can make the following summary:

- A model of fuel cladding corrosion was developed to describe the effect of physical and chemical parameters of Zr alloys under LWR conditions. The choice was made of chemical parameters which influence on Zr corrosion and can be considered during reactor operation.
- The activation energy of oxidation process is calculated on the base of an ideal mixed oxide formation model. The calculation formulae were verified on the base of experimental data on fuel cladding corrosion in the autoclave and NPPs LWR reactors.
- The success of such approach makes possible to propose a generalized model for calculating the corrosion of different Zr alloys in all types of water chemistry environments of old and new LWRs.

### 3. CONCLUSIONS

A model was developed to explain pressure drop rise in-core and deposits redistribution in the core and in the primary circuit of NPP with WWER-440. The physical-chemical basis of the model is the transport corrosion products dependence on temperature, pHT value of coolant, and correlation between rates of corrosion products (Fe) formation (after steam generators decontamination) and their removing from the circuit.

The deposits along fuel rod bring to sub boiling and results in a acceleration of corrosion products and boron precipitation on the fuel cladding surface increase of nuclide activation period and coolant radioactivity. Activity of Co-58 is the indicator of deposits growth acceleration.

A model was developed to predict the corrosion of Zr alloys under LWR conditions, which take into account the physical parameters, water chemistry and alloy composition.

## REFERENCES

- [1] ZAREMBO, V.I., KRITSKII, V.G., SLOBODOV, A.A., PUCHKOV, L.V., Solubility of magnetite under the conditions of reducing medium in the water of a nuclear power station at elevated temperature," *At. Energ.* **64** (1988) 223–225.
- [2] FRATTINI, P., BLANDFORD, E., HUSSEY, D., etc., Modeling axial offset anomaly. *Proc. Water Chemistry of Nuclear Reactor System*, San Francisco, California. CD disk, (2004) 455–461.
- [3] ROSENBERG, R.J., TERÄSVIRTA, R., HALIN, M., SUKSI, S., Investigation of iron deposits on fuel assemblies of the Loviisa 2 WWER-440 reactor. In *proc. Water Chemistry of Nuclear Reactor Systems 7*, BNES, Bournemouth (1996). 27 – 33.
- [4] INTERNATIONAL ATOMIC ENERGY AGENCY, Corrosion of Zirconium Alloys in Nuclear Power Plants. IAEA-TECDOC-684, IAEA, Vienna (1993).
- [5] PYECHA, T.D., BAIN, G.M., McINTEER, W.A., PHAM, C.H., External cladding corrosion of B&W-designed PWR fuel rods through burnups of 50 GWD/MtU", IAEA Technical Committee on External Cladding Corrosion in Water Power Reactors, Cadarache, France, (1985).
- [6] KRITSKIJ, V.G., PETRIK, N.G., BEREZINA, I.G., DOILNITSINA, V.V., Effect of water chemistry and fuel operation parameters on Zr+1%Nb cladding corrosion, IAEA Meeting on Influence of Water Chemistry on Fuel Cladding Behaviour. Řež, Czech Republic, (1993). IAEA-TECDOC-927, IAEA, Vienna (1997) 23–43.
- [7] JEONG, Y.H., RUHMANN, H., GARZAROLLI, F., Influence of alkali metal hydroxides on corrosion of Zr-based alloys. IAEA Influence of water chemistry on fuel cladding behaviour. Proceedings of a Technical Committee meeting held in Řež, Czech Republic, 1993. IAEA-TECDOC-927, IAEA, Vienna (1997) 161–192.
- [8] MAROTO, A.J.G., et al., Growth and characterisation of oxide layers on zirconium alloys, IAEA Meeting on Influence of Water Chemistry on Fuel Cladding Behaviour. Řež, Czech Republic, IAEA-TECDOC-927, IAEA, Vienna (1997).
- [9] KRITSKIJ, A.V., Rastvorimost produktov korrozii zirkoniya i hroma v vodnih rastvorah pri 298–623 K, Avtoreferat dissertatsii na sooiskanie uchyonoj stepeni kandidata himicheskikh nauk. S. Petersburg (1992).
- [10] AMAEV, A.D., et al., Obosnovanie vybora zirkonievogo splava dl'a obolochek tvelov seriynyh energeticheskikh reaktorov WWER-440, Trudy nauchno-tehnicheskoy konferentsii "Atomnaya energetika, toplivnye tsikly, radiatsionnoe materialovedenie". Ul'yanovsk, Russian Federation, (1970).
- [11] PARFENOV, B.G., GERASIMOV, V.V., VENEDICTOVA, G.I., Corrosion of zirconium and its alloys. M. Atomizdat, (1967).
- [12] Thermodynamic Properties of Inorganic Substances. Guidebook. ZEFIROVA A.P., Atomizdat, (Ed.) (1965).

# FORMATION OF CORROSIVE DEPOSITS AND THEIR IMPACT ON OPERATIONAL SAFETY OF FUEL ELEMENTS IN CANDU REACTOR

I. PIRVAN, M. MIHALACHE  
Institute for Nuclear Research,  
115400 Mioveni,  
Pitesti, Romania

## Abstract

Interaction between fuel element cladding and water coolant plays an important role in normal operation, can have a dominant role in accidental situations and can lead to failure of fuel rods and activity release. For the future, the tendency will be to increase the coolant temperature, extend fuel residence time in the reactor core (for higher burnup) and increase the heat flux. This can lead to increased probability of fuel failures due to waterside corrosion, corrosion products accumulation and deposition. In order to prevent cladding failures, the coolant chemistry must be monitored and controlled in order to reduce the amount of deposited crud and the oxygen potential. Corrosive deposits together with aqueous corrosion influence the performance of fuel elements by increase of temperature on cladding surface or changes in the coolant chemistry (increase of water pH), phenomena which lead to cladding failures. The process of corrosion products formation on zircaloy-4 fuel cladding surface and their consequences was evidenced by performing of experiments in: autoclaves circuits assembled in a by-pass loop of a CANDU-6 Reactor at NPP Cernavoda; irradiation loop of the TRIGA Reactor, and in laboratory static autoclaves. The determination of corrosion and the characterization of crud deposits on the zircaloy-4 surfaces were performed using gravimetric method, metallographic and electronic microscopy, and gamma spectrometry analysis and impedance electrochemical spectroscopy (EIS) determinations. The experimental results showed that the composition, thickness and evolution of corrosive deposits on fuel assembly surfaces depend very much on operational conditions, such as steady state operation, water chemistry conditions (pH and oxygen concentration) and different oxidation conditions of cladding surface.

## 1. INTRODUCTION

The formation, transport and deposition of the corrosion products in nuclear systems are very important and must be considered by operators of nuclear plants.

The extended fuel residence time in the reactor core for higher burnup can lead to increased probability of fuel failures due to water side corrosion, corrosion products accumulation and deposition. Fuel rods can become covered with deposits of corrosion products, which have precipitated from the coolant during operation.

Crud deposits affect the fuel rod performance by an immediate consequence which is a cladding temperature increase. The ultimate damage which results from such a temperature increase is a perforation of the cladding. Also, crud deposits are very porous, and in PHWR this porosity can potentially cause concentration chemical species (lithium) within the deposits, which can be detrimental to cladding performance from zircaloy-4 alloy. Moreover boiling inside crud porosity may decrease the local hydrogen concentration. Oxidizing species, such as  $H_2O_2$  formed by radiolysis, may be concentrated in the crud and corrosion can be accelerated. In addition, the crud on cladding behaves as a thermal barrier and the activated crud released back to coolant would increase radiation dose rate around the circuit.

Precipitation of crud deposits in the core must be avoided as far as possible, as it can lead to fouling of the fuel, loss of heat transfer efficiency, fuel failures, increased radiation fields and to neutronic disturbances in the core.

The deposition rate on surfaces is controlled by the concentration of impurities in the coolant, the pH of the water and the surface temperature. In order to prevent cladding failures, the coolant chemistry must be monitored and controlled in order to reduce the amount of deposited crud and oxygen potential.

## 2. EXPERIMENTAL

The process of corrosion products formation on zircaloy-4 fuel cladding surface and their consequences was evidenced by performing of some experiments in:

- Autoclaves circuits assembled in a by-pass loop of a CANDU-6 Reactor at NPP Cernavoda;
- Irradiation loop of the TRIGA Reactor;
- Laboratory static autoclaves.

The corrosion products formation on fuel cladding surface during steady state operation was followed by exposition of zircaloy-4 coupons in autoclaves circuits assembled in a by-pass loop of CANDU-6 Reactor at NPP Cernavoda.

The chemistry conditions for autoclaves circuits were standard conditions for the reactor, which comply with the chemical control and diagnostic parameters for steady state operation of CANDU-6 Reactor [1].

The determination of corrosion and the characterization of crud deposits on the zircaloy-4 alloy surface were performed using gravimetric method, metallographic and electronic microscopy, and gamma spectrometry analysis and impedance electrochemical spectroscopy (EIS) determinations [2].

To performing of experiments in irradiation loop of the TRIGA Reactor used the experimental fuel assembly presented in Fig. 1.



*FIG. 1. Experimental fuel assembly.*

The corrosion testing conditions in loop were:

- LiOH solution, pH = 9.5 –10.5 and conductivity < 100 mS/cm;
- O<sub>2</sub> concentration < 50 ppb;
- Maximum temperature at fuel rod surface = 300°C and pressure = 10.6 MPa;
- Coolant flow = 3 l/h;
- Linear power = 420 W/cm and burnup = 190 MW·h/kgU.

Taking into account that the water chemistry (pH and O<sub>2</sub> concentration) has an important role in formation of corrosion products, CANDU fuel claddings were tested in irradiation loop in the following conditions:

- LiOH solution, pH >10.5, (pH ~11.7);
- O<sub>2</sub> concentration >100 ppb;
- Maximum temperature at fuel rod surface = 330°C and pressure = 10.6 –10.7 MPa;
- Debit = 1.45 – 1.5 l/s;
- Linear power = 250 W/cm and burnup = 110 MW·h/kgU.

An assessment of crud and the impact of this on cladding corrosion were performed by sending of fuel claddings to the hot cell for examination and destructive evaluation [3].

The destructive examinations included cutting transverse cross-sections of the cladding for metallographic examinations. These examinations were performed to measure the thickness of crud and to evidence the effect of these deposits on fuel rod material corrosion, this effect being evidenced and by eddy current control.

The quantity of the adherent corrosion products was dependent of thickness and especially physical–chemical characteristics of the initial zirconium oxide films. To evidence this fact, as well as the impact of corrosive deposit on zircaloy-4 alloy oxidation and hydriding, a lot of laboratory experiments performed in static autoclaves at different temperature on zircaloy-4 coupons, used in PHWR systems [4, 5].

Analysis of the corrosive deposits, oxidation and hydriding of zircaloy-4 alloy were performed using, gravimetric analysis, metallographic and electronic microscopy examinations and electrochemical spectroscopy impedance determinations.

### 3. RESULTS

#### 3.1. Corrosive deposits formed on fuel claddings during steady state operation of CANDU reactor.

The deposition of crud was gravimetric determined from the coupons of zircaloy-4 alloy inserted in reactor outlet autoclaves (310°C) and reactor inlet autoclaves (260°C) during 825 exposure days. Fig. 2 presents the results of total, adherent and loose crud.

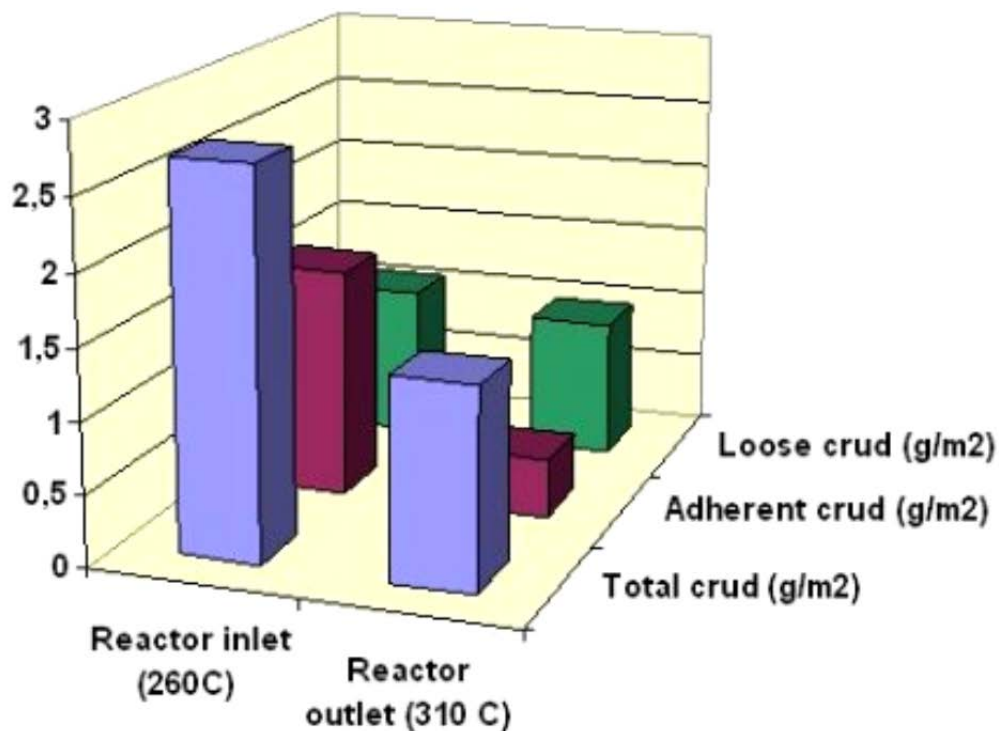
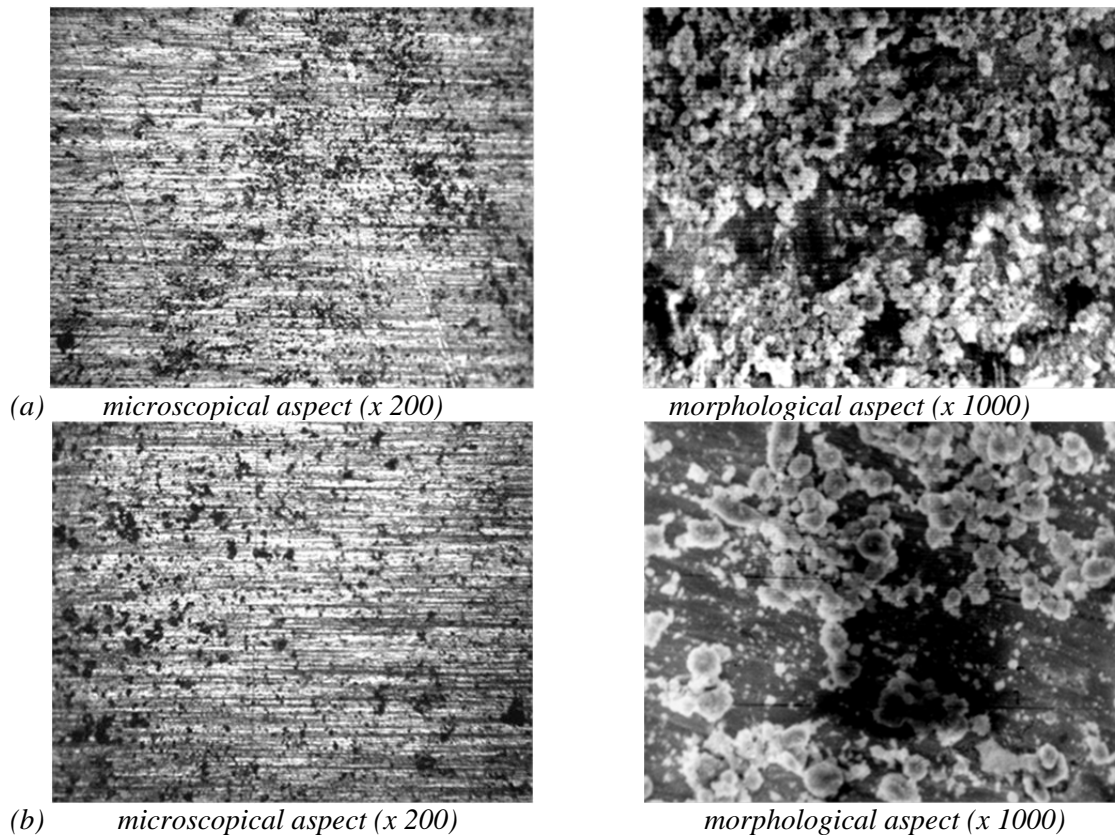


FIG. 2. Total, adherent and loose crud on zircaloy-4 coupons after 825 exposure days.

The values of crud thus obtained are in agreement with the theories that explain the mechanism of generation of corrosion products in CANDU reactors with carbon steel feeders [6, 7]. The coupons from inlet reactor autoclaves (260°C) have larger deposits since the coolant is probably still supersaturated in iron respect the solubility value and present a larger percentage (60%) of adherent crud deposited on the surface. The coupons inserted in outlet reactor autoclaves (310°C) show smaller values of total deposits and a smaller percentage of adherent crud (30%), this difference can be

attributed to the presence of particulate matter that is formed by erosion of crystals recently precipitated.

Corrosion products deposits in shape of black magnetite crystalides were evidenced on the coupons surface, Fig. 3.



*FIG. 3. Deposits of the corrosion products on zircaloy-4 coupons surface after 825 exposure days: (a) reactor inlet autoclaves and (b) reactor outlet autoclaves.*

These deposits were in shape of fine, relatively numerous and adherent magnetite crystalides on coupons inserted in reactor inlet autoclaves and the bigger and relatively rare were on coupons inserted in reactor outlet autoclaves.

The thickness of crud was measured from the metallographic samples. The thickness of the film with adherent corrosion products was about 3–5.5  $\mu\text{m}$ .

The corrosive deposits presented a non-adherent exterior layer with increased porosity and an adherent and non-porous interior layer, with similar porosity of the zirconium oxide (Fig. 4).

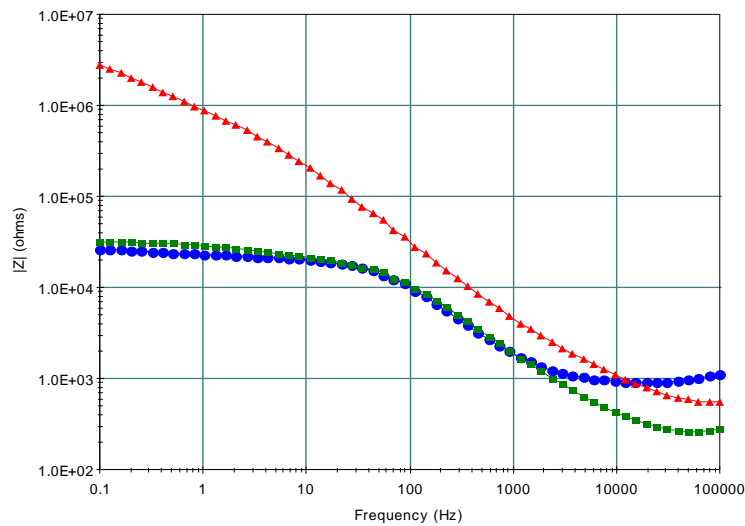


FIG. 4. Impedance/frequency variation for: (blue)-oxidized zircaloy-4 coupon; (red)-zircaloy-4 coupon with total corrosive deposits; (green)-zircaloy-4 coupon with adherent corrosive deposits.

Radionuclides determined by gamma spectrometry were generally,  $^{54}\text{Mn}$ ,  $^{60}\text{Co}$ ,  $^{95}\text{Zr}$ ,  $^{95}\text{Nb}$ . A bigger variety of radionuclides as:  $^{65}\text{Zn}$ ,  $^{59}\text{Fe}$ ,  $^{103}\text{Ru}$ ,  $^{124}\text{Sb}$ ,  $^{125}\text{Sb}$ ,  $^{141}\text{Ce}$ , after 568 exposure days was evidenced.

Visual examination of fuel rods after 190 exposure days, in normal water chemistry, in irradiation loop evidenced presence of very fine, black magnetite deposits on Zy-4 sheath surface (Fig. 5).

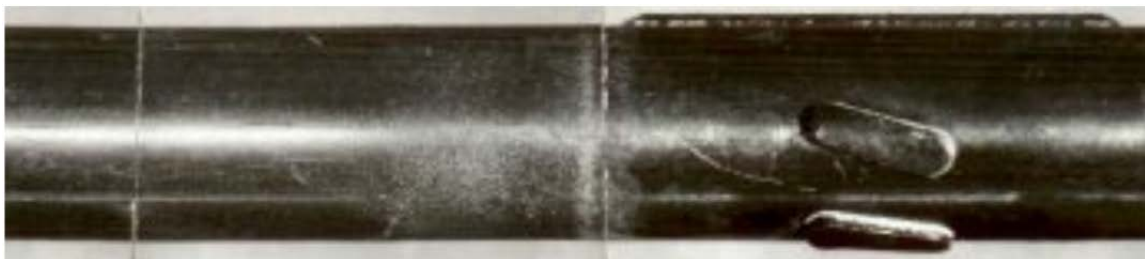


FIG. 5. Magnetite deposits on zircaloy-4 sheath surface.

Corrosive deposits formed in normal water chemistry conditions did not influence oxidation and hydriding of cladding material. Thus, the corrosion rate was about  $0.276\text{--}0.313\ \mu\text{m}/\text{dm}^2\text{day}$  and metallographic examination evidenced presence of uniform zirconium oxide, having a thickness of  $2\text{--}3\ \mu\text{m}$  and an acceleration hydriding did not happen after 825 operation days (Fig. 6). Morphology of hydrides was similarly with that of coupons tested in identical conditions from out reactor experiments.

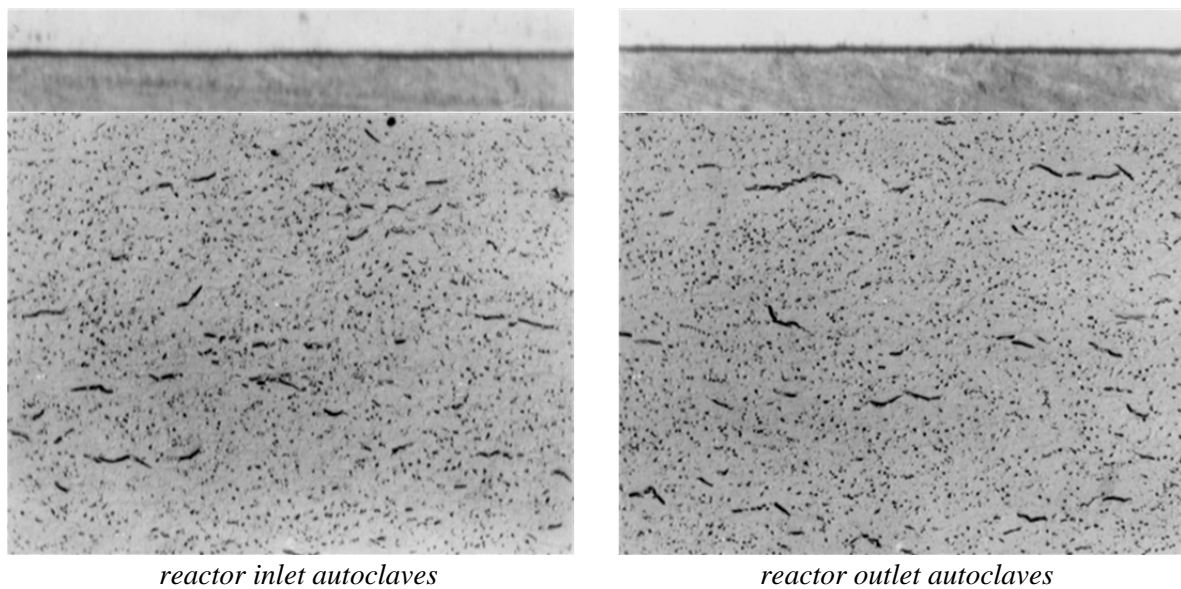


FIG. 6. Aspect of oxides (x500) and hydrides (x250) formed on Zy-4 coupons after 825 days.

### 3.2. Corrosive deposits formed on fuel claddings in abnormal water chemistry conditions

In presence of abnormal water chemistry conditions, such as  $\text{pH} > 10.5$  (about 11.7) adjusted with LiOH or  $\text{O}_2$  concentration  $> 100 \text{ppb}$  (cca 200ppb), abundant corrosive deposits were evidenced. Thus, crud deposits on fuel rods have been observed during visual examination after 90 and 180 irradiation days (Fig. 7).

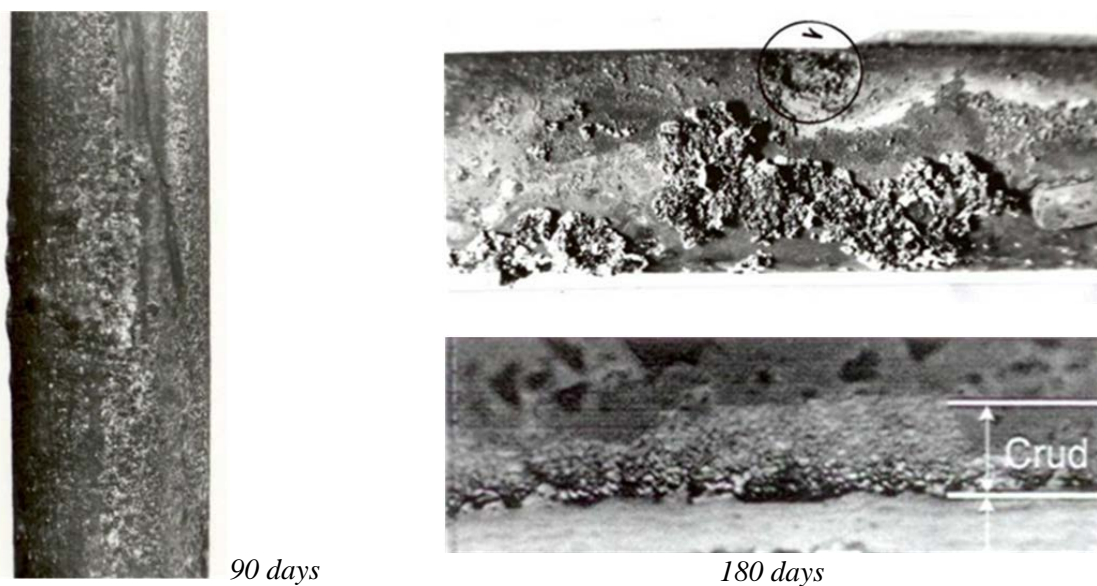


FIG. 7. Deposits of corrosion products on CANDU fuel rods tested in TRIGA reactor.

No uniform, brown-reddish and whitish-gray deposits were observed. Some of them were adherent, but others were removed relatively easily. Cracked layer of deposits was observed, the cracks being radial or parallel oriented toward wall sheath, fact that conducted to stratified aspect of the crud deposits. XRD analysis of deposits evidenced the presence of the following elements: Fe, Sn, Sb, Cr, Ni, Zn, Ti, Mg, Cu, Li and Zr. The thickness of deposits varied from  $60 \mu\text{m}$  to  $110 \mu\text{m}$ .

Fuel crud is a poor thermal conductor and in the absence of boiling, conduction through the crud layer is the principal mode of heat transfer, leading to temperature gradient of the order of  $1^{\circ}\text{C}$  per micrometer of deposit thickness at a heat flux of about  $1\text{ MW/m}^2$ .

Therefore, formation of these adherent crud deposits, with thickness about  $100\mu\text{m}$ , provided an additional thermal barrier resulting in an increase of temperature at oxide metal interface that conducted to the enhancement of Zy-4 sheath waterside corrosion.

Thus, after the removing of these deposits, a strong corroded surface of sheath was observed, being presented nodular corrosion, Fig. 8a. White zirconium oxide nodules had a thickness of  $340\mu\text{m}$  and a diameter around  $4\text{ mm}$  (Fig. 8b). They presented concentric cracks with nodule nucleus, but zones around of nodules were covered with a non-adherent oxide layer having a no uniform thickness from  $25\text{--}68\mu\text{m}$ .



*FIG. 8. Nodular corrosion on CANDU fuel rod Zy-4 cladding tested 90 days in TRIGA reactor using irradiation capsule.*

By eddy current control of sheath with thick deposits (Fig. 9a) was evidenced the perforation of the sheath (Fig. 9(b)), but the metallographic examination confirmed this phenomenon (Fig. 9 (c)) [3].

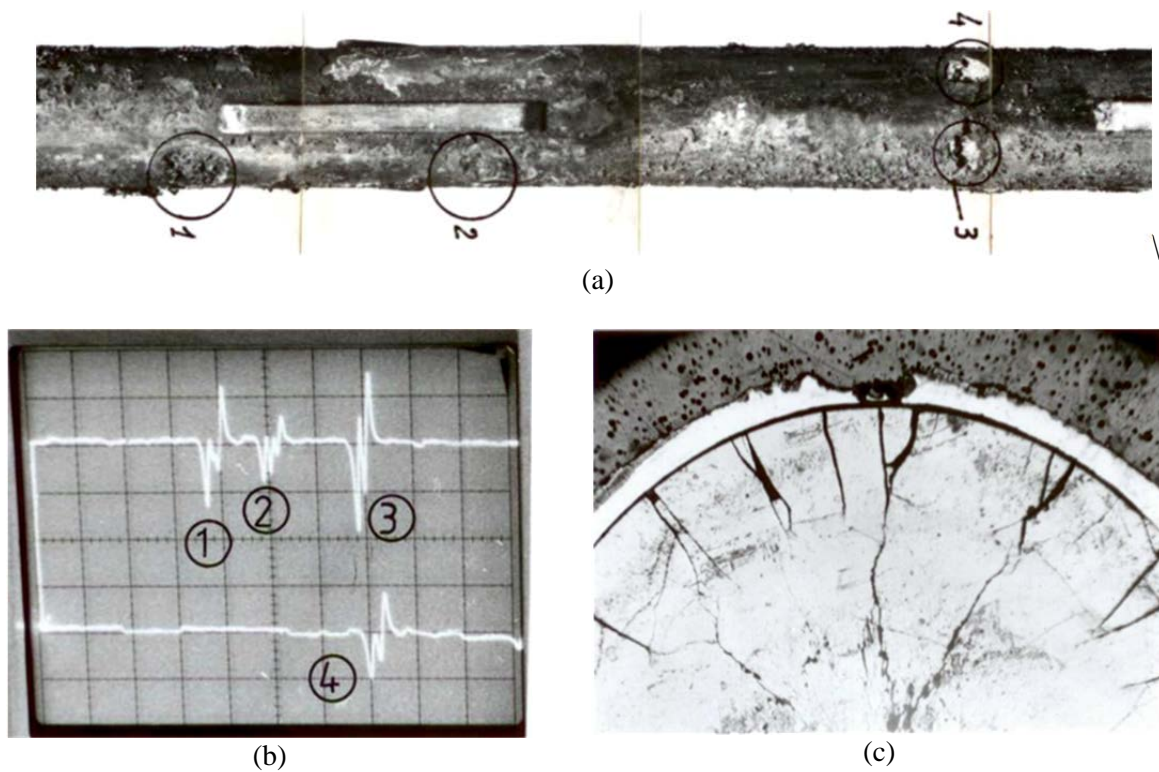


FIG. 9. Defects determined by eddy current control and metallographic examination on CANDU fuel rod.

At bigger temperature of 500°C considerable oxygen diffusion from nodular oxides in zirconium adjacent material was evidenced and influenced mechanical resistance, by material hardening and structural modifications, as well as oxidation kinetics of zircaloy-4 [8]. Reference [9] describes the influence of fuel crud build-up on corrosion of zirconium alloys.

By oxygen diffusion from oxide nodules, cracks that propagated in material were presented (Fig. 10).

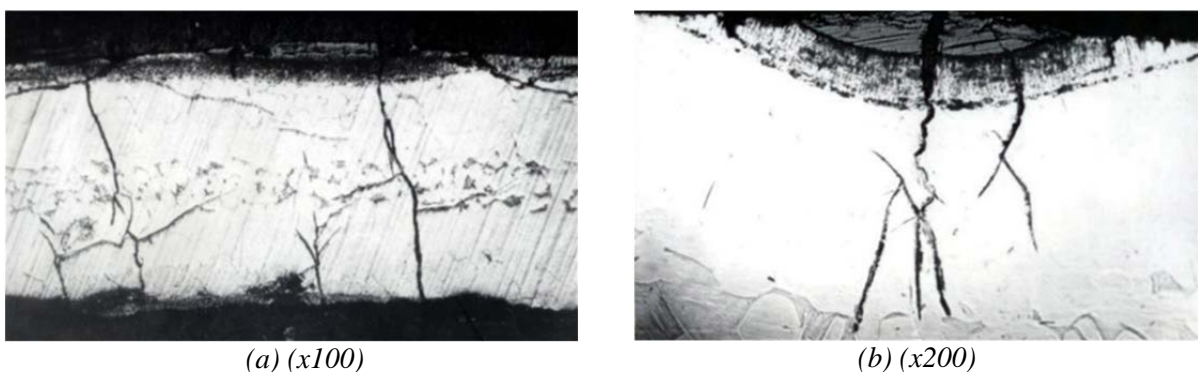


FIG. 10 Cracks in zircaloy-4 material after diffusion of 4563ppm  $O_2$  (a) and 6753ppm  $O_2$  (b) from nodular oxides.

The thick and porous oxide films and corrosion deposits will alter the local water chemistry (for example, increase of pH) and will conduct to appearance of nucleate boiling beside, local increase of temperature, due to modifications of thermal gradients.

Laboratory experiments showed that the local increase of lithium concentration by increase of pH leads to acceleration of oxidation and hydriding process, Fig. 11.

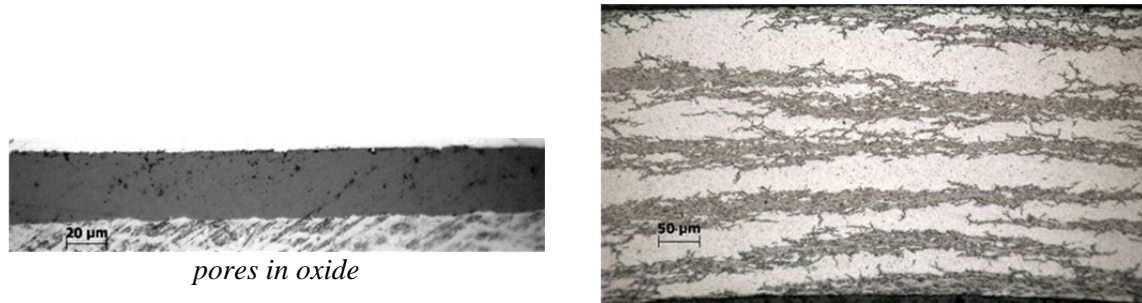


FIG. 11. Aspect of zirconium oxide and hydrides on zircaloy-4 coupons tested 20 days in LiOH solution pH=12.3 at 310°C and 10Mpa.

The Li<sup>+</sup> incorporation into oxide leads to modification of oxide nucleation or growth and the dissolution and re-precipitation of oxide, these being reasons for the accelerated corrosion in LiOH solution. Also high LiOH concentration may affect the barrier layer of oxide, as well as its microstructure.

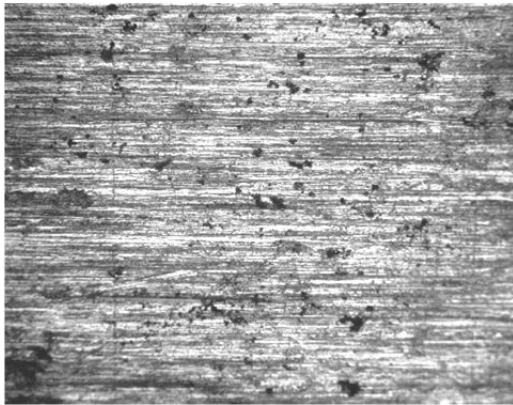
Lithium enrichment is promoted by boiling conditions leading to a local over concentration of lithium at the wall of the cladding and in the pores of the crud deposit and of the oxide films.

### 3.3. Corrosive deposits formed on zircaloy-4 coupons with different oxidation conditions

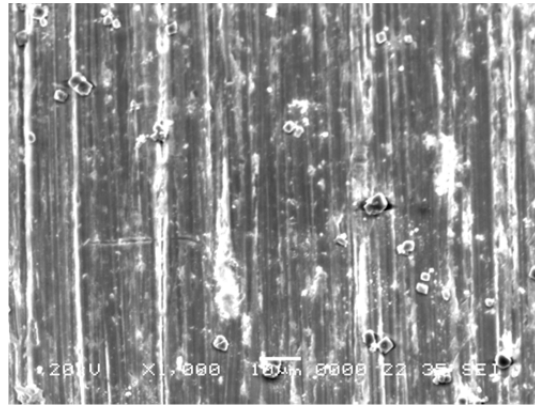
A lot of laboratory experiments performed on Zy-4 coupons oxidized at different temperature [4] evidenced that the quantity of the adherent corrosion products was dependent of thickness and especially physical-chemical characteristics of the initial zirconium oxide films. Thus, in the case of compact and adherent oxides (1–1.5µm), formed at 310°C, a small quantity of corrosion products was determined (Fig. 12).



*aspect of oxide and deposits in transverse section (x 500)*



*microscopical aspect (x 200)*



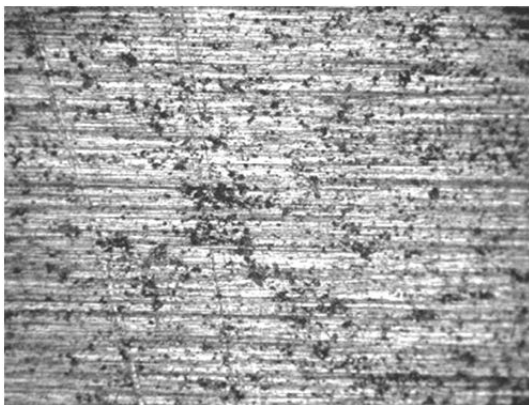
*morphological aspect (x 1000)*

*FIG. 12. Microscopical and morphological aspect of the adherent deposits on oxidized samples with oxide of 1-1.5µm.*

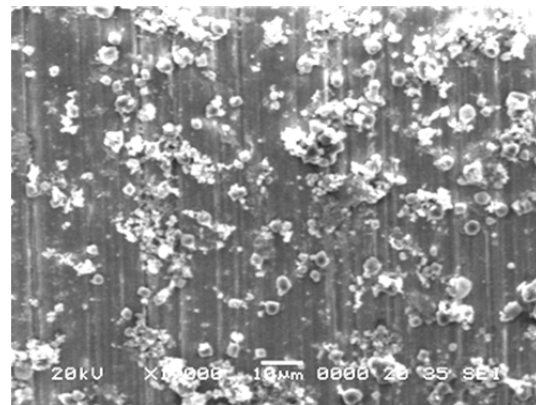
By optical and scanning electronic microscopy analysis, presence of relative fine and adherent corrosion products (orthorombic crystals of  $\text{Fe}_3\text{O}_4$  and hexagonal crystals of  $\text{Fe}_2\text{O}_3$ ) with isolated or less crowded aspect was evidenced on oxidized surfaces with zirconium oxide about  $5\mu\text{m}$  thickness, formed at  $350^\circ\text{C}$  (Fig. 13).



*aspect of oxide and deposits in transverse section (x 500)*



*microscopical aspect (x 200)*



*morphological aspect*

*FIG. 13. Microscopical and morphological aspect of the adherent deposits on oxidized samples with oxide of 4.5-5µm.*

On oxidized surfaces in steam at 400°C with thicker oxides (8–12 μm) and porous character, the adherent deposits of corrosion products with a crowded aspect were formed and they were much more numerous (Fig. 14).

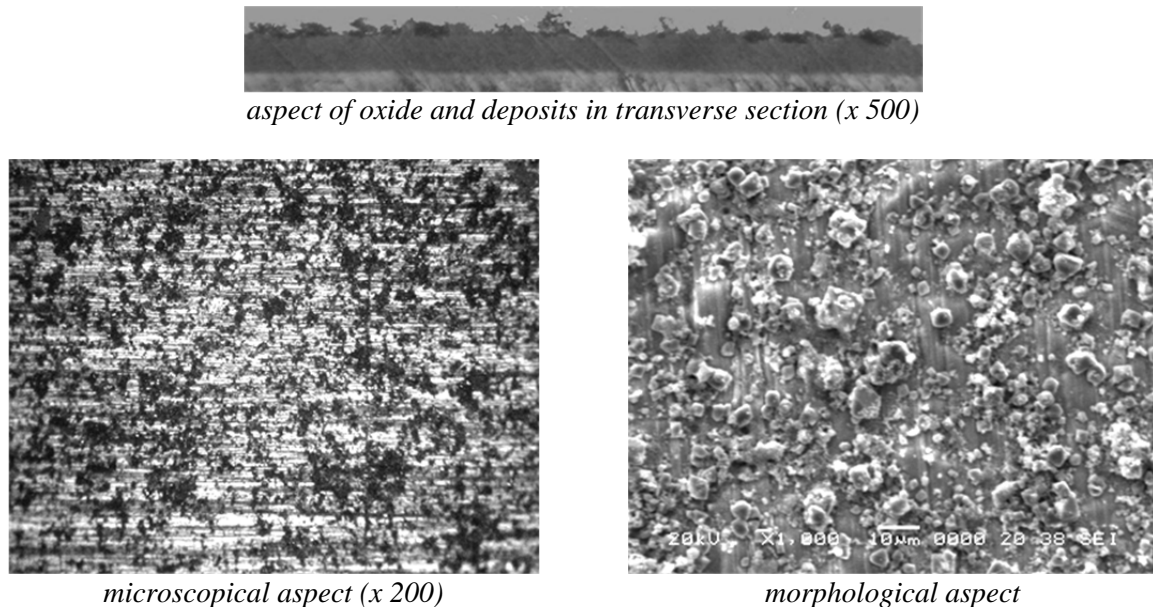


*FIG. 14. Microscopical and morphological aspect of the adherent deposits on oxidized samples with oxide of 10–12 μm.*

Both gravimetric analysis and microscopical analysis evidenced that the adherence of corrosion deposits increased with the thickness and especially with the porosity of zirconium oxides; a significant quantity of the corrosion deposits incorporates in pores and lateral cracks of oxides, phenomenon evidenced by EIS determinations.

The presence of the corrosive deposits did not influence significantly the corrosion process of coupons having initial oxides with thicknesses up to 4–5.5 μm. Thus, after the exposition of these coupons during 60 days at 360°C (17 MPa) in LiOH solution with pH=10.5 the adherent and uniform oxides were formed (Fig. 15(a)) and moderate hydriding process took place (Figs 17(a) and (b)).

In the case of initial oxidized coupons with thinner oxides of 7 μm, the presence of corrosive deposits accelerated the oxidation and hydriding leading to formation of some non-adherent, non-uniform and porous zirconium oxides generated from oxides with nodular character (Fig. 15(b)). The porous character of these oxide films was evidenced by EIS determinations, when the penetration of the electrolyte in pores and cracks conducted at significant decrease of slope and phase angles values after 48 hours and respectively 72 hours from immersion in Na<sub>2</sub>SO<sub>4</sub> 0.2M solution, as well as at significant decrease of total impedance in the range of low frequencies, Fig. 16. The electrolyte filled pores and cracks from the thicker oxides, and the respective surfaces behaved similarly with non-covered surfaces with oxides (impedance/frequency graph is parallel with abscissa — curve three and four from Fig. 16).

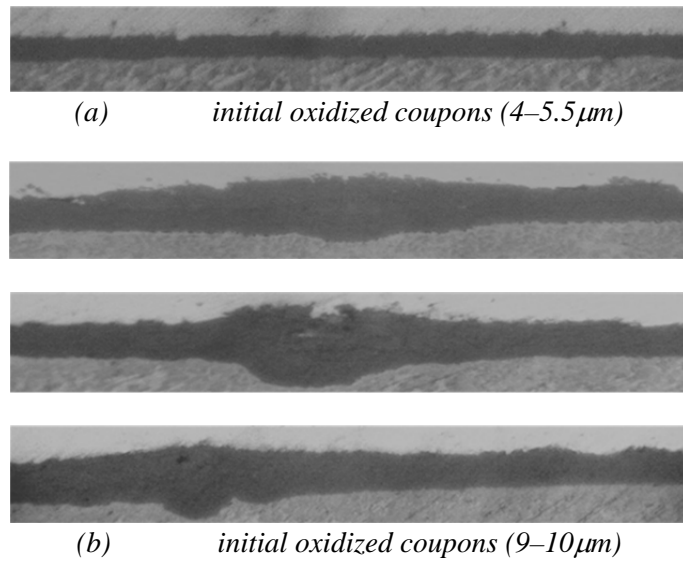


FIG. 15. Aspect of oxides after 60 testing days at 360°C (17MPa) in LiOH solution (pH=10.5) of Zy-4 coupons having initially different oxide films and corrosive deposits on their surface (x500).

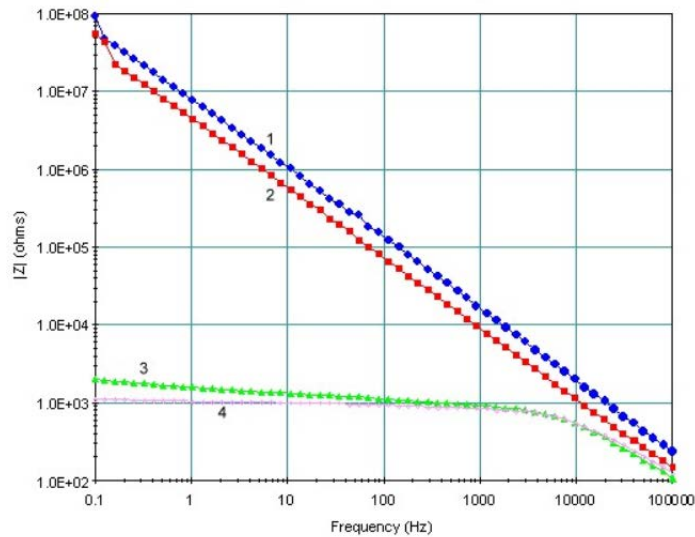


FIG. 16. Bode curves registered on Zy-4 samples (initial oxidized — oxide over 7 μm and with corrosion deposits) after testing at high temperature and pressure and immersed different periods in Na<sub>2</sub>SO<sub>4</sub> 0.2M solution: 1–30 min; 2–24 h; 3–48 h and 4–72 h.

These oxide films permitted the access of hydrogen at oxide-metal interface and a high hydrogen quantity was absorbed in material (600–800 ppm H<sub>2</sub>) and numerous hydrides were formed (Figs 17(c) and (d)).

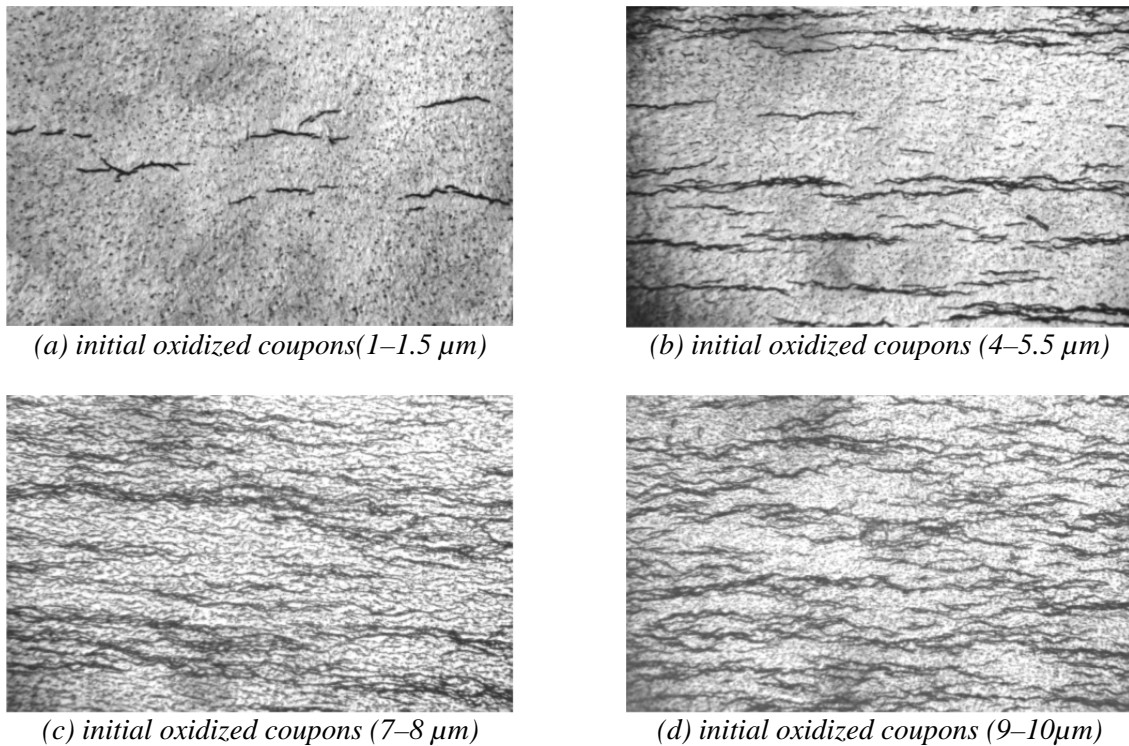


FIG. 17. Morphology of hydrides formed on Zy-4 coupons with corrosive deposits and having different initial oxidation condition, after 60 testing days at 360°C (17MPa in LiOH solution pH=10.5 (x250)).

#### 4. CONCLUSIONS

- Corrosion of zirconium components and crud deposits on their surface in water cooled reactors are dangerous phenomena capable of limiting substantially their service life. Thick and porous oxide films and corrosion deposits may alter the local water chemistry (for example, increase of pH) and may conduct to appearance of nucleate boiling beside, local increase of temperature, due to modifications of thermal gradients;
- The composition, thickness and evolution of crud of fuel assembly surfaces depend very much on operational condition, such as steady state operation, water chemistry conditions or different oxidation conditions of surface;
- During steady state operation of Candu reactor with chemistry standard conditions, black and adherent magnetite cristallites, preceded by carbon steel feeders corrosion, have precipitated from primary coolant on zircaloy-4 coupons surface. A bigger quantity of deposits on coupons from inlet reactor autoclaves was observed, this aspect being characteristic in CANDU reactors with carbon steel feeders;
- Presence of these corrosion deposits on surface did not influence oxidation and hydriding of zircaloy-4 alloy;
- In abnormal water chemistry conditions (pH>10.5 or oxygen concentration >100 ppb) and presence of irradiation CANDU fuel rods presented thick, non-adherent and porous deposits, with stratified aspect. These deposits provided an additional thermal barrier resulting in an

increase of temperature at the oxide-to-metal interface, that conducted to the enhancement of zircaloy-4 waterside corrosion, in the shape of nodular corrosion, and finally to perforation of sheath;

- Laboratory experiments evidenced that the quantity of the adherent corrosion deposits increased with the thickness and especially with the porosity of initial zirconium oxide films; a significant quantity of the corrosion deposits incorporates in pores and lateral cracks of thicker oxide films;
- Presence of the corrosive deposits on zircaloy-4 initial oxidized surfaces, with thicker oxide films (about 7  $\mu\text{m}$ ), accelerated oxidation and hydriding process of alloy, leading to formation of some non-adherent, non-uniform and porous zirconium oxides generated from oxides with nodular character and numerous hydrides in material.

## REFERENCES

- [1] MARCIULESCU, O., Operating manual – primary heat transport system chemistry control, Cernavoda NPP (1997).
- [2] PIRVAN, I., DIACONU C., VELCIU L., SORESCU A., Corrosion analysis of the coupons from Y1-Y4 autoclaves assembled in by-pass of CANDU-6 reactor, at NPP-Cernavoda, Internal Report, INR. Pitesti, Nr.6229.
- [3] PIRVAN, M., DOBRIN, R.,ALEXA, A.,CRĂCIUNESCU, T., Post-irradiation examination of CANDU 69–74 fuel rods in a loop of TRIGA reactor at INR-Pitesti, Internal Report INR. Pitesti, Nr, 2846.
- [4] PIRVAN, I.,RADULESCU, M.,MIHALACHE, M.,Corrosion behaviour of zircaloy-4 samples in presence of corrosion products deposits, Internal Report INR. Pitesti, Nr, 7758.
- [5] PIRVAN, I.,RADULESCU, M., PIRVAN, M.,Crud deposits and potential impact on cladding material in CANDU-6 PHWR, International Symposium in Nuclear Energy, Bucuresti, Romania, (2007).
- [6] BURRILL, K.A., Internal report on modeling of transport of radioactive substances in the primary circuit of water-cooled reactors, Toronto, 1997, (1981).
- [7] MILLER, D.G., BURRILL, K.A., Corrosion/98, NACE, Houston, (1998) paper no.335.
- [8] PIRVAN, I., ROTH, M., VELCIU, L., Corrosion and mechanical behaviour of CANDU fuel rods having different oxidation grades, INR Internal Report, Nr.3887.
- [9] CHEN, J., ROSBORG, B., The possible influence of fuel crud build-up and water chemistry on waterside corrosion of zirconium alloys, Proceedings of a Technical Committee Meeting, Hluboka ned Vltavou, IAEA-TECDOC-1128, IAEA, Vienna (1999).

# THE MECHANISMS FOR HEAT TRANSFER IN CRUD COATED LIGHT WATER REACTOR FUEL AND THEIR CONSEQUENCES

S.P. WALKER, I. HAQ, N. CINOSI, M. BLUCK, G.F. HEWITT  
Imperial College,  
London, United Kingdom

## Abstract

PWR fuel tends to become coated with crud which contains “chimneys” penetrating down to the metal surface. This provides an opportunity for wick-boiling to occur. This is associated with the generation of high concentrations of dissolved species within the crud, and a consequent increase in the local saturation temperature. We present here detailed, coupled two dimensional models of these processes, which allow the three linked phenomena, of heat conduction, advection and diffusion of species in the water, and flow of the water itself, to be modeled and their aggregate effect to be seen. The fuel thermal performance is characterized in terms of an effective crud thermal conductivity derived from the use of this model, and the non-linear dependence this effective thermal conductivity has on parameters such as crud thickness and pore density is determined.

## 1. INTRODUCTION

Crud formation in water-cooled reactors has caused operational problems from the beginning of nuclear power, and continues to do so. Crud layers (see Fig. 1 and Fig. 2) are chemically very complex, resulting from the deposition of various species present within the coolant. Some, like boron, are added deliberately, and others are present essentially as corrosion products from other parts of the coolant circuit. They cause a variety of problems, including increased cladding corrosion, by either increased cladding temperatures or changed chemical conditions, or some combination thereof, and power distortions and reductions due to the undesirable accretion of boron onto the surface of the cladding [1, 2].

In this paper we develop a two dimensional, coupled, model of some of the main phenomena thought to contribute to these effects, with the aim of predicting cladding temperatures and concentrations of dissolved material in the coolant in the pores of the crud.

In Section 1 we discuss the background to the problem. In Section 2 the possible thermal effects of crud, were it to behave as a conductive layer, are investigated. In Section 3 the possibility that crud heat transfer is actually predominantly a wick-boiling process is addressed, and a model to investigate this is described and investigated.

In Section 4 the thermal performance of crud coated fuel, in the presence of wick boiling, is addressed, and its ‘effective thermal conductivity’ determined. Conclusions are drawn and further necessary work identified in Section 5.

## 2. BACKGROUND

Most PWR fuel becomes coated with various deposits, collectively termed ‘crud’ [3]. It takes a variety of physical and chemical forms that change over the life of the fuel, but largely comprises corrosion products from primary circuit components. It is generally believed to play a role in fuel failure. The mechanism for this is uncertain, but is believed to be some combination of (i) the crud may raise the local clad temperature, and (ii) aggressive dissolved species are concentrated in the crud [4–7]. Studies of crud feature, for example, in the “Zero fuel failure by 2010” INPO initiative.

There is a wide variety of physical and chemical forms and species that collectively are termed ‘crud’, and this diversity naturally make analysis and quantification of its effects uncertain. There is an extensive literature on the subject; a selection that gives the most useful background for present purposes is cited here. In particular, a very helpful description of the various (and changing) forms of

crud is provided by [3], as part of a discussion of the difficulties inherent in the identification and characterization of crud formation over the ~50 000 fuel rods of a PWR.

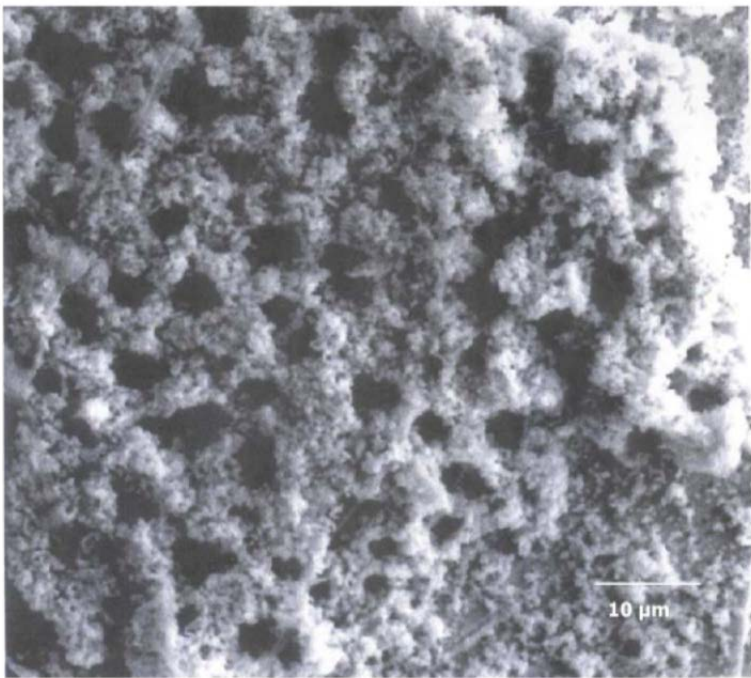


FIG. 1. Top view of PWR crud (extent of photograph about 60 μm). Note the presence of 'chimneys' [2].

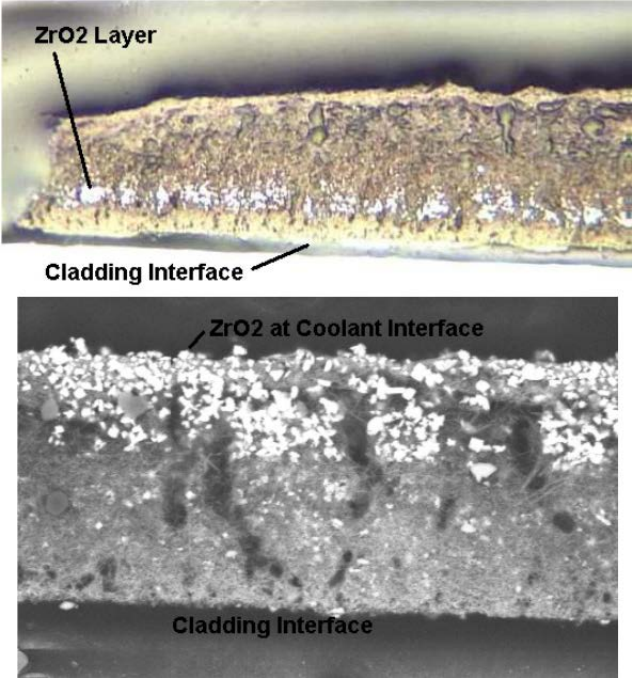


FIG. 2. Sections through crud. Note the sectioned 'chimneys'. Photographs reproduced from Byers [3].

### 3. THERMAL EFFECTS OF CRUD

The surface roughness of the fuel rod and the associated coolant pressure drop and fuel coolant heat transfer coefficient will all be influenced by the presence of the crud. We will not address this aspect further here, but rather will focus on the transmission of heat through the crud layer.

The conductivity of the fluid filled crud can be estimated, in terms of the thermal conductivities of the two phases, and the void fraction  $\varepsilon$  in the crud, from the Maxwell formula [8]:

$$k_{CRUD} = k_{FLUID} \left[ \frac{1 - \left(1 - a \frac{k_{SOLID}}{k_{FLUID}}\right)(1 - \varepsilon)}{1 + (a - 1)(1 - \varepsilon)} \right] \quad (1)$$

where

$$a = \left( \frac{3k_{FLUID}}{2k_{FLUID} + k_{SOLID}} \right) \quad (2)$$

In Fig. 3 is indicated the consequent dependence of crud conductivity on porosity. For relevant porosities, the conductivity is dominated by that of the fluid. Vapour filled crud is seen, naturally, to have a conductivity less than half that of water filled crud.

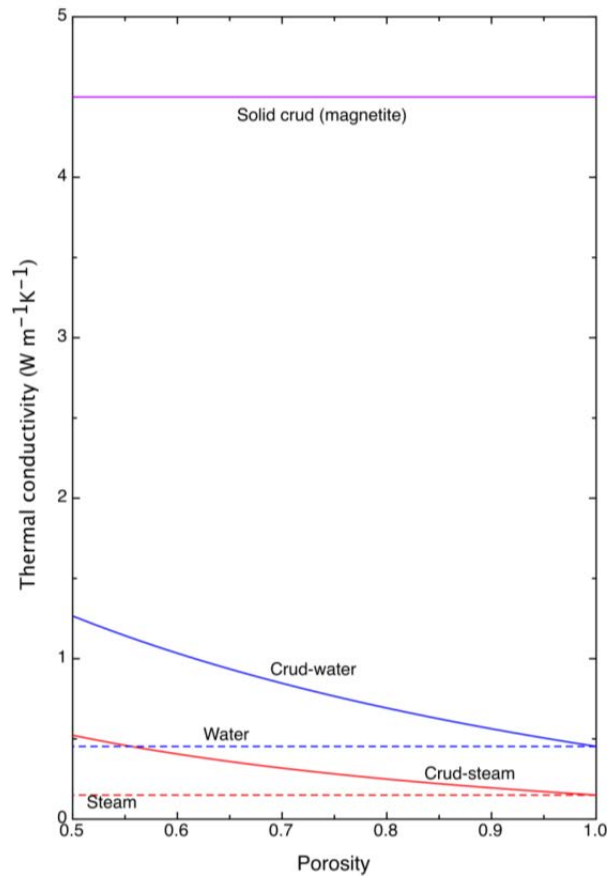


FIG. 3. Crud thermal conductivity as a function of porosity, with the porosity occupied by water and water vapour. Also indicated are the conductivity of solid crud, taken as magnetite, and of water and steam.

One mechanism for the transmission of heat to the coolant is by conduction through the crud. The crud in effect adds an additional ‘thermal resistance’, analogous, for example, to the thermal resistance presented by the pellet—clad gap.

We will here identify the modification to the fuel’s radial temperature profile caused by the crud coating. Using in (1) and (2) the parameters from Table 1 yields a water filled crud conductivity of  $0.692 \text{ Wm}^{-1}\text{K}^{-1}$ . In Fig. 4 we show the temperature profiles in the presence of crud layers of 32 and 64 microns in depth. The clad surface temperature is increased considerably, by about 3 K per  $\mu\text{m}$  of crud.

For the circumstances considered here, the bulk saturation temperature, indicated as a horizontal line on the figure, is reached about 10  $\mu\text{m}$  into the crud. Even though the small pore sizes will inhibit boiling until some temperature higher than this, there will be a layer of vapour filled crud inboard of this for cases with crud significantly more than 10  $\mu\text{m}$  thick. With a thermal conductivity about 1/3 of water filled crud, this will cause clad temperatures to be higher still.

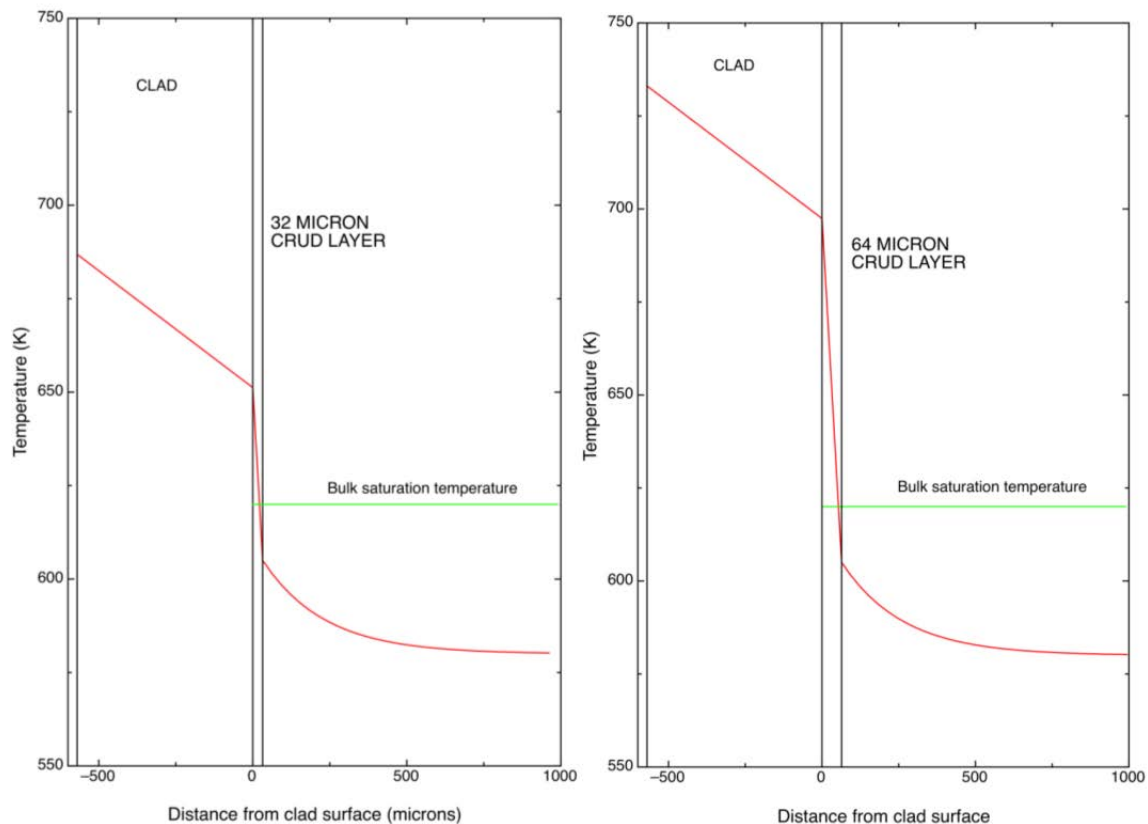


FIG. 4. Radial temperature profile with 32  $\mu\text{m}$  and 64  $\mu\text{m}$  crud layers (no wick boiling).

## 4. WICK BOILING

### 4.1. Introduction

The solid crud formed typically has a porosity of about 60–80% (although there is some inevitable uncertainty as to just how closely a posteriori measured values mirror in-reactor conditions) [4]. In addition, there are generally channels (“chimneys”) from the crud surface through its thickness down to the surface of the cladding. One consequence of this structure is that it permits a mechanism termed wick boiling, where liquid soaks through the porous crud until it reaches a region where the temperature is above the local saturation temperature, and there is a channel available for the egress of the vapour produced [10, 11].

All of these phenomena have been studied in some detail over many years.

In 1971 Macbeth [11] developed a one-dimensional hydraulic model of flow in a chimney filled crud, and studied the effect of chimney population density, although this model was not able to determine temperature distributions or solute concentrations.

TABLE 1. VALUES OF PARAMETERS EMPLOYED IN THE ANALYSES PRESENTED HERE (UNLESS STATED OTHERWISE FOR INDIVIDUAL STUDIES). COLUMN A FOR THE COMPARISONS WITH EARLIER WORK, AND COLUMN B AS THE BASIS FOR THE MODEL DEVELOPMENT IN SECTION 4

			Pan 1985	Pan 1987	Henshaw 2006	A	B
Crud thickness	$\mu\text{m}$		25	25	59	60[6]	32
Chimney centres	$\mu\text{m}$		15.96	20.6	20.6	20[6]	21
Chimney diameter	$\mu\text{m}$		5	5	5	5[6]	5
Crud porosity	$\varepsilon$	%	80	80	80	80[6]	80
Crud / water mean thermal conductivity	k	$\text{W m}^{-1}\text{K}^{-1}$	0.69	0.69		0.506[1]	0.69
Heat Flux	q	$\text{MWm}^{-2}$	1.11	1.80	1.11	1.5	1.0
System pressure	p	MPa	15.2	15.5	15.3	15.5	15.5
Boric acid diffusion coefficient	D	$\text{m}^2\text{s}^{-1}$				1.05E-08	-
Li diffusion coefficient	D	$\text{m}^2\text{s}^{-1}$		1.7E-08			
Tortuosity	$\Gamma$			0.4	0.4	0.4[6]	0.4
Coolant boron concentration	$C_b$	ppm ( $\text{gm}^{-3}$ )			1200 (4637)	1200[6]	1200
Coolant Li concentration	$C_b$	ppm ( $\text{gm}^{-3}$ )		2 (1.4)	2		
Coolant heat transfer coefficient	h	$\text{W m}^{-2}\text{K}^{-1}$				1.2E04[9]	1.2E+04
Bulk coolant temperature	T	K				590	590

In 1974 Cohen [4] developed a one-dimensional model for heat and mass transfer through a porous crud layer, along the lines of heat transfer along a fin. Heat was modeled as being conducted away from the cladding, and lost laterally via evaporation into the chimney. An inwards mass flow rate of water, sufficient to replace this evaporative loss, was then computed. From this, inter alia, an estimate of the temperature beneath the crud was obtained [4].

In 1985 Pan [8] presented a two dimensional analysis of the mechanism, computing the temperature distribution as a function of depth into the crud, and of the radial distance from the chimney. In 1987 he presented [7] an associated analysis of the concentrations reached of the various dissolved species in a chimney-populated crud, under wick boiling conditions. Whilst these analyses incorporated two dimensional effects, they are not able to allow for the various interactions between the phenomena at work. The model indicated that dissolved species concentrations increased with crud thickness, with decreasing porosity, and with increasing chimney population.

More recently, significant strides have been made in understanding of the physical chemistry of the crud, and its coupling to the associated thermal conditions, by Henshaw and colleagues [6], building upon the Cohen work. They developed a one-dimensional (through thickness) model that couples thermal hydraulics with the water chemistry. Postulating heat transfer through wick boiling, they modeled to the downward flow of water soaking through the crud, evaporating into steam at the surface of the chimneys. A particular advance of the model was to investigate the various chemical reactions taking place within the porous deposits. These reactions are generally temperature

dependent, and a degree of coupling between the reaction rates, and the temperatures caused to obtain by the species thus caused to be present, was incorporated.

In this present work we have developed a more representative two dimensional model, that couples mechanistically the processes which are in principle present; heat transfer through the wet crud, diffusive flow and boiling of the water at chimney surfaces to remove the heat, and the advection and diffusion of dissolved species. Our model also provides a framework within which the further, more sophisticated, physical chemistry analysis of Henshaw and colleagues can in due course be incorporated.

## **4.2. A coupled heat and mass transfer model**

### *4.2.1. Introduction*

As noted above, in addition to the usual convective heat transfer from the surface of the crud, the presence of the deep, slender chimneys offers the possibility of the additional heat transfer mechanism of evaporation from the surface of the chimney. The passage of heat through the crud will be by conduction through the crud itself, and through the water in the pores of the crud. Evaporation from the surface of the crud into the chimney will require a flow of water through the crud to the chimney face.

The flow of the water will take the form of the usual flow through a porous medium, drawn by the evaporative mass flux at a chimney surface, entering the crud at the face exposed to the bulk coolant, and leaving in the form of vapour formed at the walls of the chimneys.

The liquid coolant that that enters the crud in this fashion will of course contain within it whatever species are present in solution in the coolant. As discussed above, these include in particular boric acid. At the chimney surface, the evaporation will lead to the removal only of steam, and thus water flowing into the crud cannot (in the steady state) carry into the crud those species dissolved within it. What must happen is that a spatial variation of the concentration of the dissolved species will be generated, with an increase in this concentration in going from the wetted surface of the crud to the chimney. The dissolved species will diffuse down this concentration gradient (i.e. away from the chimney surface), canceling out the advection of the dissolved species associated with the flow of the water.

Everywhere, but in particular, at the chimney surface, the concentration of dissolved species will be higher than in the bulk coolant. This will have various consequences, but that of most immediate interest is that the increased concentration of dissolved species may affect the saturation temperature of the coolant, changing the thermal conditions at the chimney face.

As will be seen, these three processes are all linked. The rate of heat transfer by evaporation at the chimney wall plainly depends upon the saturation temperature there. The saturation temperature depends on the concentration of dissolved species there. The concentration depends on the advective flow, and this flow is determined by the rate of heat transfer by evaporation at the chimney wall.

In the sections that follow we will expand upon these issues, identifying the associated governing equations that describe them, and the relevant boundary conditions.

#### 4.2.2. The physical basis of the model

A schematic depiction of a chimney-filled crud, and the region analysed, is shown in Fig. 5.

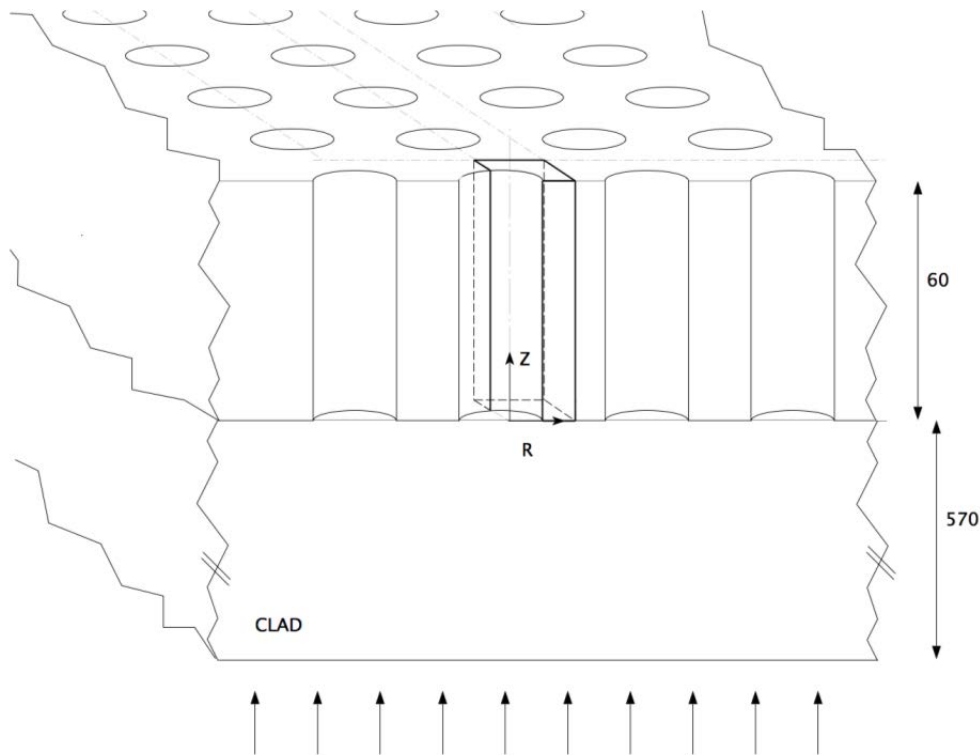


FIG. 5. A schematic diagram, showing the crud, chimneys and clad, with characteristic dimensions in microns. The region analysed in our model is indicated, along with the coordinate system used to identify the results we present.

#### 4.2.3. Heat conduction

We model the heat transfer through the wetted crud via Laplace's equation:

$$\nabla^2 T = 0 \quad (3)$$

(There is in addition advection of heat because of the flow of the water, but this is negligible; the water flow rate is tiny.) Boundary conditions are adiabatic on planes of symmetry bounding the region modeled, an imposed uniform heat flux on the inner face of the crud, and an imposed (saturation) temperature on the face of the chimney:

$$T(\mathbf{r} \in \text{CHIMNEY SURFACE}) = T_{\text{SAT}}(\mathbf{r} \in \text{CHIMNEY SURFACE}) \quad (4)$$

(One could instead employ Robin boundary conditions, with a (very high) evaporation heat transfer coefficient; the approach above effectively takes this heat transfer coefficient to be infinite. The results from both approaches are essentially identical.) The value of the saturation temperature depends on the concentration of the dissolved species. The concentrations are found from solution of equation (11) below. The main species to affect the saturation temperature, and the only one considered at present, is boron in the form of boric acid, ( $\text{H}_3\text{BO}_3$ ). The dependence of saturation temperature on boron concentration is taken from the correlation published by Deshon [1], and is shown here in Fig. 6.

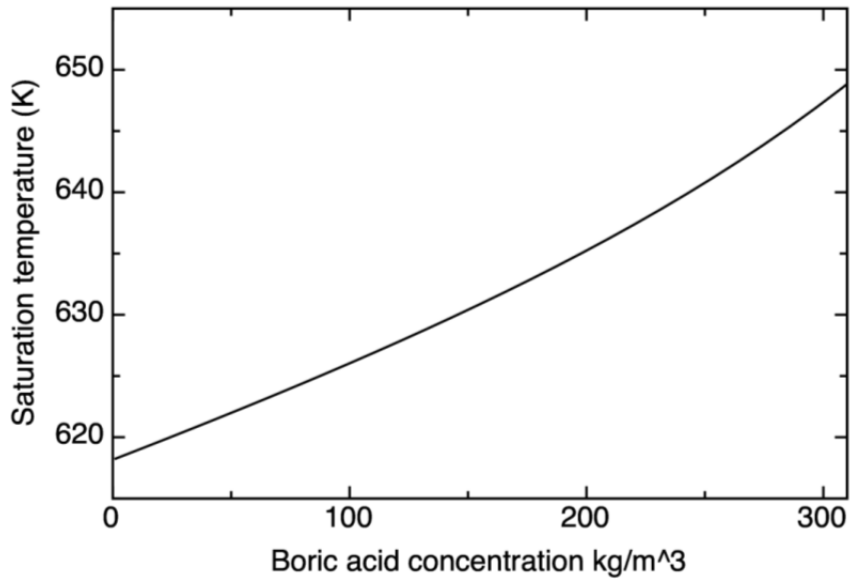


FIG. 6. The dependence on boron concentration of the saturation temperature of water at 15.55 MPa, taken from the correlation published by Deshon[1].

Interaction with the bulk coolant flow is via a specified heat transfer coefficient and bulk coolant temperature. These boundary conditions are indicated in Fig. 7.

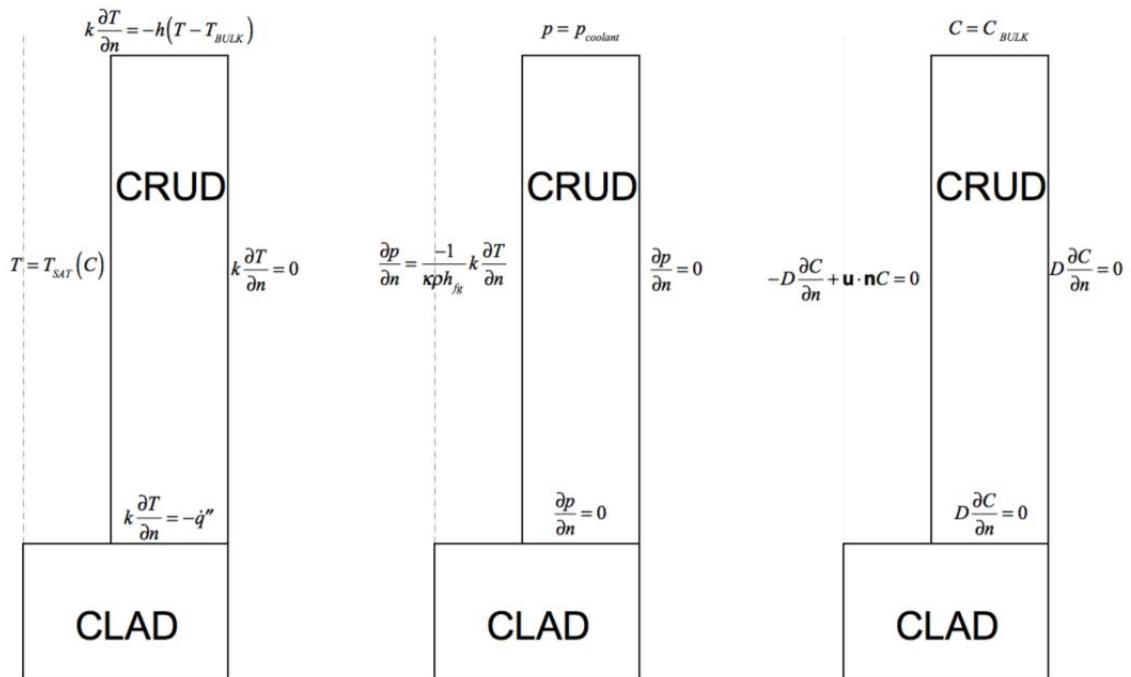


FIG. 7. Boundary conditions for (from left to right) the temperature, flow and concentration analysis.

#### 4.2.4. The diffusive flow of the coolant through the crud

The flow of water through the crud is modelled as a diffusive flow, with the local velocity related to the local pressure gradient via a flow resistance:

$$\mathbf{u} = -\kappa \nabla p \quad (5)$$

This results in a Laplace equation for the pressure distribution within the crud.

$$\nabla^2 p = 0 \quad (6)$$

Boundary conditions of no flow on planes of symmetry, and at the clad-crud interface, are employed.

At the chimney surface a spatially varying mass flow rate is imposed, based on the local heat loss rate:

$$\dot{m} h_{fg} = k \frac{\partial T}{\partial n} \quad (7)$$

This gives, in terms of the diffusive flow problem,

$$\frac{\partial p}{\partial n} = \frac{-1}{\kappa \rho h_{fg}} k \frac{\partial T}{\partial n} \quad (8)$$

These boundary conditions are indicated in Fig. 7. The numerical value of  $\frac{\partial T}{\partial n}$  for use in equation (8) is found from the solution of equation (3) above.

#### 4.2.5. The advection and diffusion of the dissolved species in the crud

Denoting the concentration of dissolved species C, and their net flow (current) J, we can write the net flow of dissolved species as the sum of advective and diffusive terms:

$$\mathbf{J} = -D \nabla C + \mathbf{u} C$$

In the steady state we have

$$\nabla \cdot \mathbf{J} = 0 \quad (10)$$

or, as ,  $\nabla \cdot \mathbf{u} = 0$

$$-D \nabla^2 C + \mathbf{u} \cdot \nabla C = 0 \quad (11)$$

The boundary condition at the crud-coolant interface is that the concentration is equal to the bulk coolant concentration. At the planes of symmetry and the clad surface the normal gradient of concentration is zero. The boundary condition at the chimney surface is that there is no net flow of dissolved species to the surface:

$$-D \frac{\partial C}{\partial n} + \mathbf{u} \cdot \mathbf{n} C = 0 \quad (12)$$

These boundary conditions are indicated in Fig. 7. The required  $\kappa \frac{\partial p}{\partial n}$  variation of the water velocity throughout the solution domain is provided by the solution of equation (6), coupled with equation (5). The boundary value of  $\mathbf{u} \cdot \mathbf{n}$ , or equivalently needed in equation (12), is found from solution of (6) above.

#### 4.2.6. The coupled solution

There are three equations to be solved; the temperature distribution in the crud, the water velocity in the crud, and the distribution of the concentration of dissolved species in the crud. Each equation has boundary condition values that depend upon the solution of one of the other equations, and an iterative approach is taken to solve them. This is shown graphically in Fig. 8.

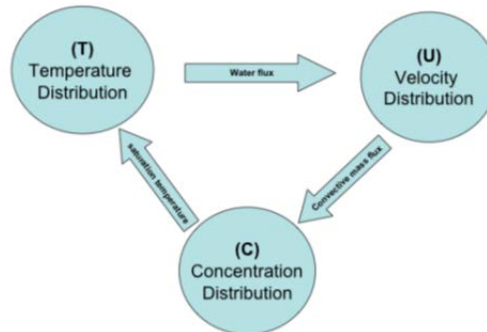


FIG. 8. The sequential, iterative solution of the three coupled problems, of temperature distribution, water flow and species concentration in the crud.

### 4.3. Numerical implementation

In Fig. 5 is indicated (one quarter) of the crud notionally associated with a single chimney. (Of course, real chimneys do not display the uniformity of diameter, or regularity of position, of that figure). We model the three-dimensional region shown as two dimensional ( $r$ - $z$ ), approximating the two symmetry planes remote from the chimney by a circular arc, centred on the chimney.

The three equations to be solved, (3), (6), and (11), are solved numerically using a finite volume scheme. The numerical approach is fairly standard, and we will not give any details here; a good introduction to the methods is provided by Versteeg [12]. The Peclet number is well below unity, so a central differencing scheme is used.

Equations (3) and (6) are in effect subsets of equation (11); they both lack the advective term but are otherwise identical. From a practical point of view, this allows some economy in code development, as the code that solves the advection — diffusion equation can be employed with minimal modification to deal with the wholly diffusive equations. For each of the three equations, once the boundary conditions are incorporated the finite volume discretization generates a sparse matrix equation. This is solved using a standard ‘line by line’ iterative solver.

In this case, of course, the equations are coupled. Boundary conditions for any one equation are available only from a solution of the other two. We accommodate this by following the procedure implicit in Fig. 8. Equation (3) is first solved for the temperature distribution, using the physical properties of water at a nominal coolant conditions. This solution is used to determine the flow-field in the crud, equation (6). This flow field is then used to determine the concentration of the dissolved species. This concentration is then used to provide a modified saturation-temperature boundary condition for the temperature solution. This sequential solution of the three equations is of course automated. In practice, we find that the convergence of this iteration is smooth and quite rapid, with converged results being achieved in typically 5–10 iterations.

#### 4.4. Validation and analysis of earlier modeling

The earlier analysis of Pan [8] in 1985 computed for a two dimensional model the radial and through-thickness variation of temperatures and water pressure in the vicinity of a crud chimney. Using the same data as Pan, and operating the present model in an uncoupled form, generates essentially identical results. Pan later extended his work [7] to address concentrations of dissolved species, and again with the same parameters employed, the present model predicts the same results. Comparisons between Pan, and the use of the present model operated in an uncoupled form, are shown in Fig. 9

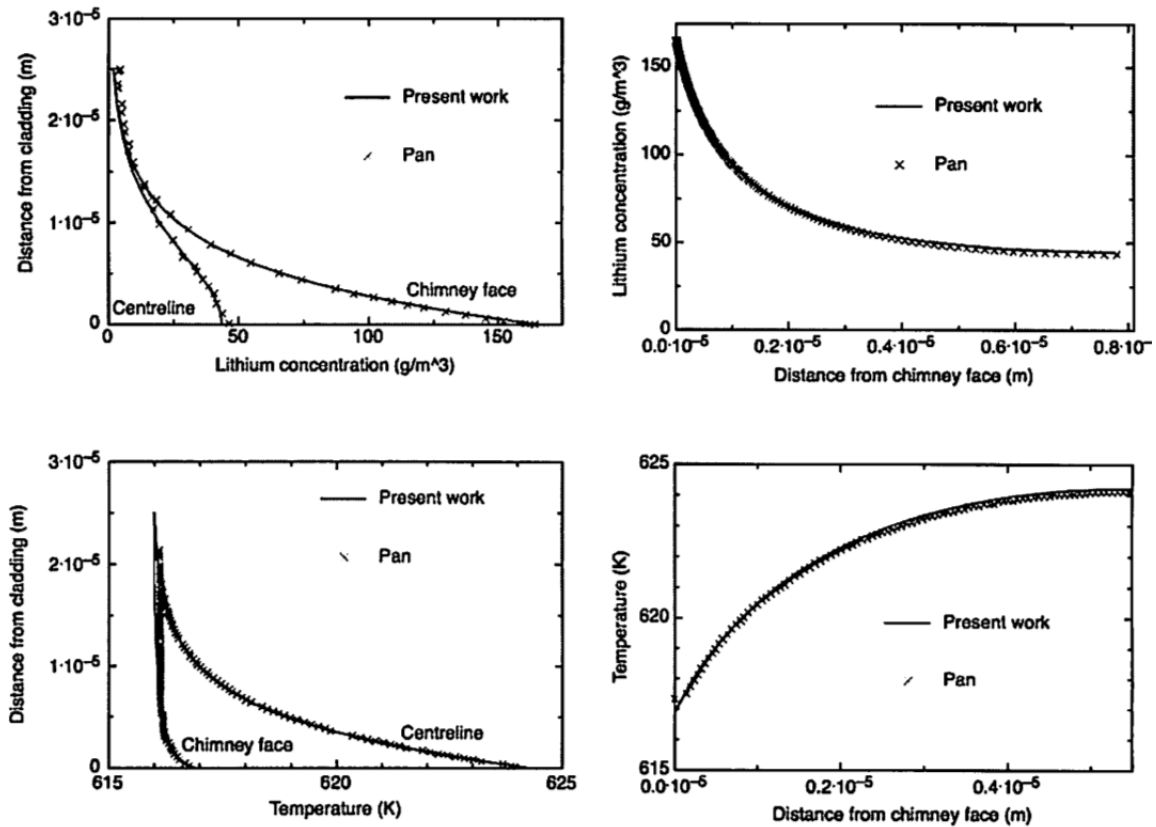


FIG. 9. The use of the present model, in uncoupled form, to analyse the cases studied by Pan. (Radial variations are shown at only  $z=0$ ; at the free surface values are prescribed as boundary conditions).

#### 4.5. Two dimensional effects, and the coupling of the phenomena

In this Section we apply the fully coupled two dimensional model, using the parameter values from Table 1. To allow comparison with earlier work, the specified heat flux is applied to the lower surface of the crud. (In Section 4 it is, more realistically, applied to the inner clad surface.)

We here analyse the crud with the present two dimensional model, with the coupling between the phenomena both incorporated and omitted. Results from this are shown in Fig. 10. The concentration of the dissolved boric acid is seen to be ~25 times the bulk value at the inter-chimney centre line, but to rise by a further factor of two to ~55 times the bulk value at the chimney face.

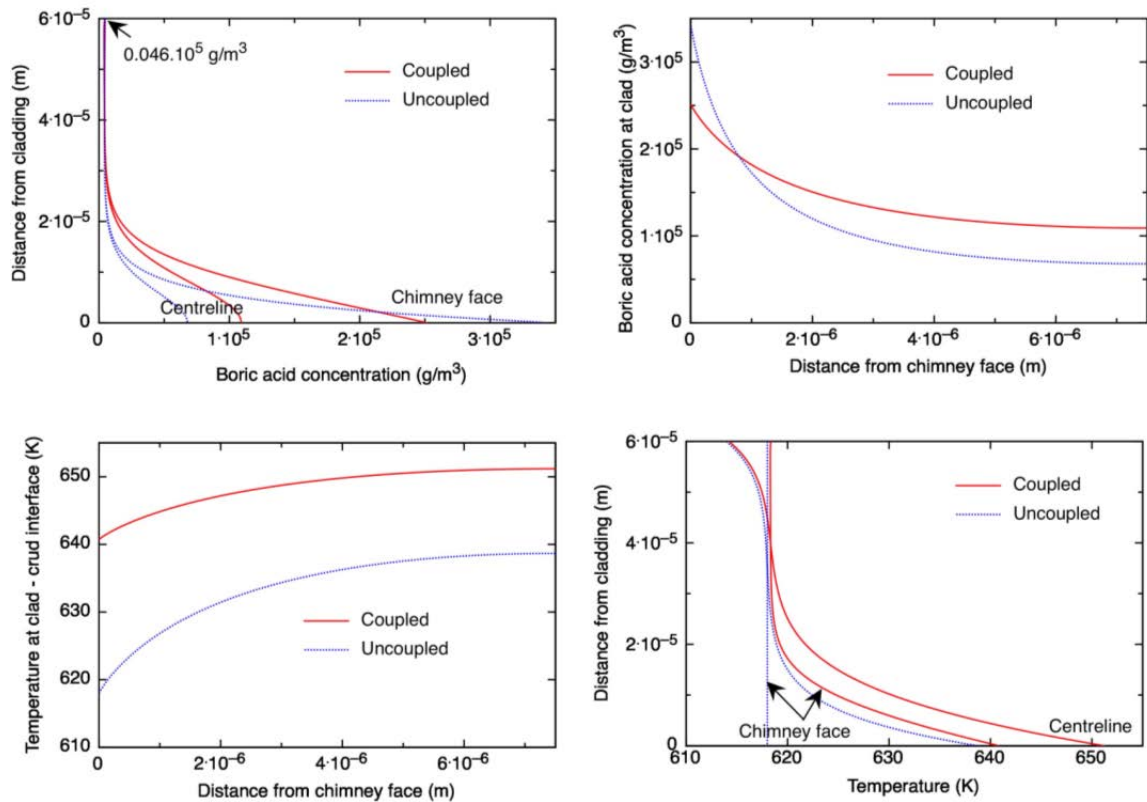


FIG. 10. A comparison of models with the coupling between the three phenomena taken into account, and omitted. (As in Fig. 9, radial variations are shown at only  $z=0$ ; at the free surface values are prescribed as boundary conditions).

## 5. THE THERMAL PERFORMANCE OF CRUD COATED FUEL

As will already be apparent, the composition and morphology of crud is very varied. It is also uncertain. Inter alia, the solubility of much of the material from which it is formed varies with temperature and pressure, which means that the crud present under reactor conditions may well have characteristics (such as pore sizes) significantly different from those of the crud on which measurements are eventually made in a laboratory. The thermal conductivity of the solid phase is uncertain, reflecting its uncertain composition, even if it were present in bulk as a homogeneous material. This is further compounded by its chaotic morphology.

An inevitable consequence of all this is that numerical values of model predictions will have large uncertainties. A realistic aim of such analysis, perhaps, will be to attempt to identify the main processes and work, their relative importance, and their dependence on the major parameters.

The numerical values of the parameters employed in the present illustrative calculations are listed in Table 1.

### 5.1. Predictions of the coupled two dimensional wick boiling model

We show in Fig. 11 the predictions of the two dimensional coupled model for the case characterized by the more moderate parameter values in column B of Table 1. Also, the heat flux is applied to the clad inner surface, and the clad is included in the thermal conduction analysis. This latter refinement causes modest (typically  $\sim 20\%$ ) increase in local predicted solute concentrations. Again, large multiples in boron concentration are predicted, along with temperatures up to  $\sim 40\text{K}$  above bulk coolant values.

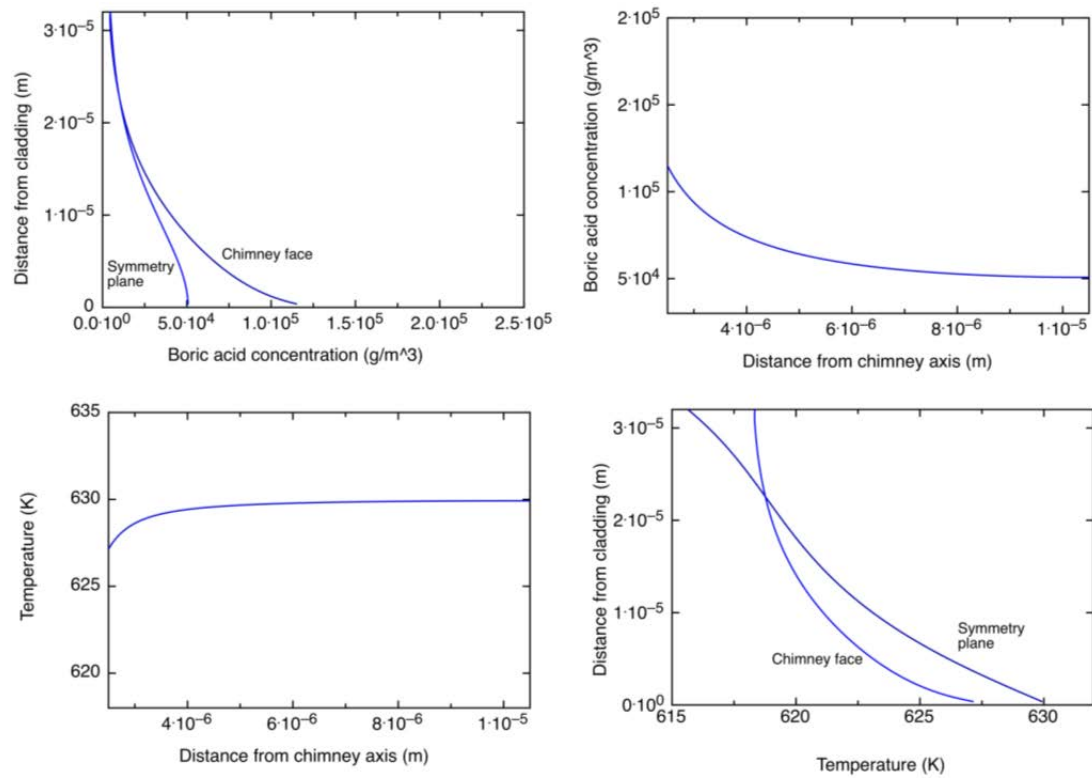


FIG. 11. Temperature and species concentration variation within the crud, with the heat flux applied at the crud inner surface.

## 5.2. Heat flux distributions predicted by the coupled two dimensional wick boiling model

A contour plot of temperatures, and a vector plot of heat flow, is shown in Fig. 12, where we indicate the temperature distribution and heat flows within, and to and from, the crud.

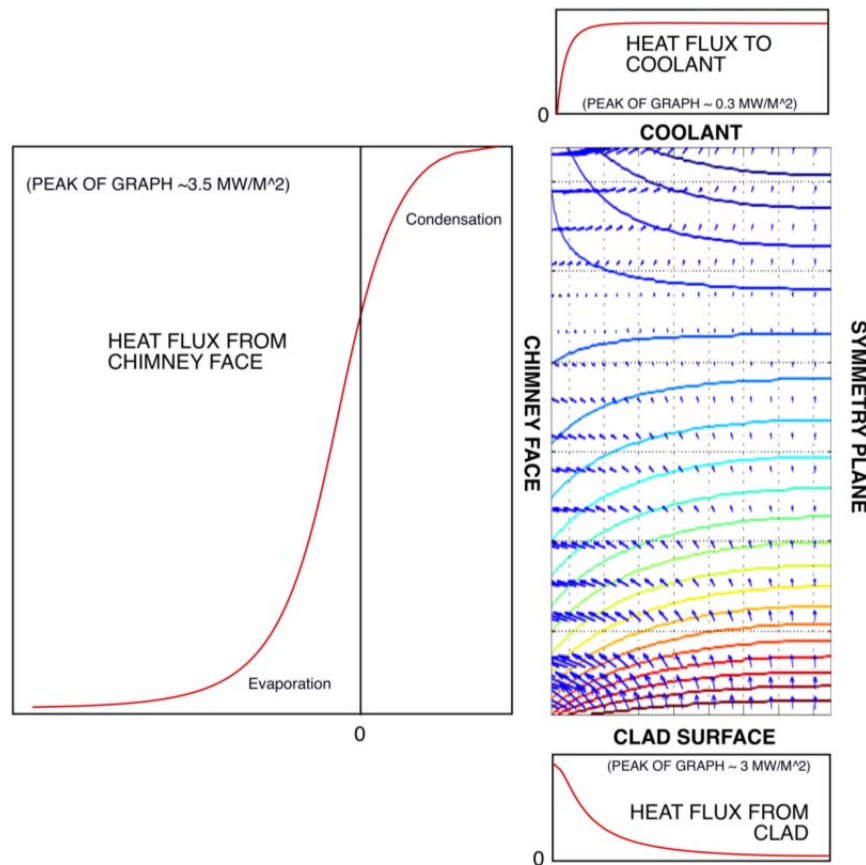


FIG. 12. Contour plot of temperatures, and a plot of heat flow vectors, in the crud. Left side chimney face, right side symmetry plane. Below, left and above: A depiction of the surface heat fluxes into the crud, into the chimney, and into the bulk coolant from the wetted crud surface.

Plainly, the mechanism that is overwhelmingly responsible for the removal of heat from the clad to the coolant is radial conduction towards the chimneys, with evaporative cooling at the chimney face. (Interestingly, the model here predicts a little condensation towards the upper part of the chimney. The magnitude of this is sensitive to the modeling of, for example, the coolant heat transfer coefficient, and it is only present for a limited range of parameter values). For the conditions employed here, about 70% of the heat is removed via net evaporation in the chimney. Associated with this, it is seen that the heat flux from the clad surface is very localized around the periphery of the chimney.

We will now seek to identify the circumstances under which this mechanism, of heat removal primarily by wick boiling, is expected to be dominant. We will then attempt to characterize the behaviour, expressing it in terms of an ‘effective thermal conductivity’ for the crud. One reason for the significance of this characterization is that it is really only this that can be measured in reactor-relevant large-scale experiments and an understanding of its appropriateness and helpfulness is necessary.

### 5.3. When is wick boiling likely to be important?

Plainly, if the chimneys are separated by many crud thicknesses, we would not expect their influence to extend over the whole fuel surface; the thermal behaviour might be expected to tend towards that depicted in Fig. 4. We will now perform analyses with a range of separations to determine the chimney density required to cause wick boiling to be the dominant mechanism for heat removal. From Fig. 12. we can see that there is only a fairly small temperature variation along the clad — crud interface, and along the crud — coolant interface. We will express and analyse results in terms

of (weighted) averages of each of these temperatures, allowing, for example, an ‘equivalent’ crud thermal conductance to be defined.

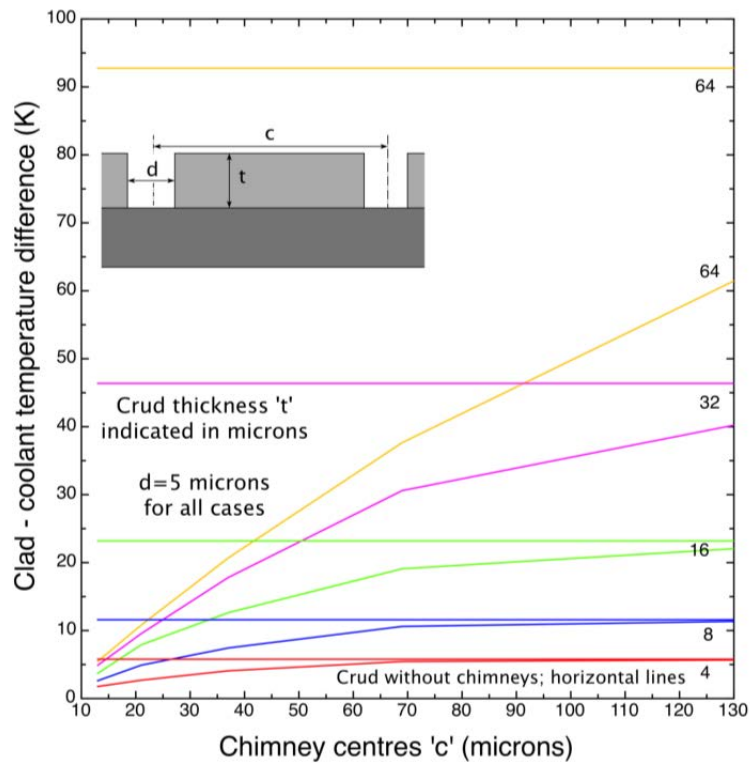


FIG. 13. Clad to coolant mean temperature difference versus chimney centres, for a range of crud thicknesses. Also shown are the temperature differences that would be present in the case of no chimneys.

In Fig. 13 we show the model’s prediction of the temperature difference, averaged over the surface, between the metal–crud and crud–water interfaces. Also shown are the corresponding temperature differences for the case of no chimneys. As the chimney separation increases, the temperature difference approaches the ‘normal’ values, as predicted by the wet crud model discussed above. The chimney spacing at which this occurs is greater for thick crud, as would be expected. For smaller chimney separations, the temperature rise through the crud is seen to be very much smaller than the simple wet crud model would predict.

The same data is presented in a different form in Fig. 14. Considering for example the well separated chimneys of the orange line, with chimney centres of 133  $\mu\text{m}$ , it is not until a crud thickness of  $\sim 30 \mu\text{m}$  that any perturbation from the ‘normal’ wet crud is observed.

For more closely spaced chimneys, the temperature rise through the crud is much reduced by the chimneys. It is notable that the temperature of the cladding is predicted to be only weakly influenced by the thickness of the crud. This is a distinct departure from the ‘wet crud’ prediction.

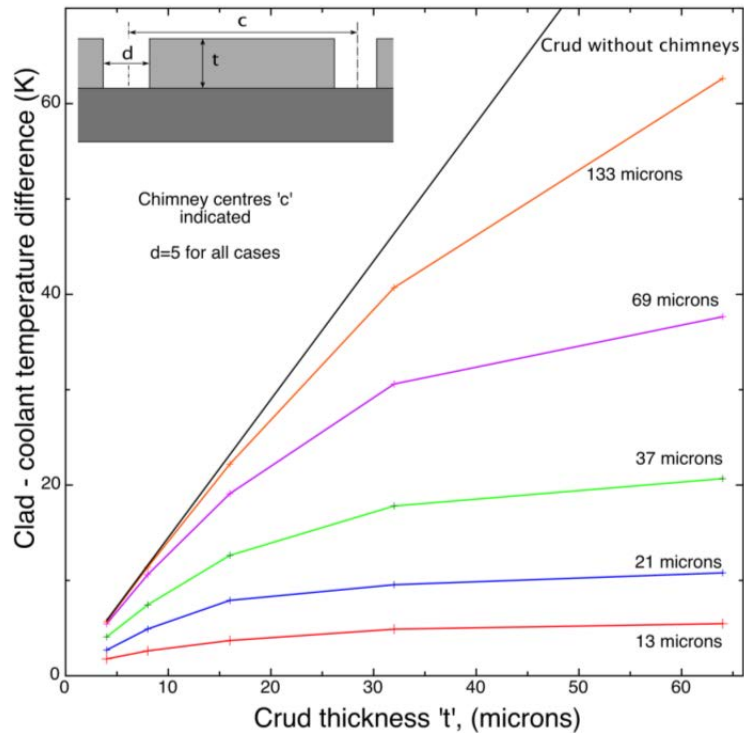


FIG. 14. Clad to coolant mean temperature difference versus crud thickness, for a range of chimney centres. Also shown is the variation of temperature difference that would be present in the case of no chimneys.

#### 5.4. Effective crud conductivity

In reactor-scale measurements of the thermal effects of crud the most natural quantity to try to measure is the temperature difference across the clad, the crud and the water-side boundary layer. (Indeed, the local bulk coolant temperature may, in addition, itself be inferred from energy conservation arguments.) From this a crud thermal conductivity can be estimated. This is one of the uses of the ‘WALT’ rig, for example [13].

We can use the results of the model to estimate equivalent crud thermal conductivity. In Fig. 15 is shown the dependence of effective thermal conductivity on crud thickness and chimney spacing. It is plain that crud thermal conductivity is very much not a ‘material property’, but varies strongly — by some orders of magnitude — according to the local geometry. Observed crud chimneys generally have separations of a few microns to ten or so microns, which indicates that this mechanism will generally be applicable.

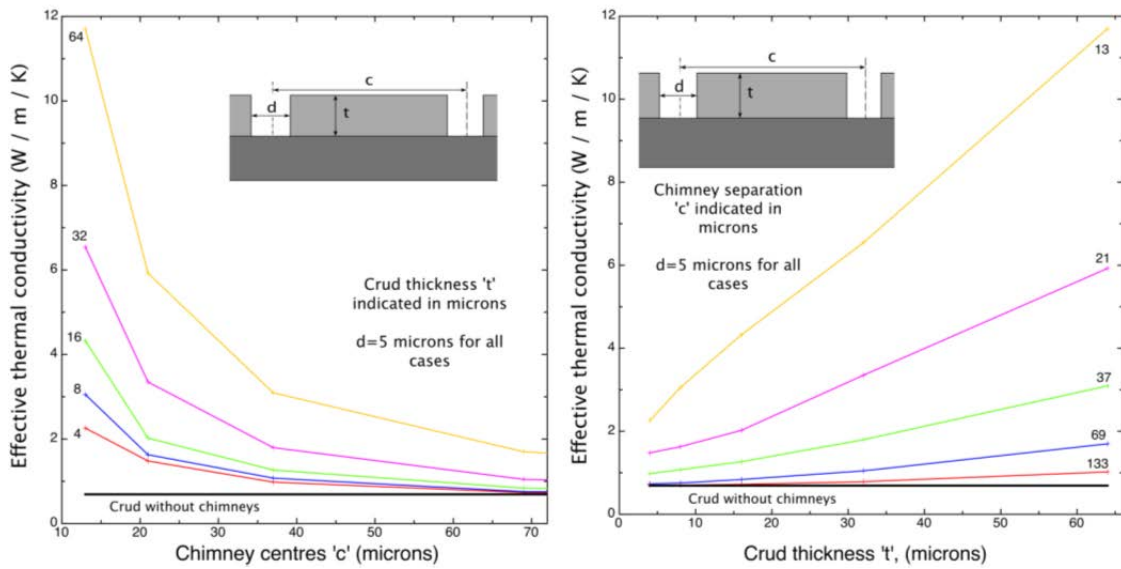


FIG. 15. Crud effective thermal conductivity as a function of chimney separation and crud thickness.

The conductivity of chimney-free wet crud is indicated also. It is convenient to combine the results, to give an approximate, but fairly robust, indication of the dependence of effective conductivity on the main parameters that affect it; the crud thickness, and the chimney separation. This is shown in Fig. 16. It is clear that the wick boiling mechanism has the ability to reduce clad temperatures significantly, over a wide parameter space.

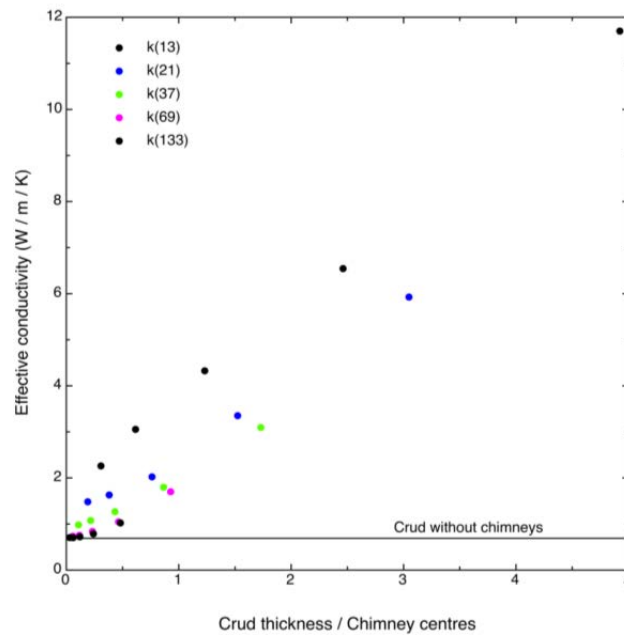


FIG. 16. The dependence of effective conductivity on crud thickness and chimney separation, obtained by aggregating the results of the previous analyses. The numbers in the legend indicate to which values of crud centre each data point corresponds.

## 6. DISCUSSION AND CONCLUSIONS

It has been shown that the usual ‘porous medium’ model of thermal conductivity predicts values that would cause very high clad temperatures, even if vapour film generation does not occur.

The role of wick boiling in crud ‘chimneys’ has been investigated using a coupled two dimensional model. Advection of the dissolved species in the coolant causes concentrations near the evaporating face to rise until diffusion back down the concentration gradient so generated balances the advection. This coupling allows the high species concentrations of dissolved species to be determined. These high concentrations cause a significant increase in the local saturation temperature. The analyses suggest that the large majority of heat loss from the fuel is then by evaporation, taking place at the chimney face.

This dramatic effect of wick boiling on the thermal performance has been quantified, and the behaviour of the crud coating has been characterized, pragmatically, in terms of an ‘effective thermal conductivity’. The dependence of this effective conductivity on the main parameter that affects it, namely the chimney separation, has been quantified. The results and methods presented should contribute to interpretation of reactor-scale measurements of crud thermal conductivity.

## REFERENCES

- [1] DESHON, J., Modeling PWR fuel corrosion product deposition and growth processes, EPRI, Palo Alto, CA 1009734 (2004).
- [2] MAHLON, J., The Simulation and study of conditions leading to axial offset anomaly in pressurized water reactors, M.Sc. Thesis M.Sc. Thesis, Georgia Institute of Technology, USA (2004).
- [3] BYERS, W. A., Pressurized water reactor core crud mapping, in 18th International Conference on Nuclear Engineering (ICONE 18), Xian China, (2010).
- [4] COHEN, P., Heat and mass transfer for boiling in porous deposits with chimneys, AICHE Symposium series, **70** (1974) 71–80.
- [5] DESHON, J., PWR axial offset anomaly (AOA), guidelines, revision 1, EPRI, Palo Alto, CA 1008102 (2004).
- [6] HENSHAW, J., et al., A model of chemistry and thermal hydraulics in PWR fuel crud deposits, J. Nucl. Mater., **353** (2006) 1–11.
- [7] PAN, C., et al., Concentration levels of solutes in porous deposits with chimneys under wick boiling conditions, Nucl. Eng. and Design, **99** (1987) 317–327.
- [8] PAN, C., JONES, B.G., Wick boiling performance in porous deposits with chimneys, in AICHE/ANS National Heat Transfer Conference Symposium on Multiphase and Heat Transfer, Denver (1985).
- [9] TODRES, N.E., KAZMI, M.S., Nuclear Systems 1, Thermal Hydraulics Fundamentals vol. 1: Hemisphere Publishing Corporation, (1989).
- [10] MACBETH, R.V., Boiling on surfaces overlaid with a porous deposit: Heat transfer rates obtained by capillary action, Atomic Energy Establishment Winfrith AEEW-R- 711 (1971).
- [11] MACBETH, R.V. et al., An investigation into the effect of crud deposits on surface temperature, dry out and pressure drop, with forced convection boiling of water at 69 bar in an annular test section, Atomic Energy Establishment Winfrith AEEW-R 705 (1971).
- [12] VERSTEEG, H.K., MALALASEKERA W., An Introduction To Computational Fluid Dynamics: The Finite Volume Method: Prentice Hall (2006).
- [13] WANG, G., et al., Methods to reduce CIPS/CILC risk for the zero fuel failure by 2010 initiative, 18th International Conference on Nuclear Engineering (ICONE 18), Xian China (2010).

# **EXPERIENCE IN DEVELOPMENT AND USE OF AN ULTRASONIC PLANT FOR FUEL ASSEMBLIES CLEANING OF A WWER-440 REACTOR CORE**

A.V. GRISHAKOV, O.P. ARKHIPOV  
OKB "GIDROPRESS", 21 Ordzhonikidze Street, 142103  
Podolsk, Moscow region

A.N. PRYTKOV  
Novovoronezh Nuclear Power Plant 3–5, 396072  
Novovoronezh

Russian Federation

## **Abstract**

The paper presents results of the use of ultrasonic cleaning of fuel assemblies at the Novovoronezh NPP.

## **1. INTRODUCTION**

The operation of RP Units 3 and 4 at Novovoronezh NPP, the Russian Federation has been constantly associated with the presence of deposits on fuel rod claddings, spacing grids and other elements of fuel assemblies. The growth of deposits during operation on elements of the fuel assemblies, leads to a growth of pressure differential on the assemblies, which then leads to a decrease in coolant flow rate through the core, and as a result, to a forced subsequent decrease in the unit power.

In 2008, regarding the units 3 and 4 at Novovoronezh NPP, a decision was made to introduce ultrasonic cleaning of fuel assemblies, as part of implementing activities on decreasing the growth of the before mentioned pressure differential at these units.

Particularly it is related to reactor vessels made of so-called "black" steels (15X2HMΦA) without protective coating and subject to decontamination washing during decontamination.

## **2. ULTRASONIC CLEANING**

### **2.1. Procedure**

Due to the novelty of the problem and the lack of experience with this procedure at Russian NPPs, it was decided to perform the cleaning of the fuel assemblies at the units 3, 4 of NV NPP in two stages. The first stage involved pilot cleaning of two fuel assemblies with their subsequent examination and inspection under a special program in a hot chamber at the NV NPP itself. The second stage involved industrial cleaning, during planned transport technological procedures (TTP), of all sealed fuel assemblies of the third or fourth years of operation of Units 3 and 4. Each stage of cleaning had its own technical requirement regarding safety of such work, taking into account, all conditions of the created equipment including emergency ones. This method of cleaning was not fundamentally new, had it already been tested and used for pilot-industrial and industrial cleaning of spent fuel assemblies (SFA) at Unit 3 of NV NPP with the help of an ultrasonic plant (UP) created for this purpose. Only tight fuel assemblies (by the results of tightness control) were subjected to industrial cleaning.





*FIG. 2. UP in standard housing, type 12. Workers of the plant and representatives of OKB “Gidropress” are examining the pump-filtering equipment. The frame in the figure highlights the cylindrical vessel of the plant, the loading chamber, hoses and insulated power cables. The pump-filtering facility and connecting flexible hoses are located on the housing of type 12 on the left.*

### **2.3. Procedure requirements at NV NPP**

It is possible to emphasize the following main requirements for the plant operator:

- A possibility to perform cleaning on one plant of both RFA and WA without additional reconstruction;
- A possibility to use regular cargo-lifting mechanisms and TTP regular tools, and as a result, only vertical working position;
- A possibility of control during cleaning of the main process parameters: flow rate, pressure differential on spent FA, temperature, dose power on the filter;
- Minimization of personnel presence, and as a rule, remote control;
- A possibility of equipment deactivation between operational periods and a possibility of intermediate storing in the reactor hall;
- A possibility of remote replacement of filtering cartridges in the filtering facility with a possibility of their subsequent utilization;
- Minimization of the ultrasonic field effect on the fuel rod cladding and fuel matrix during cleaning.

## 2.4. Ultrasonic operation

The first stage of ultrasonic cleaning of the working fuel assembly (WA) and the regulating fuel assembly (RFA) (stage of pilot-industrial operation of UP) was carried out on the 23 December 2008 within the framework of activities on decreasing the growth of the pressure differential on WWER-440 reactors of units 3 and 4 of NV NPP. Ultrasonic cleaning of 67 WA and 12 RFA from deposits with help of UP (stage of industrial operation) was carried out during preventive maintenance (PM-2009) of unit 3 from 2009-02-11 to 2009-02-28.

The WA and RFA were examined in the “hot” chamber at NV NPP after ultrasonic cleaning at the stage of pilot-industrial operation (the duration of ultrasonic influence was more than 40 minutes).

During preventive maintenance (PM-2009) ultrasonic cleaning was performed in a pulsing mode with a duration of up to 30 minutes:

- The booster pump and ultrasonic module were activated;
- SFA were placed in the ultrasonic module bottle;
- The booster pump was deactivated for 3 min.;
- The booster pump was activated for 5 min.;
- Items 3 and 4 were repeated three times (24 min.);
- SFA were extracted from the ultrasonic module bottle.

Pump deactivation was done to increase the ultrasonic effectiveness impact on deposits with zero flow rate through FA.

## 3. CONCLUSIONS

The following conclusions can be made based on the results of the examinations undertaken:

- Ultrasonic influence does not change the structure of the fuel rod cladding material and fuel pellet, nor does it affect the design of the spacing grids and the fuel assembly as a whole.
- During ultrasonic cleaning deposits are partially removed from the fuel rod surface; hard deposits in the spacing grids become more mobile (loosened) and are partially removed.
- All fuel rods maintain their tightness after ultrasonic cleaning.

Twenty-three untight fuel assemblies were detected after unit shutdown for unscheduled preventive maintenance (PM) during leak check cladding (LCC) in 2009. It is important to point out that both fuel assemblies which were subjected to ultrasonic cleaning (11 pcs.), and fuel assemblies which were not subjected to ultrasonic cleaning (12 pcs.) were untight, and there is no reason to suspect that ultrasonic cleaning was responsible for FA loss of tightness. This is also proven by the results of post-reactor studies of FA inside the hot chamber.

During subsequent operation of the unit according to the in-core instrumentation system (ICIS) temperature control data, the maximum heating was observed on the first-year operation fuel assembly in the 35th fuel loading, which is in line with the planned design distribution. Whereas in the previous years (before ultrasonic cleaning) the maximum heating was observed on third and fourth-year operation fuel assemblies (id est fuel assemblies with the largest amount of deposits).

Thus, it can be stated that fuel assemblies maintain their operability during ultrasonic cleaning (UC); UC does not increase the number of untight fuel assemblies in the core and not only does not lead to increase in the velocity of pressure growth on the reactor, but actually decreases it, which makes it possible to operate the reactor plant under permissible thermal-hydraulic conditions.

TABLE 1. THE CONTENT OF DEPOSITS — CORROSION PRODUCTS (FE, CR, NI, MN, CO), PROBABLY DEBRIS-PARTICLES AND ORGANIC SUBSTANCES. DENSITY OF DEPOSITS —  $2 \text{ g}\cdot\text{cm}^{-3}$

Quantity of element, mg/fuel rod		
Fe	Cr	Ni
5–800	3–40	2–70
Element	Weight [%]	
C	4,48–6,7	
O	26,37–31,44	
Cr	2,0–3,02	
Mn	6,11–6,67	
Fe	42,87–48,42	(essential element)
Ni	4,91–6,23	
Zr	3,51–6,47	

However, operational experience of UP at the stage of industrial operation at Units 3 and 4 of NV NPP unearthed a number of faults, the following being the main ones:

- Insufficiency of ult;
- Of filters.

Work is now underway on updating UP, which includes development of a high-gradient electromagnet filter.



# IN SITU EXPERIMENTAL DATA ON PASSIVATION OF ALLOY 690 IN HOT CONDITIONING WATER CHEMISTRY

T. SAARIO  
VTT, Espoo,  
Finland

## Abstract

The primary circuit surfaces of a new pressurized water nuclear reactor are passivated before the first fuel loading. This treatment is called hot conditioning. The main purpose of the hot conditioning is to minimise the rate of generation of soluble and insoluble corrosion products (corrosion rate), and thereby minimize the activity build-up during power operation. There is still no international consensus on optimal passivation water chemistry. Open issues are e.g. the optimal concentration of lithium and the length of the passivation treatment. New issues are the possible benefits of using boron and zinc in the water during the passivation. The report presents the first part of experimental results on Alloy 690 gained by the electrochemical impedance spectroscopy (EIS) in situ technique at  $T = 292^{\circ}\text{C}$ . These results indicate that addition of boron is highly beneficial, 1200 ppm B resulting in reduction of the estimated corrosion rate by a factor of about 2. An increase of the lithium concentration from 1 to 2 ppm Li was found to result in an increase of the estimated corrosion rate. The time to form a stable passive layer on Alloy 690 at  $T = 292^{\circ}\text{C}$  was found to be about 40 hrs. Thus, the time normally used for passivation, i.e. 300–1000 hours is certainly long enough. In experiments without boron, the conductivity was found to decrease during the experiment, indicating a possibility of lithium hide-out on the hot part of the test equipment surfaces. There are three lines of further research in optimization of the hot conditioning procedure that require attention. The first one is the lower range of Li concentration, i.e. in situ results need to be gained also for 0.5 ppm Li, in order to quantify the difference between the Japanese and Western approaches. Secondly, the effect of boron concentration should be studied in a more wide range, e.g. duplicating some of the current measurements at a level of 500 ppm B. Thirdly, the mechanism, extent and consequences of possible Li hideout during the passivation treatment should be studied in detail.

## 1. INTRODUCTION

The primary circuit of a new reactor is passivated (pre-oxidised) before loading in the first fuel. The passivation procedure is called hot conditioning which is part of the Hot Functional Testing (HFT). The main purpose of the pre-oxidation is to minimise the concentration of corrosion products in the coolant during the future power cycles, and thus minimise the activity build-up at the plant. During hot conditioning water is heated by the waste heat from the main circulation pumps, resulting in a maximum temperature of slightly less than  $300^{\circ}\text{C}$ . Pre-oxidation of system and component surfaces may also come into focus when larger system parts have been decontaminated and are possibly pre-oxidised before taking into use or e.g. in case of replacing the steam generator.

There has been a continuous development in optimization of the hot conditioning procedure during the last 30 years [1]. The aim of water chemistry development is to establish a Cr-rich stable oxide film on the surface of the primary system components, especially on steam generator tubing which represents about 70% of the surface exposed to the coolant. A Cr-rich spinel-type oxide film results in a lower corrosion product release and thus contributes to a lower level of activity build-up during power operation.

Plain deaerated water is not sufficient in establishing a reducing condition (which is needed to form the desired passivating Cr-rich spinel-type oxide film), and thus dissolved hydrogen is added (typically 25 to 35 ccH<sub>2</sub>/kgH<sub>2</sub>O). Adjustment of the high temperature pH to a value close to the solubility minimum of the main elements Fe, Ni and Cr supports formation of a Cr-rich spinel-type oxide and in PWRs is achieved by adding lithium hydroxide, LiOH. For a target pH<sub>T</sub> in the range 7.2–7.4 the concentration of Li is 0.5–1.0 ppm, respectively, in the absence of boric acid. Adding the base, LiOH, without H<sub>2</sub> would result in markedly higher corrosion product release rate, even higher than that in deaerated water [1].

The Japanese have proposed that a hot conditioning chemistry with 0.5 ppm Li + 30 ccH<sub>2</sub>/kgH<sub>2</sub>O is optimal, and showed e.g. at Tomari-1 [2], Ikata-3 [3] and Genkai-4 [4] that this chemistry results in a 10–30% reduction in does rate during the first outages, when compared to plants passivated with

de-aerated water. A further 40–60% reduction in dose rate can be gained by introducing Zn-injection (at the level of 5 ppb) during the hot conditioning, as shown for the case of Tomari-3 [5]. EDF and AREVA currently promote a hot conditioning chemistry with 1–2 ppm Li + 30 ccH<sub>2</sub>/kgH<sub>2</sub>O.

An example of the kinetics of passive film formation on different steam generator tubing materials under typical PWR operational water chemistry conditions is shown in Fig. 1. The film thickness presented in Fig. 1 consists of both the inner (in-grown) layer and the outer (deposited) layer. While the total film thickness for Alloy 690 grows continuously in a near parabolic fashion, it is presumed that the part of the inner layer which is responsible for corrosion resistance, i.e. the barrier layer, actually forms rather rapidly [6, 7].

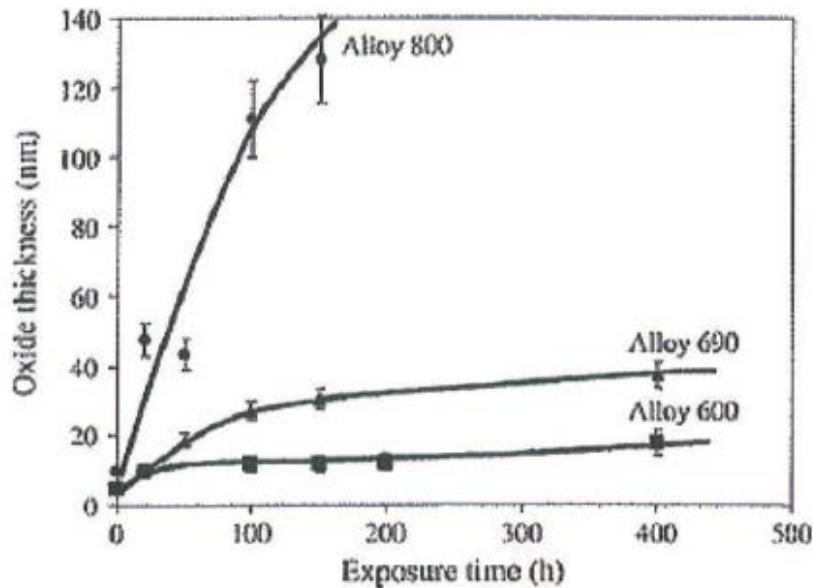


FIG. 1. Oxide thickness vs. oxidation time for alloys 600, 690 and 800, oxidised in PWR primary water at  $T = 325^{\circ}\text{C}$  (2 ppm Li, 1200 ppm B, 35 cc/kgH<sub>2</sub>O H<sub>2</sub>) [6].

Electrochemical impedance spectroscopy (EIS) is a tool that has been earlier shown to be applicable for in situ monitoring of properties of passive films forming under hot conditioning water chemistry conditions [8]. Impedance is resistance of a system to alternating current, analogous to the electric resistance of a material. According to Ohm's law voltage (V) is resistance (R) times the current (I).

$$V = R \cdot I \quad (1)$$

Simplifying, in the case of a PWR environment, one may take that the voltage is the redox-potential (-constant), resistance is equal to impedance at low frequencies and current is the corrosion current which is directly proportional to the corrosion rate. Thus, the value of impedance at low frequencies becomes inversely proportional to the corrosion rate. In general, the higher is the value of impedance at low frequency end of the spectrum, the lower is the corrosion rate. The EIS data can be formally interpreted using the mixed conduction model (MCM), as shown later in Chapter 4.1.

There is still no international consensus on the best available procedure for the water chemistry to be used during HFT. Open questions exist on the minimum length of the passivation time, the optimal concentration of Li, and the use of boric acid. In SAFIR2010-programme, in the project WATCHEM, on-line in situ electrochemical methods have been developed in cooperation with BARC, India, and UCTM, Bulgaria to monitor the passivation process and to determine the degree of success. The methods have been earlier verified for carbon steel [8]. This report contains the first part of verification results for Alloy 690.

## 2. GOAL

The main goal of the present report has been to verify the use of in situ electrochemical impedance (EIS) technique for monitoring of the progress and success of passivation of Alloy 690 during exposure to simulated hot conditioning water chemistries. A second goal was to perform a preliminary assessment of the main water chemistry parameters, i.e. lithium hydroxide and boric acid concentration, in relation to determining the optimal water chemistry for hot conditioning of a PWR plant having Alloy 690 steam generator tubing.

## 3. EXPERIMENTAL

The measurements were performed in an AISI 316 autoclave at temperature of 292°C and pressure of 100 bar. The autoclave was connected to a recirculation loop enabling refreshing of the water in the autoclave about twice in an hour. The electrolyte used was prepared from deionised water. Lithium was added as LiOH and boron as H<sub>3</sub>BO<sub>3</sub>. In the experiments where B was added, a concentration of 1200 ppm B was used, corresponding to 6867 ppm of H<sub>3</sub>BO<sub>3</sub>. Hydrogen overpressure of 1.5 bar was added to the feed water tank corresponding to about 30 cc/kgH<sub>2</sub>O (2.3 ppm) dissolved hydrogen. All potentials were measured vs. an internal reference electrode made of Pd and cathodically polarised to  $i_c = -5 \mu\text{Acm}^{-2}$  to stabilise the potential of the reference electrode at the hydrogen line (i.e. the reversible H<sub>2</sub>/H<sup>+</sup> — redox-potential, RHE). The potential was converted to the SHE scale by the Nernst equation after calculating the solution pH at the temperature. A cylinder made of Pd and placed around the specimen was used as a counter electrode.

Specimens were cut from an Alloy 690 tube (courtesy of EPRI NDE Center). The material was in annealed condition. Measurement wires (0.8 mm Ni-wires) were attached to the specimen mechanically, and the connection point was covered with several layers of PTFE-tape.

Impedance spectra were obtained with a Solartron 1287/1260 system controlled by ZPlot software (Scribner Associates) in a frequency range of 0.001 to 80,000 Hz at an a.c. voltage amplitude of 10 mV (rms). Impedance spectra were measured every ca. three hours till the end of the exposure at open circuit. The validation of the impedance spectra was performed by checking the linearity condition, i.e. measuring spectra at different signal amplitudes, and the causality using a Kramers-Kronig compatibility test. For the simulation and fitting of impedance spectra to the transfer functions derived from the kinetic model, Microcal Origin-based software has been employed.

## 4. RESULTS

### 4.1. Impedance spectra

Several successful experiments were carried out using water with 1200 ppm B as the base electrolyte into which lithium additions were made as LiOH. An example of the inlet conductivity from one of the experiments is shown in Fig. 2. First the loop was cleaned by changing all the water into ion pure water and circulating the ion pure water through the loop until conductivity was less than 0.2  $\mu\text{S}\cdot\text{cm}^{-1}$ . Then, 1200 ppm boron as H<sub>3</sub>BO<sub>3</sub> and 1 ppm of Li as LiOH were added, temperature was increased to  $T = 80^\circ\text{C}$  and nitrogen bubbling was continued in the mixing tank until dissolved oxygen level was  $\text{DO}_2 < 5$  ppb. After this, 1.5 bar hydrogen overpressure was introduced into the mixing tank and temperature was increased to  $T = 292^\circ\text{C}$ .

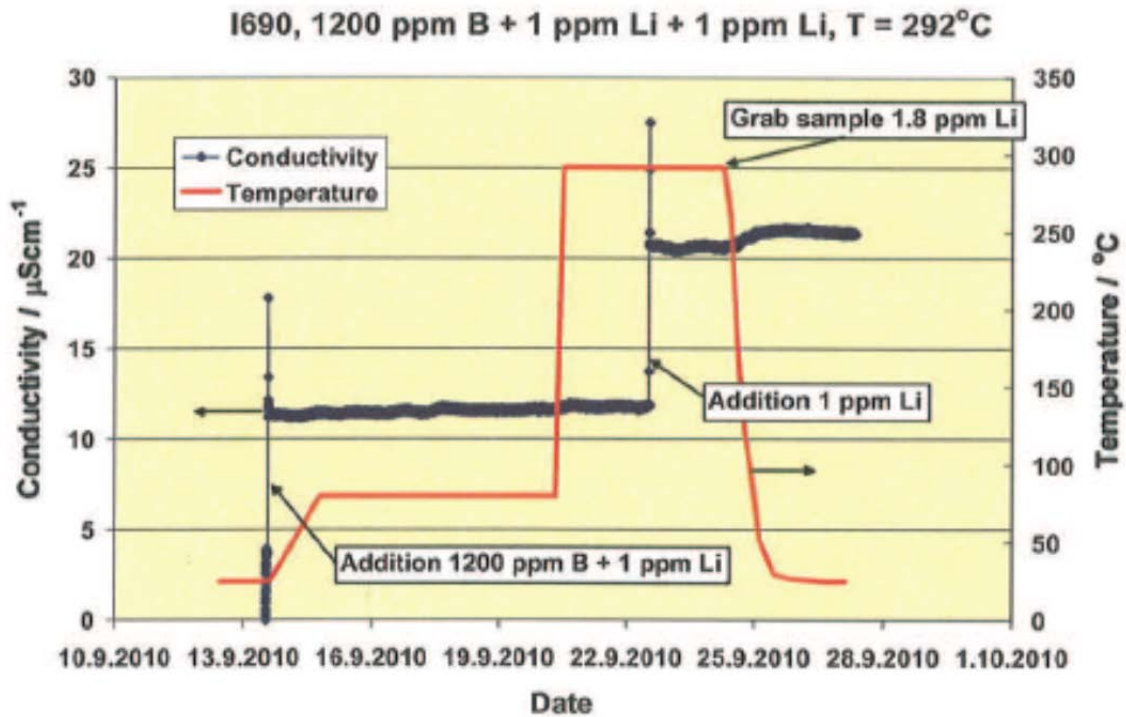


FIG. 2. Temperature and inlet conductivity ( $25^{\circ}\text{C}$ ) as a function of time in a test run where originally 1200 ppm of B and 1 ppm Li, and after stabilization of the in situ impedance spectra of Alloy 690 an additional 1 ppm Li was added as LiOH.  $[\text{H}_2] = 30 \text{ ccH}_2/\text{kgH}_2\text{O}$  from the start.

During the exposure at  $T = 292^{\circ}\text{C}$  EIS was recorded, one spectra roughly each 3 hrs. After the spectra had stabilized, an additional 1 ppm Li was injected to the mixing tank and the EIS was again recorded until the spectra stabilized, after which the test was ended and the pressure vessel was cooled down. At the end of the test a grab sample analysis for Li showed  $[\text{Li}] = 1.8 \text{ ppm}$ . The high temperature pH would be  $\text{pH}_{292\text{C}} = 6.5$  for a solution with 1200 ppm B + 1 ppm Li and  $\text{pH}_{292\text{C}} = 6.8$  for a solution with 1200 ppm B + 2 ppm Li.

Figure 3 shows a comparison of the EIS (stabilized values) measured during the experiment. The increase of Li concentration from about 1 ppm to about 2 ppm results in a decrease of the impedance value at low frequencies from about  $|Z| = 1580 \Omega\cdot\text{cm}^2$  to roughly  $970 \Omega\cdot\text{cm}^2$ . In a straightforward interpretation, this means that increasing the lithium concentration by about 100% results in an increase of the corrosion rate by roughly 60%. A more accurate interpretation of the results will be given below in Chapter 4.2, involving modelling of the impedance spectra and extraction of relevant parameters thereof describing the different processes responsible for the impedance signal.

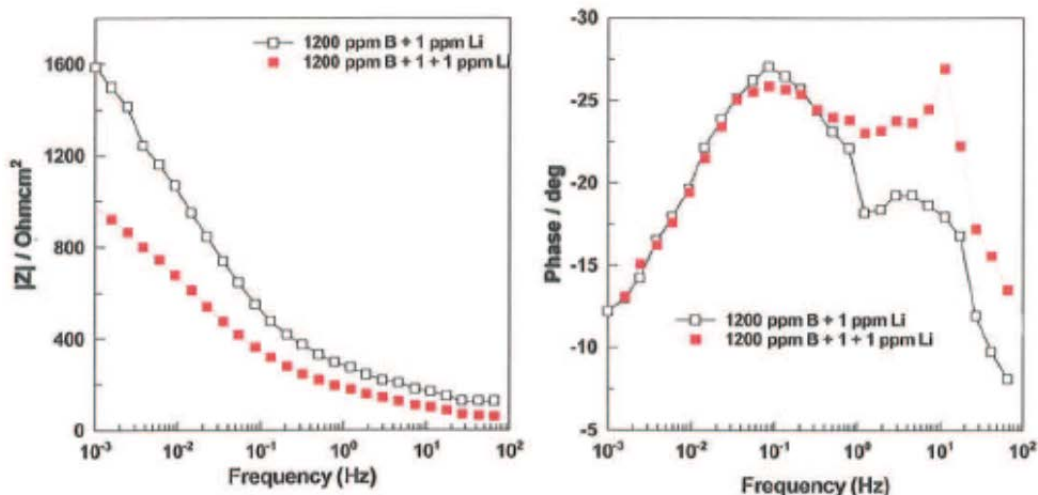


FIG. 3. The effect of increasing the lithium concentration during one single experiment from about  $[Li] = 1 \text{ ppm}$  to  $[Li] = 2 \text{ ppm}$  on the impedance magnitude (left) and phase angle (right).  $T = 292^\circ\text{C}$ ,  $[B] = 1200 \text{ ppm}$ .

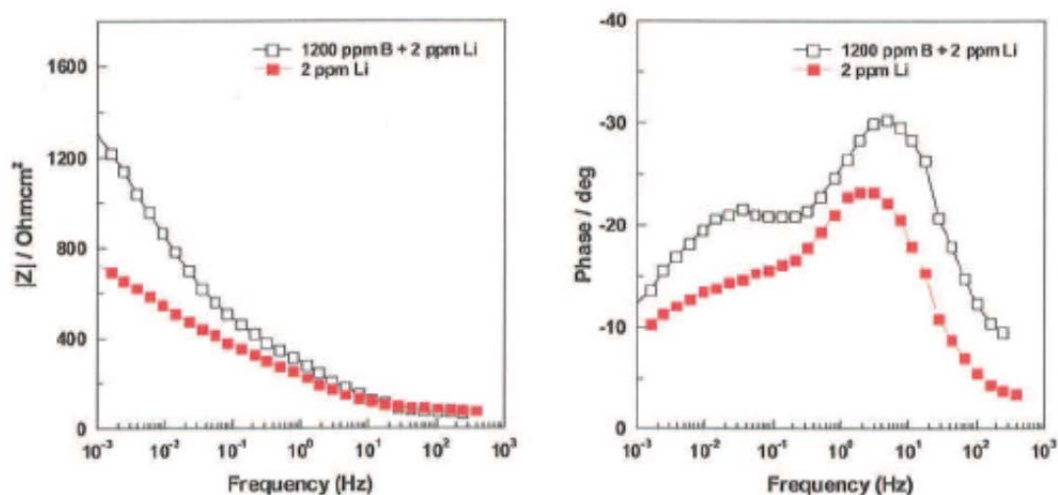


FIG. 4. Comparison of results from an experiment with  $1200 \text{ ppm B} + 2 \text{ ppm Li}$  and a separate experiment with  $2 \text{ ppm Li}$  (no B). In these experiments the chemistry was kept constant throughout the duration of each experiment.

Figure 4. shows a comparison of results from an experiment with  $2 \text{ ppm Li}$  (without any B) and a separate experiment with  $1200 \text{ ppm B} + 2 \text{ ppm Li}$ . The high temperature pH would be  $= 7.8$  for a solution with  $2 \text{ ppm Li}$  (no B), which is about  $1.0 \text{ pH-units}$  higher than that for the case with  $1200 \text{ ppm B} + 2 \text{ ppm Li}$ . In case of  $1 \text{ ppm Li}$  without B, the high temperature pH would be  $\text{pH}_{292\text{C}} = 7.4$ , about  $0.9 \text{ pH-units}$  higher than for the case with  $1200 \text{ ppm B} + 1 \text{ ppm Li}$ . In these experiments the chemistry was kept constant throughout the duration of each experiment.

In Fig. 4., despite the slightly less favourable  $\text{pH}_{292\text{C}}$ , the impedance with  $1200 \text{ ppm B}$  is clearly higher, at low frequencies by about  $70\%$ . Thus, the corrosion rate and rate of generation of soluble and insoluble corrosion products into the primary circuit would be expected to be clearly smaller in the presence of B than without it. Figure 5 shows a similar comparison with  $1 \text{ ppm Li}$  concentration. The presence of  $1200 \text{ ppm B}$  results in roughly twice as high impedance, indicating an even higher reduction in the rate of generation of soluble and insoluble corrosion products than in the case of  $2 \text{ ppm Li}$  concentration in the solution. In Fig. 6., another comparison is shown, similar to that in Fig. 3, on the effect of increasing the Li concentration from  $1 \text{ ppm}$  to  $2 \text{ ppm}$  in a solution with

1200 ppm B. In this case, the comparison is between two separate experiments, so that in both cases the chemistry has been kept constant throughout the experiment. In this case, the reduction in impedance resulting from the increase in Li concentration was roughly 25%.

A comparison of two experiments with no B, one with 1 ppm Li and the other one with 2 ppm Li, is shown in Fig. 7. Here, the decrease in impedance due to the increase of Li concentration was about 8%.

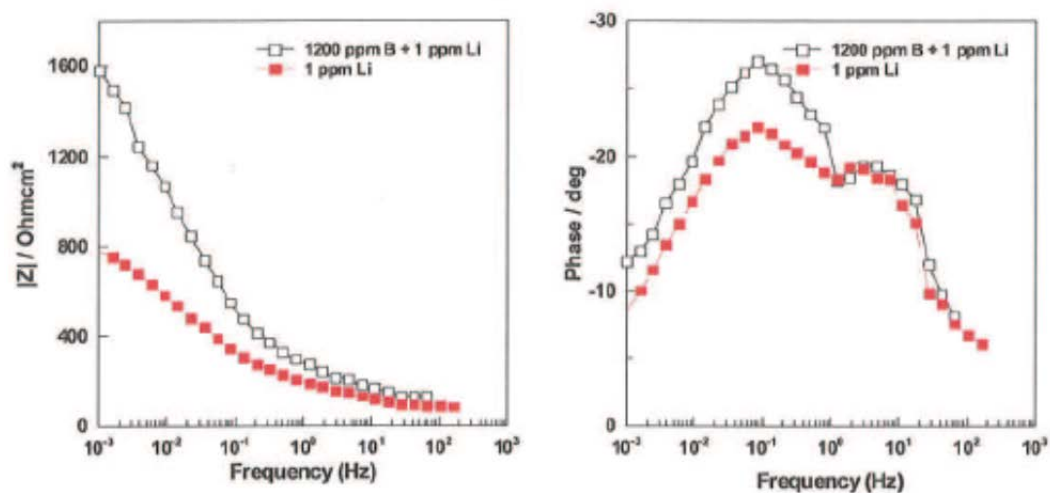


FIG. 5. Comparison of results from an experiment with 1200 ppm B + 1 ppm Li and a separate experiment with 1 ppm Li (no B). In these experiments the chemistry was kept constant throughout the duration of each experiment.

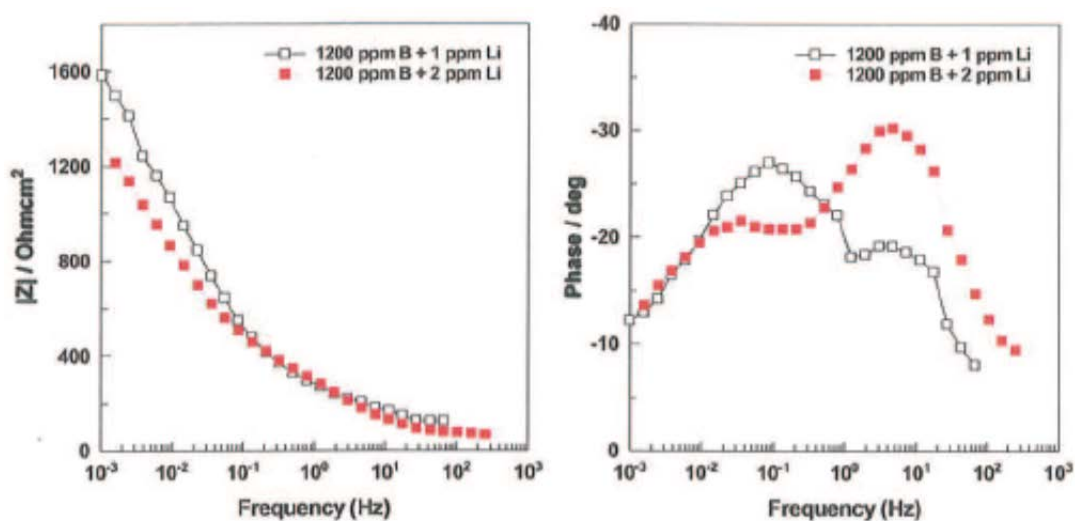


FIG. 6. Comparison of two separate experiments. The effect of increasing the lithium concentration from about  $[\text{Li}] = 1 \text{ ppm}$  to  $[\text{Li}] = 2 \text{ ppm}$  on the impedance magnitude (left) and phase angle (right).  $T = 292^\circ\text{C}$ ,  $[\text{B}] = 1200 \text{ ppm}$ .

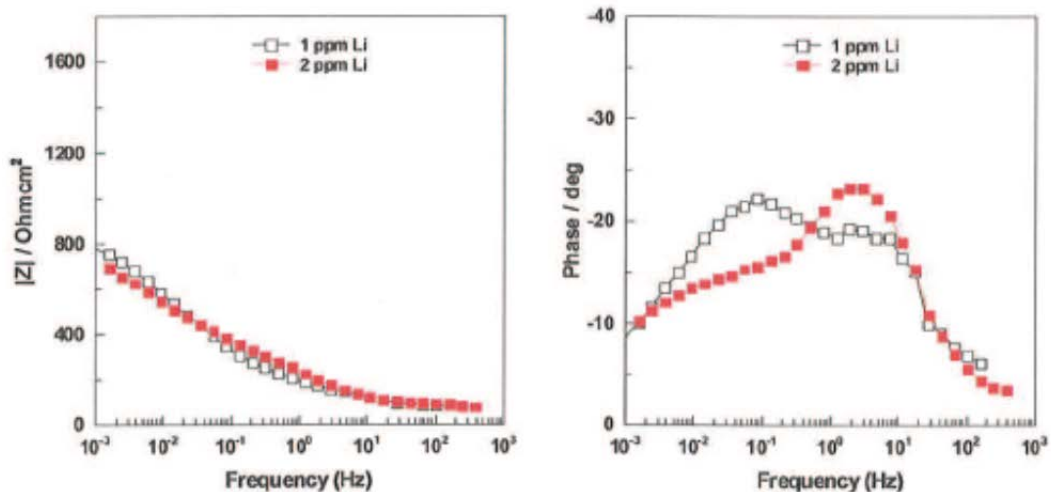


FIG. 7. Comparison of two separate experiments, the first one with lithium concentration of about  $[Li] = 1$  ppm and the second one with about  $[Li] = 2$  ppm. Impedance magnitude on the left and phase angle on the right.  $T = 292^\circ\text{C}$ ,  $[B] = 0$  ppm.

The exposure time for stabilization of the impedance spectra may be taken as the minimum time needed to achieve a stable passive layer. In case of carbon steel under PHWR hot conditioning conditions stabilization of the impedance spectra occurred within 30–40 hours [8], in agreement with the estimates (based on conventional ex situ techniques) for achieving a stable magnetite film on the surface [8]. Figures 8 and 9 show the impedance spectra measured as a function of exposure time for 1200 ppm B + 1 ppm Li and 1.3 ppm Li (no B), respectively. In both cases stabilization of the spectra is evident within about 30 to 40 hours of exposure. An interesting point is that the impedance is larger in the beginning of the exposure and decreases until stabilization occurs. This is exactly the opposite to the behaviour of carbon steel [8]. One possible explanation to this phenomena could be that on Alloy 690 under PWR conditions, the first about 3 nm thick layer forming within less than one minute is almost purely  $\text{Cr}_2\text{O}_3$  [7]. Transformation of this layer to the normally observed  $\text{Cr}_2\text{FeO}_4$  spinel oxide could be resulting in the observed behaviour. In the case of carbon steel, the layer is magnetite,  $\text{Fe}_3\text{O}_4$ , and only the thickness of the layer changes as a function of the exposure time without any changes in the layer crystallography.

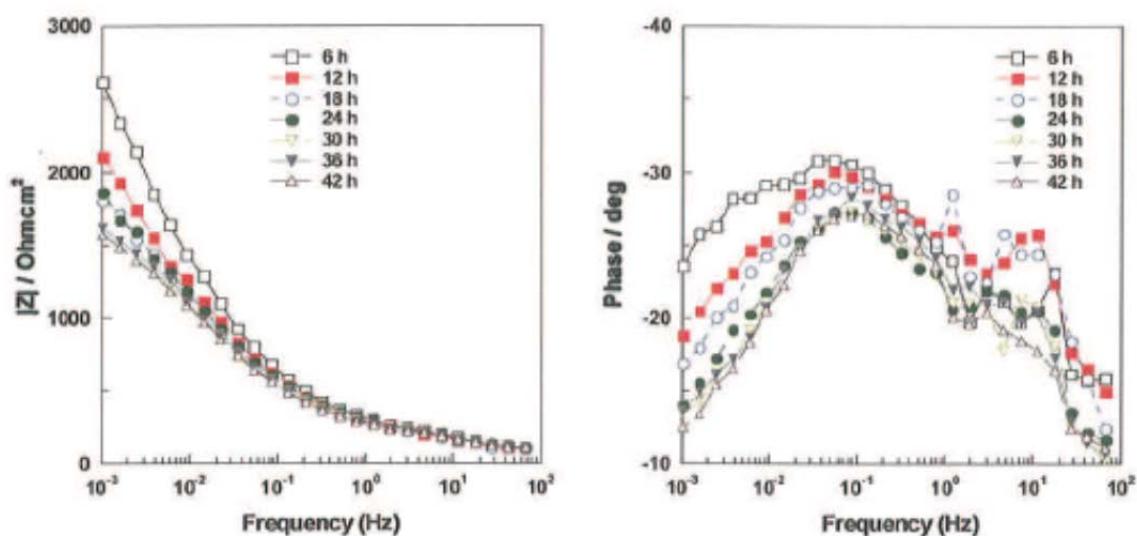


FIG. 8. The effect of exposure time on stabilization of EIS. Impedance magnitude (left) and phase angle (right). Lithium concentration  $[Li] = 1$  ppm,  $[B] = 1200$  ppm,  $T = 292^\circ\text{C}$ .

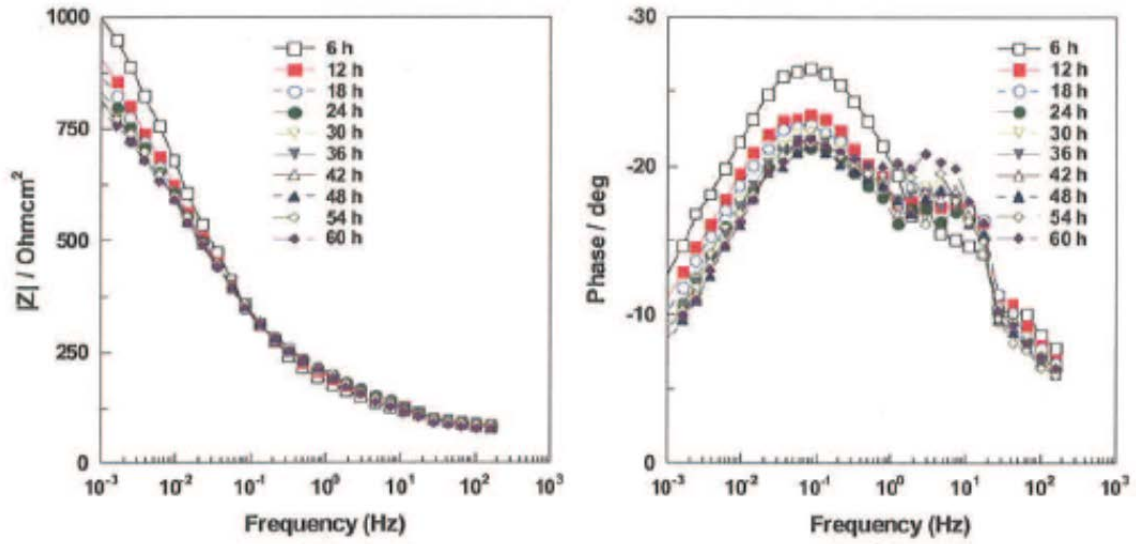


FIG. 9. The effect of exposure time on stabilization of EIS. Impedance magnitude (left) and phase angle (right). Lithium concentration  $[Li] = 1.3$  ppm,  $T = 292^\circ\text{C}$ ,  $[B] = 0$  ppm.

#### 4.2. Modelling the impedance response

Following the line of reasoning in /8/, the overall impedance of the Alloy 690 / oxide / coolant system can be written as being a sum of the resistance of the electrolyte,  $R_{ci}$ , and the impedances of the barrier layer and the outer deposited layer,  $Z_b$  and  $Z_{out}$ , respectively,

$$Z = R_{ci} + Z_b + Z_{out} \quad (2)$$

For the impedance of the outer layer, trials of different distributed functions demonstrated that the so-called Havriliak-Negami impedance [9] gave the best fit to the experimental data

$$Z_{out} = \frac{R_{out}}{\left[1 + (j\omega R_{out} C_{out})^u\right]^n} \quad (3)$$

Here  $C_{out}$  and  $R_{out}$  are the capacitance of the outer layer and the apparent resistance of defect migration through that layer, whereas  $u$  and  $n$  are fractional exponents. The Havriliak-Negami response represents a generalization of the Constant Phase Element (CPE) to account for asymmetric capacitive loops. The Havriliak-Negami element has been proposed originally for polymer dispersions and can be regarded according to the original authors as the impedance of a two phase mixture, which seems to be a good approximation for the outer layer of oxide.

The impedance of the barrier layer is given by the sum of the impedances characterizing its electric properties and ionic transport through it in parallel

$$Z_b = \left(Z_c^{-1} + Z_{ion}^{-1}\right)^{-1} \quad (4)$$

The electronic contribution to the impedance,  $Z_c$ , is related to the spatial variation of the steady-state concentration of oxygen vacancies in the oxide, which creates a positive ionic space charge that requires electronic compensation to achieve electro neutrality. The following expression for  $Z_c$  has been derived earlier [9]:

$$Z_c = \frac{RT}{2j\omega F \bar{E} \epsilon \epsilon_0} \ln \left[ \frac{1 + j\omega \rho_d \epsilon \epsilon_0 e^{\frac{RT}{2F\bar{E}t_b}}}{1 + j\omega \rho_d \epsilon \epsilon_0} \right] \quad (5)$$

and

$$\rho_d = \frac{RTk_1}{F^2 D_e k_2}, \epsilon \quad (5)$$

Where  $\rho_d$  is the dielectric constant of  $\text{Fe}_2\text{CrO}_4$  spinel oxide, assumed to be equal to 25,  $\epsilon$  is the dielectric permittivity of free space,  $\omega$  is the angular frequency and  $D_e$  is the diffusion coefficient of the electronic current carriers.

On the other hand, the impedance due to the motion of oxygen vacancies,  $Z_{ion}$ , has been shown [9] to be well approximated by

$$Z_{ion} = R_t + \frac{RT}{4F^2 k_1 \left[ 1 + \sqrt{1 + \frac{j\omega(RT)^2}{(FE)^2 D_o}} \right]} \quad (6)$$

The above described model for the transport of electronic and ionic charge carriers through the oxide film is known as the mixed conduction model (MCM). The kinetic and transport parameters, namely, the rate constant of oxidation at the alloy/barrier layer interface,  $k_1$ , the diffusion coefficient of oxygen vacancies,  $D_o$ , the field strength in the barrier layer,  $E$ , the charge transfer resistance at the alloy/oxide interface,  $R_i$ , the  $\rho_d \epsilon$  parameter defined in Eq. (5), as well as the parameters characterizing the outer layer ( $C_{out}$  and  $R_{out}$ ) were estimated using non-linear least square fitting of the experimental spectra to the transfer function derived in the previous paragraph. Statistical weighting was used for the experimental data set and the errors of parameter estimation were multiplied by the square root of the reduced  $\chi^2$ -value resulting from the fit. In spite of the relatively large number of parameters, this resulted in a sufficient number of degrees of freedom in the system in order to obtain statistically reliable values of the kinetic parameters.

TABLE 1. IMPEDANCE MODEL FITTING RESULTS

Param	Unit	1 ppm Li	2 ppm Li	1 ppm Li 1200 ppm B	1 + 1 ppm Li 1200 ppm B	2 ppm Li 1200 ppm B
C	$\mu\text{F}\cdot\text{cm}^{-2}$	53.8	81	36.5	36	22.5
p	-	0.07	0.0685	0.0736	0.0716	0.0713
$\rho_d \epsilon$	$\Omega\cdot\text{cm}$	4.94E6	5.31E6	1.20E7	6.04E6	4.43E6
$R_t$	$\Omega\cdot\text{cm}^2$	76.7	216.9	1.1	27.0	25.0
$k_1$	$\text{mol}\cdot\text{cm}^{-2}\cdot\text{s}^{-1}$	7.57E-12	9.96E-12	2.12E-12	5.16E-12	3.96E-12
$R_{out}$	$\Omega\cdot\text{cm}^2$	4.7	13.9	50.3	35.6	127.3
$C_{out}$	$\text{F}\cdot\text{cm}^{-2}$	1.97E-4	7.4E-5	4.6E-4	1.42E-3	4.5E-4
$D_o$	$\text{cm}^2\cdot\text{s}^{-1}$	6.1E-17	5.9E-17	9.8E-18	2.9E-17	2.6E-17
field	$\text{V}\cdot\text{cm}^{-1}$	86294	99252	92758	88242	90869
thickness	nm	40.3	35.8	35.7	38.5	37.6

In the oxidation of Alloy 690, the possible rate limiting processes can be a) the rate of oxidation at the alloy/barrier layer interface (described by the parameter  $k_1$ ) or b) the transport of oxygen/oxygen

vacancies through the existing film (described by the parameter  $D_o$ ). Dissolution of the oxide / hydrolysis of metal cations at the film/electrolyte interface are typically fast in comparison with the two preceding steps and are thus assumed not to be rate limiting.

As shown in Table 1, in the case of 1 ppm Li, the rate constant of oxidation at the alloy/barrier layer interface decreases by roughly a factor of 3.5 due to addition of 1200 ppm B. Simultaneously, the diffusion constant  $D_o$  decreases by roughly a factor of 6. In case of 2 ppm Li, the decrease in the same parameters due to addition of 1200 ppm B is less, roughly 2.5 and 2.3, respectively. In the case of 2 ppm Li, as the effect on both parameters is almost the same, it is difficult to say which one of the processes is rate determining. However, in the case of 1 ppm Li the effect of B is about twice as strong on the diffusion rate, indicating that at least in this case the rate determining step of oxidation and corrosion is the diffusion of oxygen/oxygen vacancies through the barrier layer. The difference in the parameters for the solution containing only Li (i.e. between 1 and 2 ppm Li) is relatively small.

### 4.3. Conductivity data

The pressure vessel used for the tests was made of AISI316L, and had been cleaned of surface oxides with glass pebble blasting and further passivated for 72 hours at 292°C in PWR water. The total exposure time of the pressure vessel to high temperature PWR water at the end of the experiments described in this report was not more than 1000 hrs. Thus, the thickness of the oxides on the pressure vessel surfaces was relatively small. During the experiments where only LiOH was added, the conductivity was found to decrease as a function of test duration. Figure 10 shows an example of a test where, after cleaning the loop with ion exchangers until conductivity was  $\gamma < 0.2 \mu\text{S}\cdot\text{cm}^{-1}$ , first temperature was increased to  $T = 80^\circ\text{C}$ , then dissolved oxygen was removed by nitrogen bubbling, then 1.5 bar overpressure of hydrogen gas was added to the mixing tank and finally a target concentration of 1.0 mg/l (ppm)  $\text{Li}^+$  was added to the water volume as LiOH. The ion exchanger was accidentally left on for a short period right after the addition of the Li. This is seen as a rapid decrease of conductivity. A second addition of Li was made after shutting off the ion exchanger, resulting in a slight overshoot of the starting Li concentration. Already during the equilibration time at  $T = 80^\circ\text{C}$  before heating up some decrease of conductivity can be noticed, the rate of decrease increasing after heating up to  $T = 292^\circ\text{C}$ . The water grab sample at the end of the test showed 1.3 ppm Li.

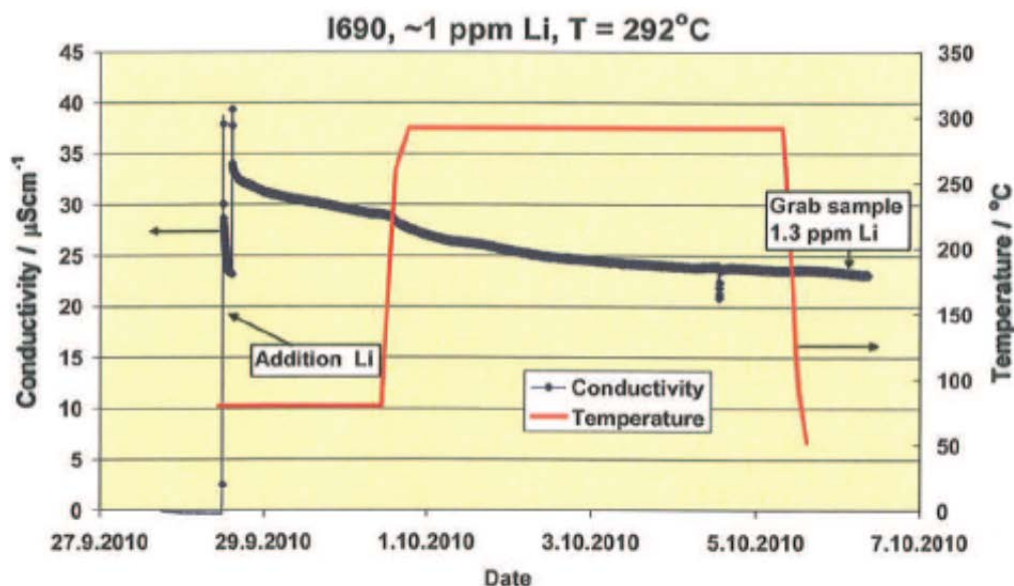


FIG. 10. Conductivity (25°C) as a function of time in a test run where originally a target concentration of 1.0 ppm Li was added as LiOH.  $[\text{H}_2] = 30 \text{ ccH}_2/\text{kgH}_2\text{O}$  from the start.

Another example of the conductivity is shown in Fig. 11. In this test run, the target Li-concentration was 2.2 ppm. Similarity to Fig. 10 for water with about 1 ppm Li, the conductivity

decreases rather steadily as a function of time. The water grab sample at the end of this test showed 2.2 ppm Li. A check was made on the stability of the conductivity sensors so that water with 2.2 ppm Li (no B) was circulated through them, without passing through the high temperature section of the experimental system. In a one week test no change in the sensor signal was noticed, indicating that the decrease of conductivity is solely due to adsorption of Li on the surfaces within the high temperature section of the system.

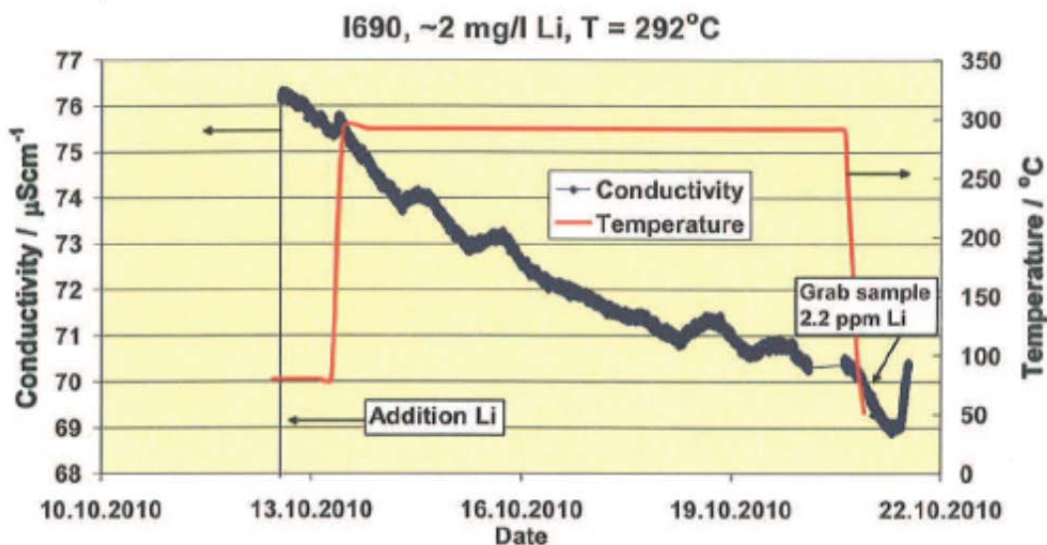


FIG. 11. Conductivity (25°C) as a function of time in a test run where originally a target concentration of 2.2 ppm Li was added as LiOH.  $[H_2] = 30 \text{ ccH}_2/\text{kgH}_2\text{O}$  from the start.

## 5. CONCLUSIONS

Based on the in situ electrochemical impedance data gained so far it seems evident that the formation and stabilization of the barrier layer part of the oxide forming on both carbon steel and Alloy 690 in lithiated high temperature water takes place during the first 40 hours of the exposure. Taking into account that the typically proposed exposure time during hot conditioning period is between 300 and 1000 hours, the passivation time is more than adequate.

At the exposure temperature of  $T = 292^\circ\text{C}$ , the impedance magnitude and thereby the rate of generation of soluble and insoluble corrosion products increases only slightly when lithium concentration increases from 1 to 2 ppm, in absence of boron. The introduction of 1200 ppm B into the coolant increases the impedance magnitude by roughly 100% in comparison with the case of 1 ppm Li concentration and slightly more in case of 2 ppm Li concentration. This indicates that addition of boron decreases dramatically the rate of generation of soluble and insoluble corrosion products for Alloy 690.

Through the modelling of the impedance spectra using the Mixed Conduction Model (MCM) approach, parameters relevant to the different processes involved in corrosion of Alloy 690 in simulated hot conditioning environment could be derived. The diffusion coefficient of oxygen through the barrier layer part of the oxide is of the order of  $D_o = 10^{-17} \cdot \text{cm}^2\text{s}^{-1}$ . The diffusion coefficient decreases roughly by a factor of 6 when the boron concentration increases from 0 to 1200 ppm, and by a factor of about 2, for lithium concentrations of 1 and 2 ppm, respectively. Simultaneously the reaction rate constant for the oxidation of Alloy 690 at the alloy / oxide interface decreases by roughly a factor of 2.5. The analysis of the impedance spectra through the MCM thus corroborates the straightforward analysis given above in 4.1, indicating specifically that addition of boron into the coolant is highly beneficial and that increasing the lithium concentration is detrimental to the quality of the passive layer on Alloy 690.

There are three lines of further research in optimization of the hot conditioning procedure that require attention. The first one is the lower range of Li concentration, i.e. in situ results need to be

gained also for 0.5 ppm Li, in order to quantify the difference between the Japanese and Western approaches. Secondly, the effect of boron concentration should be studied in a more wide range, e.g. duplicating some of the current measurements at a level of 500 ppm B. Thirdly, the mechanism, extent and consequences of possible Li hideout during the passivation treatment should be studied in detail.

## 6. SUMMARY

The primary circuit surfaces of a new pressurized water nuclear reactor are passivated before the first fuel loading. This treatment is called hot conditioning. The main purpose of the hot conditioning is to minimize the rate of generation of soluble and insoluble corrosion products (corrosion rate), and thereby minimize the activity build-up during power operation. There is still no international consensus on optimal passivation water chemistry. Open issues are e.g. the optimal concentration of lithium and the length of the passivation treatment. New issues are the possible benefits of using boron and zinc in the water during the passivation.

This report presents the first part of experimental results on Alloy 690 gained by the electrochemical impedance spectroscopy (EIS) in situ technique at  $T = 292^{\circ}\text{C}$ . These results indicate that addition of boron is highly beneficial, 1200 ppm B resulting in reduction of the estimated corrosion rate by a factor of about 2. An increase of the lithium concentration from 1 to 2 ppm Li was found to result in a higher estimated corrosion rate. The time to form a stable passive layer on Alloy 690 at  $T = 292^{\circ}\text{C}$  was found to be about 40 hrs. Thus, the time normally used for passivation, i.e. 300–1000 hours, is certainly long enough. In experiments without boron, the conductivity was found to decrease during the experiment, indicating a possibility of lithium hide-out on the hot part of the test equipment surfaces.

There are three lines of further research in optimization of the hot conditioning procedure that require attention. The first one is the lower range of Li concentration, i.e. in situ results need to be gained also for 0.5 ppm Li, in order to quantify the difference between the Japanese and Western approaches. Secondly, the effect of boron concentration should be studied in a more wide range, e.g. duplicating some of the current measurements at a level of 500 ppm B. Thirdly, the mechanism, extent and consequences of possible Li hideout during the passivation treatment should be studied in detail.

## REFERENCES

- [1] SAARIO, T., KINNUNEN, P., Literature survey on optimisation of hot functional test procedure. VTT Research Report VTT-R-08070-07 (2008) 15.
- [2] YAMADA, E., SUZUKI, S., HIRAO, T., HASHIMOTO, Y., HISAMUNE, K., YOKOYAMA, J., Corrosion rate reduction by chemical control during hot functional testing, Proc. JAIF International Conference on Water Chemistry in Nuclear Power Plants, Fukui, Japan (1991) 151–156.
- [3] KADOYA, M., Countermeasures for radiation dose reduction at Ikata Unit No.3, Proc. 10. International Congress of the International Radiation Protection Association, Hiroshima, Japan (2000) paper number P-6a-296.
- [4] ITO, A., MURATA, K. AND YOKOYAMA, J., Water chemistry during startup testing at the latest PWR: Genkai Unit No. 4, Proc. JAIF International Conference on Water Chemistry in Nuclear Power Plants, Kashiwazaki, Japan (1998) 806–811.
- [5] HAYAKAWA, H., MINO, Y., NAKAHAMA, S., AIZAWA, Y., NISHIMURA, T., UMEHARA, R., SHIMIZU, Y., KOGAWA, N. OJIMA, Z., Zinc injection from hot functional test (HFT) in Tomari Unit 3.
- [6] MACHET, A., GALTAYRIES, A., MARCUS, P., COMBRADE, P., JOLIVET, P. SCOTT, P. XPS study of oxides formed on nickel-base alloys in high-temperature and high-pressure water. Surf. Interface Anal. **34**, (2002), 197–200.

- [7] COMBRADE, P., SCOTT, P.M., FOUCAULT, M., ANDRIEU, E. MARCUS, P. Oxidation of Ni base alloys in PWR water: oxide layers and associated damage to the base metal. Proceedings of the 12th International Conference on Environmental Degradation of Materials in Nuclear Power System — Water Reactors. Edited by ALLEN, T.R., KING, P.J., NELSON L. (Eds.) TMS (The Minerals, Metals & Materials Society), (2005).
- [8] BOJINOV, M., GAONKAR, K., GHOSH, S., KAIN, V., KUMAR, K., SAARIO, T., Characterisation of the oxide layer on carbon steel during hot conditioning of primary heat transport systems in heavywater reactors. Cor. Sci. **51** (2009) 1146–1156.
- [9] BOJINOV, M., FABRICIUS, G., KINNUNEN, P., LAITINEN, T., MAKELA, K., SAARIO, T., SUNDHOLM, G., Electrochemical study of the passive behaviour of Ni-Cr alloys in a borate solution — a mixed-conduction model approach. J. Electroanal. Chem. **504** (2001) 29–44.



# OPTIMIZATION OF WATER CHEMISTRY TO CONTROL CRUD DEPOSITION ON FUEL CLAD IN INDIAN PRESSURIZED HEAVY WATER REACTORS

S. VELMURUGAN, S.V. NARASIMHAN  
Water and Steam Chemistry Division, BARC Facilities  
Kalpakkam – 603 102  
Tamilnadu, India

## Abstract

Deposition of corrosion products in the core structural materials especially in the fuel clad can cause problem of radiation field build up in the out of core surfaces. Hence, efforts have to be made to control deposition of corrosion products in the clad and other zircaloy components. There are 18 reactors in India, 16 are pressurized heavy water reactors. The PHWRs is a tube type reactor and it has a separate moderator system and boron addition is not carried out in the heavy water primary coolant. By controlling the lithium concentration, the  $\text{pH}_a$  of the heavy water coolant is controlled at a desired value so that deposition of corrosion products in the clad and other zircaloy components is minimized. Hydrogen injection is also carried out to maintain the reducing chemistry condition. The presence of hydrogen and alkaline chemistry condition in the primary coolant feeders and headers are made of carbon ensures the formation of magnetite and mixed ferrites as corrosion products in the primary coolant system structural materials. In PHWRs, the steel and the magnetite ( $\text{Fe}_3\text{O}_4$ ) formed over the carbon steel is the dominant corrosion product. Dissolution of magnetite from the out of core structural materials and its deposition in the incore surfaces are highly dependent on the  $\text{pH}_a$ . Dissolution of magnetite from carbon steel is aided by flow accelerated corrosion (FAC) observed on carbon steel feeders. Hence, the chemistry of the heavy water coolant has to be adjusted in such a way that it minimizes deposition in the core and at the same time minimizes flow accelerated corrosion. Full primary coolant system chemical decontamination is being carried out in Indian PHWRs, before any major shut down activity. The added chemicals apart from removing the oxide film over the out of core structural materials, is expected to remove the corrosion product oxides deposited over the clad and other zircaloy structural materials. This is evident from lower radiation field build up subsequent to chemical decontamination. This paper presents on the water chemistry specification followed in Indian PHWRs, the observation of FAC and its role in the transport and deposition of corrosion products, the effect of chemical decontamination and the facilities built to study the deposition of corrosion products in the zircaloy material.

## 1. INTRODUCTION

Deposition of corrosion products in the in-core zircaloy surfaces is a cause of concern for the plant operators as it causes problem of radiation field, neutron flux variation and corrosion. Hence, efforts are being made world over to control deposition of corrosion products in the clad and other zircaloy components. The problem is common to BWRs, PWRs and also to PHWRs and other reactors. In India there are 16 PHWRs, of them 14 are 220 MWe and 2 of them are 540 MWe PHWRs. Zircaloy is used as fuel clad, pressure tubes and as calendria tubes. PHWRs are tube type reactors. It is fuelled by natural uranium. It has a separate moderator system. Boron/gadolinium addition is carried out in the moderator during shutdown/startup or during the pre-equilibrium core operation. Hence, the primary heavy water coolant does not contain boron. Only lithium is added to make the pH of the coolant alkaline. Hydrogen is added to control the radiolytic production of oxygen.

In the primary coolant system apart from zircaloy, carbon steel and Incoloy-800/Monel-400 are used as structural materials. As the deposition in core zircaloy components arises from the formation of corrosion products from carbon steel and steam generator tube materials, control of crud deposition in the core is closely linked to the corrosion of out-of-core structural materials which in turn is controlled by primary heavy water coolant chemistry in PHWRs. The chemistry of the primary heavy water coolant is optimized in such a way that there is a balance between crud deposition in the core and carbon steel corrosion in the out-of-core.

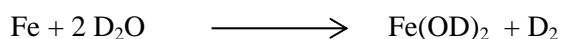
## 2. CHEMISTRY SPECIFICATION

The chemistry specification for the primary heat transport (PHT) system of Indian PHWRs is given in Table 1.

TABLE 1. CHEMISTRY SPECIFICATION FOR PHT SYSTEM OF INDIAN PHWRs

S. No	Parameter/ Constituent	Sampling Frequency	NRV	Action levels		
				<u>AL#1</u>	<u>AL #2</u>	<u>AL #3</u>
1.	pH <sub>a</sub> at 25°C	Once / day	>10.2 to <10.5	10.2 – 10.0 10.5 – 10.6 (240 h)	< 10.0 – 9.0 >10.6 – 10.8 (48 h)	< 9.0 >10.8
2.	Dissolved oxygen (µg / lit)	By DO analyzer or grab measurement — Thrice / week	<10	≥10 (240 h)	≥20 (48 h)	≥ 100

The pH<sub>a</sub> of the primary heavy water coolant is specified as 10.2–10.5 and the dissolved oxygen is controlled at < 10 ppb. Hydrogen is injected and maintained at a concentration range of 2–10 ml/kg. Under these reducing conditions, magnetite and ferrites are formed as corrosion products. As carbon steel is the major structural material, magnetite dominates the corrosion product inventory.



Corrosion of carbon steel feeders and headers is an important factor in the transportation of corrosion products. As carbon steel releases large amount of crud during the initial stages, hot conditioning of the primary coolant system is carried out before criticality of the reactor. It is done without the fuel in the core so that the crud does not settle on the fuel surfaces. During this period of hot conditioning, a uniform coating of magnetite is formed over the carbon steel surfaces. This magnetite film is protective which restricts the corrosion and corrosion release from carbon steel and other surfaces. The corrosion products released from carbon steel and other surfaces are transported through the heavy water primary coolant. Deposition in the in-core surfaces is heavily dependent on the chemistry condition of the coolant. The pH<sub>a</sub> is kept at > 10 so that positive temperature coefficient of solubility of magnetite is ensured. However, in order to ensure a cleaner core pH<sub>a</sub> 25°C of 10.5–10.6 is desirable. Achieving this pH<sub>a</sub> range is limited by the requirement of controlling flow accelerated corrosion.

## 3. FLOW ACCELERATED CORROSION

Flow accelerated corrosion has been observed to occur in carbon steel feeders especially in the core outlet feeders. Certain locations in feeder bends/elbows undergo wall thinning at rates much higher than the straight sections of the carbon steel feeders. Presence of FAC has been confirmed by the observation of scallops in the outlet feeders and observation of lower wall thicknesses in feeder elbows during in service inspection of feeders. It has been reported that flow accelerated corrosion rate goes through a minimum as a function of pH in the temperature range 150–190°C, while such a dependence is not very clearly available at 300°C. Thus, FAC puts a constraint in maintaining a higher pH to achieve a cleaner core. At present the pH<sub>a</sub> is controlled in the range of 10.2 to 10.3. Investigations are going on to study the effect of pH<sub>a</sub> on flow accelerated corrosion at 300°C and on radiation field buildup.

#### 4. DEPOSITION OF ANTIMONY ON ZIRCALOY SURFACES

Release of  $^{122}\text{Sb}$  and  $^{124}\text{Sb}$  activities have been observed during shut down periods. This is attributed to the release of antimony from the primary coolant pump seals and bearings. The antimony thus released from these components settle down on the clad and other zircaloy components. The chemical form of antimony in the core surface is uncertain. Release of activated antimony occurs during shutdown maintenance. Hydrazine addition is being evaluated for its effectiveness in preventing the release of antimony activities during shut down.

#### 5. EFFECT OF FULL SYSTEM CHEMICAL DECONTAMINATION

Full primary coolant system chemical decontamination is carried out to reduce the radiation field build in Indian PHWRs. The chemicals added remove the magnetite film from the carbon steel surfaces. Its effect on non-carbon steel surfaces such as steam generator surfaces is marginal. The added chemical formulation reacts with magnetite film present over carbon steel surfaces and the pH of the solution increases to 5.0. Under these conditions, the efficiency of the removal of magnetite/ferrites from core zircaloy and out-of-core steam generator surfaces is less efficient. However, as the inventory of oxides deposited over zircaloy surfaces is less, significant removal of oxides deposited over the core zircaloy surfaces is expected. A study in this regard is required. Operation of the reactor subsequent to the chemical decontamination has not resulted in change in crud deposition behaviour.

#### 6. CONCLUSIONS

In PHWRs, there is a need to balance the mutually opposing requirement of maintaining a clean core by having high pH and to reduce the flow accelerated corrosion in feeders by having  $\text{pH}_a$  closer to 10.

Full system chemical decontamination of primary coolant circuit has not altered the crud deposition behaviour.



## APPENDIX PROPOSED FORM FOR REPORTING CRUD SAMPLING MEASUREMENTS

Plant	Country	Contact Person		Reactor Type	Fuel Cycle Length	Chemistry Regime of RC system (normal power operation)		
		name	email			pH <sub>(300)</sub> or pH <sub>(T)</sub>	alkaline reagent for pH control	Dissolved Hydrogen/Oxygen concentration
					months			

Primary circuit materials		Corrosion products analysing from the coolant (average values during operation)			Analysis of crud/deposits scraped from primary equipment internal and/or fuel cladding surfaces (manual scraper or automated scraper)					
SG tubing	Vessel	Fuel assembly (cladding, grids etc.)	Chemical analysis (concentration of Fe (or other metals) in the coolant)	Radiochemical analysis (radioisotope activity in coolant — <sup>54</sup> Mn, <sup>58</sup> Co)	"Sampling from" specification: FA (Cycles in core, Burnup); Primary equipment surface	Crud mass and area of crud scraping	Crud colour, thickness (estimate from mass/area) and microstructure	Elemental content	Radioisotope content	Individual crud flakes analysis (structure and elemental content)

	<b>OPTIONAL</b>		
NOTE — for more use worksheet (APPENDIX)	Corrosion products analysing from the coolant (high temperature coolant sampling at steady-state, during shutdown, startup and during power transients) — soluble and insoluble forms		
	Chemical analysis (concentration in the coolant)	Radiochemical analysis (activated corrosion products)	Microstructural and elemental analysis of crud particles

## ABBREVIATIONS

BWR	boiling water reactor
CANDU	Canadian type pressurized heavy water reactor (Canadian Deuterium Uranium)
CIPS	crud induced power shift
CRP	coordinated research programme
FAC	flow assisted corrosion
HFT	hot functional testing
HWR	heavy water reactors
IRI	incomplete (control rod) insertion
LWR	light water reactor
MTR	materials test reactor
NPP	nuclear power plant
ONLC	on-line noble metal addition
PCMI	pellet clad mechanical interaction
PHWR	pressurized heavy water reactor
PWR	pressurized water reactor
SCC	stress corrosion cracking
SG	steam generator
SNB	sub-cooled nucleate boiling
WWER	Russian designed pressurized light water reactor



## LIST OF PARTICIPANTS

O. Arkhipov	Gidropress, Moscow, Russian Federation.
E. Arsenina	Khmelnitski NPP, Kiev, Ukraine.
P.J. Bennett	Halden Reactor Project, Halden, Norway.
I. Berezina	VNIPIET, St Petersburg, Russian Federation.
H. Glasbrenner	Swiss Federal Nuclear Safety Inspectorate (ENSI), Villigen, Switzerland.
B. Gong	Nuclear Power Institute of China, Chengdu, China.
A. Grishakov	Gidropress, Moscow, Russian Federation.
D.H. Lister	University of New Brunswick, Fredericton, Canada.
V. Marukhyan	Armenian NPP, Metsamor, Armenia.
M. Miklos	NRI, Řež, Czech Republic.
I. Pirvan	INR, Pitesti, Romania.
T. Saario	VTT Technical Research Centre of Finland, Espoo, Finland.
V. Sankaralingam	BARC, Kalpakkam, Tamil Nadu, India.
K. Scherbinin	Khmelnitsky NPP, Kiev, Ukraine.
J. Schunk	Paks NPP, Paks, Hungary.
X. Shi	Shanghai Nuclear Engineering Research and Design Institute, Shanghai, China.
V. Shishov	JSC VNIINM, Moscow, Russian Federation.
M. Tretyakov	KIPT, Kiev, Ukraine.
M. Usman	Pakistan Atomic Energy Commission, Islamabad, Pakistan.
S.P. Walker	Imperial College, London, United Kingdom.
N. Zaharieva	INRNE, Sofia, Bulgaria.
V. Zuyok	KIPT, Kiev, Ukraine.





## Where to order IAEA publications

In the following countries IAEA publications may be purchased from the sources listed below, or from major local booksellers. Payment may be made in local currency or with UNESCO coupons.

### AUSTRALIA

DA Information Services, 648 Whitehorse Road, MITCHAM 3132  
Telephone: +61 3 9210 7777 • Fax: +61 3 9210 7788  
Email: service@dadirect.com.au • Web site: <http://www.dadirect.com.au>

### BELGIUM

Jean de Lannoy, avenue du Roi 202, B-1190 Brussels  
Telephone: +32 2 538 43 08 • Fax: +32 2 538 08 41  
Email: jean.de.lannoy@infoboard.be • Web site: <http://www.jean-de-lannoy.be>

### CANADA

Bernan Associates, 4501 Forbes Blvd, Suite 200, Lanham, MD 20706-4346, USA  
Telephone: 1-800-865-3457 • Fax: 1-800-865-3450  
Email: customercare@bernan.com • Web site: <http://www.bernan.com>

Renouf Publishing Company Ltd., 1-5369 Canotek Rd., Ottawa, Ontario, K1J 9J3  
Telephone: +613 745 2665 • Fax: +613 745 7660  
Email: order.dept@renoufbooks.com • Web site: <http://www.renoufbooks.com>

### CHINA

IAEA Publications in Chinese: China Nuclear Energy Industry Corporation, Translation Section, P.O. Box 2103, Beijing

### CZECH REPUBLIC

Suweco CZ, S.R.O., Klecakova 347, 180 21 Praha 9  
Telephone: +420 26603 5364 • Fax: +420 28482 1646  
Email: nakup@suweco.cz • Web site: <http://www.suweco.cz>

### FINLAND

Akateeminen Kirjakauppa, PO BOX 128 (Keskuskatu 1), FIN-00101 Helsinki  
Telephone: +358 9 121 41 • Fax: +358 9 121 4450  
Email: akatilaus@akateeminen.com • Web site: <http://www.akateeminen.com>

### FRANCE

Form-Edit, 5, rue Janssen, P.O. Box 25, F-75921 Paris Cedex 19  
Telephone: +33 1 42 01 49 49 • Fax: +33 1 42 01 90 90  
Email: formedit@formedit.fr • Web site: <http://www.formedit.fr>

Lavoisier SAS, 145 rue de Provigny, 94236 Cachan Cedex  
Telephone: +33 1 47 40 67 02 • Fax +33 1 47 40 67 02  
Email: romuald.verrier@lavoisier.fr • Web site: <http://www.lavoisier.fr>

### GERMANY

UNO-Verlag, Vertriebs- und Verlags GmbH, Am Hofgarten 10, D-53113 Bonn  
Telephone: +49 228 94 90 20 • Fax: +49 228 94 90 20 or +49 228 94 90 222  
Email: bestellung@uno-verlag.de • Web site: <http://www.uno-verlag.de>

### HUNGARY

Librotrade Ltd., Book Import, P.O. Box 126, H-1656 Budapest  
Telephone: +36 1 257 7777 • Fax: +36 1 257 7472 • Email: books@librotrade.hu

### INDIA

Allied Publishers Group, 1st Floor, Dubash House, 15, J. N. Heredia Marg, Ballard Estate, Mumbai 400 001,  
Telephone: +91 22 22617926/27 • Fax: +91 22 22617928  
Email: alliedpl@vsnl.com • Web site: <http://www.alliedpublishers.com>

Bookwell, 2/72, Nirankari Colony, Delhi 110009  
Telephone: +91 11 23268786, +91 11 23257264 • Fax: +91 11 23281315  
Email: bookwell@vsnl.net

### ITALY

Libreria Scientifica Dott. Lucio di Biasio "AEIOU", Via Coronelli 6, I-20146 Milan  
Telephone: +39 02 48 95 45 52 or 48 95 45 62 • Fax: +39 02 48 95 45 48  
Email: info@libreriaaeiou.eu • Website: [www.libreriaaeiou.eu](http://www.libreriaaeiou.eu)

## **JAPAN**

Maruzen Company Ltd, 1-9-18, Kaigan, Minato-ku, Tokyo, 105-0022  
Telephone: +81 3 6367 6079 • Fax: +81 3 6367 6207  
Email: journal@maruzen.co.jp • Web site: <http://www.maruzen.co.jp>

## **REPUBLIC OF KOREA**

KINS Inc., Information Business Dept. Samho Bldg. 2nd Floor, 275-1 Yang Jae-dong SeoCho-G, Seoul 137-130  
Telephone: +02 589 1740 • Fax: +02 589 1746 • Web site: <http://www.kins.re.kr>

## **NETHERLANDS**

De Lindeboom Internationale Publicaties B.V., M.A. de Ruyterstraat 20A, NL-7482 BZ Haaksbergen  
Telephone: +31 (0) 53 5740004 • Fax: +31 (0) 53 5729296  
Email: books@delindeboom.com • Web site: <http://www.delindeboom.com>

Martinus Nijhoff International, Koraalrood 50, P.O. Box 1853, 2700 CZ Zoetermeer  
Telephone: +31 793 684 400 • Fax: +31 793 615 698  
Email: info@nijhoff.nl • Web site: <http://www.nijhoff.nl>

Swets and Zeitlinger b.v., P.O. Box 830, 2160 SZ Lisse  
Telephone: +31 252 435 111 • Fax: +31 252 415 888  
Email: info@swets.nl • Web site: <http://www.swets.nl>

## **NEW ZEALAND**

DA Information Services, 648 Whitehorse Road, MITCHAM 3132, Australia  
Telephone: +61 3 9210 7777 • Fax: +61 3 9210 7788  
Email: service@dadirect.com.au • Web site: <http://www.dadirect.com.au>

## **SLOVENIA**

Cankarjeva Zalozba d.d., Kopitarjeva 2, SI-1512 Ljubljana  
Telephone: +386 1 432 31 44 • Fax: +386 1 230 14 35  
Email: import.books@cankarjeva-z.si • Web site: <http://www.cankarjeva-z.si/uvoz>

## **SPAIN**

Díaz de Santos, S.A., c/ Juan Bravo, 3A, E-28006 Madrid  
Telephone: +34 91 781 94 80 • Fax: +34 91 575 55 63  
Email: compras@diazdesantos.es, carmela@diazdesantos.es, barcelona@diazdesantos.es, julio@diazdesantos.es  
Web site: <http://www.diazdesantos.es>

## **UNITED KINGDOM**

The Stationery Office Ltd, International Sales Agency, PO Box 29, Norwich, NR3 1 GN  
Telephone (orders): +44 870 600 5552 • (enquiries): +44 207 873 8372 • Fax: +44 207 873 8203  
Email (orders): book.orders@tso.co.uk • (enquiries): book.enquiries@tso.co.uk • Web site: <http://www.tso.co.uk>

### **On-line orders**

DELTA Int. Book Wholesalers Ltd., 39 Alexandra Road, Addlestone, Surrey, KT15 2PQ  
Email: info@profbooks.com • Web site: <http://www.profbooks.com>

### **Books on the Environment**

Earthprint Ltd., P.O. Box 119, Stevenage SG1 4TP  
Telephone: +44 1438748111 • Fax: +44 1438748844  
Email: orders@earthprint.com • Web site: <http://www.earthprint.com>

## **UNITED NATIONS**

Dept. I004, Room DC2-0853, First Avenue at 46th Street, New York, N.Y. 10017, USA  
(UN) Telephone: +800 253-9646 or +212 963-8302 • Fax: +212 963-3489  
Email: publications@un.org • Web site: <http://www.un.org>

## **UNITED STATES OF AMERICA**

Bernan Associates, 4501 Forbes Blvd., Suite 200, Lanham, MD 20706-4346  
Telephone: 1-800-865-3457 • Fax: 1-800-865-3450  
Email: customercare@bernan.com • Web site: <http://www.bernan.com>

Renouf Publishing Company Ltd., 812 Proctor Ave., Ogdensburg, NY, 13669  
Telephone: +888 551 7470 (toll-free) • Fax: +888 568 8546 (toll-free)  
Email: order.dept@renoufbooks.com • Web site: <http://www.renoufbooks.com>

**Orders and requests for information may also be addressed directly to:**

### **Marketing and Sales Unit, International Atomic Energy Agency**

Vienna International Centre, PO Box 100, 1400 Vienna, Austria  
Telephone: +43 1 2600 22529 (or 22530) • Fax: +43 1 2600 29302  
Email: sales.publications@iaea.org • Web site: <http://www.iaea.org/books>



